

Exploration of Bis(imino)pyridine Iron Alkoxides for the Synthesis of Novel Degradable Polymers

Author: Kayla R. Delle Chiaie

Persistent link: <http://hdl.handle.net/2345/bc-ir:108245>

This work is posted on [eScholarship@BC](#),
Boston College University Libraries.

Boston College Electronic Thesis or Dissertation, 2018

Copyright is held by the author, with all rights reserved, unless otherwise noted.

Exploration of Bis(imino)pyridine Iron Alkoxides for the Synthesis of Novel Degradable Polymers

Kayla R. Delle Chiaie

A dissertation
submitted to the Faculty of
the department of Chemistry
in partial fulfillment
of the requirements for the degree of
Doctor of Philosophy

Boston College

Morrissey College of Arts and Sciences
Graduate School

December 2018

© Copyright 2018 Kayla R. Delle Chiaie

Exploration of Bis(imino)pyridine Iron Alkoxides for the Synthesis of Novel Degradable Polymers

Kayla Rose Delle Chiaie

Advisor: Professor Jeffery Byers

Abstract: This dissertation discusses the development of a family of iron complexes and their role in the synthesis of degradable polymers. Chapter one will introduce the different areas of redox-switchable polymerization. In chapter two the synthesis of block copolymers containing a polyester and polyether block is presented. The application redox-switchable polymerization to form a copolymer with two fundamentally distinct backbone functionalities and their characterization is discussed. In chapter three the synthesis of a degradable cross-linked polymer through a novel redox-triggered cross linking event is summarized. In chapter four, a detailed mechanistic study of iron-complex catalyzed epoxide polymerization is examined and a unique mechanistic scheme is proposed. Lastly, in chapter five the synthesis and characterization of a formally iron(I) complex is presented. This complex shows remarkable catalytic activity towards ring-opening polymerization.

Table of Contents

Chapter 1	Redox-Switchable Polymerization.....	xiii
1.1	Introduction.....	1
1.2	Ring-Opening Metathesis Polymerization (ROMP).....	2
1.3	Radical and Cationic Polymerizations.....	5
1.4	Coordination-Insertion Olefin Polymerization.....	7
1.5	Ring-Opening Polymerization.....	9
1.6	References.....	16
Chapter 2.	Block Copolymerization of Cyclic Diesters and Epoxides Catalyzed by Bis(imino)pyridine Iron Bis(alkoxide) Complexes	21
2.1	Introduction.....	21
2.2	Epoxide homopolymerization	25
2.3	Redox-Switchable Epoxide Polymerization.....	26
2.4	Redox-Switchable Block Copolymerization.....	27
2.5	Conclusions.....	35
2.6	Experimental.....	36
2.7	References.....	43
Chapter 3	Redox-triggered Crosslinking of a Degradable Polymer.....	50
3.1	Introduction.....	50
3.2	Synthesis of dual functionalized monomer.....	52
3.3	Homopolymerization of 3.9.....	54
3.4	Conclusions.....	67
3.5	Experimental.....	68
3.6	References.....	77

Chapter 4 : Mechanistic Investigation of Epoxide Polymerization by Cationic

Bis(imino)pyridine Iron Bis(alkoxide) Complexes	82
4.1 Introduction	82
4.2 Cationic vs. Coordination-Insertion Mechanism	85
4.3 Anion effects.....	89
4.4 Kinetic Analysis.....	91
4.5 Kinetic Modeling.....	94
4.6 Ligand Effects.....	96
4.7 Molecular Weight and Dispersity.....	102
4.8 Conclusions.....	103
4.9 Experimental.....	104
4.10 References	109

Chapter 5 Ring-Opening Polymerization with a Formally Iron(I)

Bis(imino)pyridine Mono(alkoxide) Complex	114
5.1 Introduction.....	114
5.2 Synthesis and Characterization of bis(imino)pyridine iron alkoxides	117
5.3 Polymerizations Catalyzed with Formally Iron(I) Complexes	126
5.4 Copolymerization Reactions with Low Strain Monomers.....	132
5.5 Conclusions.....	136
5.6 Experimental.....	138
5.7 References	150

Appendix A Differential Scanning Calorimetry and Thermogravimetric Analysis

Thermograms 161

Appendix B Nuclear Magnetic Resonance (NMR) Spectra	175
---	-----

B.1	NMR Spectra from Chapter 3.....	175
B.2	NMR Spectra from Chapter 4.....	177
Appendix C	X-ray crystal structure data from Chapter 5.....	182

List of Tables

Table 2.1. Polymerization of epoxides catalyzed by 2.2 ^a	26
Table 2.2. Redox-controlled diblock copolymerization of lactide (L) and cyclohexene oxide (CHO).....	29
Table 2.3. Redox-controlled diblock copolymerization of cyclohexene oxide (CHO) and lactide (L).....	32
Table 3.1. Properties of polymers obtained from the redox-triggered crosslinking of random copolymers containing lactide and epoxy cyclic diester 3.9 ^a	59
Table 4.1. Rate constants (k_{obs}) for different bis(imino)pyridine ligands using 0.2 mol % of the complex in deuterated dichloromethane at -30°C.....	98
Table 5.1. Zero-field ⁵⁷ Fe Mössbauer parameters for iron complexes 5.3 and 5.1 ^{a,b}	121
Table 5.2. Selected bond distances and angles for the X-ray crystal structure of 5.3b and structures of 5.3a and 5.3b optimized at the M06-L level	125
Table 5.3. Polymerization of (<i>rac</i>)-lactide catalyzed by 5.1 and 5.3	128
Table 5.4. Polymerization studies with complexes 5.3b and 5.1b ^a	130
Table C. 1 Crystal data and structure refinement for Fe(PDI)(neopentoxide) (5.3b)	182
Table C. 2 Bond lengths [Å] and angles [°] for Fe(PDI)(neopentoxide) (5.3b)	183

List of Figures

Figure 2.1. Redox-controlled polymerization of cyclohexene oxide in PhCl (0.91M with 2.2 (2.0 mol%)	27
Figure 2.2. DOSY-NMR spectra of a) isolated block copolymer (Table 2.2, entry 1) and b) a mixture of polylactide and polyether homopolymers of similar molecular weight and [PLA]:[PCHO] ratio.....	34
Figure 3.1. Crosslinking techniques.....	50
Figure 3.2. Molecular weight (M_n , ●) and molecular weight distribution (M_w/M_n , ◐) vs. conversion for the polymerization of 3.9 catalyzed by iron-based complex 3.1 ..	55
Figure 3.3. Determination of reactivity ratios for copolymerization 3.9 and lactide catalyzed by 3.1	61
Figure 3.4. T_g (●) and swellability (◐) of polymers obtained from redox-triggered crosslinking reactions at various [3.9]: lactide feed compositions. Lines connecting the datum are merely meant to guide the eye to emphasize the trend and are not mathematical fits to model the data	65
Figure 4.1. Redox-controlled polymerization of cyclohexene oxide in PhCl (0.91M) with 4.1 (2 mol%)	87
Figure 4.2. a) Assignment of triads in the ^{13}C NMR of the polymer obtained from polymerization with 4.2. b) triad region of the ^{13}C NMR for polymer obtained from polymerization with ferrocenium hexafluorophosphate. i (iso) and s (syndio) indicate relative tacticity of triads.....	88
Figure 4.3. Kinetic data of cyclohexene oxide polymerization with different equivalents of BAR_4^{F}	91

Figure 4.4. Kinetic data for the polymerization of cyclohexene oxide using 0.2 mol % of complex 4.2 in deuterated dichloromethane at -30 °C	93
Figure 4.5. Determination of order in iron for cyclohexene oxide polymerization using x mol % of complex 4.2 in deuterated dichloromethane at -30 °C	94
Figure 4.6. Kinetic modeling of 1 st order (top: goodness of fit = $1.4e^{-7}$) versus 2 nd order (bottom: goodness of fit = $5.4e^{-9}$) in monomer using COPASI. Intermediates shown are used to illustrate the kinetic model used to obtain these fits	95
Figure 4.7. UV-vis data for 4.2 and 4.2f at 0.53 M in dichloromethane	99
Figure 4.8. Kinetic data and determination of the order in the catalyst for complex 4.3	100
Figure 5.1. Iron bis(imino)pyridine alkoxide complexes used in ring opening polymerization reactions and their application in redox-switchable polymerization reactions	115
Figure 5.2. Monomers explored for ring-opening polymerization	116
Figure 5.3. X-ray crystal structure of complex 4.3b with thermal ellipsoids represented at the 50% probability level. Hydrogen atoms are omitted for clarity. Fe-N1 = 2.14Å, Fe-N2 = 1.99Å, Fe-N3 = 2.15Å. O-Fe-N1 = 107.9°, O-Fe-N2 = 163.0°, O-Fe-N3 = 105.3°, N1-Fe-N2 = 75.3°, N1-Fe-N3 = 145.6°, N2-Fe-N3 = 75	118
Figure 5.4. Frozen-toluene EPR spectrum of complex 4.3b in red showing simulated spectrum in blue with the parameters given in the text	119
Figure 5.5. Mössbauer spectrum of 5.3b.....	120
Figure 5.6. Variable temperature magnetic susceptibility (χ^*T) data for complex 3b obtained in the solid state using a SQUID magnetometer operating at 1.00 Tesla	

from 5 K to 300 K. The line was a result from a fit to the data to give $g = 2.44$, $D = -21.65$ and $E/D = 0.2$	123
Figure 5.7. Mulliken spin densities (a.u.) for quartet 4.3b (left) and doublet 4.3b (right). M06-L electronic energies in kcal mol ⁻¹ . L = bis(imino)pyridine	124
Figure A. 1 DSC trace of a 3.9 homopolymerization catalyzed by 3.1.	161
Figure A. 2 TGA trace of a 3.9 homopolymerization catalyzed by 3.1.	161
Figure A. 3 DSC trace of a 3.9 homopolymerization catalyzed by 3.2.	162
Figure A. 4 TGA trace of 3.9 homopolymerization catalyzed by 3.2.	162
Figure A. 5 DSC trace of a 3.9:lactide (9:1) copolymerization before oxidation.	163
Figure A. 6 TGA trace of a 3.9:lactide (9:1) copolymerization before oxidation.	163
Figure A. 7 DSC trace of a 3.9:lactide (3:1) copolymerization before oxidation.	164
Figure A. 8 TGA trace of a 3.9:lactide (3:1) copolymerization before oxidation.	164
Figure A. 9. DSC trace of a 3.9:lactide (1:1) copolymerization before oxidation.	165
Figure A. 10 TGA trace of a 3.9:lactide (1:1) copolymerization before oxidation.	165
Figure A. 11 DSC trace of a 3.9:lactide (1:3) copolymerization before oxidation.	166
Figure A. 12 TGA trace of a 3.9:lactide (1:3) copolymerization before oxidation.	166
Figure A. 13 DSC trace of a 3.9:lactide (1:9) copolymerization before oxidation.	167
Figure A. 14 TGA trace of a 3.9:lactide (1:9) copolymerization before oxidation.	167
Figure A. 15 DSC trace of a 3.9 homopolymerization.	168
Figure A. 16 TGA trace of a 6 homopolymerization after the iron(II) to iron(III) switch.	168
Figure A. 17 DSC trace of a 3.9 homopolymerization obtained after the iron(III) to iron(II) switch.	169

Figure A. 18 TGA trace of a 3.9 homopolymerization obtained after the iron(III) to iron(II) switch.	169
Figure A. 19 DSC trace of a 3.9:lactide (9:1) copolymerization after oxidation.....	170
Figure A. 20 TGA trace of a 3.9 lactide (9:1) copolymerization after oxidation.	170
Figure A. 21 DSC trace of a 3.9:lactide (3:1) copolymerization after oxidation.....	171
Figure A. 22 TGA trace of a 3.9:lactide (3:1) copolymerization after oxidation.	171
Figure A. 23 DSC trace of a 3.9:lactide (1:1) copolymerization after oxidation.....	172
Figure A. 24 TGA trace of a 6:lactide (1:1) copolymerization after oxidation.	172
Figure A. 25 DSC trace of a 3.9:lactide (1:3) copolymerization after oxidation.....	173
Figure A. 26TGA trace of a 6:lactide (1:3) copolymerization after oxidation.	173
Figure A. 27 DSC trace of a 3.9:lactide (1:9) copolymerization after oxidation.....	174
Figure A. 28 TGA trace of a 3.9:lactide (1:9) copolymerization after oxidation.	174
Figure B. 1 ¹ H NMR (600 MHz) of 3.8 CDCl ₃	175
Figure B. 2 ¹³ C NMR(600 MHz) of 3.8 CDCl ₃	175
Figure B. 3 ¹ H NMR (600 MHz) of 3.9 CDCl ₃	176
Figure B. 4 ¹³ C NMR(600 MHz) of 3.9 CDCl ₃	176
Figure B. 5 ¹ H-NMR (500MHz) of 4.2 in CD ₂ Cl ₂	177
Figure B. 6 ¹ H-NMR (500MHz) of 4.2b in CD ₂ Cl ₂	177
Figure B. 7 ¹ H-NMR (500MHz) of 4.2c in CD ₂ Cl ₂	178
Figure B. 8 ¹ H-NMR (500MHz) of 4.2d in CD ₂ Cl ₂	178
Figure B. 9 ¹ H-NMR (500MHz) of 4.2e in CD ₂ Cl ₂	179
Figure B. 10 ¹ H-NMR (500MHz) of 4.2f in CD ₂ Cl ₂	179
Figure B. 11 ¹ H-NMR (500MHz) of 4.2g in CD ₂ Cl ₂	180

Figure B. 12 $^1\text{H-NMR}$ (500MHz) of 4.2h in CD_2Cl_2	180
Figure B. 13 $^1\text{H-NMR}$ (500MHz) of 4.2i in CD_2Cl_2	181
Figure B. 14 $^1\text{H-NMR}$ (500MHz) of 4.3 in CD_2Cl_2	181

List of Schemes

Scheme 1.1. Tuning of ROMP catalysts through redox of ferrocene-based ligand	3
Scheme 1.2. Mechanism of reversible ROMP by the use of a pyrilium-based catalyst	4
Scheme 1.3. <i>e</i> ATRP of methacrylate by use of a copper-TREN catalyst (M= monomer, P = polymer) ³⁰	5
Scheme 1.4. Switchable RAFT of methyl methacrylate by the use of NAD coenzyme	6
Scheme 1.5 Photo-redox switchable ATRP 1.4* is active for polymerization ³¹	6
Scheme 1.6. The simplified mechanism for redox-controlled cationic polymerization and subsequent block copolymerization ³³	7
Scheme 1.7. Redox-moderated olefin polymerization catalysts.....	8
Scheme 1.8. Reversible activation/inactivation of a titanium alkoxide ROP catalyst ²⁴	9
Scheme 1.9. Y and In-based redox-switchable polymerizations of lactide and trimethylene carbonate.....	10
Scheme 1.10. Redox-switchable copolymerization of L-lactide and caprolactone	11
Scheme 1.11. Redox-switchable lactide polymerization using cerium catalysts.....	12
Scheme 1.12. Redox-switchable copolymerization of lactide and epoxides by use of iron-based catalysts.....	13
Scheme 1.13. Electrochemically switchable copolymerization of lactide and cyclohexene oxide.....	15
Scheme 2.1. Orthogonal reactivity of cyclic diester and epoxide monomers.....	25
Scheme 3.1. Redox-triggered crosslinking.....	52
Scheme 3.2. Synthesis of cyclic diester 3.9	53
Scheme 3.3. Synthesis and copolymerization of 3.5-sat. with lactide.....	62

Scheme 3.4. Mechanistic hypothesis to explain why copolymerizations of lactide and 3.9 results in lower molecular weight and more polydisperse polymer compared to homopolymerization reactions. Intermediates such as 3.10 and 3.11 sequester the catalyst in unreactive states so that insertions of 3.9 are slower and monomer insertions after incorporating 3.9 (<i>k</i> _{obs'}) are slower than monomer insertions after incorporating lactide (<i>k</i> _{obs}).....	63
Scheme 3.5. a) Targeted monomer 3.12. b) Reaction of 3.1 with cyclohexene oxide in the presence of oxygen	66
Scheme 4.1. Reversible reduction and oxidation of 4.1 and 4.1-red	84
Scheme 4.2. Different epoxide ring-opening polymerization mechanisms.....	86
Scheme 4.3. Proposed mechanism for iron complex catalyzed epoxide polymerization	101
Scheme 5.1 Synthesis of iron mono(alkoxide) complexes 5.3	117
Scheme 5.2. Some copolymerization reactions catalyzed by 5.3b	134
Scheme 5.3. Proposed explanation for the chemoselectivity observed in copolymerization reactions involving (<i>rac</i>)-lactide and ϵ -caprolactone	136

Acknowledgements

I would like to thank everyone who enabled the completion of my Ph.D. at Boston College. Firstly, I would like to express my gratitude and appreciation for my thesis advisor Prof. Jeffery Byers for his guidance throughout my doctoral research. Over the years, Jeff has taught me to be a careful and rigorous chemist and has even managed to instill in me a deep love of kinetics.

I would like to thank the faculty and staff at the Boston College Chemistry Department. In particular Dale, Ian, and Lynne in the main office for always being available and willing to answer any question I could imagine. Additionally, a lot of the data shown in Chapter four would not have been collected without TJ and Jing teaching and allowing me to run low temperature NMR experiments.

None of the work in this dissertation would have been possible without the help of my fellow Byers Lab members (past and present) and collaborators. I was given the great privilege of collaborating with students in the Betley Lab (Matt Wilding and Diana Iovan), Swager Lab (Lionel Moh), and Cramer Lab (Büsra Dereli and Manuel Ortuño). Within the group, I have worked closely on projects with Ashley Biernesser, Lauren Yablon, Julia Curley, Miao Qi, and Alex Sudyn and appreciate all of the time and effort they have put into the research in these chapters. I would also like to acknowledge Miao Qi, Julia Curley, Stella Gonsales, Michael Crockett, Alex Sudyn, Alex Wong, and Emma Edelstein for their friendship, without which coming to lab everyday would not have been nearly as enjoyable (and my crossword puzzles far less complete). Specifically, I feel a heartfelt gratitude for my close friend and superb mentor Ashley Biernesser who has been

a remarkable friend, colleague/co-author, and fundamental source of support in all aspects of my life.

Lastly, I am overwhelmed with gratitude for the support, love, and encouragement my family has given me throughout every phase of my education. I am so grateful to both of my parents, my father for cultivating a love and respect for learning from a very young age and my mother for being an excellent example of an assertive and perseverant woman in the workplace. I had the immense pleasure of living with my sister, Krystal for most of my doctoral work and am so thankful that she was always there to help me decompress after a rough day in lab. Her mental and emotional support throughout my entire life has given me the strength and confidence to pursue any goal.

Chapter 1 Redox-Switchable Polymerization

1.1 Introduction

Primary structure (i.e. sequence and microstructure) are linked to macroscopic polymer properties.¹⁻⁶ This relationship has led to the necessary development of highly controllable polymerization reactions that result in fine control over composition and sequence. The advent of living polymerization reactions has provided a means to target such well-defined materials.^{4,7} Until recently, the best way to tune sequence of living polymerizations was through manipulations involving precise and ordered additions of different monomers as well as exploiting previously determined reactivity ratios, which describe the relative rates of insertions of various monomers in a copolymerization reaction.^{7,8} This approach becomes unfeasible as the complexity of the desired polymer increases due to the need for previous monomers to either be entirely consumed or have comparable reactivity ratios.

A unique opportunity to improve the limitations of the systems as mentioned above involves the growing field of switchable polymerization.^{9,10} Here, the chemical reactivity of a polymerization catalyst is selectively toggled between multiple states that are active or inactive towards different polymerization reactions with external stimuli. Switchable polymerizations are present in the literature for the on/off switch of several monomers for a variety of polymerization types and stimuli, including ring-opening metathesis polymerizations,¹¹⁻¹³ radical polymerizations,¹⁴⁻¹⁶ coordination-insertions olefin polymerizations,^{17,18} and ring-opening polymerizations.¹⁹⁻²⁴ However, this technique has more recently been used to chemoselectively discriminate between

different pools of monomers to afford new classes of polymeric materials with highly complex structures.

Due to the ubiquity of metal complexes for many different types of polymerization and their low redox potentials, an attractive stimulus for switchable polymerization is redox control. Through relatively low redox potentials, the oxidation/reduction of transition metal complexes is an accessible way to influence the polymerization activity of catalysts. Changing the oxidation state of the metal complexes can be done using chemical oxidants, photochemical oxidants, or even electrochemistry, the latter of which offers the advantage of being highly programmable.

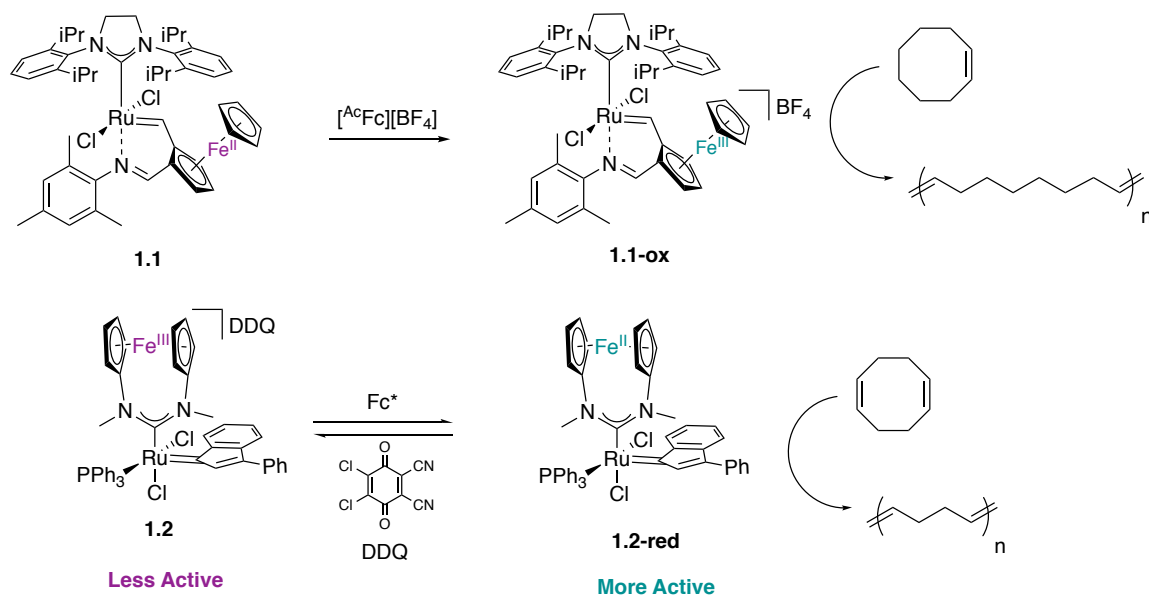
1.2 Ring-Opening Metathesis Polymerization (ROMP)

ROMP is a powerful and diverse strategy for the controlled synthesis of polymers from cyclic olefins. This method had already afforded unique polymer architectures accessible through the sequential addition of different monomers such as gradient copolymers.^{25,26} Moreover, ROMP is highly accessible due to a variety of commercially available catalysts and a broad monomer scope.

In 2013, Plenio et al. reported a triggered ROMP that modulated a latent ferrocene group appended to the alkylidene ligand of a catalyst inspired by the Hoveyda modification to Grubbs' 2nd generation ruthenium-based catalyst (Scheme 1.1, **1.1**).²¹ Upon oxidation, the decreased electron donating capability of the N-heterocyclic carbene ligand promoted ligand dissociation necessary for the initiation of the catalyst towards cyclooctene polymerization.²⁷ Notably, there was no report of the subsequent reduction of the complex. Later that same year, Bielawski and coworkers reported a ROMP catalyst that incorporated the ferrocene unit into the N-heterocyclic carbene (NHC) ligand that is

common to many commercially available olefin metathesis catalysts.²⁸ When the ligand was oxidized (Scheme 1.1, **1.2**) it was far less active towards the polymerization of cyclooctadiene, and in the reduced state (**1.2-red**) it was highly active towards the polymerization. This switch used 2,3-dichloro-5,6-cyano-1,4-benzoquinone (DDQ) and decamethylferrocene (Fc*) to oxidize and reduce the complexes, respectively (Scheme 1.1).

Scheme 1.1. Tuning of ROMP catalysts through redox of ferrocene-based ligand

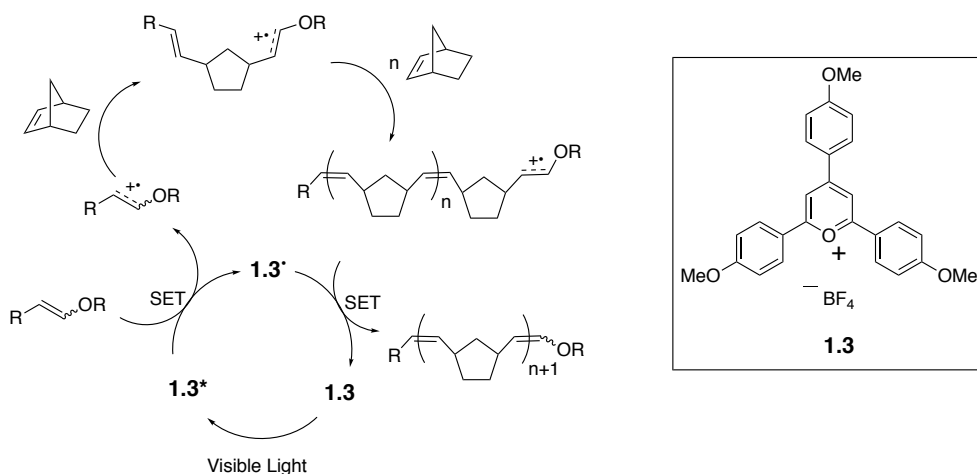


The relative rates of the complexes were $k_{\text{red}}/k_{\text{ox}} = 37.5$, which is not a chemoselective switch. Since the oxidation and reduction were reversible, an "on/off/on" experiment could be carried out starting with the reduced species as the catalysts until about 25% conversion was achieved. Upon addition of DDQ, the conversion was attenuated, and subsequently, when Fc* was added, conversion continued but only at about 30% of the initial rate which suggests some catalyst decomposition may have occurred.²⁸

This same group also reported a similar system based on oxidation and reduction of the commercially available Grubbs second-generation complex.²⁹ In this example, oxidation of the catalyst leads to insolubility of the catalyst and subsequent attenuation of polymerization activity. Here, $k_{\text{red}}/k_{\text{ox}} = 80$, an improvement on the previous system. However, after the on/off/on switch, ROMP proceeded with only ~25% of initial activity but was able to access multiple switches. The on/off switch in this system was attributed to the solubility change of the catalyst in this system as opposed to the direct electronic attenuation of the catalyst.

More recently, Boydston and co-workers developed a switchable metal-free ROMP system (Scheme 1.2).¹¹ The metal-free system used the photoexcitation of a pyrilium catalyst (**1.3**) to oxidize an electron-rich vinyl ether. The cationic intermediate formed was then able to activate norbornene towards ROMP. A single-electron transfer then allowed for the reversible reduction of the cationic propagating chain end. Multiple switches were possible without loss of activity, and in the absence of light, no polymerization was observed giving a truly “off” state, leading to excellent temporal control over the growth of the polymer.

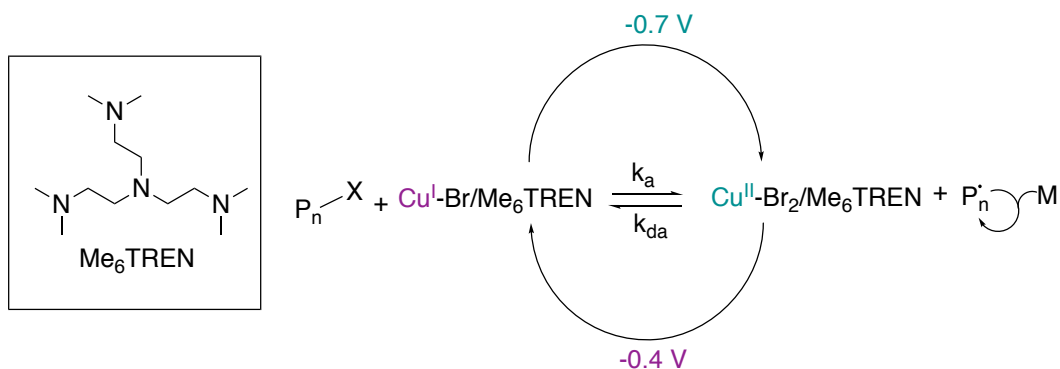
Scheme 1.2. Mechanism of reversible ROMP by the use of a pyrilium-based catalyst



1.3 Radical and Cationic Polymerizations

Radical-mediated polymerizations have utilized redox switches to modulate reactivity. Useful methods include atom transfer radical polymerization (ATRP) and reversible addition-fragmentation chain transfer (RAFT) systems. In 2011, Matyjaszewski expanded the use of their powerful ATRP system to incorporate an electrochemical on/off switch, aptly named eATRP.^{14,30} ATRP is controlled by an equilibrium between an active propagating species and dormant polymer chains (k_a/k_{da}). The electrochemically switchable ATRP was achieved using a $\text{Cu}^{\text{II}}\text{Br}_2/\text{Me}_6\text{TREN}$ catalyst and ethyl-2-bromopropionate as an initiator (Scheme 1.3).

Scheme 1.3. eATRP of methacrylate by use of a copper-TREN catalyst (M= monomer, P = polymer)³⁰

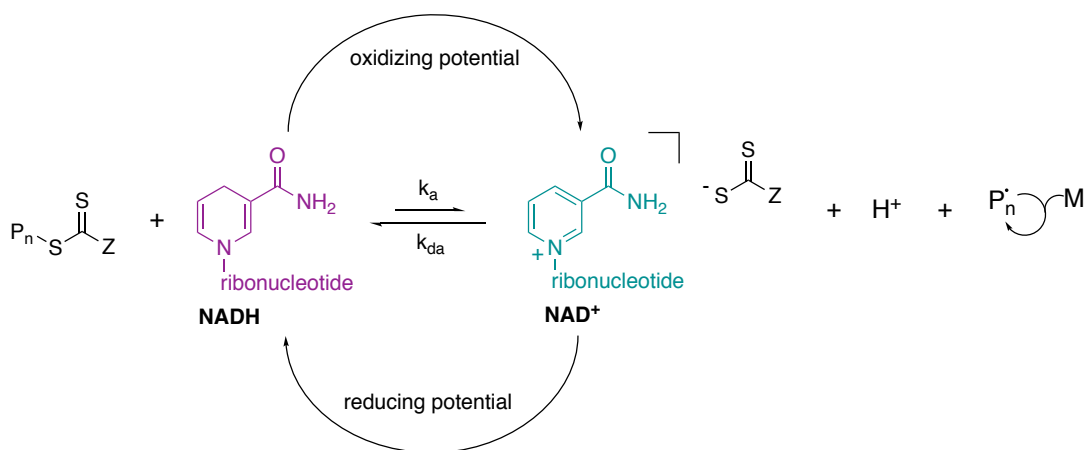


eATRP is capable of multiple switches and produces very well defined polymers with narrow dispersities. Importantly, the switch here does not directly change the catalyst but influences the already present equilibrium between the active state and inactive state, copper(II) vs. copper(I) respectively. Because of the pre-existing equilibrium, continuous application of current is required which may complicate automated setups.

In 2017, Yan et al. extended this strategy to a reversible addition-fragmentation chain transfer (RAFT) polymerization using a coenzyme (nicotinamide adenine

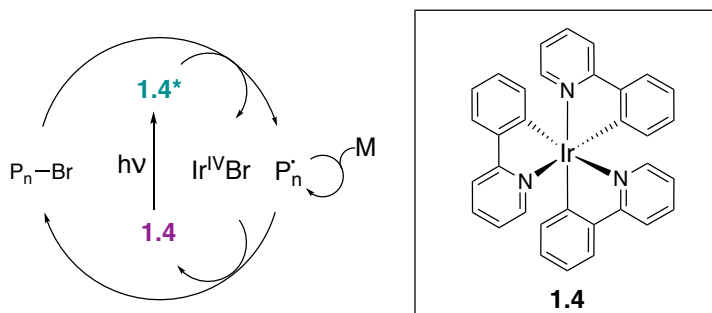
dinucleotide: NAD^+) catalyst (Scheme 1.4, NAD^+).¹⁶ One advantage of this system is that it does not rely on metal catalysts but organic coenzymes. This system is amenable to less activated RAFT monomers such as styrene.

Scheme 1.4. Switchable RAFT of methyl methacrylate by the use of NAD coenzyme



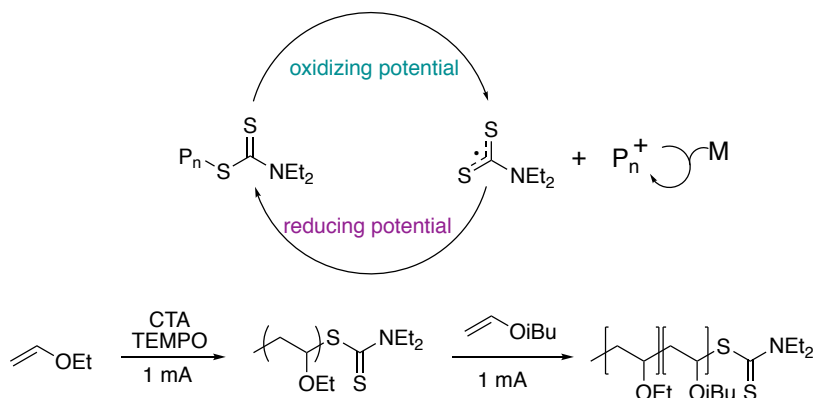
In 2012, Hawker and Fors published a photoredox controlled ATRP (Scheme 1.5).³¹ Here, an iridium-based photocatalyst is used to generate the radical necessary to initiate ATRP of acrylates. The polymerization was well controlled with narrow dispersities (<1.25) and good agreement between theoretical and experimental molecular weight. In the absence of light, no conversion was observed, allowing for multiple switches. Photo-redox polymerizations have been utilized for patterning of devices through the use of photomasks.³²

Scheme 1.5 Photo-redox switchable ATRP 1.4* is active for polymerization³¹



In 2018, Fors and co-workers extended this method to include an electrochemically controlled cationic RAFT polymerization (Scheme 1.6).³³ Here, an oxidizing potential activates the dithiocarbamate chain transfer agent (CTA) to form a radical cation capable of performing the polymerization of vinyl ethers. Subsequent application of a reducing potential re-caps the chain end of the polymer. Due to the complication of the polymer being deposited onto the electrode, TEMPO was added as a radical mediator to give homogenous oxidation of the CTA. With this system in hand, Fors and co-workers were able to polymerize a variety of activated and less activated vinyl ethers and even some less activated monomers like *para*-methoxy styrene. Because of the very high chain end fidelity of the system, block copolymers were easily accessed through sequential addition and multiple switching. However, the Fors system does require continuous application of current.

Scheme 1.6. The simplified mechanism for redox-controlled cationic polymerization and subsequent block copolymerization³³



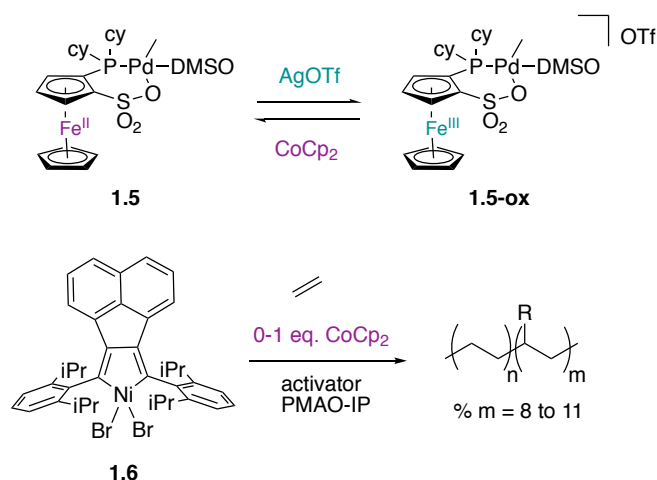
1.4 Coordination-Insertion Olefin Polymerization

In comparison to radical mediated polymerizations, redox-controlled polymerization of small olefins is logistically more difficult to carry out due to gaseous monomers and continuous feeding of monomers.⁹ Additionally, olefin polymerizations

often require high pressures, complicating the *in situ* addition of redox reagents. Lastly, olefin polymerizations often require methylaluminoxane as a cocatalyst, which can reduce in situ oxidized complexes. In 2015, Chen and co-workers developed a redox-controlled polymerization that did not need any cocatalyst.¹⁷ With a phosphine-sulfonate palladium-based catalyst (**1.5**) they were able to modulate olefin polymerization activity with oxidation of the ferrocene moiety installed on **1.5** (Scheme 1.7). They observed that **1.5** was four to six times more active towards ethylene polymerization than the oxidized **1.5-ox**.

Additionally, **1.5** produced poly(ethylene) of higher molecular weights. Similar activities were seen for the copolymerization of ethylene and methyl acrylate. **1.5-ox** led to less methyl acrylate incorporation in these copolymerizations. These catalysts showed the opposite reactivity towards norbornene oligomerization, the reduced **1.5** was inactive, and the oxidized **1.5-ox** was active.

Scheme 1.7. Redox-moderated olefin polymerization catalysts



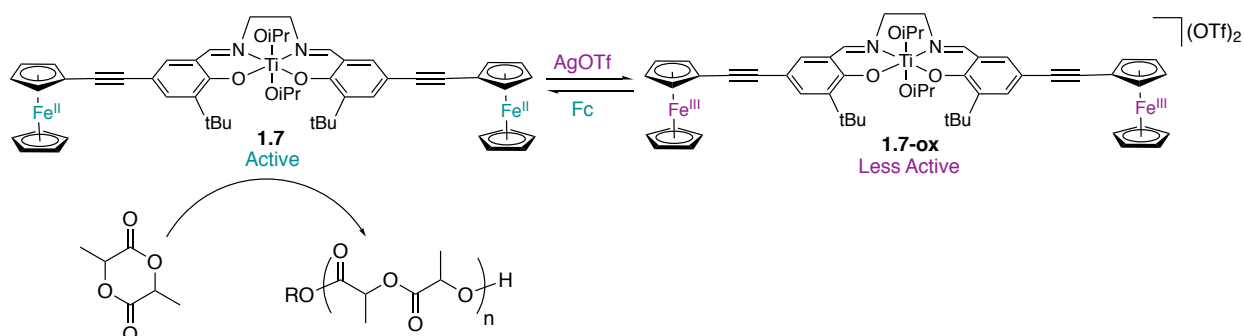
In 2016, Long and co-workers reported that a partial or full reduction of a nickel diimine catalyst (**1.6**) could be used to modulate branching density in ethylene polymerization.¹⁸ Increasing the amount of cobaltocene reductant resulted in a decrease

in branching density from 11% to 8% (Scheme 1.7). Importantly, they were able to isolate high molecular weight poly(ethylene) from these polymerizations, but the redox reaction was not reversible.

1.5 Ring-Opening Polymerization

Switchable polymerization has been extended to ring-opening polymerization, which often forms degradable polyesters. Gibson and Long reported the earliest example of a redox-controlled ring-opening polymerization in 2006.²⁴ They incorporated a ferrocene unit onto a salen-type ligand of a titanium alkoxide complex (Scheme 1.8, **1.7**).

Scheme 1.8. Reversible activation/inactivation of a titanium alkoxide ROP catalyst²⁴

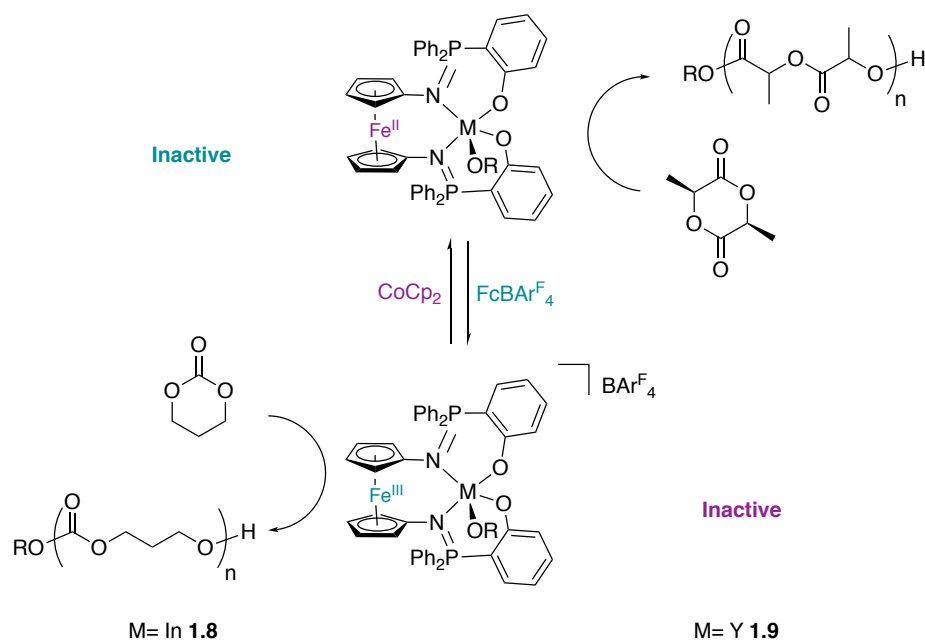


The fully oxidized Fe^{III} (**1.7-ox**) was less active towards the ROP of lactide, but the reduced **1.7** form was active at 70 °C. *In situ* oxidation of the catalyst decreased the electron density at the titanium center, which hindered the polymerization ($k_{\text{red}}/k_{\text{ox}} \sim 30$). In contrast, *in situ* reduction of the ferrocene unit resulted in complete reactivation of the complex for the ring-opening polymerization of lactide. This system produced polymers with narrow dispersities ($M_w/M_n < 1.2$) and remained narrow even after multiple redox-switching events.

In 2011, Diaconescu and coworkers reported a similar system with a remote ferrocene unit that regulated polymerization activity for different cyclic monomers

(Scheme 1.9).³⁴ They incorporated a ferrocene-appended phosphine Schiff base ligand onto both indium (**1.8**) and yttrium (**1.9**) alkoxide complexes. The yttrium-based catalyst was active for the ROP of L-lactide in the reduced state and could be turned “off” by the oxidation of the ferrocene unit to give an inactive catalyst. Importantly, the system could be switched multiple times without suffering a loss in activity when it was in the “on” state. Well-defined molecular weight polymers were obtained from these experiments with narrow dispersities (1.03-1.07). The catalyst exhibited orthogonal reactivity for the polymerization of trimethylene carbonate with the indium-based catalysts (**1.8**), the oxidized catalyst was active, and the reduced catalyst was inactive for the polymerization. The authors reasoned that this switch in reactivity is due to a balance between monomer binding and the activation barrier for the nucleophilic attack of the bound alkoxide.

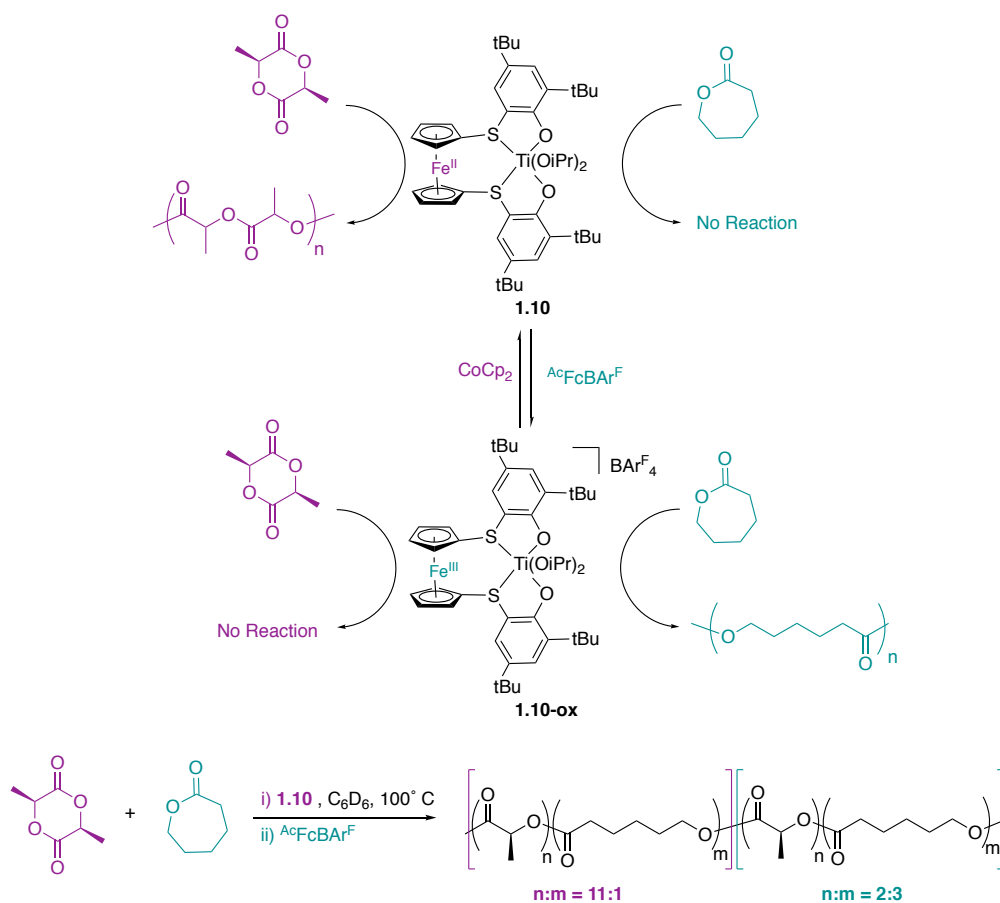
Scheme 1.9. Y and In-based redox-switchable polymerizations of lactide and trimethylene carbonate



In 2014, the Diaconescu group expanded the above system to include a series of zirconium and titanium-based catalysts with ferrocenyl substituents.³⁵ In the reduced

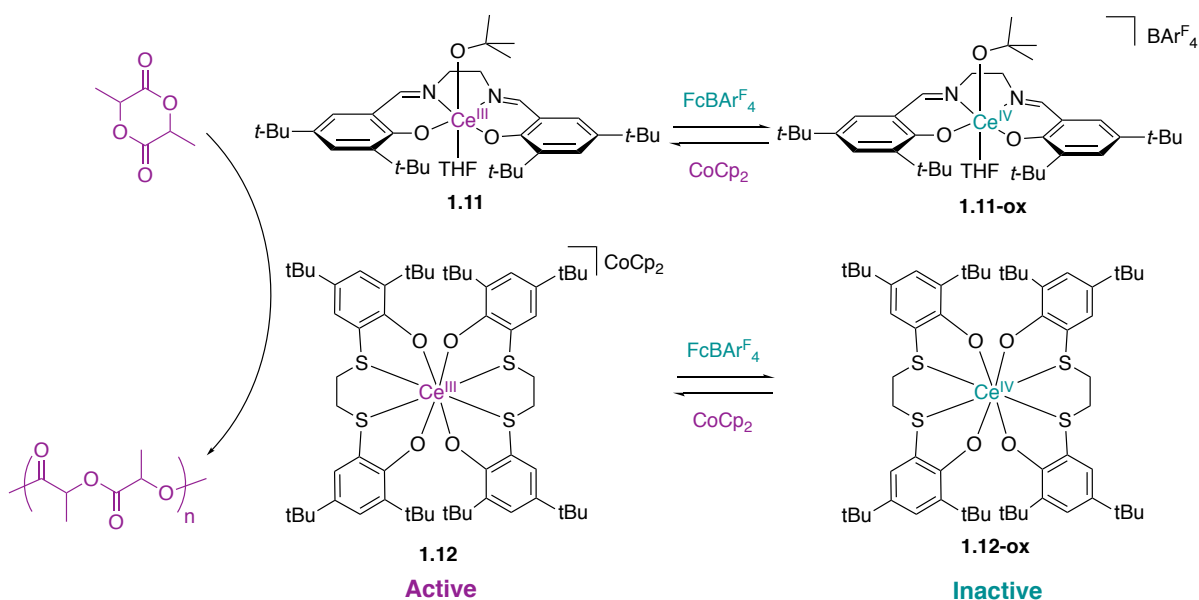
states, the Zr and Ti complexes were active towards the ROP of L-lactide at 100 °C but were inactive towards the homopolymerization of caprolactone. The opposite reactivity was observed when the complexes were oxidized (Scheme 1.10). The orthogonal reactivity enabled a one-pot synthesis of a polyester copolymer by use of the titanium-based catalyst (**1.10**). However, the fidelity of the switch was not maintained from the homopolymerization reactions to the copolymerization reaction. The “imperfect” switch led to the incorporation of the other monomer during switching, a drawback of this catalyst system.

Scheme 1.10. Redox-switchable copolymerization of L-lactide and caprolactone



Instead of remote oxidation of a moiety on the ligand, it was found that reactivity could be attenuated by the direct oxidation and reduction of the metal center of a ROP catalyst. In 2011, the Diaconescu group reported a cerium(III)salen alkoxide catalyst (**1.11**) that was capable of the ROP of lactide.³⁶ Oxidation of the complex led to the cationic cerium(IV) analogue (**1.11-ox**) that was inactive for lactide ROP (Scheme 1.11). Multiple switches were reported without significant losses in polymerization rate. However, slightly broad molecular weight distributions were observed (1.53-1.73). In 2013, Okuda and co-workers published a similar system using a cerium-OSSO catalyst (**1.12**).¹⁹ Notably, both catalysts were active in the Ce(III) state and inactive in the Ce(IV) state.

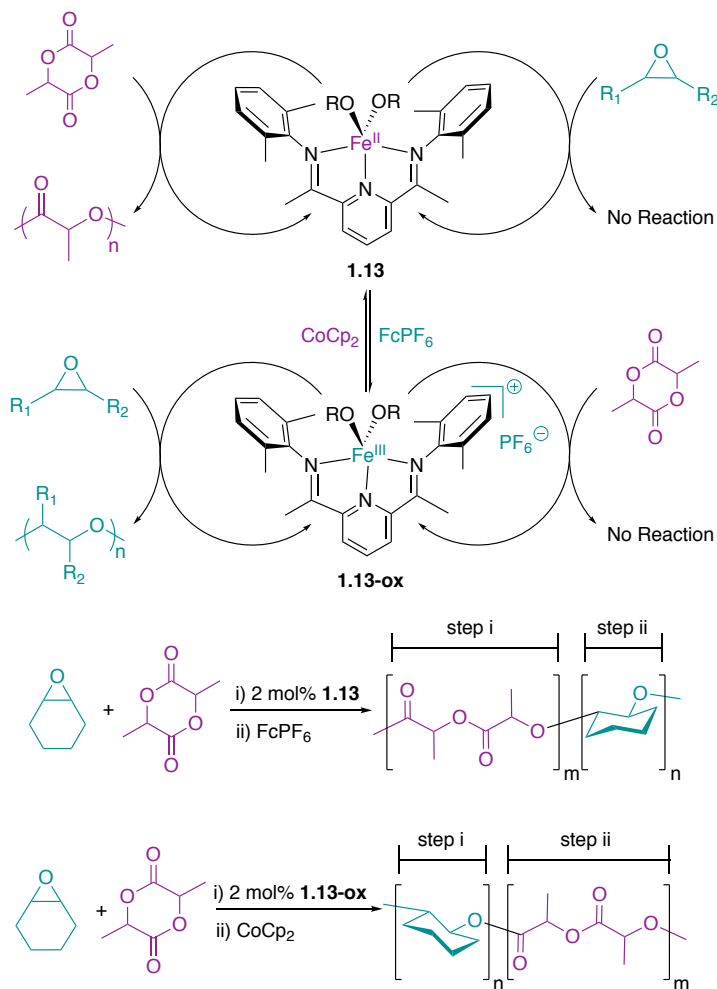
Scheme 1.11. Redox-switchable lactide polymerization using cerium catalysts



In 2013, the Byers group reported a redox-switchable bis(imino)pyridine iron bis(alkoxide) catalyst for the ROP of lactide.²³ The cerium-based system was highly robust and capable of multiple redox-switches with no loss in activity and marked the first example of a redox-switchable ring-opening polymerization reaction mediated by

iron that was both the site for redox activity and the site for the polymerization reaction. The same redox activity and site for polymerization proved to be valuable for the application of the catalyst for redox switchable copolymerization reactions. In 2016, the iron-catalyzed system was expanded to include a second monomer (epoxides) that displayed orthogonal reactivity.²² Lactide was readily polymerized by the formally Fe(II) complex (**1.13**) and inactive with the cationic, formally Fe(III) complex (**1.13-ox**). In contrast, epoxides showed complementary reactivity being active when the catalyst was in the iron(III) oxidation state and inactive when the catalyst was in the iron(II) oxidation state (Scheme 1.12).

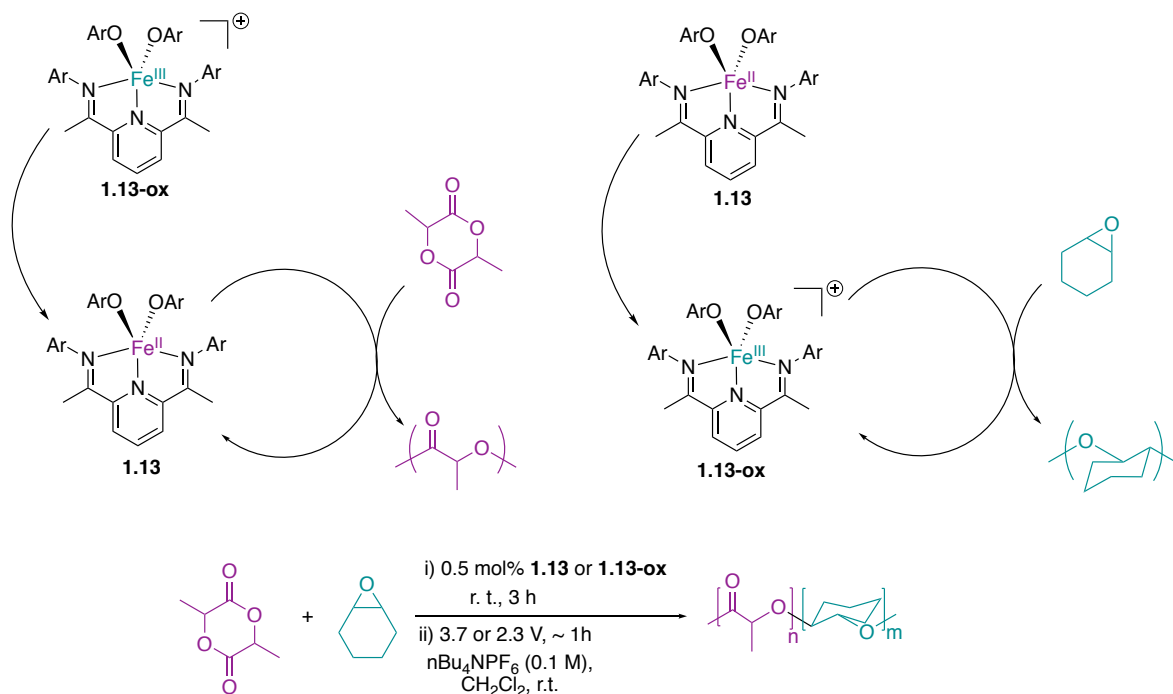
Scheme 1.12. Redox-switchable copolymerization of lactide and epoxides by use of iron-based catalysts



An advantage of the Byers system compared to the Diaconescu system was that the switch, in this case, was completely chemoselective. No conversion of either monomer was observed in each monomer's respective "off" state (e.g., Fe(III) for lactide and Fe(II) for epoxide). As seen in Scheme 1.12 the one-pot block copolymerization of cyclohexene oxide and *rac*-lactide could be carried out in both the Fe(II) to Fe(III) direction and the Fe(III) to Fe(II) direction. Both reactions afforded well-defined block copolymers where the oxidation state of the catalyst could control the sequence. Compared to the Diaconescu work, this reaction provided a copolymer that was made up of two characteristically distinct polymers, polyester and polyether. Considering the diverse physical and mechanical properties that can result from copolymers containing chemically distinct repeat units, the capability for sequence control to be dictated from the catalyst oxidation state holds excellent promise for the development of novel copolymeric structures that have unique and diverse properties. The Diaconescu group published a similar system in 2016.³⁷

Since the discovery of the iron-based catalyst, the Byers group reported the first example of an electrochemically controlled ROP.²⁰ Here, the same iron-based catalysts from above were regulated through the application of electrical current as opposed to the manual addition of solid redox reagents. This procedure produced a similarly chemoselective reaction for the polymerizations of lactide and epoxides that could also be used for the production of block copolymers (Scheme 1.13). Compared to chemical redox reagents, the electrochemical method has a distinct advantage in that it could be easily configured to automatic systems, high-pressure systems, and may be capable of producing more complex polymer architectures through fine regulation of the potential.

Scheme 1.13. Electrochemically switchable copolymerization of lactide and cyclohexene oxide



Conclusions

The field of redox-switchable polymerization has seen significant growth in the last two decades. The work described in this thesis has focused on the development of the redox-switchable copolymerization of lactide and epoxides and the study of the epoxide polymerization mechanism (Chapters 2 and 4 respectively). In the Byers lab, we have also developed a redox-triggered crosslinking polymerization that required the synthesis of a monomer with both cyclic diester and epoxide functionality (Chapter 3). Lastly, we have developed and characterized a family of formally iron(I) catalysts for use in various polymerization reactions (Chapter 5). The development of the systems mentioned above has led to the synthesis of a new diverse family of degradable polymers.

1.6 References

- (1) Seeberger, P. H. Automated Oligosaccharide Synthesis. *Chem. Soc. Rev.* **2008**, *37* (1), 19–28.
- (2) Ryu, D. Y.; Shin, K.; Drockenmuller, E.; Hawker, C. J.; Russell, T. P. A Generalized Approach to the Modification of Solid Surfaces. *Science (80-.)*. **2005**, *308* (5719), 236–239.
- (3) Malmström, E. E.; Hawker, C. J. Macromolecular Engineering via “Living” Free Radical Polymerizations. *Macromol. Chem. Phys.* **1998**, *199* (6), 923–935.
- (4) Matyjaszewski, K. Macromolecular Engineering by Controlled/living Ionic and Radical Polymerizations. *Macromol. Symp.* **2001**, *174* (1), 51–67.
- (5) Matyjaszewski, K. Macromolecular Engineering: From Rational Design through Precise Macromolecular Synthesis and Processing to Targeted Macroscopic Material Properties. *Prog. Polym. Sci.* **2005**, *30* (8–9), 858–875.
- (6) Lutz, J. F. A Controlled Sequence of Events. *Nat. Chem.* **2010**, *2* (2), 84–85.
- (7) Odian, G. *Principles of Polymerization*; John Wiley & Sons, Inc.: Hoboken, NJ, USA, 2004.
- (8) Carlotti, S.; Peruch, F. Cyclic Monomers: Epoxides, Lactide, Lactones, Lactams, Cyclic Silicon-Containing Monomers, Cyclic Carbonates, and Others. In *Anionic Polymerization: Principles, Practice, Strength, Consequences and Applications*; Springer Japan: Tokyo, 2015; pp 191–305.
- (9) Teator, A. J.; Lastovickova, D. N.; Bielawski, C. W. Switchable Polymerization Catalysts. *Chem. Rev.* **2016**, *116* (4), 1969–1992.

- (10) Lüning, U. Switchable Catalysis. *Angew. Chemie - Int. Ed.* **2012**, *51* (33), 8163–8165.
- (11) Ogawa, K. A.; Goetz, A. E.; Boydston, A. J. Metal-Free Ring-Opening Metathesis Polymerization. *J. Am. Chem. Soc.* **2015**, *137* (4), 1400–1403.
- (12) Varnado, C. D.; Rosen, E. L.; Collins, M. S.; Lynch, V. M.; Bielawski, C. W. Synthesis and Study of Olefin Metathesis Catalysts Supported by Redox-Switchable diaminocarbene[3]ferrocenophanes. *Dalt. Trans.* **2013**, *42* (36), 13251–13264.
- (13) Savka, R.; Foro, S.; Gallei, M.; Rehahn, M.; Plenio, H. Oxidation-Triggered Ring-Opening Metathesis Polymerization. *Chem. - A Eur. J.* **2013**, *19* (32), 10655–10662.
- (14) Chmielarz, P.; Fantin, M.; Park, S.; Isse, A. A.; Gennaro, A.; Magenau, A. J. D.; Sobkowiak, A.; Matyjaszewski, K. Electrochemically Mediated Atom Transfer Radical Polymerization (eATRP). *Prog. Polym. Sci.* **2017**, *69*, 47–78.
- (15) Chen, C. Redox-Controlled Polymerization and Copolymerization. *ACS Catal.* **2018**, *8*, 5506–5514.
- (16) Sang, W.; Xu, M.; Yan, Q. Coenzyme-Catalyzed Electro-RAFT Polymerization. *ACS Macro Lett.* **2017**, *6* (12), 1337–1341.
- (17) Chen, M.; Yang, B.; Chen, C. Redox-Controlled Olefin (Co)Polymerization Catalyzed by Ferrocene-Bridged Phosphine-Sulfonate Palladium Complexes. *Angew. Chemie - Int. Ed.* **2015**, *54* (51), 15520–15524.

- (18) Anderson, W. C.; Rhinehart, J. L.; Tennyson, A. G.; Long, B. K. Redox-Active Ligands: An Advanced Tool to Modulate Polyethylene Microstructure. *J. Am. Chem. Soc.* **2016**, *138* (3), 774–777.
- (19) Sauer, A.; Buffet, J. C.; Spaniol, T. P.; Nagae, H.; Mashima, K.; Okuda, J. Switching the Lactide Polymerization Activity of a Cerium Complex by Redox Reactions. *ChemCatChem* **2013**, *5* (5), 1088–1091.
- (20) Qi, M.; Dong, Q.; Wang, D.; Byers, J. A. Electrochemically Switchable Ring-Opening Polymerization of Lactide and Cyclohexene Oxide. *J. Am. Chem. Soc.* **2018**, *140* (17), 5686–5690.
- (22) Biernesser, A. B.; Chiaie, K. R. D.; Curley, J. B.; Byers, J. A. Block Copolymerization of Lactide and an Epoxide Facilitated by a Redox Switchable Iron-Based Catalyst. *Angew. Chemie - Int. Ed.* **2016**, *55* (17), 5251–5254.
- (23) Biernesser, A. B.; Li, B.; Byers, J. A. Redox-Controlled Polymerization of Lactide Catalyzed by Bis(imino)pyridine Iron Bis(alkoxide) Complexes. *J. Am. Chem. Soc.* **2013**, *135* (44), 16553–16560.
- (24) Gregson, C. K. A.; Gibson, V. C.; Long, N. J.; Marshall, E. L.; Oxford, P. J.; White, A. J. P. Redox Control within Single-Site Polymerization Catalysts. *J. Am. Chem. Soc.* **2006**, *128* (23), 7410–7411.
- (25) Bielawski, C. W.; Grubbs, R. H. Living Ring-Opening Metathesis Polymerization. *Prog. Polym. Sci.* **2007**, *32* (1), 1–29.
- (26) Breslow, D. S. Metathesis Polymerization. *Prog. Polym. Sci.* **1993**, *18* (6), 1141–1195.

- (27) Thiel, V.; Hendann, M.; Wannowius, K. J.; Plenio, H. On the Mechanism of the Initiation Reaction in Grubbs-Hoveyda Complexes. *J. Am. Chem. Soc.* **2012**, *134* (2), 1104–1114.
- (28) Arumugam, K.; Varnado, C. D.; Sproules, S.; Lynch, V. M.; Bielawski, C. W. Redox-Switchable Ring-Closing Metathesis: Catalyst Design, Synthesis, and Study. *Chem. - A Eur. J.* **2013**, *19* (33), 10866–10875.
- (29) Rosen, E. L.; Varnado, C. D.; Arumugam, K.; Bielawski, C. W. Metal-Centered Oxidations Facilitate the Removal of Ruthenium-Based Olefin Metathesis Catalysts. *J. Organomet. Chem.* **2013**, *745–746*, 201–205.
- (30) Magenau, A. J. D.; Strandwitz, N. C.; Gennaro, A.; Matyjaszewski, K. Electrochemically Mediated Atom Transfer Radical Polymerization. *Science* **2011**, *332* (6025), 81–84.
- (31) Fors, B. P.; Hawker, C. J. Control of a Living Radical Polymerization of Methacrylates by Light. *Angew. Chemie - Int. Ed.* **2012**, *51* (35), 8850–8853.
- (32) Corrigan, N.; Shanmugam, S.; Xu, J.; Boyer, C. Photocatalysis in Organic and Polymer Synthesis. *Chem. Soc. Rev* **2016**, *45*, 6165.
- (33) Peterson, B. M.; Lin, S.; Fors, B. P. Electrochemically Controlled Cationic Polymerization of Vinyl Ethers. *J. Am. Chem. Soc.* **2018**, *140* (6), 2076–2079.
- (34) Broderick, E. M.; Guo, N.; Vogel, C. S.; Xu, C.; Sutter, J.; Miller, J. T.; Meyer, K.; Mehrkhodavandi, P.; Diaconescu, P. L. Redox Control of a Ring-Opening Polymerization Catalyst. *J. Am. Chem. Soc.* **2011**, *133* (24), 9278–9281.
- (35) Wang, X.; Thevenon, A.; Brosmer, J. L.; Yu, I.; Khan, S. I.; Mehrkhodavandi, P.; Diaconescu, P. L. Redox Control of Group 4 Metal Ring-Opening Polymerization

- Activity toward L -Lactide and ϵ -Caprolactone. *J. Am. Chem. Soc.* **2014**, *136* (32), 11264–11267.
- (36) Broderick, E. M.; Guo, N.; Wu, T.; Vogel, C. S.; Xu, C.; Sutter, J.; Miller, J. T.; Meyer, K.; Cantat, T.; Diaconescu, P. L. Redox Control of a Polymerization Catalyst by Changing the Oxidation State of the Metal Center. *Chem. Commun.* **2011**, *47* (35), 9897–9899.
- (37) Quan, S. M.; Wang, X.; Zhang, R.; Diaconescu, P. L. Redox Switchable Copolymerization of Cyclic Esters and Epoxides by a Zirconium Complex. *Macromolecules* **2016**, *49* (18), 6768–6778.

Chapter 2. Block Copolymerization of Cyclic Diesters and Epoxides Catalyzed by Bis(imino)pyridine Iron Bis(alkoxide) Complexes

2.1 Introduction

Poly(lactic acid) (PLA) is a biodegradable and biocompatible material that has been used in the production of food packaging, textiles, fibers, and medical devices or implants.^{2,3} PLA is ideal for use in such materials because it can readily degrade in the environment to reduce unseemly and potentials environmentally damaging accumulation of plastic material. Moreover, it can be tailored to degrade at a certain pace within the body to transfer stress back to injured areas at a slow rate suitable for recovery which has made it a popular polymer in biomedical engineering. Unfortunately, PLA has some undesirable properties, such as, poor oxygen barrier, low glass transition temperature (T_g , and brittleness that have limited its use. Common strategies used to improve the mechanical properties of polymers are adding plasticizers or making blends of multiple polymers to create materials with hybrid properties.^{4,5} However, these have not been successful for improving the properties of PLA because the polylactide units are highly crystalline, and tend to form larger crystalline units quickly causing the polymer to phase separate from both plasticizers and blends. The phase separation leads to loss of the hybrid material properties. Some strategies to improve the PLA properties without phase separation are to synthesize stereoregular or cross-linked PLA or copolymers containing PLA.²

Copolymers are an attractive option because they not only improve the mechanical properties of some polymers but they show promise for tuning certain properties: rate of degradation, crystallinity, strength, toughness, etc.³ There are two main strategies for the synthesis of copolymers that contain poly(lactic acid): sequential or concurrent ring-opening polymerization of lactide with a suitable comonomer that is also capable of undergoing ring-opening polymerization⁴⁻¹⁴ or the use of hydroxyl end group-functionalized polymers that are used as macroinitiators for lactide polymerization.¹⁵⁻¹⁷

Several different comonomers have been used with lactide for the sequential or concurrent ring-opening polymerization reactions to produce copolymers that contain poly(lactic acid). Common comonomers include other cyclic esters,^{12,13,17} cyclic carbonates,¹⁸⁻²⁰ and epoxides.^{14,21-24}

The most commonly synthesized copolymer with lactide incorporates glycolide.⁶ Block and random copolymers that contain lactide and glycolide have been used extensively in active food packaging,²⁵ tissue engineering,²⁶ and drug delivery.²⁷⁻²⁹ Glycolide copolymers slightly increase the hydrophilicity of the polymer compared to poly(lactic acid)³⁰ and alter the lifetime of the materials.^{31,32} As the glycolic content increases, the polymer becomes more susceptible to degradation due to the absence of the backbone methyl group associated with the glycolide blocks. There are many synthetic protocols for the production of these polymers, including random lactide-glycolide copolymers.⁴⁻⁶ Glycolide often has a higher reactivity towards ROP than lactide meaning that it will easily form block copolymers. However, there are often high rates of transesterification, which can ultimately lead to more “random” sequences. Additionally, Hoye et al. have shown the ability to create a random copolymer by adding the glycolide

slowly over the course of the polymerization.⁵ Due to the insolubility of glycolide in many organic solvents, many of the copolymerization reactions are carried out in the melt. Tin octanoate [Sn(oct)₂] is commonly used as the catalyst although there are notable examples that use 1,8-diazabicyclo[5.4.0]-undec-7-ene(DBU),⁵ aluminum(III) isopropoxide [Al(Oi-Pr)₃],⁶ and zinc(II) lactate.⁴

Cyclic esters have been successfully employed as comonomers with lactide.^{7-14,18} Copolymers that incorporate lactide and caprolactone are common and well studied. Poly(caprolactone) is also biodegradable, and block copolymers containing caprolactone and lactide have been shown to exhibit improved thermal and mechanical properties, such as an increase in elongation at break from 5% to 90% compared to poly(*L*-lactic acid) (PLLA).^{9,33} Additionally, due to increased drug permeability these block copolymers are suitable for drug delivery and tissue regeneration applications.^{8,14,34} It should be noted that redox-controlled polymerization of ϵ -caprolactone and lactide has been explored by Diaconescu and coworkers.¹⁰

Another class of suitable comonomers for ring opening copolymerization with lactide is cyclic carbonates. The most common of these is 1,3-dioxan-2-one, which is more commonly known as trimethylene carbonate. Copolymers of lactide and trimethylene carbonate are commonly made by the copolymerization of both monomers using tin catalysts.^{11,14-15,18,34-36} Nevertheless, copolymers can also be made through the concurrent ring-opening copolymerization of lactide and trimethylene carbonate using Mg(OEt)₂/Ti(O^tBu)₄,¹⁵ (R)-2,2'-[1,1'-binaphthyl-2,2'-diylbis(nitrylomethylidene)]-diphenolate aluminum isopropoxide,¹⁹ and zirconium(IV) acetylacetonate as the catalysts.¹⁶ The blocky and statistical copolymers that result from such procedures have

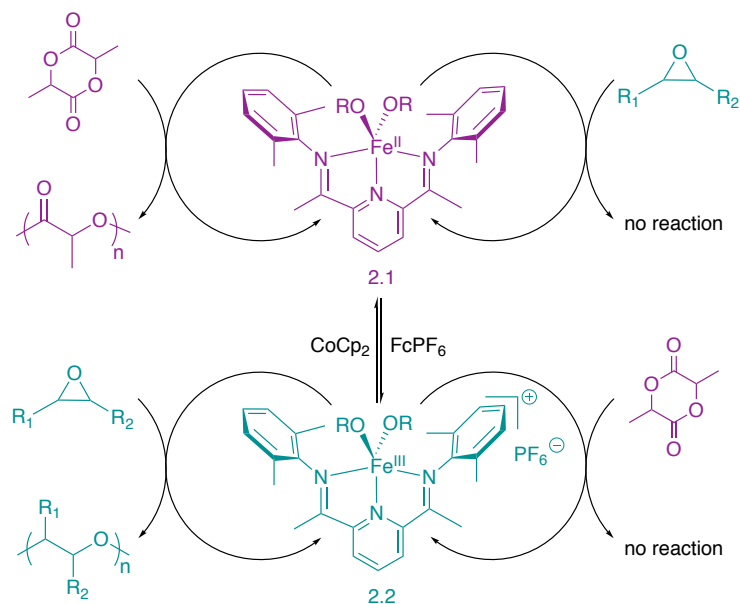
been developed for the controlled release of biologically active agents. Additionally, increasing the length of the trimethylene carbonate block can improve the mechanical properties of the polymer. Flexibility increases up to 210% have been observed.^{14,18,32, 36}

Many other less common comonomers have been polymerized with lactide. Bhowmick et al. have reported the synthesis of an ABA block copolymer containing δ -valerolactone and lactide through sequential ROP with Sn(oct)₂ as the catalyst.¹⁷ This polymer adopted a lamellar morphology and has been investigated for drug delivery. Cross et al. have synthesized both blocky and random copolymers of lactide and β -butyrolactone using aluminum salen and salan complexes.³⁸ In 2014, Hillmyer et al. reported the block copolymerization of lactide and β -methyl- δ -valerolactone to yield materials with tunable thermal and mechanical properties that resemble thermoplastic elastomers.³⁹ Interestingly, under certain conditions they observe the formation of a gradient copolymer with a narrow polydispersity.

In our recent work, we have targeted the formation of diblock copolymers of PLA and poly(cyclohexene oxide) using redox switchable polymerization with bis(imino)pyridine iron(II) bis(alkoxide) and the analogous cationic bis(imino)pyridine iron(III) bis(alkoxide) complexes.⁴⁰ We hypothesized that the different reactivity of iron(II) and iron(III) complexes would be amenable to developing a chemoselective block copolymerization with a second monomer that has orthogonal reactivity to lactide. In this way, we could synthesize a variety of microstructures from the same monomer feedstock by switching the oxidation state of the catalyst to dictate which monomer polymerizes. We discovered that epoxides have such reactivity and utilized the complementary reactivity of epoxides and lactide for the synthesis of block copolymers.

In these reactions, iron(II) serves as the active oxidation state for lactide polymerization, while iron(III) is the active oxidation state for epoxide polymerization (Scheme 2.1). This synthetic methodology provides rapid access to block copolymers that are promising candidates for drug delivery devices⁴¹ and as biodegradable thermoplastic elastomers.⁴²

Scheme 2.1. Orthogonal reactivity of cyclic diester and epoxide monomers

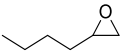


2.2 Epoxide homopolymerization

During preliminary investigations, we found that while the iron(II) alkoxide **2.1** is completely inactive for hexene oxide polymerization, exposing small amounts of the cationic iron(III) alkoxide **2.2** (0.2 mol%) to neat hexene oxide lead to polymer with a number average molecular weight of 6.5 kg/mol and a dispersity (M_w/M_n) of 2.0 after 24 hours (Table 2.1, entry 1). In addition to hexene oxide, iron(III) alkoxide **2.2** was a good catalyst to polymerize a variety of other epoxide monomers. Monosubstituted, 1,2-disubstituted (entry 4), and 1,1-disubstituted epoxides (entry 3) were competent substrates for the polymerization reaction although polymerization of isoprene oxide led to low yields of low molecular weight polymer (entry 3). Compared to the other

monomers examined, styrene oxide demonstrated broader dispersities as a consequence of a bimodal molecular weight distribution observed in the GPC trace (entry 5).

Table 2.1. Polymerization of epoxides catalyzed by **2.2**^a

	Epoxide	M_n^b	M_w/M_n	%Yield ^c
1		6.5	2.0	57
2		4.6	1.7	69
3		1.9	1.7	28
4		22.1	1.9	36
5		12.7/0.7 ^d	1.3/1.5	51
6 ^e		22.6	2.3	81

^aNeat epoxide with 0.2 mol% **2** for 24 h at 24 °C. ^bkg/mol; determined by GPC relative to polystyrene standards. ^cdetermined by mass. ^dbimodal distribution. ^eIn PhCl (2.1 M).

Iron(III) alkoxide **2.2** proved to be a particularly active catalyst for the polymerization of the highly strained cyclohexene oxide (CHO). Attempted polymerization of this substrate in neat epoxide resulted in a significant exotherm and the rapid formation of a viscous gel-like solution that could not be stirred. The use of solvent was required to mitigate the significant exotherm observed during neat epoxide polymerization reactions (entry 6). Importantly, when cyclohexene oxide was treated with the iron(II) complex **2.1**, no polymerization occurred.

2.3 Redox-Switchable Epoxide Polymerization

To combine the epoxide polymerization with the redox-switchable lactide polymerization, the *in situ* redox-switchable polymerizations of cyclohexene oxide was realized (Figure 2.1). A polymerization reaction of cyclohexene oxide in chlorobenzene was allowed to reach 40% conversion, at this time cobaltocene was added to reduce the cationic formally iron(III) complex to the inactive iron(II) state. After 40 minutes, no further conversion of cyclohexene oxide was observed. Ferrocenium hexafluorophosphate was added to re-oxidize the complex back to the original cationic iron(III) state. After oxidation, cyclohexene oxide proceeded at a similar rate to that before oxidation. The reaction stalled out around 60%. We have recently determined that this is due to some product inhibition and can be improved by using a more weakly coordinating anion. Further studies of the epoxide polymerization mechanism can be found in Chapter 5.

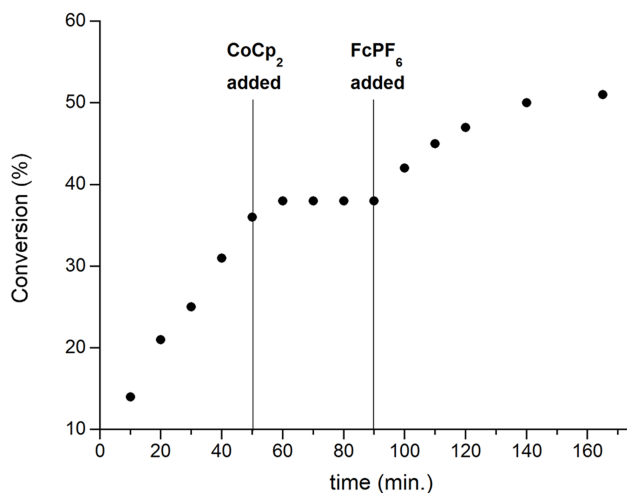


Figure 2.1. Redox-controlled polymerization of cyclohexene oxide in PhCl (0.91M with 2.2 (2.0 mol%))

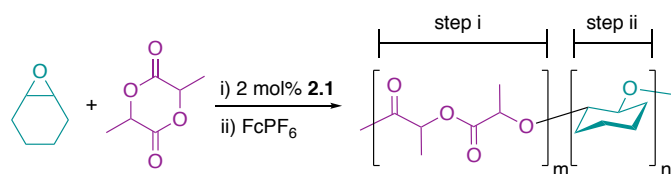
2.4 Redox-Switchable Block Copolymerization

To combine the redox-switchable polymerizations of epoxides and lactide, starting with the iron(II) alkoxide **2.1**, a 1:1 mixture of cyclohexene oxide and lactide in

chlorobenzene at room temperature lead to the clean polymerization of lactide without any incorporation of the cyclohexene oxide monomer. The chemoselectivity of the reaction was clear from the absence of polyether resonances in the ^1H NMR spectrum of the polymer. The molecular weight obtained from this reaction ($M_n = 11.9$ kg/mol) is identical to the molecular weight of poly(lactic acid) obtained in the absence of cyclohexene oxide in chlorobenzene. The only observable difference between this lactide polymerization reaction and a lactide polymerization reaction carried out without cyclohexene oxide was a slight decrease in reaction rate (40 min. vs. 20 min. to reach >95% conversion in the presence and absence of cyclohexene oxide, respectively), which likely arises from competitive binding of the epoxide and lactide to the Fe(II) catalyst. Although only poly(lactic acid) was observed when the catalyst was in the Fe(II) oxidation state, oxidation of the catalyst to Fe(III) led to clear evidence for the formation of poly(cyclohexene oxide) in the ^1H NMR spectrum. GPC analysis of the reaction mixture showed a broad dispersity ($M_w/M_n = 2.2$), leading us to surmise that the copolymer contained some polyether homopolymer.⁴³ The reaction mixture was precipitated into acetone to remove homopolyether side product, and the soluble material was then precipitated into hexanes to isolate the copolymer product. GPC analysis of isolated copolymer showed a single peak with a dispersity of 1.5; however, a decrease in molecular weight was observed from the first to the second step (entry 1, Table 2.2). The Diaconescu group has also observed this decrease in molecular weight in a similar system.⁴⁴ An increase in molecular weight of the copolymers may not be observed as expected because the M_n determined by refractive index detector is calibrated against polystyrene standards, and the correction factors for the formed copolymers are

unknown. GPC analysis was performed with a light scattering detector, which showed comparable values with the refractive index detector for polylactide, but largely different values for the polyether and copolymer products. By using the light scattering detector to characterize the molecular weight of the polymer, the isolated copolymer had $M_n = 37.5$ kg/mol, which is consistent with the formation of a diblock copolymer, showing an increase in M_n from the first step. Precipitation of the copolymer product resulted in a 70% yield, based on the mass of recovered polymer products (copolymer and homopolyether).

Table 2.2. Redox-controlled diblock copolymerization of lactide (L) and cyclohexene oxide (CHO)



	After step <i>i</i>				After step <i>ii</i> and precipitation ^a					
	M_n^b	M_w/M_n	% CHO ^c	% L ^c	M_n^b	M_w/M_n	% CHO ^c	% L ^c	m:n ^c	% Copolym. ^d
1	11.9	1.2	0	98	10.2 (37.5)	1.5	69	98	7:1	67
2 ^e	11.2 (12.1)	1.2	0	98	9.2 (27.2)	1.5	89	98	7:1	65
3 ^f	10.0	1.2	0	99	3.5 (20.1)	1.4	71	98	5:1	23
4 ^g	4.5	1.3	0	35	1.7 (27.0)	2.0	32	36	4:1	68

Reaction run at room temperature in chlorobenzene. ^aIsolated by precipitation from acetone and hexanes. ^bkg/mol, determined by GPC with RI detector relative to polystyrene standards; values in parentheses from LS detector. ^cpercent conversion determined by ¹H NMR. ^dpercent copolymer determined from mass of isolated copolymer/mass of total polymer. ^eEpoxide added in second step after oxidant. ^f[CHO]:[L] = 5:1 ([CHO] = 0.80M). ^gStep *i* carried out for 15 min.

Furthermore, the reaction was performed with each monomer sequentially, where the epoxide monomer wasn't introduced until after the completion of lactide polymerization and oxidation of the iron catalyst. Control experiments (entry 2, Table 2.2) showed that the FcPF₆ oxidant also polymerizes cyclohexene oxide on its own, although it results in slower reaction rates, lower polymer molecular weights and broader polydispersities (2.0 mol% FcPF₆ gives 25% conversion after 3 hrs., M_n = 4.7 kg/mol, PDI = 3.8) than complex **2.2**. In the one-pot reaction, it is assumed that the electron transfer of the oxidation reaction is much faster than initiation of polymerization by FcPF₆, although it is possible that a small amount of epoxide homopolymerization is initiated before the oxidation reaction is complete. By performing the block copolymerization with the sequential addition of monomers, the oxidation reaction takes place in the absence of epoxide monomer, such that the FcPF₆ should be consumed before cyclohexene oxide is added to the reaction. Polymers of similar molecular weights and composition to the one-pot reaction resulted (entry 2, Table 2.2), which shows that performing the reaction in one-pot has no detrimental effects due to homopolymerization initiation by FcPF₆ compared to adding monomers sequentially.

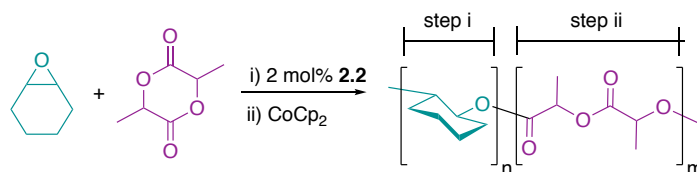
Varying the ratio of monomers used could alter the composition of the copolymers. When copolymerization was carried out with five equivalents of epoxide relative to lactide, slightly higher incorporation of epoxide into the copolymer was observed, however, a lower yield of copolymer was obtained due to the increased formation of homopolyether when the epoxide concentration is higher (entry 3, Table 2.2).

The switch in chemoselectivity observed by oxidizing the Fe(II) catalyst was further demonstrated by carrying out the lactide polymerization to partial completion prior to oxidation and subsequent epoxide polymerization (entry 4, Table 2.2). Analysis of the ^1H NMR spectrum of this reaction after oxidation of the catalyst resulted in the polymerization of cyclohexene oxide with no further incorporation of lactide monomer.

After promising results demonstrated that diblock copolymers could be synthesized by starting with lactide polymerization and switching to epoxide polymerization, the reverse order was then investigated starting with the iron(III) alkoxide complex **2.2** to initiate epoxide polymerization followed by reduction with cobaltocene to halt epoxide polymerization and trigger lactide polymerization. The epoxide polymer had $M_n = 1.2$ kg/mol and a dispersity of 1.9 (Table 2.3, entry 1) after reacting for 3 hours in the presence of lactide. Relatively low conversion of the cyclohexene oxide monomer was observed (22%) which may be due to inhibition by lactide through competitive binding, as described above. Although the somewhat broad dispersities observed in this reaction suggested that polymer termination may be occurring, attempts to form block copolymers were still made by exposing the reaction to cobaltocene to reduce the iron(III) epoxide polymerization catalyst to an iron(II) complex suitable for lactide polymerization. We were pleased to find that this procedure led to the rapid consumption of lactide without any further conversion of epoxide as indicated in the ^1H NMR spectrum of the reaction mixture. GPC analysis after copolymer precipitation showed one peak that underwent an increase in molecular weight according to both the refractive index and light scattering detectors and a decrease in molecular weight distribution when the cobaltocene reductant was added to the reaction ($M_n = 10.6$

kg/mol, $M_w/M_n = 1.4$). This observation was, once again, consistent with the production of a block copolymer, and the decrease in dispersity of the copolymer product may be due to the high percentage of narrow dispersity polylactide in the copolymer product. Isolation of the copolymer by precipitation resulted in 95% yield based on the mass of polymer products, and only a minimal amount of homopolyether was collected, showing that minimal termination is occurring in the first step. This mass recovery suggests that the broad dispersities observed in the epoxide polymerization are due to slow initiation rather than termination events (see more in Chapter 4).

Table 2.3. Redox-controlled diblock copolymerization of cyclohexene oxide (CHO) and lactide (L)



	After step <i>i</i>				After step <i>ii</i> and precipitation ^a					
	M_n^b	M_w/M_n	% CHO ^c	% L ^c	M_n^b	M_w/M_n	% CHO ^c	% L ^c	m:n ^c	% Copolym. ^d
1	1.2 (22.8)	1.9	22	0	10.6 (30.9)	1.4	22	97	9.0:1	95
2 ^e	7.4 (9.7)	1.8	42	0	12.5 (20.5)	1.4	42	98	9.0:1	84
3 ^f	1.2	2.0	50	0	5.8 (34.6)	1.4	51	99	3.3:1	53
4 ^{f,g}	2.2	2.4	21	0	11.6 (30.1)	1.4	22	98	3.2:1	48

^aIsolated by precipitation from acetone and hexanes. ^bkg/mol, determined by GPC with RI detector relative to polystyrene standards; values in parentheses from LS detector. ^cpercent conversion determined by ¹H NMR. ^dpercent copolymer determined from mass of isolated copolymer/mass of total polymer. ^eLactide added in the second step after reductant. ^f[CHO]:[L] = 5:1 ([CHO] = 0.80M). ^gStep *i* carried out for 30 min.

To reach higher conversion of the epoxide monomer, sequential polymerization of epoxide followed by lactide was performed (entry 2) and gave 42% conversion of epoxide in the first step. Sequential polymerization led to the formation of a polymer mixture that incorporated both monomers and had a similar GPC trace and NMR spectrum compared to reactions carried out with both monomers in solution. Higher epoxide conversions and increased epoxide content in the copolymer could also be achieved by performing the reaction with increased epoxide concentration, so that [CHO]:[L] was 5:1 (entry 3, Table 2.3). This reaction resulted in a diblock copolymer with [PLA]:[PCHO] = 3.3:1, however, a lower yield of the copolymer (53%) resulted due to increased formation of homopolyether at higher epoxide concentrations.

Although no further conversion of the epoxide was observed in the second step of these reactions while the catalyst is in the iron(II) oxidation state, we had previously observed that the epoxide polymerizations do not reach full conversion. Therefore to demonstrate the chemoselectivity of the iron catalyst in this polymerization, we studied diblock copolymerizations at the higher epoxide concentration ([CHO]:[L] = 5:1) in which the first step was performed for only 30 minutes, where only 21% conversion of CHO was observed compared to 51% after 3 hours (entry 4 vs. entry 3, Table 2.3). Full lactide conversion was observed, without any further conversion of the epoxide upon addition of the reducing reagent CoCp₂. This outcome demonstrates the redox control over the diblock copolymerization, showing that reducing the catalyst can halt epoxide conversion.

In addition to GPC and solubility, DOSY-NMR was used to distinguish the formation of block copolymer versus a blend of homopolymers. DOSY-NMR has been

shown to be an effective method for characterization of block copolymers, as it can be used to identify blends of polymers from observation of multiple diffusion coefficients. DOSY-NMR of the isolated block copolymers from a redox-switching reaction starting with lactide polymerization and followed by epoxide polymerization showed signals for the polylactide and polyether all at the same diffusion coefficient ($D = 9.5 \times 10^{-11} \text{ m}^2/\text{s}$). In contrast, DOSY-NMR of a mixture of homopolymers of similar molecular weight showed two distinct diffusion coefficients at 1.59 and $1.28 \times 10^{-10} \text{ m}^2/\text{s}$, that corresponded to NMR peaks of the polylactide and polyether, respectively (Figure 2.2). Block copolymers formed from the iron(III) to iron(II) copolymerization (epoxide polymerization followed by lactide polymerization) also showed signals at a single diffusion coefficient ($D = 1.06 \times 10^{-10} \text{ m}^2/\text{s}$), which supports that block copolymers are formed in this direction as well.

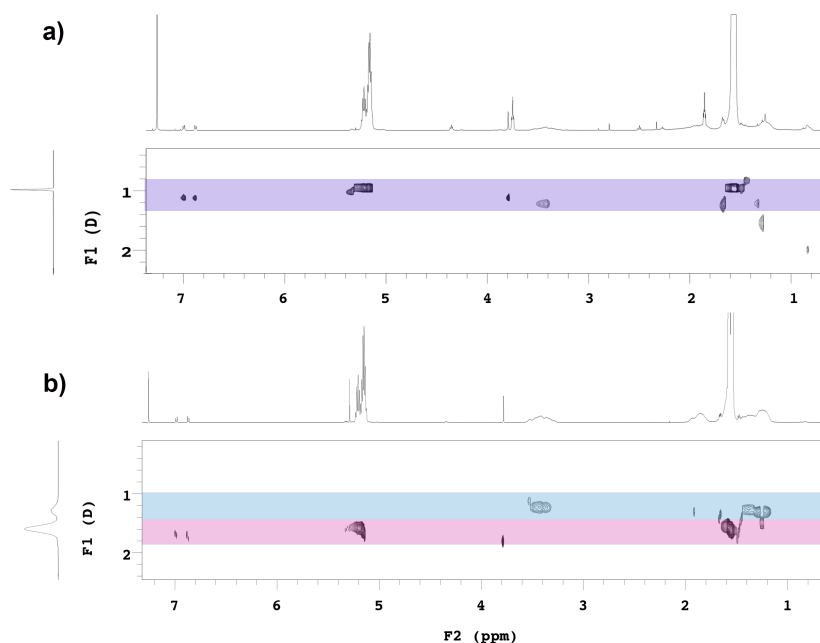


Figure 2.2. DOSY-NMR spectra of a) isolated block copolymer (**Table 2.2**, entry 1) and b) a mixture of polylactide and polyether homopolymers of similar molecular weight and [PLA]:[PCHO] ratio

2.5 Conclusions

Cationic, formally iron(III) bis(alkoxide) catalysts supported by bis(imino)pyridine ligands were found to be effective catalysts epoxide for polymerization. While complexes in the formally iron(III) oxidation state were active for epoxide polymerization, complexes in the formally iron(II) oxidation state were completely inactive. This trend is opposite to what was observed previously for lactide polymerization. To take advantage of the difference in chemoselectivity between Fe(II) and Fe(III) complexes, redox switchable block copolymerization reactions were carried out starting with both monomers present in solution. Diblock copolymers were formed starting with lactide or epoxide polymerization when either an Fe(II)–Fe(III) or Fe(III)–Fe(II) redox switch is employed, respectively. Remarkably, in both cases, incorporation of the lactide was not observed during epoxide polymerization and vice versa. In a previous report of redox-controlled block copolymerization of lactide and ϵ -caprolactone carried out by the Diaconescu group, the reaction was not wholly chemoselective. The resulting copolymer was more accurately described as poly[block(PLA-minor-PCL)-block(PCL-minor-PLA)].¹¹

This chapter demonstrates for the first time that changes in the oxidation state of a catalyst can lead to a complete change in chemoselectivity in a chemical reaction. The change in chemoselectivity was used for the synthesis of block copolymers, but the concept of redox-switchable catalysis can be extended to the synthesis of small molecules as well. In the future, we plan to improve the fidelity of the block copolymerization reaction through modifications to the bis(imino)pyridine ancillary ligand as well as through mechanistic studies. Finally, the versatility of iron as a catalyst for many

transformations opens the possibility to find alternative monomers that may be applied in redox-switchable copolymerization reactions or related copolymerization reactions.

2.6 Experimental

General Considerations. Unless stated otherwise, all reactions were carried out in oven-dried glassware in a nitrogen-filled glove box or with standard Schlenk line techniques. Solvents were used after passage through a solvent purification system under a blanket of argon and then degassed briefly by exposure to vacuum. Nuclear magnetic resonance (NMR) spectra were recorded at ambient temperature on Varian spectrometers operating at 400-600 MHz. Gel permeation chromatography (GPC) was performed on an Agilent GPC220 in THF at 40 °C with three PL gel columns (10 μ m) in series. Molecular weights and molecular weight distributions were determined from the signal response of the RI detector relative to polystyrene standards. Molecular weights were also determined with a light scattering detector for selected samples. Polymer products were separated with a Beckman Coulter J2-MC Centrifuge with Rotor 17.0 at 2500 RPM at 10 °C for 7.0 minutes. Spectra and GPC curves of polymers can be found in a previous thesis.⁴³

Lactide was obtained from Frinton Laboratories and was recrystallized from ethyl acetate followed by recrystallization from toluene and dried *in vacuo* prior to polymerization. Cyclohexene oxide was obtained from Sigma Aldrich and was dried over CaH₂ and distilled prior to polymerization. Chlorobenzene was obtained from Acros Organics and passed through silica prior to use. Other methods used to dry chlorobenzene led to irreproducible results in epoxide polymerization reactions. Complexes **2.1** and **2.2** were synthesized as described previously.⁴³

Generic procedure for the polymerization of epoxides with complex 2.2. In a glove box, iron(III) bis(alkoxide) complex **2.2** (0.0163 g, 0.0198 mmol) and epoxide (9.9 mmol) were added to a seven mL vial. The mixture was allowed to stir 24 hours at room temperature. Unreacted epoxide monomer was removed *in vacuo* and conversion was determined from the mass of the recovered polymer product. The reaction mixture was analyzed by GPC (RI) to determine the molecular weight and molecular weight distribution of the polymers.

Polymerization of cyclohexene oxide with complex 2.2. In a glove box, iron(III) bis(alkoxide) complex **2.2** (0.0163 g, 0.0198 mmol) in chlorobenzene (2.0 mL) was added to a seven mL vial containing cyclohexene oxide (1.00g, 10.2 mmol) in chlorobenzene (2.0 mL). The mixture was allowed to stir 24 hours at room temperature. Unreacted epoxide monomer was removed *in vacuo* and conversion was determined from the mass of the recovered polymer product. The mixture was analyzed by GPC (RI) to determine the molecular weight and molecular weight distribution of the polymers.

Redox switchable polymerization of cyclohexene oxide. In a glove box, iron(III) bis(alkoxide) complex **2.2** (0.0250 g, 0.0306 mmol) in chlorobenzene (0.8 mL) was added to a 7 mL vial containing cyclohexene oxide (0.150 g, 1.53 mmol) in chlorobenzene (0.7 mL) at room temperature. After 50 min., cobaltocene (0.0058 g, 0.0306 mmol) was added to the reaction mixture, and the color changed from blue to brown. At $t = 90$ min., ferrocenium hexafluorophosphate (0.0101 g, 0.0305 mmol) was added, and the mixture turned blue-brown. Aliquots were removed periodically from the mixture and terminated by addition of wet CDCl_3 outside of a glove box. The conversion was determined by analysis of spectra by integration of ^1H NMR methine peaks of the

remaining cyclohexene oxide (3.1 ppm) versus the methine peaks of the polyether (3.2-3.6 ppm). Each aliquot was analyzed by GPC (RI) to determine the molecular weight and molecular weight distribution of the polymers.

Diblock copolymerization of lactide/cyclohexene oxide by an Fe^{II} to Fe^{III} redox switch, one pot. In a glove box, iron(II) bis(alkoxide) complex **2.1** (0.0094 g, 0.014 mmol) in chlorobenzene (2.0 mL) was added to a seven mL vial containing (*rac*)-lactide (0.10 g, 0.70 mmol) and cyclohexene oxide (0.068 g, 0.70 mmol for 1:1 [CHO]:[L], or 0.0343 g, 3.50 mmol for 5:1 [CHO]:[L]) in chlorobenzene (2.0 mL) at room temperature. After one hour, ferrocenium hexafluorophosphate (0.0050 g, 0.015 mmol) was added to the mixture, and the color changed from purple-brown to blue. The mixture was allowed to stir for three hours and then was removed from a glove box and quenched with wet THF (0.5 ml). The remaining volatiles were removed *in vacuo*, and the mixture was dissolved in a minimal amount of dichloromethane (2 ml) and precipitated into acetone (100 mL). After being allowed to stir for one hour, the turbid mixture was centrifuged and poured through a 0.02 μm polypropylene (PP) filter membrane to collect homopolyether in the precipitate and copolymer with a small amount of low molecular weight homopolyether in the filtrate. After the fluid was dried *in vacuo*, the material collected in the acetone filtrate was redissolved in minimal dichloromethane (2 ml) and precipitated into stirring hexanes (100 mL). After the solution was allowed to stir for one hour, the mixture was centrifuged and poured through a 0.02 μm PP filter membrane to collect the copolymer in the precipitate and low molecular weight homopolyether in the filtrate.

To monitor the progress of the reaction, aliquots were removed periodically from the mixture and terminated by addition of wet CDCl_3 . Lactide conversion was determined by the integration of ^1H NMR methine peaks of the remaining lactide (5.0 ppm) versus the methine peaks of polylactide (5.2 ppm). Epoxide conversion was determined by mass of the polymer product before precipitation, taking into account the theoretical mass of polylactide and lactide. The polymers were analyzed by GPC to determine molecular weight and molecular weight distribution after each step of the reaction and each precipitation. The ratio of polylactide to polyether ([PLA]:[PCHO]) of the reaction mixtures were determined by ^1H NMR by integrating the methine polyether peak (3.2-3.6 ppm) versus the methine polylactide peak (5.2 ppm). Percent copolymer was determined by copolymer mass/total polymer mass where the “copolymer mass” is the mass of the polymer isolated in the hexanes precipitate and the “total polymer mass” is the “copolymer mass” plus any polymeric material isolated from the acetone precipitate and hexanes filtrate. Approximately 10% of polymer is lost during precipitation and handling of the polymers, so the unpurified polymer mass is not used in this calculation.

Diblock copolymerization of lactide/cyclohexene oxide by an Fe^{II} to Fe^{III} redox switch, sequential monomer addition. In a glove box, iron(II) bis(alkoxide) complex **2.1** (0.0094 g, 0.014 mmol) in chlorobenzene (2.0 mL) was added to a 7 mL vial containing (*rac*)-lactide (0.10g, 0.70 mmol) in chlorobenzene (2.0 mL) at room temperature. After one hour, ferrocenium hexafluorophosphate (0.0050 g, 0.015 mmol) was added to the mixture at which point the mixture immediately turned from purple-brown to blue. The solution was allowed to stir for five minutes to ensure that the oxidation reaction occurred prior to addition of the epoxide monomer. Cyclohexene oxide

(0.068g, 0.70 mmol) was then added. The solution was allowed to stir for three hours and was then removed from a glove box and quenched with wet THF (0.5ml). Chlorobenzene and unreacted cyclohexene oxide were removed *in vacuo*. Precipitations were performed as described for the one-pot polymerization to isolate copolymer products.

Diblock copolymerization of cyclohexene oxide/lactide by an Fe^{III} to Fe^{II} redox switch, one pot. In a glove box, iron(III) bis(alkoxide) complex **2.2** (0.00113 g, 0.014 mmol) in chlorobenzene (2.0 mL) was added to a 7 mL vial containing (*rac*)-lactide (0.10 g, 0.70 mmol) and cyclohexene oxide (0.068 g, 0.70 mmol for 1:1 [CHO]:[L], or 0.0343 g, 3.50 mmol for 5:1 [CHO]:[L]) in chlorobenzene (2.0 mL) at room temperature. After three hours, cobaltocene (0.0026 g, 0.014 mmol) was added to the reaction mixture, and the color changed from blue to brown. The reaction was allowed to stir for one hour and then was removed from a glove box and quenched with wet THF (0.5 mL). The remaining volatiles were removed *in vacuo*. The mixture was dissolved in minimal dichloromethane (2.0 mL) and precipitated into stirring acetone (100 mL). After stirring one hour, the mixture was centrifuged and poured through a 0.02 μm polypropylene (PP) filter membrane to collect homopolyether in the precipitate and copolymer with a small amount of low molecular weight homopolyether in the filtrate. After drying *in vacuo*, the material collected in the acetone filtrate was redissolved in minimal dichloromethane (2.0 mL) and precipitated into stirring hexanes (100 mL). After stirring one hour, the mixture was centrifuged and poured through a 0.02 μm polypropylene (PP) filter membrane to collect the copolymer in the precipitate and low molecular weight homopolyether in the filtrate.

Aliquots were removed periodically from the reaction mixture and terminated by addition of CDCl_3 to monitor the progress of the reaction. Lactide conversion was determined by ^1H NMR by integrating the methine peaks of the remaining lactide (5.0 ppm) versus the methine peaks of polylactide (5.2 ppm). Epoxide conversion was determined by mass of the polymer product before precipitation, taking into account the theoretical mass of polylactide and lactide. The polymers were analyzed by GPC to determine molecular weight and molecular weight distribution after each step of the reaction and each precipitation. The ratio of polylactide to polyether ([PLA]:[PCHO]) of the reaction mixtures were determined by ^1H NMR by integrating the methine polyether peak (3.2-3.6 ppm) versus the methine polylactide peak (5.2 ppm). Percent copolymer was determined by copolymer mass/total polymer mass where the “copolymer mass” is the mass of the polymer isolated from the hexanes precipitation and the “total polymer mass” is the “copolymer mass” plus any polymeric material isolated from the acetone filtrate and hexanes precipitates. Approximately 10% of polymer is lost during precipitation and handling of the polymers, so the unpurified polymer mass is not used in this calculation.

Diblock copolymerization of cyclohexene oxide/lactide by an Fe^{III} to Fe^{II} redox switch, sequential monomer addition. In a glove box, iron(III) bis(alkoxide) complex **2.2** (0.00113 g, 0.014 mmol) in chlorobenzene (2.0 mL) was added to a 7 mL vial containing cyclohexene oxide (0.068 g, 0.70 mmol) in chlorobenzene (2.0 mL) at room temperature. After three hours, cobaltocene (0.0026 g, 0.014 mmol) was added to the mixture at which point the solution immediately turned from blue to brown. The solution was allowed to stir an additional five minutes to ensure that the reduction

reaction occurred prior to addition of the lactide monomer. Then (*rac*)-lactide (0.10 g, 0.70 mmol) was added to the reaction as a solid. The solution was allowed to stir for one hour and was then removed from a glove box and quenched by the addition of wet THF (0.5 ml). The remaining volatile materials were removed *in vacuo*, and precipitations were performed as described for the one-pot polymerization to isolate copolymer products.

2.7 References

- (1) Biernesser, A. B.; Delle Chiaie, K. R.; Curley, J. B.; Byers, J. A. Block Copolymerization of Lactide and an Epoxide Facilitated by a Redox Switchable Iron-Based Catalyst. *Angew. Chemie - Int. Ed.* **2016**, *55* (17), 5251–5254.
- (2) Byers, J. A.; Biernesser, A. B.; Delle Chiaie, K. R.; Kaur, A.; Kehl, J. A. Catalytic Systems for the Production of Poly(lactic Acid); 2017; pp 67–118.
- (3) Odian, G. *Principles of Polymerization*; John Wiley & Sons, Inc.: Hoboken, NJ, USA, 2004.
- (4) Kreiser-Saunders, I.; Kricheldorf, H. R. Poly lactones. 39 - Zn Lactate-Catalyzed Copolymerization of L-Lactide with Glycolide or ϵ -Caprolactone. *Macromol. Chem. Phys.* **1998**, *199* (6), 1081–1087.
- (5) Qian, H.; Wohl, A. R.; Crow, J. T.; MacOsko, C. W.; Hoyer, T. R. A Strategy for Control Of “random” copolymerization of Lactide and Glycolide: Application to Synthesis of PEG- B -PLGA Block Polymers Having Narrow Dispersity. *Macromolecules* **2011**, *44* (18), 7132–7140.
- (6) Dechy-Cabaret, O.; Martin-Vaca, B.; Bourissou, D. Controlled Ring-Opening Polymerization of Lactide and Glycolide. *Chem. Rev.* **2004**, *104* (12), 6147–6176.
- (7) Huang, M. H.; Li, S.; Vert, M. Synthesis and Degradation of PLA-PCL-PLA Triblock Copolymer Prepared by Successive Polymerization of ϵ -Caprolactone and DL-Lactide. *Polymer (Guildf)*. **2004**, *45* (26), 8675–8681.
- (8) Shen, Y.; Zhu, K. J.; Shen, Z.; Yao, K. M. Synthesis and Characterization of Highly Random Copolymer of ϵ -Caprolactone and D,L-Lactide Using Rare Earth Catalyst. *J. Polym. Sci. Part A Polym. Chem.* **1996**, *34* (9), 1799–1805.

- (9) Qian, H.; Bei, J.; Wang, S. Synthesis, Characterization and Degradation of ABA Block Copolymer of L-Lactide and ϵ -Caprolactone. *Polym. Degrad. Stab.* **2000**, *68* (3), 423–429.
- (10) Chamberlain, B. M.; Jazdzewski, B. A.; Pink, M.; Hillmyer, M. A.; Tolman, W. B. Controlled Polymerization of DL-Lactide and ϵ -Caprolactone by Structurally Well-Defined Alkoxo-Bridged Di- and triyttrium(III) Complexes. *Macromolecules* **2000**, *33* (11), 3970–3977.
- (11) Wang, X.; Thevenon, A.; Brosmer, J. L.; Yu, I.; Khan, S. I.; Mehrkhodavandi, P.; Diaconescu, P. L. Redox Control of Group 4 Metal Ring-Opening Polymerization Activity toward L -Lactide and ϵ -Caprolactone. *J. Am. Chem. Soc.* **2014**, *136* (32), 11264–11267.
- (12) Nuyken, O.; Pask, S. D. Ring-Opening Polymerization-An Introductory Review. *Polymers (Basel)*. **2013**, *5* (2), 361–403.
- (13) Penczek, S.; Szymanski, R.; Duda, A.; Baran, J. Living Polymerization of Cyclic Esters - A Route to (Bio)degradable Polymers. Influence of Chain Transfer to Polymer on Livingness. *Macromol. Symp.* **2003**, *201* (1), 261–269.
- (14) Dove, A. P. Controlled Ring-Opening Polymerisation of Cyclic Esters: Polymer Blocks in Self-Assembled Nanostructures. *Chem. Commun.* **2008**, No. 48, 6446–6470.
- (15) Silvino, A. C.; Rodrigues, A. L. C.; De Jesus, K. F.; Dias, M. L. Synthesis and Characterization of Statistical Copolymers of Trimethylene Carbonate and L-Lactide Using Mg(II)/Ti(IV) Mixed Alkoxides as Initiator System. *Eur. Polym. J.* **2014**, *57*, 66–74.

- (16) Dobrzynski, P.; Kasperczyk, J. Synthesis of Biodegradable Copolymers with Low-Toxicity Zirconium Compounds. V. Multiblock and Random Copolymers of L-Lactide with Trimethylene Carbonate Obtained in Copolymerizations Initiated with zirconium(IV) Acetylacetonate. *J. Polym. Sci. Part A Polym. Chem.* **2006**, *44* (10), 3184–3201.
- (17) Kasyapi, N.; Bhowmick, A. K. Nanolamellar Triblock of Poly-D,L-Lactide- δ -Valerolactone-D,L-Lactide with Tuneable Glass Transition Temperature and Crystallinity for Use as a Drug-Delivery Vesicle. *RSC Adv.* **2014**, *4* (52), 27439–27451.
- (18) Ajellal, N.; Carpentier, J. F.; Guillaume, C.; Guillaume, S. M.; Helou, M.; Poirier, V.; Sarazin, Y.; Trifonov, A. Metal-Catalyzed Immortal Ring-Opening Polymerization of Lactones, Lactides and Cyclic Carbonates. *Dalt. Trans.* **2010**, *39* (36), 8363–8376.
- (19) Socka, M.; Duda, A.; Adamus, A.; Wach, R. A.; Ulanski, P. Lactide/trimethylene Carbonate Triblock Copolymers: Controlled Sequential Polymerization and Properties. *Polym. (United Kingdom)* **2016**, *87*, 50–63.
- (20) Broderick, E. M.; Guo, N.; Vogel, C. S.; Xu, C.; Sutter, J.; Miller, J. T.; Meyer, K.; Mehrkhodavandi, P.; Diaconescu, P. L. Redox Control of a Ring-Opening Polymerization Catalyst. *J. Am. Chem. Soc.* **2011**, *133* (24), 9278–9281.
- (21) Chisholm, M. H.; Navarro-Llobet, D.; Simonsick, W. J. A Comparative Study in the Ring-Opening Polymerization of Lactides and Propylene Oxide. *Macromolecules* **2001**, *34* (26), 8851–8857.

- (22) Guillaume, S. M.; Kirillov, E.; Sarazin, Y.; Carpentier, J. F. Beyond Stereoselectivity, Switchable Catalysis: Some of the Last Frontier Challenges in Ring-Opening Polymerization of Cyclic Esters. *Chem. - A Eur. J.* **2015**, *21* (22), 7988–8003.
- (23) Mai, S. M.; Abbot, A.; Norton, D.; McKean, R.; Ryan, A. J. Synthesis and Characterization of Block Copolymers of Polyoxyethylene and Polylactide with Different Architectures. *Macromol. Chem. Phys.* **2009**, *210* (10), 840–851.
- (24) Masutani, K.; Kimura, Y. Chapter 1. PLA Synthesis. From the Monomer to the Polymer. In *Poly(lactic acid) Science and Technology: Processing, Properties, Additives and Applications*; The Royal Society of Chemistry, 2015; pp 1–36.
- (25) Catalá, R.; López-Carballo, G.; Hernández-Muñoz, P.; Gavara, R. PLA and Active Packaging. In *Poly(lactic acid) Science and Technology: Processing, Properties, Additives and Applications*; The Royal Society of Chemistry, 2015; pp 243–265.
- (26) Mooney, D. J.; Breuer, C.; McNamara, K.; Vacanti, J. P.; Langer, R. Fabricating Tubular Devices from Polymers of Lactic and Glycolic Acid for Tissue Engineering. *Tissue Eng.* **1995**, *1* (2), 107–118.
- (27) Xu, Q.; Czernuszka, J. T. Controlled Release of Amoxicillin from Hydroxyapatite-Coated Poly(lactic-Co-Glycolic Acid) Microspheres. *J. Control. Release* **2008**, *127* (2), 146–153.
- (28) Athanasiou, K. A.; Niederauer, G. G.; Agrawal, C. M. Sterilization, Toxicity, Biocompatibility and Clinical Applications of Polylactic Acid/polyglycolic Acid Copolymers. *Biomaterials* **1996**, *17* (2), 93–102.

- (29) Tsuji, H. Poly(Lactic Acid). In *Bio-Based Plastics*; John Wiley & Sons Ltd, 2013; pp 171–239.
- (30) Kranz, H.; Ubrich, N. Physicomechanical Properties of Biodegradable Poly (D, L - lactide) and Poly (D, L-lactide-co-glycolide) Films in the Dry and Wet States. *J. Pharm. Sci.* **2000**, *89* (12), 1558-1566.
- (31) Chu, C.-C. Biodegradable Polymeric Biomaterials. *Biomaterials* **2007**, 6-1-6–22.
- (32) Miller, R. A.; Brady, J. M.; Cutright, D. E. Degradation Rates of Oral Resorbable Implants (Polylactates and Polyglycolates): Rate Modification with Changes in PLA/PGA Copolymer Ratios. *J. Biomed. Mater. Res.* **1977**, *11* (5), 711–719.
- (33) Gramlich, W. M. Toughening Polylactide with Phase-Separating Complex Copolymer Architectures. *Macromol. Chem. Phys.* **2015**, *216* (2), 145–155.
- (34) Zhang, L.; Li, N.; Wang, Y.; Guo, J.; Li, J. Ring-Opening Block Copolymerization of ϵ -Caprolactone with L-Lactide Catalyzed by N-Heterocyclic Carbenes: Synthesis, Characteristics, Mechanism. *Macromol. Res.* **2014**, *22* (6), 600–605.
- (35) Jelonek, K.; Kasperczyk, J.; Li, S.; Dobrzynski, P.; Jarzabek, B. Controlled Poly(l-Lactide-Co-Trimethylene Carbonate) Delivery System of Cyclosporine A and Rapamycine - The Effect of Copolymer Chain Microstructure on Drug Release Rate. *Int. J. Pharm.* **2011**, *414* (1–2), 203–209.
- (36) Guerin, W.; Helou, M.; Carpentier, J. F.; Slawinski, M.; Brusson, J. M.; Guillaume, S. M. Macromolecular Engineering via Ring-Opening Polymerization: L-Lactide/trimethylene Carbonate Block Copolymers as Thermoplastic Elastomers. *Polym. Chem.* **2013**, *4* (4), 1095–1106.

- (37) Grijpma, D. W.; Van Hofslot, R. D. A.; Supèr, H.; Nijenhuis, A. J.; Pennings, A. J. Rubber Toughening of Poly(lactide) by Blending and Block Copolymerization. *Polym. Eng. Sci.* **1994**, *34* (22), 1674–1684.
- (38) Cross, E. D.; Allan, L. E. N.; Decken, A.; Shaver, M. P. Aluminum Salen and Salan Complexes in the Ring-Opening Polymerization of Cyclic Esters: Controlled Immortal and Copolymerization of Rac- β -Butyrolactone and Rac-Lactide. *J. Polym. Sci. Part A Polym. Chem.* **2013**, *51* (5), 1137–1146.
- (39) Xiong, M.; Schneiderman, D. K.; Bates, F. S.; Hillmyer, M. A.; Zhang, K. Scalable Production of Mechanically Tunable Block Polymers from Sugar. *Proc. Natl. Acad. Sci.* **2014**, *111* (23), 8357–8362.
- (40) Biernesser, A. B.; Chiaie, K. R. D.; Curley, J. B.; Byers, J. A. Block Copolymerization of Lactide and an Epoxide Facilitated by a Redox Switchable Iron-Based Catalyst. *Angew. Chemie - Int. Ed.* **2016**, *55* (17), 5251–5254.
- (41) Cho, H. K.; Cho, J. H.; Jeong, S. H.; Cho, D. C.; Yeum, J. H.; Cheong, I. W. Polymeric Vehicles for Topical Delivery and Related Analytical Methods. *Arch. Pharm. Res.* **2014**, *37* (4), 423–434.
- (42) Bishai, M.; De, S.; Adhikari, B.; Banerjee, R. Copolymerization of Lactic Acid for Cost-Effective PLA Synthesis and Studies on Its Improved Characteristics. *Food Sci. Biotechnol.* **2013**, *22*, 73–77.
- (43) Biernesser, A. B. Synthesis of Divers Degradable Polymers by Redox-Switchable Iron-Based Catalysis, Boston College, 2016.

- (44) Quan, S. M.; Wang, X.; Zhang, R.; Diaconescu, P. L. Redox Switchable Copolymerization of Cyclic Esters and Epoxides by a Zirconium Complex. *Macromolecules* **2016**, *49* (18), 6768–6778.

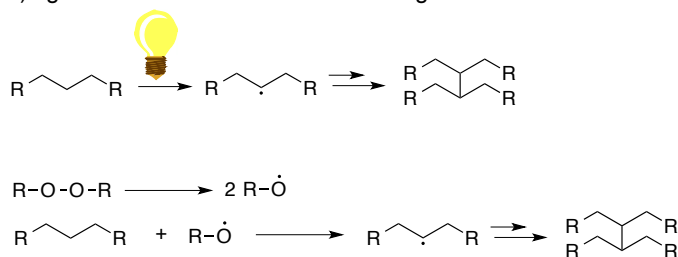
Chapter 3 Redox-triggered Crosslinking of a Degradable

Polymer

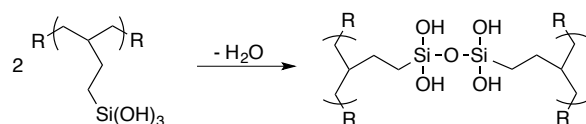
3.1 Introduction

Since the discovery of vulcanized rubber in the 19th century, cross-linked polymers have been utilized for many applications including automobile tires,¹ biological tissue engineering,² dental fillings,³ food packaging,⁴ pulsatile drug delivery systems,⁵ photolithography,¹ paints and coatings,¹ and adhesives.² Compared to thermosets and thermoplastics, cross-linked polymers are normally strong, tough, and solvent resistant, which make them suitable for all of the above applications.⁶ Nevertheless, application of cross-linked polymers in some areas has enjoyed less success due to synthetic limitations. Chemical crosslinks are often formed with light or radical initiators to form radicals that can recombine to form chemical bonds (Figure 3.1a).⁷

a) Light and radical induced cross linking



b) Condensation cross linking



c) Redox-triggered cross linking

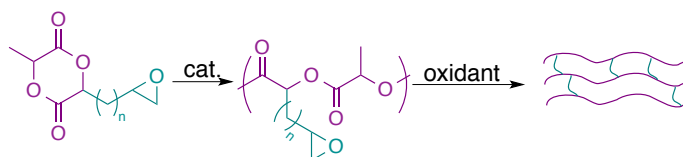


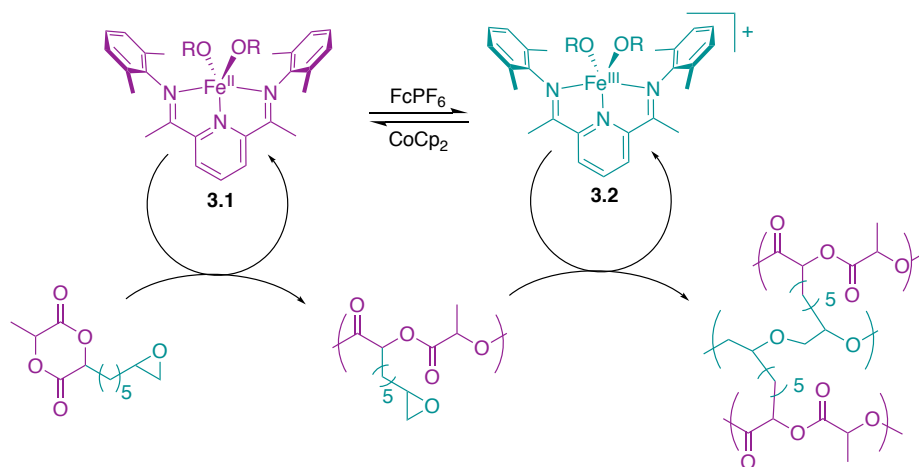
Figure 3.1. Crosslinking techniques

These methods have enjoyed significant success in lithography and coatings technologies, but the site of crosslinking and crosslinking density can be difficult to control. Moreover, light-driven processes are sometimes limited to thin films due to light penetration that extends only a few millimeters. Since polymerization only occurs in areas that are exposed to light, shadows can also be problematic, especially for coating applications. Condensation reactions serve as an alternative to UV irradiation (Figure 3.1b)⁷, but these types of reactions sometimes require elevated temperatures or the need to store polymer precursors separately (e.g., epoxy resins).⁸ On the other hand, these methods are not limited to thin films, and they demonstrate better control over where and to what degree crosslinking occurs.

In this chapter, we describe a new way to trigger crosslinking that complements the existing methodologies (Scheme 3.1). In this method, we take advantage of an iron complex that demonstrates orthogonal reactivity for ring opening polymerization reactions of cyclic diesters and epoxides, depending on the oxidation state of the catalyst. (Chapter 2) The advantages that the complementary reactivity of these iron-based complexes afford have recently been enumerated for the redox-controlled block copolymerization of an epoxide and lactide,⁹ which Diaconescu and coworkers have also observed with different catalysts and monomers.¹⁰ In general, switchable catalysis has started to gain traction as a new way to assemble complex small molecules and macromolecules.^{11–13} We now extend the utility of switchable catalysis into the realm of crosslinking reactions by exploiting the redox-switching capabilities of the iron-based catalysts, which can be triggered upon oxidation. This switching capability provides the temporal control common to irradiation techniques without complications from

shadowing. It maintains control over the site and degree of crosslinking without the need to store precursors separately. Moreover, the process is a new way to crosslink poly(lactic acid), a biodegradable alternative to the slowly degrading and oil-derived polymers commonly used today.¹⁴⁻¹⁷

Scheme 3.1. Redox-triggered crosslinking



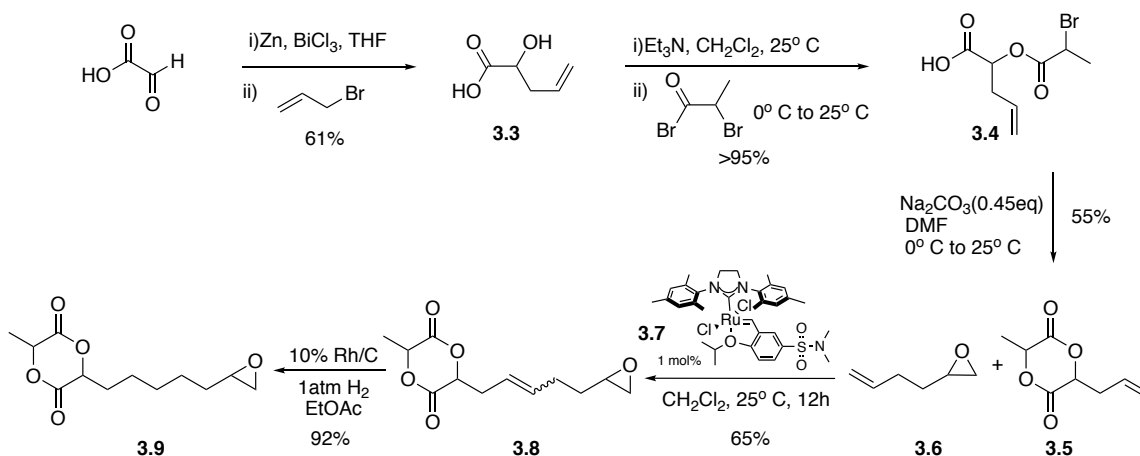
3.2 Synthesis of dual functionalized monomer

To carry out redox-triggered cross-linking polymerizations, we first needed to synthesize a monomer that had both cyclic diester and epoxide functionalities (Scheme 3.2). Zou and co-workers had reported the synthesis of allyl substituted cyclic diester **3.5**. The first step of this synthesis was a bismuth mediated Barbier-type allylation of glyoxylic acid to form carboxylic acid **3.3**.¹⁸ This step proceeded with good yields and was previously optimized by Lauren Yablon.

The esterification of **3.3** was performed in nearly quantitative yields with triethylamine and bromopropionyl bromide to yield compound **3.4**. The cyclization of **3.4** was initially problematic giving a moderately low yield of 30% and required large amounts of anhydrous DMF. Through optimization, it was determined that reagent grade

DMF could be used without hindering the yield. Additionally, it was found that this reaction gave higher yields when run on a large scale (25 g starting material) to deliver the desired product (55%).

Scheme 3.2. Synthesis of cyclic diester **3.9**



Cross-metathesis between **3.5** and the commercially available epoxy alkene **3.6** catalyzed by metathesis catalyst **3.7** (Scheme 3.2) an analog of the Hoveyda-Grubbs second generation catalyst.^{19,20} Cross-metathesis of **3.5** with epoxy alkene **3.6** gave epoxide-functionalized cyclic diester **3.8**. Notably, **3.5** does not readily homodimerize and has therefore been classified as a type three alkene for cross-metathesis.¹⁹ A good deal of time was spent optimizing this reaction because it initially gave a yield of only 20%. The cross-metathesis product was also not stable at room temperature for more than a day due to residual ruthenium-based impurities present in the isolated compound. Because of this isolation issue and the high cost of these catalysts, the catalyst loading was dropped from 3.0% to 1.0% without diminishing the yield. It was determined that a good amount of product was being lost or decomposed during column purification. To ameliorate this issue, this material was purified on a silica gel column with a moderate

flow rate to reduce the amount of time the compound was exposed to the silica gel. This procedure improved yields to 50%. The remaining gain in yield came from periodically exposing the reaction mixture to vacuum. This lower pressure removed ethylene and drove the equilibrium for the cross-metathesis reaction forward, improving conversion and giving a decent yield of 65%. It is important to note that starting material **3.5**, **3.6**, and the dimer of **3.6** are easily isolated from the reaction mixture yielding near quantitative yield based on recovered starting material (>95%). Elaboration of **3.8** to the saturated epoxy cyclic diester **3.9** was achieved in a straightforward fashion and high yields (92%).

3.3 Homopolymerization of 3.9

To assess the feasibility of a redox-triggered crosslinking reaction, **3.9** was exposed to iron(II) complex **3.1** (Scheme 3.1). As was observed previously for lactide, **3.9** underwent polymerization in a controlled fashion with polymer demonstrating M_w/M_n of 1.4 and a linear relationship between molecular weight and conversion being observed (Figure 3.2). Notably, no conversion of the epoxide side chain was seen during this polymerization. The molecular weights obtained were slightly higher than the theoretical molecular weights (e.g., in Figure 3.2) at 66% conv., the observed M_n is 11.2 kg/mol while the theoretical M_n is 8.0 kg/mol). Since this discrepancy varies slightly depending on the batch of **3.9** used; we attribute the small differences between theoretical and observed molecular weights to minor impurities (<1%) in the monomer. Notably, the polymerization of **3.9** occurred at a slower rate compared to lactide ($k_{obs}(\mathbf{3.9}) = 0.14 \times 10^{-4} \text{ s}^{-1}$ vs. $k_{obs}(\text{lactide}) = 1.66 \times 10^{-4} \text{ s}^{-1}$), a likely consequence of competitive binding from the epoxide and cyclic diester moieties of **3.9**. This outcome was in line with our previous

observations for lactide polymerization reactions catalyzed by **3.1**, which were slower when epoxides are present (Chapter 2).⁹

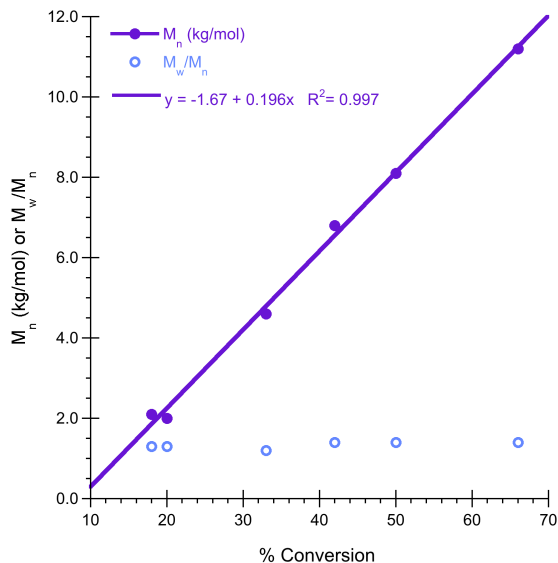


Figure 3.2. Molecular weight (M_n , ●) and molecular weight distribution (M_w/M_n , ○) vs. conversion for the polymerization of **3.9** catalyzed by iron-based complex **3.1**

After polymerization of the cyclic diester moiety in **3.9** reached 95% conversion, the catalyst was oxidized *in situ* with ferrocenium hexafluorophosphate (FcPF_6). Oxidation of **3.1** was evident by an immediate color change from purple to blue, a color change that we previously noted during similar oxidation reactions (Chapter 2).^{9,21} Upon removal of the solvent, a polymeric material resulted that was insoluble in all solvents tested, even at elevated temperatures. Such insolubility precluded polymer characterization by solution state ^1H NMR spectroscopy, but it was hypothesized that catalyst oxidation gave rise in the polymerization of the epoxide side chains, thereby giving rise to in cross-linked polyester. As confirmation of this hypothesis, the thermal

properties of the polymer obtained after catalyst oxidation were determined and compared to the polymer obtained prior to catalyst oxidation (entry 1, Table 3.1). As expected for the cross-linked polymer, the thermal stability and glass transition temperature for the polymer recovered after catalyst oxidation ($T_d = 299$ °C and $T_g = 74$ °C, respectively) was larger than the polymer isolated prior to catalyst oxidation ($T_d = 190$ °C and $T_g = 15$ °C, respectively). Moreover, when the insoluble polymer obtained after catalyst oxidation was subjected to acid-catalyzed hydrolysis, degradation of the polyester subunits occurred. Analysis of the resulting oligomers by ^1H NMR spectroscopy revealed the presence of ether linkages, which is consistent with the formation of polyether crosslinks that occurred upon catalyst oxidation.

Despite visual evidence that the catalyst was rapidly oxidized by the oxidant and prior evidence that catalyst oxidation with FcPF_6 is faster than epoxide polymerization,⁹ we considered the possibility that FcPF_6 was carrying out the crosslinking reaction instead of the oxidized iron-based catalyst.²² To rule out this possibility, the epoxide-functionalized polyester was synthesized and exposed to FcPF_6 . Upon removal of the solvent, the polymer was still soluble, and there was negligible evidence for conversion of the epoxide functionality by ^1H NMR. Therefore, the oxidant is not a competent catalyst for the redox-triggered crosslinking reaction.

For further verification that the iron(III) catalyst was the active species for crosslinking, an experiment was designed to demonstrate that catalyst oxidation occurs significantly faster than epoxide polymerization. Due to the low activity of iron-based catalysts for the polymerization of epoxides derived from α -olefins, we suspected that the crosslinking reaction only occurred upon solvent removal. ^1H NMR experiments and

redox-switchable lactide polymerization experiments²¹ suggest that the redox reaction between **3.1** and FcPF₆ takes no longer than a few seconds (See Chapter 2). Thus, if crosslinking requires concentrating the reaction mixture, then the catalyst has ample time to undergo oxidation prior to crosslinking. To test this hypothesis, polymerization of **3.9** was carried out to high conversion with catalyst **3.1**. FcPF₆ was then added to the reaction mixture, which resulted in the immediate color change suggestive of catalyst oxidation. Instead of immediately removing the solvent, the reaction mixture was allowed to stir for an additional 24 hours, and then cobaltocene (CoCp₂) was added to the reaction to reduce the catalyst back to the iron(II) oxidation state. Consistent with our expectation, removal of the solvent at this stage led to no evidence for crosslinking by ¹H NMR. Moreover, when the same reaction was repeated without the addition of CoCp₂, the cross-linked polymer was obtained upon removing the solvent. This outcome confirmed that crosslinking does not occur until the reaction mixture is concentrated. Since 24 hours is ample time to ensure full catalyst oxidation, it is unlikely that the oxidant is responsible for the crosslinking reaction.

To demonstrate the versatility of this redox-triggered crosslinking reaction, the polymerization was also run in the reverse direction where the epoxide is polymerized first with the catalyst in the iron(III) oxidation state followed by crosslinking induced by catalyst reduction (i.e., iron (III) to iron (II) redox switch). For this reaction, **3.9** was exposed to isolated **3.2**. After polymerization of the epoxide functionality reached high conversion (85%), the catalyst was reduced *in situ* with cobaltocene (CoCp₂). Upon removal of the solvent, an insoluble material was once again produced that precluded analysis by solution state ¹H NMR spectroscopy. As was done previously for the polymer

obtained from the iron(II) to iron(III) redox switch, the thermal properties of the polymer were determined to confirm that crosslinking had occurred (entry 2, Table 3.1). Although T_d and T_g are consistent with the formation of a cross-linked polymer ($T_d = 305$ °C and $T_g = 14$ °C), the polymer obtained from the iron(III) to iron(II) switch had different thermal properties compared to the polymer obtained from the iron(II) to iron(III) switch (*cf.* entries 1 and 2, Table 3.1). This disparity in thermal transitions suggests a greater degree of crosslinking occurring for the latter situation. At the current stage, it is not clear why the two reactions behave differently, but it may be associated with the incomplete conversions observed for epoxide polymerization for the iron(III) to iron(II) switch or to a greater propensity for intramolecular rather than intermolecular reactions occurring for the iron(III) to iron(II) switch compared to the iron(II) to iron(III) switch.

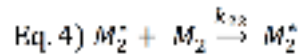
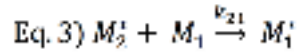
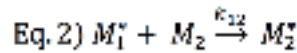
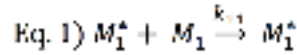
To further demonstrate the utility of a redox-triggered crosslinking reaction, random copolymerization reactions were carried out between **3.9** and (*rac*)-lactide at various **3.9**: lactide feed ratios (Table 3.1). In every instance, complete conversion of the lactide and cyclic diester **3.9** was observed, once again occurring with selective ring opening of the cyclic diester functional groups before catalyst oxidation. However, unlike the homopolymerization of either **3.9** or (*rac*)-lactide, copolymerization reactions containing both monomers proceeded to give low molecular weight polymer with broad polydispersities that are neither characteristic of a living process nor of a reaction proceeding with a single, catalytically active species (Table 3.1). The reactions proceeded at approximately half the rate compared to homopolymerization of **3.9**.

Table 3.1. Properties of polymers obtained from the redox-triggered crosslinking of random copolymers containing lactide and epoxy cyclic diester 3.9^a

	[3.9]: [lactide]	Before Crosslinking				After Crosslinking			
		M _n ^b (kg/mol)	M _w /M _n ^b	T _d ^c (°C)	T _g ^d (°C)	T _d ^c (°C)	T _g ^d (°C)	% Swelling ^e	% Gel Fraction
1	1:0	12.7	1.4	190	15 ^f	299	74	283 ±55	83±7
2 ^g	1:0	0.8	1.5	283	-7.0	305	14	357 ±78	52±9
3	9:1	1.5	2.5	190	22	291	61	431 ±136	72±11
4	3:1	1.6	3.9	116	-38	299	55	499 ±182	71±1
5	1:1	3.3	4.6	120	-18	217	49	551 ±55	81±7
6	1:3	2.8	2.8	215	24 ^f	220	44	644 ±135	66±1
7	1:9	6.7	1.6	222	-20	291	43	1092 ±343	69±4

^aReactions run with **3.1** as the catalyst and then in situ oxidation to **3.2** with FcPF₆. ^bDetermined from GPC relative to polystyrene standards. ^cOnset decomposition temperature determined by TGA. ^dGlass transition temperature determined by DSC. ^eDetermined in THF. ^fMelting temperatures also observed for these samples. ^gThis reaction was run starting with **3.2** and then in situ reduction to **3.1** with CoCp₂.

To gain some insight into this unexpected behavior, monomer reactivity ratios were determined for copolymerization reactions by altering the feed ratio and analyzing the relative reactivity of the two monomers at low conversions. The reactivity ratios were determined assuming the terminal model of copolymerization following the method described previously.²³ To determine reactivity ratios, polymerization reactions were carried out, and conversion was analyzed by GC at low conversions (ideally below 70%). At high conversion, the co-monomer feed will affect the copolymer composition, but at low conversion, the copolymer composition will be based on the inherent reactivity of each monomer to undergo polymerization. The primary assumption of this method is that copolymerization rate is only dependent on the last unit of the propagating chain. Based on this theory there are four possible propagation reactions:



Here equations 1 and 4 are considered self-propagation and equations 2 and 3 are cross propagation. Above each reaction is the rate constant for each reaction. Reactivity ratios are abbreviated as r_1 and r_2 .

$$\text{Eq. 5) } r_1 = \frac{k_{11}}{k_{12}} \quad r_2 = \frac{k_{22}}{k_{21}}$$

If $r > 1$ then the monomer preferentially adds itself, but if $r < 1$ it will more likely add the comonomer. The reactivity ratios are incorporated into the copolymerization equation 6:

$$\text{Eq. 6) } \frac{d[M_1]}{d[M_2]} = \frac{[M_1](r_1[M_1] + [M_2])}{[M_2](r_2[M_2] + [M_1])}$$

Here $\frac{d[M_1]}{d[M_2]}$ is equal to the copolymer composition. Further manipulation of this equation with linear least-squares regression analysis can give equations G and F.

$$\text{Eq. 7) } G = \frac{\frac{[M_1]}{[M_2]} \left(\frac{d[M_1]}{d[M_2]} - 1 \right)}{\left(\frac{d[M_1]}{d[M_2]} \right)} \quad F = \frac{\left(\frac{[M_1]}{[M_2]} \right)^2}{\left(\frac{d[M_1]}{d[M_2]} \right)}$$

Here $\frac{[M_1]}{[M_2]}$ is the initial comonomer feed. A plot of G is plotted against F to yield a straight line with slope r_1 and the intercept r_2 .

This analysis resulted in $r_{lactide} = 2.8$ and $r_{3.6} = 0.08$ ($r_{lactide} * r_6 = 0.22$), which reflects a propensity to incorporate lactide regardless of whether lactide or **3.9** was the last inserted monomer. The reactivity ratios also suggest a polymer microstructure that is mostly poly(lactic acid) with subunits of **3.9** occasionally inserted.

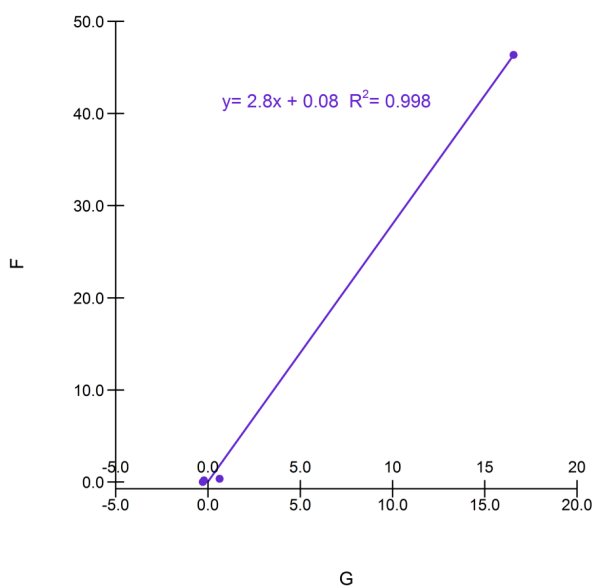
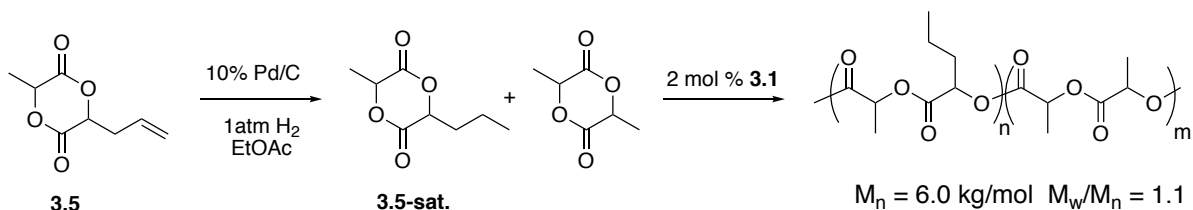


Figure 3.3. Determination of reactivity ratios for copolymerization **3.9** and lactide catalyzed by **3.1**

The possibility that the lower molecular weight control observed in copolymerization experiments were a manifestation of the different ring strain between **3.9** and lactide was ruled out with copolymerization reactions carried out between lactide and a saturated version of monomer **3.5** (Scheme 3.3). As expected, these copolymerization reactions occurred with the clean conversion of both monomers and good control over molecular weight and molecular weight distribution. For example, when a 1:1 mixture of monomers and 2 mol% catalyst was used, polymer with $M_n = 6.0$ kg/mol (theor $M_n = 7.2$ kg/mol) and $M_w/M_n = 1.1$ was obtained. Notably, **3.5** itself is not active for ROP catalyzed by **3.1**.

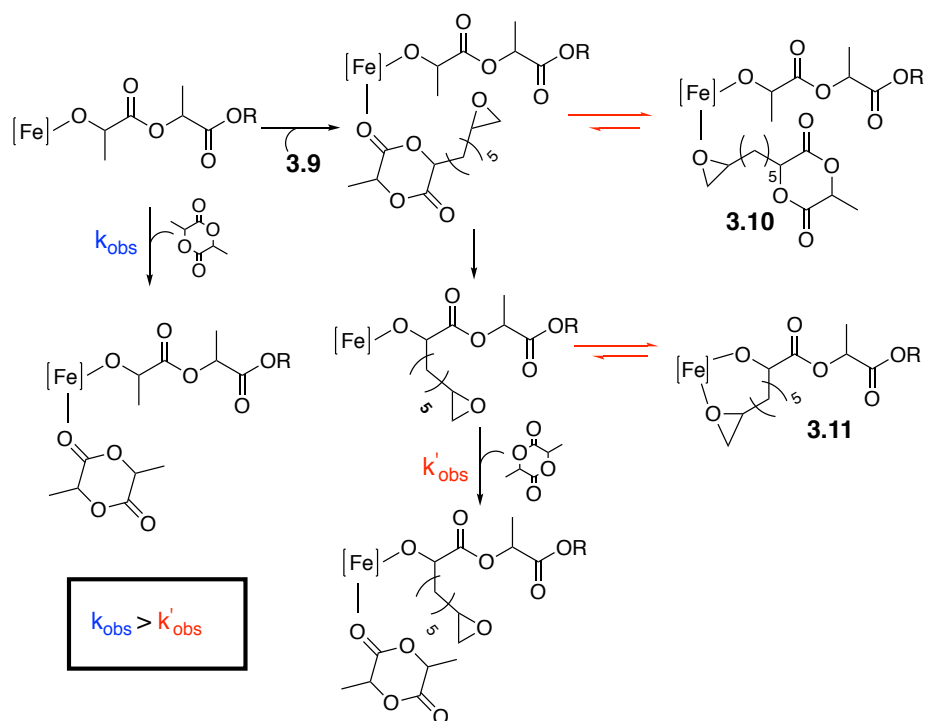
Scheme 3.3. Synthesis and copolymerization of 3.5-sat. with lactide.



With a difference in ring strain between **3.9** and lactide being ruled out as a potential reason for the lower molecular weight control observed in the copolymerization reactions compared to the corresponding homopolymerization reactions, we hypothesize that competitive binding of the epoxide moiety could explain the different behavior in **3.9** with the catalyst. If the epoxide moiety in **3.9** binds to the catalyst instead of the cyclic diester moiety, then the lactide monomer would be expected to be more reactive than **3.9** because binding of **3.9** would lead to an intermediate that would be inactive towards polymerization (i.e., **3.10** in Scheme 3.4). Moreover, compared to lactide, ring-opening polymerization of **3.9** positions an epoxide proximal to the metal so that chelation can occur from the growing polymer chain (i.e. **3.11** in Scheme 3.4). Due to these binding events, propagation is slower after incorporating **3.9** compared to propagation after inserting lactide because the coordinated epoxide competes with the next incoming monomer. As a result, multiple propagating species undergo polymerization at different rates, which ultimately leads to the broader polydispersities observed in the copolymerization reactions compared to narrower polydispersities being observed for both homopolymerizations of lactide and **3.9**. While the validity of this mechanistic hypothesis has not been rigorously tested, it is noteworthy that polymers with narrow molecular weight distributions are not advantageous in crosslinking applications.

Monodisperse polymers may be a disadvantage because they are often difficult to process.²⁴

Scheme 3.4. Mechanistic hypothesis to explain why copolymerizations of lactide and **3.9** results in lower molecular weight and more polydisperse polymer compared to homopolymerization reactions. Intermediates such as **3.10** and **3.11** sequester the catalyst in unreactive states so that insertions of **3.9** are slower and monomer insertions after incorporating **3.9** (k'_{obs}) are slower than monomer insertions after incorporating lactide (k_{obs}).



Despite this minor complication, redox-triggered crosslinking reactions in copolymers containing lactide and **3.9** were nevertheless achieved similarly as the homopolymerization reaction by removing most of the solvent from the reaction mixture after oxidizing the catalyst with FcPF_6 . Crosslinking was once again evident from the poor polymer solubility in all solvents after the reaction was allowed to proceed for one hour at room temperature.

Further verification for the existence of crosslinking in these polymers was achieved by analysis of the materials by thermogravimetric analysis (TGA), differential

scanning calorimetry (DSC), and swelling tests (entries 1 and 3-7, Table 3.1). TGA of the polymers revealed that the thermal stability (i.e., T_d) was significantly affected by crosslinking the polymer (upwards of 180 °C), but only minimally affected by the amount of **3.9** in the cross-linked copolymer. In contrast, significant increases in the glass transition temperature (T_g) were observed for the cross-linked polymers, which became more substantial as the amount of **3.9** was increased in the copolymer (Figure 3.4). This trend is consistent with an increase in crosslinking density and a decrease in chain mobility that results from crosslinking.^{25,26} The cross-linked polymers demonstrated glass transition temperatures that were up to 30 °C higher than atactic poly(lactic acid) ($T_g \sim 45$ °C).²⁷ The increase in T_g that was observed is more significant than previously observed for cross-linked poly(lactic acid) obtained from polymer irradiation.^{14,28-30} We attribute the significant changes in T_g that we observe to the synthetic methodology used for crosslinking here, which results in more complete and uniform crosslinking thereby maximally affecting polymer thermal properties.

Consistent with the high degree of crosslinking was the high gel fractions that were unilaterally observed for all cross-linked materials (Table 3.1). Still, the trend observed for the degree of swelling in the cross-linked polymers was contrary to our expectations. All cross-linked polymers experienced swelling of at least 200% (wt./wt.) when exposed to tetrahydrofuran (THF), but the amount of swelling increased as the amount of **3.9** decreased in the feed (Figure 3.4). Polymer samples with 10% of **3.9** in the feed demonstrated maximal swelling capabilities reaching nearly 1100% when exposed to THF. That the cross-linked polymers with the least amount of **3.9** demonstrated, the most swelling is surprising because it was assumed that these polymers had the lowest

crosslinking density. In general, swelling capacity for cross-linked polymers increases with increasing crosslink density as long as the polymer is not extensively cross-linked.³¹ Nevertheless, the general trend breaks down for highly cross-linked materials, which swell less due to restricted intramolecular motions. The fact that swelling increased as the amount of **3.9** decreased coupled with the observation that T_g increased at higher concentrations of **3.9** is most consistent with densely cross-linked materials being formed in the iron(II) to iron(III) redox switch (entries 1, 3-7). The situation appears to be somewhat different for the iron(III) to iron(II) switch (entry 2, Table 3.1), where less extensive crosslinking has occurred.

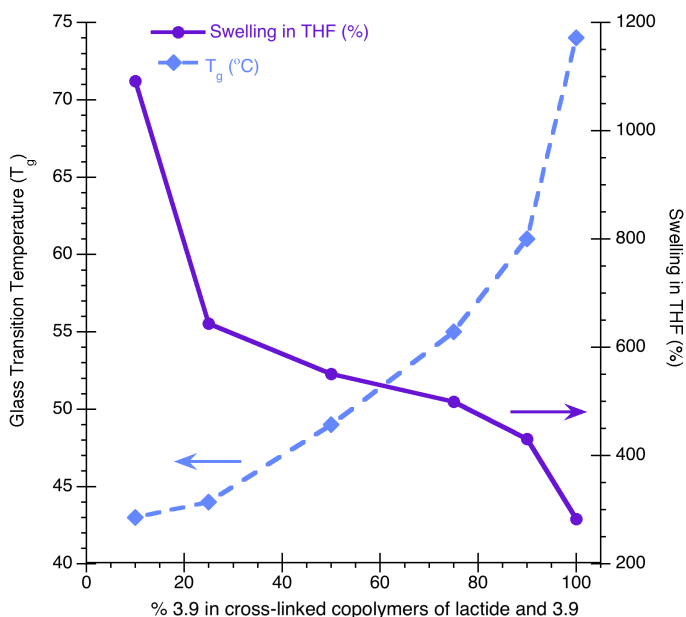
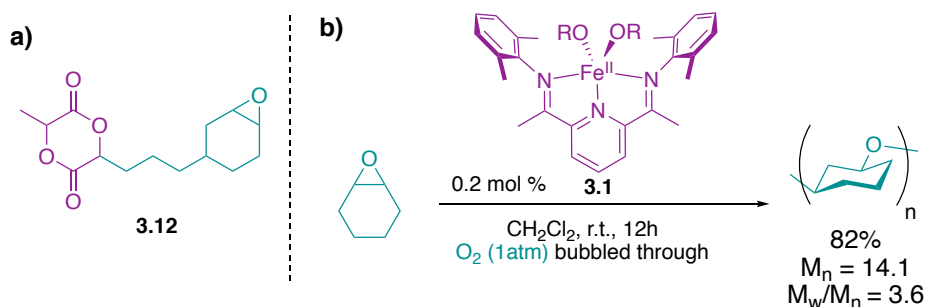


Figure 3.4. T_g (•) and swellability (◊) of polymers obtained from redox-triggered crosslinking reactions at various [3.9]: lactide feed compositions. Lines connecting the datum are merely meant to guide the eye to emphasize the trend and are not mathematical fits to model the data

We have more recently been studying a variant of **3.9** that contains a more strained epoxide moiety (Scheme 3.5a, **3.12**). We hypothesized that with a more reactive epoxide we might be able to trigger the crosslinking by using oxygen gas as the oxidant. In addition to being a "green" oxidant, utilizing oxygen would remove the need to add external oxidants and perhaps enable oxidation in the solid state. To test this hypothesis, experiments were performed by exposing cyclohexene oxide to **3.1** and then bubbling oxygen through the solution (Scheme 3.5). After 12 hours 82% conversion was observed. We have since synthesized **3.12** but have been unable to trigger crosslinking with oxygen as the oxidant. Future studies will focus on developing conditions for oxygen-triggered crosslinking

Scheme 3.5. a) Targeted monomer **3.12**. b) Reaction of **3.1** with cyclohexene oxide in the presence of oxygen



In addition to thermal properties, we plan to investigate the mechanical properties of these cross-linked materials. To do this, we have developed a method for producing thin films out of the material. Due to the insolubility of the cross-linked polymer, basic solvent casting of the final polymer is not possible. Instead, a solution of the pre-cross-linked material is added to a disposable aluminum weighing dish. A solution of oxidant is then added, and the solvent is allowed to evaporate. The oxidation begins the crosslinking inside the film vessel, and subsequent slow evaporation of solvent forms a film. Film

thickness can be tuned by changing either the amount of solution added or the size of the pan. Once the solvent appears to be completely evaporated, the pan was slowly heated to prevent the formation of bubbles. Then the final curing took place in a vacuum oven at 45 °C. These final films can be carefully removed from the aluminum pan by peeling the aluminum from the sides and bottom of the film. Punching out disks is then sufficient to make films for dynamic mechanical analysis. However, films prepared through the copolymerization and crosslinking of lactide and **3.9** appear to be very brittle. Future studies in this area will focus on adding exogenous epoxide monomer to form more malleable films that are more suitable for mechanical property testing.

3.4 Conclusions

In this chapter, we present a new strategy for the synthesis of cross-linked polyesters that relies on the redox-switching capabilities of an iron-based catalyst. Moreover, we provide a way to access cross-linked polymers derived from poly(lactic acid). Although poly(lactic acid) has been extensively studied, few examples explore its crosslinking. Cross-linked poly(lactic acid) is most commonly achieved by high energy light^{28,32} or electron beam irradiation,²⁹ which can be inefficient thereby leading to low levels of crosslinking. End group functionalization of poly(lactic acid) followed by crosslinking has been reported in some success,³³ although this method requires post-synthetic functionalization of polymers, which often suffer from incomplete conversions.

Beyond providing access to cross-linked poly(lactic acid), we have been able to demonstrate how the exquisite chemoselectivity of the Fe(II) and Fe(III) oxidation states of the catalyst can be used to control the onset of polymer crosslinking. Redox-triggered crosslinking reactions involving disulfide bridges,³⁴ the crosslinking reactions reported

here are the first examples where crosslinking reactions can be controlled by redox reactions; they are the first that involves the use of a ring opening polymerization catalyst that demonstrates orthogonal reactivity for two different functional groups. The newly introduced strategy is advantageous compared to light triggered processes because the method is not limited to thin films or prone to shadowing effects. Compared to two-part resins, the method may also be advantageous because the degree of crosslinking can be theoretically controlled by catalyst reduction, which will stop the crosslinking reaction. While we have not yet demonstrated that such control is possible, this proof-of-principle study justifies a more in-depth study in which this type of reactivity can be investigated. Until recently, we have been limited due to the need to concentrate the polymerization to observe crosslinking. Excitingly, we have recently determined that switching to a less coordination counter anion allows for crosslinking to occur without the need to concentrate the reaction mixture (see Chapter 4 for anion screen). Regulating crosslinking density through in situ reductions will be explored with this anion. Future studies will include an investigation into different epoxy cyclic diester monomers. Alternative oxidation strategies will be pursued as well. Finally, considering the lack of information regarding cross-linked poly(lactic acid), a more thorough study of the properties of the cross-linked polymers is warranted, including a detailed exploration of the polymer mechanical properties and degradation profiles.

3.5 Experimental

General Considerations. Unless stated otherwise, all reactions were carried out in oven-dried glassware in nitrogen-filled glove box or using standard Schlenk line techniques. Solvents were used after passage through a solvent purification system under

a blanket of argon and then degassed briefly by exposure to vacuum. Acros Organics supplied the glyoxylic acid. zinc, allyl bromide, 2-bromopropionyl bromide, triethylamine, sodium carbonate, and rhodium on activated carbon were purchased from Sigma-Aldrich. TCI America provided bismuth(III) chloride. Fisher Scientific supplied hydrochloric acid, magnesium sulfate, and solvents. 1,2-epoxy-5-hexene was purchased from Gelest, Inc. Hoveyda-Grubbs 2nd Generation and Zhan's catalysts were purchased through Strem. (*rac*)-Lactide was supplied by Frinton Laboratories and was recrystallized from ethyl acetate followed by recrystallization from toluene and dried *in vacuo* prior to use. Zinc was activated with hydrochloric acid, dried over P₂O₅, and stored under an inert atmosphere. Nuclear magnetic resonance (NMR) spectra were recorded at ambient temperature on a Varian spectrometer (¹H and ¹H{¹H} 500 MHz, and ¹³C{¹H} 125 MHz) in CDCl₃ and are referenced versus shifts of solvents containing residual protic impurities. The line listing for the ¹H NMR spectra are reported as chemical shift in ppm (multiplicity, number of protons, coupling constant in Hz, assignment). High-resolution mass spectra were obtained at the Boston College Mass Spectrometry Facility using JEOL AccuTOF DART. The automatic column used was a Teledyne ISCO CombiFlash® R_f using RediSep R_f Gold columns, TLC plates were run using Merck TLC Silica gel 60 F₂₅₄ glass plates and stained with KMnO₄ or PMA stains.

Gel permeation chromatography (GPC) was performed on an Agilent GPC220 in THF at 40 °C with three PL gel columns (10µm) in series and recorded with a refractive index detector. Molecular weights and molecular weight distributions were determined from the signal response of the refractive index (RI) detector relative to polystyrene standards.

Gas chromatography (GC) was performed with a Shimadzu GC-2014 GC-FID (SHRXL-5MS column 15 m x 0.25 mm x 0.25 μ m). The GC method used was 30-250 $^{\circ}$ C, 15.33 minutes, and 0.5 mL sample size with tetradecane as an internal standard.

All differential scanning calorimetry (DSC) measurements were performed on a TA instruments Q10-0311 for three heating cycles from -80 $^{\circ}$ C to 300 $^{\circ}$ C at a ramp of 10 $^{\circ}$ C/min. Thermogravimetric analysis (TGA) measurements were performed on a TA Instruments Q50 from room temperature to 800 $^{\circ}$ C at a ramp of 20 $^{\circ}$ C/min. TGA and DSC were performed at MIT using instruments in the Swager group.

Synthesis of 2-Hydroxypent-4-enoic Acid (3.3). In a dry atmosphere glove box, glyoxylic acid monohydrate (20 g, 0.22 mol) was added to a 3-neck round bottom flask (1L) with a 180 $^{\circ}$ joint, rubber septum, and a thermometer. The round bottom flask was brought out of the glove box and connected to a Schlenk line, and dry THF (590 mL) was added. Zinc (30 g, 0.46 mol) and bismuth trichloride (96 g, 0.30 mol) was cooled to 0 $^{\circ}$ C. The zinc was added in two portions to the round bottom flask through the side arm under a positive pressure of nitrogen. Bismuth trichloride was added in four portions to the round bottom flask under a positive pressure of nitrogen, making sure the temperature did not rise above 10 $^{\circ}$ C. The reaction slurry turned gray upon the addition of zinc and turned dark blue/black upon addition of the bismuth trichloride. The slurry stirred for 3 hours at 0 $^{\circ}$ C. Allyl bromide (26 mL, 0.30 mol) was added dropwise to the flask. The reaction flask was put under an atmosphere of nitrogen and allowed to stir overnight at 4 $^{\circ}$ C. The reaction was quenched with 1 M HCl (1000 mL) and allowed to stir for 3 hours at 25 $^{\circ}$ C. The slurry was filtered through celite. The organic phase was washed three times with diethyl ether (100 mL). The combined organic phases were washed three

times with brine (100 mL), dried over magnesium sulfate, filtered, and concentrated to give white crystals (16.9 g, 67%). The product was used without further purification. ^1H NMR (500 MHz, CDCl_3) δ 5.83 (ddt, $J = 17.2, 10.0, 7.2$ Hz, 1H, CH), 5.21 (dd, $J = 13.5, 9.1$ Hz, 2H, CH_2), 4.36 (dd, $J = 6.1, 4.9$ Hz, 1H, CH), 2.72 – 2.43 (m, 2H, CH_2); ^{13}C NMR (150 MHz, CDCl_3): δ 38.51, 69.86, 119.67, 132.03, 178.90; IR (neat) 3451.74, 3401.12, 2909.37, 1707.29, 1209.51, 1070.59, 917.76, 874.37 cm^{-1} ; HRMS (ESI+) Calcd. for $\text{C}_5\text{H}_9\text{O}_3$ $[\text{M}+\text{H}]^+$: 117.05517; Found 117.05574. Spectroscopic data matches what is reported in the literature.¹⁸

Synthesis of 2-(2-Bromopropanoyloxy)pent-4-enoic Acid (3.4). On the Schlenk line under nitrogen, 2-bromopropionyl bromide (12.25 mL, 117 mmol) and dichloromethane (329 mL) were added to a 2-neck round bottom flask (1L) and cooled to 0 °C. A solution of triethylamine (16.3 mL, 11.82 g, 117 mmol) and 2-hydroxypent-4-enoic acid (13.59 g, 117 mmol) in dichloromethane (120 mL) was added dropwise to the round bottom flask. The solution was allowed to stir at 25 °C for 24 hours. The organic phase was washed three times with water (100 mL) and washed once with brine (300 mL). The organic phase was washed three times from the aqueous phase using dichloromethane (100 mL). The combined organic phases were dried over magnesium sulfate, filtered, and concentrated to give a dark yellow oil as a mixture of diastereomers (29 g, quant.). The product was used without purification. ^1H NMR (500 MHz, CDCl_3), a mixture of two diastereomers that could not be resolved. δ 10.92 (s, 1H), 5.88 – 5.68 (m, 1H, CH), 5.19 (dd, $J = 2.5, 1.3$ Hz, 1H, CH), 5.13 (t, $J = 9.4, 8.1, 3.0$ Hz, 2H, CH_2), 4.54 – 4.28 (q, 1H, CH), 2.77 – 2.42 (m, 2H, CH_2), 1.82 (d, $J = 9.9, 7.6, 5.5$ Hz, 3H, CH_3); ^{13}C (150 MHz, CDCl_3): δ 175.58, 174.44, 169.87, 169.59, 131.48, 131.41, 119.46,

72.64, 72.55, 39.96, 39.71, 39.30, 35.28, 21.86, 21.65; HRMS (ESI+) Calcd. for $C_8H_{12}BrO_4$ $[M+H]^+$: 250.99190; Found 250.99164. Spectroscopic data matches what is reported in the literature.¹⁸

Synthesis of 3-Allyl-6-methyl-1,4-dioxane-2,5-dione (3.5). A solution of 2-(2-Bromopropanoyloxy)pent-4-enoic acid (25.0 g, 99.6 mmol) in DMF (800 mL) was added dropwise using an addition funnel over 5 hours to a slurry of sodium carbonate (4.80 g, 43.3 mmol) in DMF (3200 mL) in a 3-neck round bottom flask (5L) at 0 °C. The reaction slurry was stirred at 25 °C for 24 hours. The reaction solution was concentrated, and acetone was added to precipitate the sodium salts. The mixture was filtered and concentrated to give a yellow oil. The product was purified by flash column chromatography using elution gradient as a mixture of diastereomers (100% hexanes to 70% hexanes and 30% ethyl acetate, $KMnO_4$ stain) to give a colorless oil (R_f = 0.37 in 70/30 hexanes/EtOAc, 9.3 g, 55%). 1H NMR (600 MHz, $CDCl_3$) diastereomers could not be resolved. δ 5.82 (m, J = 17.1, 10.2, 7.0 Hz, 1H, CH), 5.33 – 5.18 (m, 2H, CH_2), 5.08 – 4.99 (m, 1H, CH), 4.95 (d, J = 7.3, 4.5 Hz, 1H, CH), 2.85 – 2.66 (m, 2H, CH_2), 1.65 (d, J = 21.1, 6.9 Hz, 3H, CH_3).; ^{13}C NMR (150 MHz, $CDCl_3$): δ 167.52, 166.65, 166.06, 165.30, 130.76, 130.00, 121.01, 119.83, 76.01, 75.12, 72.74, 72.25, 36.09, 33.99, 17.59, 15.65; IR (neat) 1752.40, 1227.14, 1072.27 cm^{-1} ; HRMS (ESI+) Calcd. for $C_8H_{11}O_4$ $[M+H]^+$: 171.06573; Found 171.06503. Spectroscopic data matches what is reported in the literature.¹⁸

Synthesis of 3-methyl-6-(5-(oxiran-2-yl)pent-2-en-1-yl)-1,4-dioxane-2,5-dione (3.8) Compound **3.5** (2.000 g, 11.75 mmol) and 1,2-epoxy-5-hexene (**3.6**) (4.00 mL, 3.480 g 35.5 mmol) were dissolved in dichloromethane (30 mL) in a 2-neck round

bottom flask (50 mL). The solution was degassed by freeze-pump-thaw three times. Then Zhan's catalyst (**3.7**) (220 mg, 0.35 mmol) was added as a solid in one portion via the side arm. The reaction solution was stirred for 24 hours at 25 °C with brief exposure to vacuum periodically until the TLC of the reaction mixture indicated no further conversion. The crude reaction mixture was purified by column chromatography using a gradient of solvents (15% ethyl acetate and 85% hexanes to 30% ethyl acetate and 70% hexanes) to afford a light brown oil as a mixture of diastereomers ($R_f = 0.30$ and 0.31 , 1.8 g, 65%) Reaction followed using 30% hexanes/70% ethyl acetate and staining with KMnO_4 . The unreacted starting material was also collected from the column ($R_f = 0.73$, 0.50 g, 30%). ^1H NMR (500 MHz, CDCl_3) δ 5.71 (dt, $J = 19.0, 10.0$ Hz, 1H, CH), 5.53 (dt, $J = 24.1, 8.1$ Hz, 1H, CH), 5.08 – 4.94 (m, 1H, CH), 4.90 (dd, $J = 7.0, 4.6$ Hz, 1H, CH), 2.91 (dd, $J = 6.3, 3.8$ Hz, 1H, CH), 2.74 (m, 3H, CH and CH_2), 2.48 (dd, $J = 8.7, 5.9$ Hz, 1H, CH), 2.38 – 2.08 (m, 2H, CH_2), 1.78 – 1.42 (m, 5H, CH_3 and CH_2); ^{13}C NMR (150 MHz, CDCl_3): δ 167.43, 166.54, 135.02, 122.87, 75.59, 72.31, 51.77, 47.08, 33.09, 31.99, 29.03, 15.84; IR (neat) 2923.55, 1758.82, 1274.80, 1231.34; HRMS (ESI+) Calcd. for $\text{C}_{12}\text{H}_{16}\text{O}_5$ $[\text{M}+\text{H}]^+$: 241.10760; Found 241.10853.

Synthesis of 3-methyl-6-(5-(oxiran-2-yl)pentyl)-1,4-dioxane-2,5-dione (3.9**)**

Rhodium on activated carbon (170 mg) and ethyl acetate (10 mL) was added to a 2-neck, 50 mL, round bottom flask, equipped with a septum and a 3-way joint, under nitrogen. The solution was degassed by brief exposure to vacuum and backfilling with nitrogen three times. Compound **3.8** (1.7 g, 7.1 mmol) was then added to the flask via the side arm under positive pressure nitrogen. The flask was evacuated and backfilled with hydrogen (1 atm) from a balloon through the 3-way joint three times. The reaction was allowed to

stir under hydrogen for 4 hours at 25 °C and monitored by staining with KMnO₄ until the compound no longer stained, indicating the absence of alkenes. The reaction mixture then filtered through celite and concentrated to afford a colorless oil that was >95% pure with a small amount of an aldehyde impurity (1.6 g, 96%). ¹H NMR (600 MHz, CDCl₃) diastereomers could not be resolved. δ 5.01 (m, *J* = 11.9, 6.9 Hz, 1H, CH), 4.93 – 4.82 (m, 1H, CH), 2.87 (s, 1H, CH), 2.72 (dd, *J* = 4.9, 4.0 Hz, 1H, CH), 2.43 (dd, *J* = 5.0, 2.7 Hz, 1H, CH), 2.18 – 1.87 (m, 2H, CH₂), 1.65 (d, *J* = 14.8, 7.6 Hz, 3H, CH₃), 1.61 – 1.27 (m, 8H, 4 CH₂); ¹³C NMR (150 MHz, CDCl₃); IR (neat) 2931.95, 2860.66, 1758.31, 1450.59, 1233.69; HRMS (ESI+) Calcd. for C₁₂H₁₈O₅ [M+H]⁺:243.12329; Found 243.12325.

Representative procedure for redox-triggered polymerization of 3.9. In the glovebox, a 7 mL vial with a stir bar was charged with **3.9** (100 mg, 0.413 mmol) as a solution in dichloromethane (1.36 mL). In a separate 4 mL vial, a solution of **3.1** (5.5 mg, 8.2 mmol) in dichloromethane (1 mL) was prepared and immediately added to the solution of **3.9**. The reaction was allowed to stir at room temperature for 24 hours. Ferrocenium hexafluorophosphate (2.7 mg, 8.2 mmol) was then added the vial, and the reaction was stirred for four hours at room temperature. The reaction was brought out of the glove box and concentrated (quantitative). To obtain pre-crosslinked polymer, the reaction mixture was removed from glovebox prior to oxidation and dried *in vacuo*.

Procedure for redox-triggered polymerization of 3.9 starting with 3.2. In the glovebox, a 7 mL vial with a stir bar was charged with **3.9** (100 mg, 0.413 mmol) as a solution in dichloromethane (1.00 mL). In a separate 4 mL vial, a solution of **3.2** (6.7 mg, 8.2 mmol) in dichloromethane (1.0 mL) was prepared and immediately added to the

solution of **3.9**. The reaction was allowed to stir at room temperature for 48 hours. Cobaltocene (1.6 mg, 8.2 mmol) was then added the vial, and the reaction was stirred for four hours at room temperature. The reaction was concentrated (quantitative) in the glovebox. To obtained pre-crosslinked polymer, the reaction mixture was removed from glovebox prior to reduction and dried *in vacuo*.

Representative procedure for redox-triggered copolymerization of 3.9 and lactide. In a 7 mL vial with a stir bar was added **3.9** (60.6 mg, 250 mmol) and lactide (36 mg, 0.25 mmol), which was dissolved in dichloromethane (0.5 mL). In a separate 4 mL vial, **3.1** (6.7 mg, 10 mmol) was dissolved in dichloromethane (1 mL), and the catalyst solution was added to the solution containing the monomers. The reaction was allowed to stir at room temperature for 24 hours. Ferrocenium hexafluorophosphate (13.3 mg, 10.0 mmol) was then added to the vial, and the reaction was stirred for 4 hours at room temperature. The solvent was removed concentrated to give an insoluble polymer mass. To obtained pre-crosslinked polymer, the reaction mixture was removed from glovebox prior to oxidation and dried *in vacuo*.

Procedure for redox-triggered copolymerization of 3.9 using ferrocenium hexafluorophosphate. In the glovebox, a 7 mL vial with a stir bar was charged with **3.9** (121 mg, 0.50 mmol) as a solution in dichloromethane (1.0 mL). In a separate 4 mL vial, a solution of **3.1** (6.7 mg, 10 mmol) in dichloromethane (1.0 mL) was prepared and immediately added to the solution of **3.9**. The reaction was allowed to stir at room temperature for 24 hours. The reaction was then removed from the glovebox, and the polymer was precipitated into methanol. The resulting polyester **7** was brought back into the box and dissolved in dichloromethane (1.0 mL). Ferrocenium hexafluorophosphate

(3.3 mg, 10 mmol) was then dissolved in dichloromethane (0.5 mL) and added to the vial, and the reaction was stirred for twenty-four hours at room temperature. The reaction was brought out of the glove box and concentrated (quantitative).

Procedure for copolymerization of lactide and 3.5-sat. In a 7 mL vial with a stir bar was added lactide (36 mg, 250 mmol) and **3.5** (43 mg, 250 mmol), which was dissolved in dichloromethane (0.5 mL). In a separate 4 mL vial, **3.1** (6.7 mg, 10 mmol) was dissolved in dichloromethane (1 mL), and the catalyst solution was added to the solution containing the monomers. The reaction was allowed to stir at room temperature for 24 hours. The solvent was removed and dried *in vacuo*.

Representative procedure for swelling experiments. A known mass of polymer (5-10mg) was added to a vial and submerged in tetrahydrofuran (THF). After soaking for 24 hours, THF was carefully removed, and swollen polymer was briefly dried to remove surface solvent. Polymer vial was reweighed, and mass of absorbed THF was calculated. This was repeated three times.

Representative procedure for degradation experiments. A known mass of cross-linked polymer was added to a vial and stirred in 10% hydrochloric acid in tetrahydrofuran for 36h. This time and acid concentration were determined to degrade polyester linkages fully. This yielded an oligomeric polyether with a $M_n = 500$ and a polydispersity of 2.0 and an average yield above 85%.

3.6 References

- (1) Finch, C. a. Cross-Linked Polymers: Chemistry, Properties and Applications. American Chemical Society Symposium Series No. 367. Edited by R. A. Dickie, S. S. Labana and R. S. Bauer, American Chemical Society, Washington DC, 1988, *Br. Polym. J.* **1990**, 22 (4), 359–359.
- (2) Gómez-Mascaraque, L. G.; Méndez, J. A.; Fernández-Gutiérrez, M.; Vázquez, B.; San Román, J. Oxidized Dextrins as Alternative Crosslinking Agents for Polysaccharides: Application to Hydrogels of Agarose-Chitosan. *Acta Biomater.* **2014**, 10 (2), 798–811.
- (3) Shalaby, S. W.; Salz, U. *Polymers for Dental and Orthopedic Applications*; CRC Press, 2006; Vol. 2006.
- (4) Maitra, J.; Shukla, V. K. Cross-Linking in Hydrogels - A Review. *Am. J. Polym. Sci.* **2014**, 4 (2), 25–31.
- (5) Raut, N. S.; Deshmukh, P. R.; Umekar, M. J.; Kotagale, N. R. Zinc Cross-Linked Hydroxamated Alginates for Pulsed Drug Release. *Int. J. Pharm. Investig.* **2013**, 3 (4), 194–202.
- (6) Song, S. W.; Jeong, Y.; Kwon, S. Photocurable Polymer Nanocomposites for Magnetic, Optical, and Biological Applications. *IEEE J. Sel. Top. Quantum Electron.* **2015**, 21 (4), 324–335.
- (7) Tamboli, S. M.; Mhaske, S. T.; Kale, D. D. *Properties of High-Density Polyethylene Filled with Waste Crosslinked Foam.*

- (8) Chruściel, J. J.; Leśniak, E. Modification of Epoxy Resins with Functional Silanes, Polysiloxanes, Silsesquioxanes, Silica and Silicates. *Prog. Polym. Sci.* **2015**, *14*, 67–121.
- (9) Biernesser, A. B.; Chiaie, K. R. D.; Curley, J. B.; Byers, J. A. Block Copolymerization of Lactide and an Epoxide Facilitated by a Redox Switchable Iron-Based Catalyst. *Angew. Chemie - Int. Ed.* **2016**, *55* (17), 5251–5254.
- (10) Wang, X.; Thevenon, A.; Brosmer, J. L.; Yu, I.; Khan, S. I.; Mehrkhodavandi, P.; Diaconescu, P. L. Redox Control of Group 4 Metal Ring-Opening Polymerization Activity toward L -Lactide and ϵ -Caprolactone. *J. Am. Chem. Soc.* **2014**, *136* (32), 11264–11267.
- (11) Teator, A. J.; Lastovickova, D. N.; Bielawski, C. W. Switchable Polymerization Catalysts. *Chem. Rev.* **2016**, *116* (4), 1969–1992.
- (12) Blanco, V.; Leigh, D. A.; Marcos, V. Artificial Switchable Catalysts. *Chem. Soc. Rev.* **2015**, *44* (15), 5341–5370.
- (13) Guillaume, S. M.; Kirillov, E.; Sarazin, Y.; Carpentier, J. F. Beyond Stereoselectivity, Switchable Catalysis: Some of the Last Frontier Challenges in Ring-Opening Polymerization of Cyclic Esters. *Chem. - A Eur. J.* **2015**, *21* (22), 7988–8003.
- (14) Dechy-Cabaret, O.; Martin-Vaca, B.; Bourissou, D. Controlled Ring-Opening Polymerization of Lactide and Glycolide. *Chem. Rev.* **2004**, *104* (12), 6147–6176.
- (15) Lunt, J. Large-Scale Production, Properties and Commercial Applications of Polylactic Acid Polymers. *Polym. Degrad. Stab.* **1998**, *59* (1–3), 145–152.

- (16) Dove, A. P. Controlled Ring-Opening Polymerisation of Cyclic Esters: Polymer Blocks in Self-Assembled Nanostructures. *Chem. Commun.* **2008**, No. 48, 6446–6470.
- (17) Albertsson, A. C.; Varma, I. K. Recent Developments in Ring Opening Polymerization of Lactones for Biomedical Applications. *Biomacromolecules* **2003**, *4* (6), 1466–1486.
- (18) Zou, J.; Hew, C. C.; Themistou, E.; Li, Y.; Chen, C. K.; Alexandridis, P.; Cheng, C. Clicking Well-Defined Biodegradable Nanoparticles and Nanocapsules by UV-Induced Thiol-Ene Cross-Linking in Transparent Miniemulsions. *Adv. Mater.* **2011**, *23* (37), 4274–4277.
- (19) Chatterjee, A. K.; Choi, T. L.; Sanders, D. P.; Grubbs, R. H. A General Model for Selectivity in Olefin Cross Metathesis. *J. Am. Chem. Soc.* **2003**, *125* (37), 11360–11370.
- (20) Garber, S. B.; Kingsbury, J. S.; Gray, B. L.; Hoveyda, A. H. Efficient and Recyclable Monomeric and Dendritic Ru-Based Metathesis Catalysts. *J. Am. Chem. Soc.* **2000**, *122* (34), 8168–8179.
- (21) Biernesser, A. B.; Li, B.; Byers, J. A. Redox-Controlled Polymerization of Lactide Catalyzed by Bis(imino)pyridine Iron Bis(alkoxide) Complexes. *J. Am. Chem. Soc.* **2013**, *135* (44), 16553–16560.
- (22) Wang, T.; Chen, J. W.; Li, Z. Q.; Wan, P. Y. Several Ferrocenium Salts as Efficient Photoinitiators and Thermal Initiators for Cationic Epoxy Polymerization. *J. Photochem. Photobiol. A Chem.* **2007**, *187* (2–3), 389–394.

- (23) Odian, G. *Principles of Polymerization*; John Wiley & Sons, Inc.: Hoboken, NJ, USA, 2004.
- (24) Wilkinson, A. N.; Ryan, A. J. *Polymer Processing and Structure Development*; Ryan, A. J., Wilkinson, A. N., Eds.; Kluwer Academic Publishers: Dordrecht, The Netherlands, 1998.
- (25) Fink, J. K. Bismaleimide Resins. In *Reactive Polymers Fundamentals and Applications*; William Andrew Publishing: Oxford, 2013; pp 269–301.
- (27) Becker, J. M.; Pounder, R. J.; Dove, A. P. Synthesis of Poly(lactide)s with Modified Thermal and Mechanical Properties. *Macromol. Rapid Commun.* **2010**, *31* (22), 1923–1937.
- (28) Quynh, T. M.; Mitomo, H.; Nagasawa, N.; Wada, Y.; Yoshii, F.; Tamada, M. Properties of Crosslinked Polylactides (PLLA & PDLA) by Radiation and Its Biodegradability. *Eur. Polym. J.* **2007**, *43* (5), 1779–1785.
- (29) Bee, S. T.; Ratnam, C. T.; Sin, L. T.; Tee, T. T.; Wong, W. K.; Lee, J. X.; Rahmat, A. R. Effects of Electron Beam Irradiation on the Structural Properties of Polylactic Acid/polyethylene Blends. *Nucl. Instruments Methods Phys. Res. Sect. B Beam Interact. with Mater. Atoms* **2014**, *334*, 18–27.
- (30) Nijenhuis, A. J.; Grijpma, D. W.; Pennings, A. J. Crosslinked Poly (L-Lactide) and Poly (ϵ -Caprolactone). **1996**, *37* (13), 2783–2791.
- (31) Dickie, R. A.; Labana, S. S.; Bauer, R. S. Preface. In *Cross-linked polymers: Chemistry, Properties, and Applications*; American Chemical Society: Washington D.C., 1988; pp ix–ix.

- (32) Jin, F.; Hyon, S. H.; Iwata, H.; Tsutsumi, S. Crosslinking of poly(L-Lactide) by γ -Irradiation. *Macromol. Rapid Commun.* **2002**, *23* (15), 909–912.
- (33) Helminen, A. O.; Korhonen, H.; Seppala, J. V. Crosslinked Poly (Ester Anhydride)s Based on Poly(epsilon-Caprolactone) and Polylactide Oligomers. *J. Polym. Sci. Part A Polym. Chem.* **2003**, *41*, 3788–3797.
- (34) Chan, N.; Yee, N.; An, S. Y.; Oh, J. K. Tuning Amphiphilicity/temperature-Induced Self-Assembly and in-Situ Disulfide Crosslinking of Reduction-Responsive Block Copolymers. *J. Polym. Sci. Part A Polym. Chem.* **2014**, *52* (14), 2057–2067.

Chapter 4 : Mechanistic Investigation of Epoxide Polymerization by Cationic Bis(imino)pyridine Iron Bis(alkoxide) Complexes

4.1 Introduction

Epoxide opening reactions have been a prominent part of synthetic organic chemistry owing to the ease of epoxide synthesis and their reactivity for ring opening when exposed to various nucleophiles. These reactions afford many complex products depending on the nucleophile used.¹⁻⁴ Subsequently, the mechanisms of epoxide opening reactions have been widely studied for decades.¹ Epoxides serve as prominent monomers used to synthesize polyether materials due to the versatility and high ring strain associated with epoxide monomers.^{5,6} Polyether-based materials are commercially used for a wide variety of commercial “plastic” applications due to their unique, characteristic properties. Owing to the polymer C-O-C backbone, these materials exhibit high flexibility, low glass transition temperatures, and significant hydrophilicity dependent on the monomer.⁷ These properties do not belong to the analogous all-carbon counterparts, polyolefins. Epoxides such as ethylene oxide and propylene oxide can undergo polymerization that occurs by a variety of mechanisms including anionic (base-initiated),^{8,9} cationic (acid-initiated),^{10,11} and metal-catalyzed coordination-insertion polymerizations.^{7,12}

Throughout the development of the ring-opening polymerization of epoxides, iron-based catalysts have played a central role. In pioneering work, Baggett and Pruitt of Dow chemical developed the use of iron-based catalysts for the isospecific

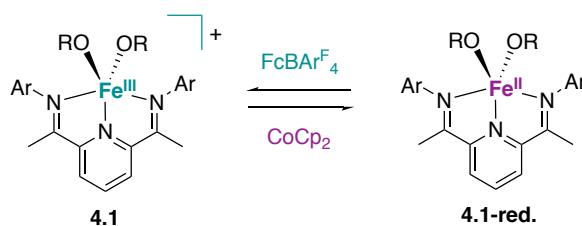
polymerization of propylene oxide.^{13–15} The combination of iron(III) chloride and propylene oxide used yielded a complex mixture of iron products that was not well defined but was nevertheless active for polymerization. Subsequently, a variety of iron-based hydrates with and without additional ligands have been used for epoxide polymerization.^{16,17} Despite the prominent use of iron-based catalysts for epoxide polymerization industrially, there has been much debate regarding the mechanism of polymerization. Through the hydrolysis of products from studies combining iron halide and alcohols, Borkovec and Colclough have shown that iron alkoxides are likely the active species for these polymerization reactions.^{17,18} However, for iron-based complex, catalyzed polymerizations several variations of the active site have been proposed ranging from monomeric, bimetallic, trinuclear, and even polymeric multimetallic species.^{19–22} Despite its important role in early developments for epoxide polymerization, to the best of our knowledge, a detailed kinetic analysis of epoxide polymerization catalyzed by a discrete iron complex has not been reported. Notably, kinetic studies have been done with a cobalt-based catalyst.²³

Since their original discovery, the use of iron-based catalysts for epoxide polymerization reactions has mostly remained dormant.^{16,18} In 2016, we reported the redox-switchable polymerization of epoxides using a cationic formally iron(III) complex (**4.1**). Notably, the reduced bis(imino)pyridine iron(II) bis(alkoxide) complex (**4.1-red.**) is inactive for epoxide polymerization.^{24–26} As discussed in Chapter 2, we have shown that diblock copolymers of poly(lactic acid) and poly(cyclohexene oxide) can be synthesized through a redox-switchable copolymerization (Figure 3.1) and applied to a redox-triggered cross-linking. We have recently been able to use electrochemistry to replace the

chemical redox reagents for this reaction.²⁷ Notably, the report by Miao is the first example where electrochemistry has been used to alter the chemoselectivity of a catalyst completely.

However, a limitation to the redox-switchable polymerization reactions catalyzed by bis(imino)iron complexes is that the epoxide polymerization does not have the characteristics of a living polymerization system (e.g., fast initiation, limited termination events, etc.). The non-living nature of this epoxide polymerization makes it difficult to synthesize multiblock copolymers with well-defined block lengths that would result from multiple redox-switching events. Moreover, there is modest control over the molecular weight of the polyether blocks obtained in these copolymers. Notwithstanding, this disadvantage does not affect the redox-triggered crosslinking discussed in Chapter 3. In an effort directed towards addressing these limitations, we explored the mechanism of the epoxide polymerization reaction catalyzed by iron-based catalysts. It is expected that this study will reveal the key features of the polymerization reaction that have thus far limited their use for the synthesis of multiblock copolymers with redox-switchable catalysis.

Scheme 4.1. Reversible reduction and oxidation of 4.1 and 4.1-red



Finally, the mechanistic features uncovered in this study provide valuable insights into how transition metal catalysts can affect epoxide-opening reactions in general. Such information will be invaluable for the continued development of transition metal-based

catalysts used for epoxide-opening reactions, which have broad utility for the assembly of biologically relevant small molecules and complex macromolecular architectures.

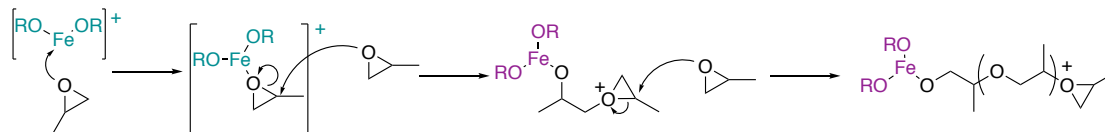
4.2 Cationic vs. Coordination-Insertion Mechanism

Three types of mechanisms that have been proposed for epoxide polymerization: anion initiated, cation initiated, and coordination-insertion mechanisms.^{1,3,5} Anionic initiated mechanisms begin with a nucleophilic attack on the epoxide by a negatively charged species followed by ring opening of the epoxide to form an alkoxide intermediate that then becomes the propagating nucleophile (Error! Not a valid bookmark self-reference).^{8,9} A cationic initiated pathway begins with Lewis acid activation of the epoxide and subsequent nucleophilic attack by another equivalent of epoxide to form an epoxonium intermediate that serves as the propagating species.^{10,11} Finally, metal-catalyzed coordination-insertion mechanisms first bind the epoxide to a metal alkoxide, which activates it for nucleophilic attack. Then a bound nucleophile either on the same metal center or a different metal center opens the epoxide to form a metal alkoxide that serves as the propagating species.^{7,12}

An anionic mechanism was quickly ruled out for the polymerization due to a control reaction where the epoxide is exposed to the relevant anion with an unreactive counter cation (tetrabutylammonium tetrakis[3,5-bis(trifluoromethyl)phenyl]borate). In this reaction, no conversion of the epoxide was seen even after multiple days. It is possible that heterolytic cleavage of an iron alkoxide occurs and the alkoxide acts as an anionic initiator for the polymerization. However, computational studies have shown that this is energetically disfavored, suggesting that this pathway might not be operative.

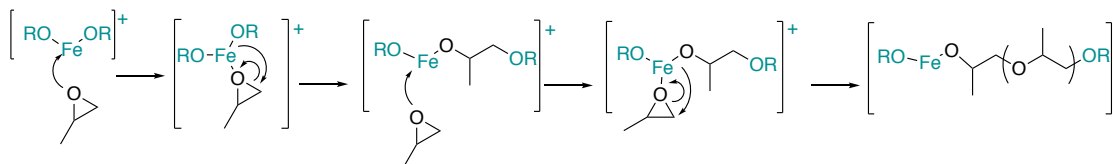
Scheme 4.2. Different epoxide ring-opening polymerization mechanisms

Cationic Ring-Opening Polymerization

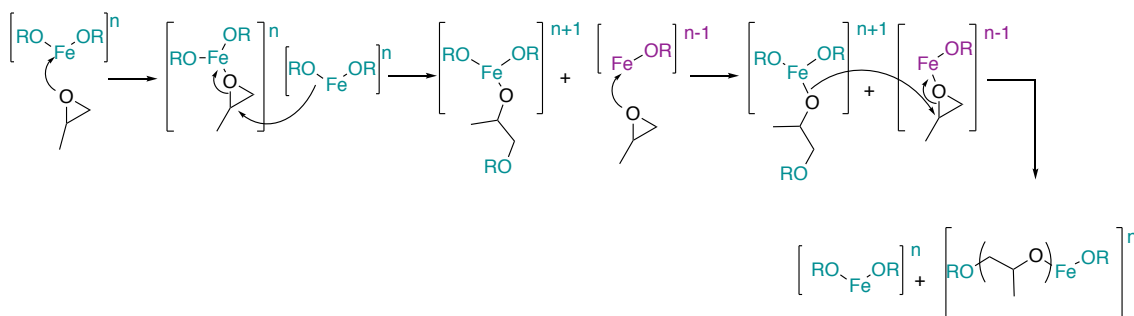


Coordination-Insertion Ring-Opening Polymerization

Monometallic



Bimetallic



With an anionic mechanism ruled out, we considered the possibility that the iron complex **4.1** used for this polymerization could proceed through a cationic initiated ring-opening polymerization mechanism (Scheme 4.2). For a cationic initiated process, the propagating species is an oxonium ion intermediate that does not involve the metal complex (Scheme 4.2). Therefore, once the polymerization reaction is initiated, it would not be affected by the subsequent reduction of the iron center of **4.1**. In contrast, for a coordination-insertion mechanism catalyzed by iron, propagation occurs directly on the iron center of **4.1**, so reduction of the iron complex would change the nature of the propagating species, which makes it more likely to halt propagation as seen in Figure 4.1. Based on the redox-control of the polymerization described in Chapter 2 and Figure 4.1,

it is unlikely that complex **4.1** was serving as a cationic initiator for the polymerization of epoxides. With an anionic mechanism ruled out, we considered the possibility that the iron complex **4.1** used for this polymerization could proceed through a cationic initiated ring-opening polymerization mechanism

Therefore, once the polymerization reaction is initiated, it would not be affected by the subsequent reduction of the iron center of **4.1**. In contrast, for a coordination-insertion mechanism catalyzed by iron, propagation occurs directly on the iron center of **4.1**, so reduction of the iron complex would change the nature of the propagating species, which makes it more likely to halt propagation as seen in Figure 4.1. Based on the redox-control of the polymerization described in Chapter 2 and Figure 4.1, it is unlikely that complex **4.1** was serving as a cationic initiator for the polymerization of epoxides.

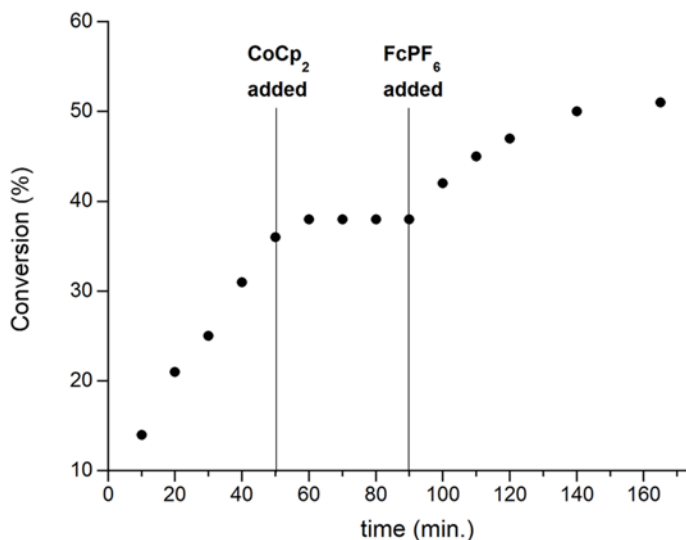


Figure 4.1. Redox-controlled polymerization of cyclohexene oxide in PhCl (0.91M) with **4.1** (2 mol%)

The polymerization of (*R*)-propylene oxide was used as a stereochemical probe in a common intermediate experiment to rule out a cation-initiated mechanism. Initiators for

cationic polymerization of epoxides (strong Lewis acids) were compared with **4.1** for the polymerization of *R*-propylene oxide. When (*R*)-propylene oxide was exposed to **4.1**, regio-irregular and stereoregular polyether was obtained (Figure 4.2a). These assignments were made using the analysis of the triads in the ^{13}C NMR previously assigned by Chisholm.²⁸ In contrast, a Lewis-acid catalyst (BF_3 etherate) or an iron-based catalyst that cannot support coordination-insertion (i.e., ferrocenium salts, Figure 4.2b) yielded polymers that were both regio- and stereo-irregular. The direct comparison shows very different microstructures of polyether being formed, ruling out a common intermediate. The stereochemical outcomes observed are inconsistent with complex **4.1** operating through a cationic-initiated polymerization mechanism. With the cationic initiated mechanism ruled out, we hypothesized that the polymerization might be proceeding through a coordination-insertion mechanism.

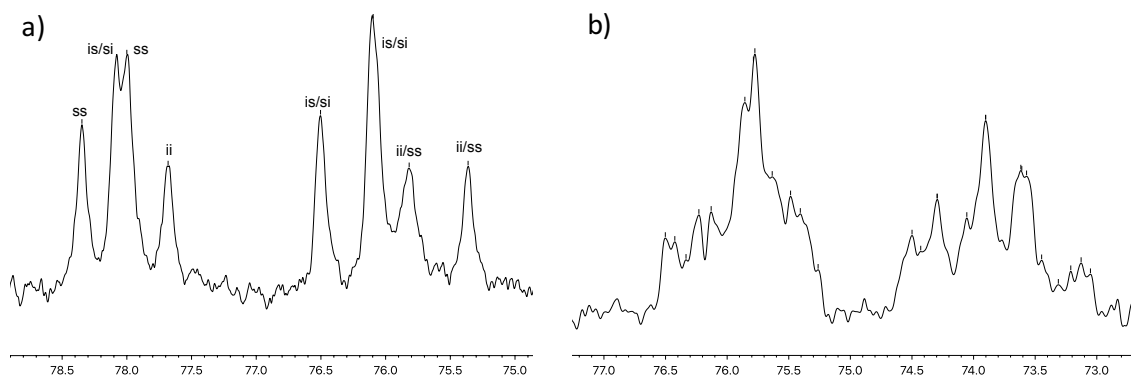


Figure 4.2. a) Assignment of triads in the ^{13}C NMR of the polymer obtained from polymerization with **4.2**. b) triad region of the ^{13}C NMR for polymer obtained from polymerization with ferrocenium hexafluorophosphate. i (iso) and s (syndio) indicate relative tacticity of triads

4.3 Anion effects

Extensive kinetic data were collected to determine if the mechanism was monometallic or bimetallic. Originally, hexafluorophosphate was used as the anion for the cationic iron complex **4.1**. Unfortunately, this counter anion precluded kinetic analysis because fast propagation and incomplete conversions prevented the collection of data over multiple half-lives. To address this issue, a less coordinating anion (tetrakis[3,5-bis(trifluoromethyl)phenyl]borate, BAr^{F_4}) was selected. The iron complex with this anion (**4.2**) allowed the collection of kinetic data over several half-lives (Figure 4.3). Collection of conversion versus time data revealed three features: a) a short but significant induction period, b) swift reaction kinetics at low to moderate conversions and c) inhibition that occurred at long reaction times. We have observed that the polymerization reaction is highly sensitive to the identity of the counteranion used. Reactions using the BAr^{F_4} anion result in the rapid consumption of the epoxide. The polymerization has a small induction period, and leads to nearly full conversion of epoxides, even at prolonged reaction times.

In contrast, reactions catalyzed by analogous iron alkoxide complexes with the hexafluorophosphonium anion (PF_6^-) resulted in a reaction that was initially fast, but that did not reach full conversion even at prolonged reaction times. Maximum conversion of 50-70% was observed, which depended on the initial concentration of the epoxide monomer: higher ultimate conversions were observed for reactions carried out at larger initial concentrations of the monomer. Catalyst decomposition in these reactions was ruled out because when a second aliquot of the monomer was added to the mixture, the epoxide polymerization reaction occurred at a similar rate as observed initially. The

addition of the second aliquot of epoxide leads to similar ultimate conversion. These results are best explained by the better coordinating ability of the PF_6^- anion compared to $[\text{BAr}^{\text{F}}_4]^-$ anion. Consistent with this hypothesis was reactions catalyzed by iron-based complexes with the tetrafluoroborate anion (BF_4^-), which were completely inactive in the polymerization reaction.^{29,30} BF_4^- is a more strongly coordinating anion than PF_6^- and, consequently, it can completely inhibit epoxide polymerization. In addition to affecting final conversion, we hypothesized that an anion binding equilibrium could be contributing to the induction periods that were commonly observed in these reactions.

To probe the anion effect on epoxide polymerization, we collected kinetic data with different amounts of BAr^{F}_4 anion using tetrabutylammonium BAr^{F}_4 ($[\text{Bu}_4\text{N}][\text{BAr}^{\text{F}}_4]$) as the source for exogenous anion (Figure 4.3). As can be seen from Figure 4.3, it was clear that anion binding played a role in the induction period; more anion led to a prolonged induction period. Figure 4.3 is consistent with anion binding being an essential contributor to the activity of the catalyst. In the future, an even less coordinating anion may be able to reduce the induction period further.

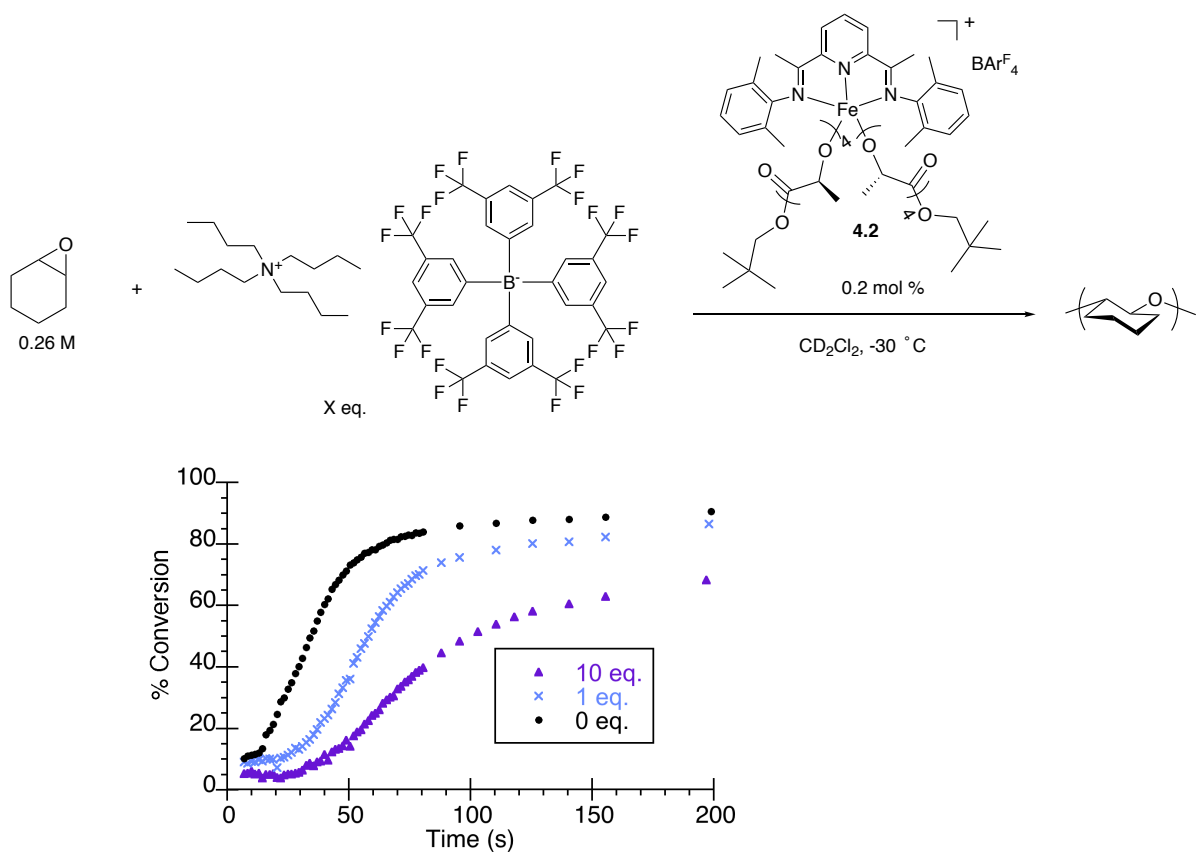


Figure 4.3. Kinetic data of cyclohexene oxide polymerization with different equivalents of BAr^{F}_4

4.4 Kinetic Analysis

To distinguish whether the polymerization reaction proceeded through a monometallic or bimetallic coordination/insertion mechanism, we turned to detailed kinetic analysis of the reaction by ^1H NMR spectroscopy.^{19–22} The goal of this study was to determine the kinetic order in epoxide and the iron-based catalyst so that a monometallic coordination-insertion mechanism could be distinguished from a bimetallic mechanism. Additionally, we hoped to determine if the polymerization was proceeding through a monometallic or bimetallic active species since both are common in other

epoxide homo- and co-polymerizations.³¹ As a result of complex kinetics, establishing the order of the reaction in the monomer and the catalyst was not straightforward.

We have found that aliphatic alkoxide initiators lead to less complicated kinetics associated with slow initiation rates that result from reactions with aromatic alkoxides.²⁴ While it is possible to synthesize cationic iron(III) catalysts with aliphatic alkoxide initiators,³² these compounds are susceptible to impurities making them difficult to obtain reproducibly. The complex was first initiated with a few units of L-lactide in the formally Fe(II) state and then oxidized to avoid these sensitive compounds (complex **4.2**). The iron(III) complexes are less prone to decomposition when lactide is inserted into the aliphatic iron(II) alkoxide before catalyst oxidation. We hypothesize that the binding of the ester carbonyl is protecting the iron center from deleterious side reactions. Moreover, such an initiator is most relevant to understand best how the catalyst behaves after a redox-switch in redox-switchable copolymerizations of lactide and epoxides. **4.2** proceeded at fast rates, reaching nearly full conversion in under two minutes at -30 ° C. The data did not fit well to any of the simple integrated rate laws for zero, first, or second-order dependence in epoxide (Figure 4.4a and b), which is likely due to the significant induction period and inhibition stages of the reaction. Considering the part of the reaction where epoxide is converting the most, second-order dependence fits are best. This initial analysis led us to conclude that the reaction is second-order in epoxide. Kinetic modeling will be discussed later that supports this conclusion.

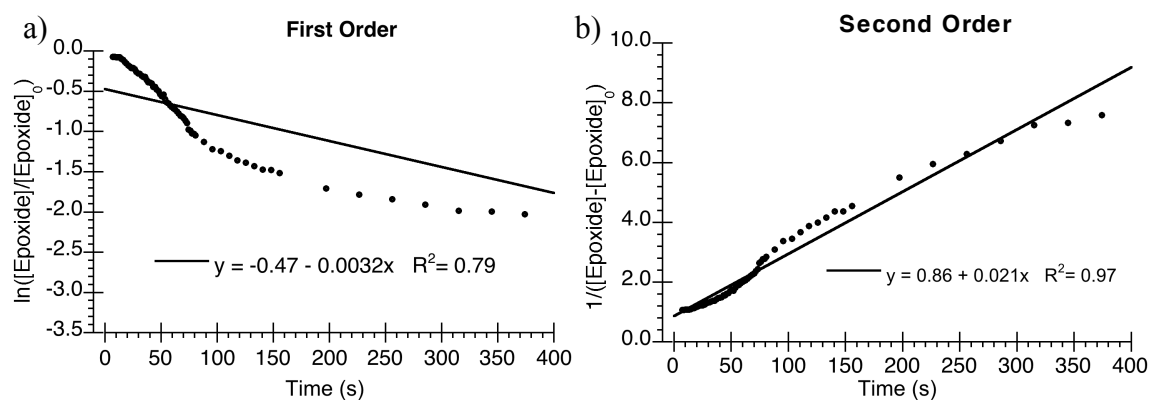


Figure 4.4. Kinetic data for the polymerization of cyclohexene oxide using 0.2 mol % of complex 4.2 in deuterated dichloromethane at -30 °C

Despite this complication, attempts were made to determine the order of the reaction in the iron catalyst three different ways. Firstly, third order apparent rate constants (k_{obs}) obtained from second order plots akin to **Figure 4.4c** were collected from reactions carried out at four different concentrations of the iron-based catalyst. Plots of k_{obs} of each run versus the concentration of **4.2** resulted in a non-zero slope straight line, suggesting that the reaction is first order in iron. Plots of $\log(k_{obs})$ vs. $\log[Fe]$ gave a slope of 1.04, which is also consistent with a reaction that is first order in iron. Lastly, the Burés method³³ was used to evaluate the reaction course and determine the order of the reaction in the iron-based complex. Unlike the other methods, this method does not require extracting observed rate constants and can be applied to reactions that are complicated by induction periods and product inhibition (such as this one).³³ Based on this method, conversion is plotted against a timescale that is normalized for catalyst concentration (Time X [Cat]ⁿ) where “n” is the order of the reaction. As was observed with the other two methods, the excellent overlap of the data was observed when n=1 was used, which is most consistent with a reaction that is first-order in iron (**Figure 4.5**).

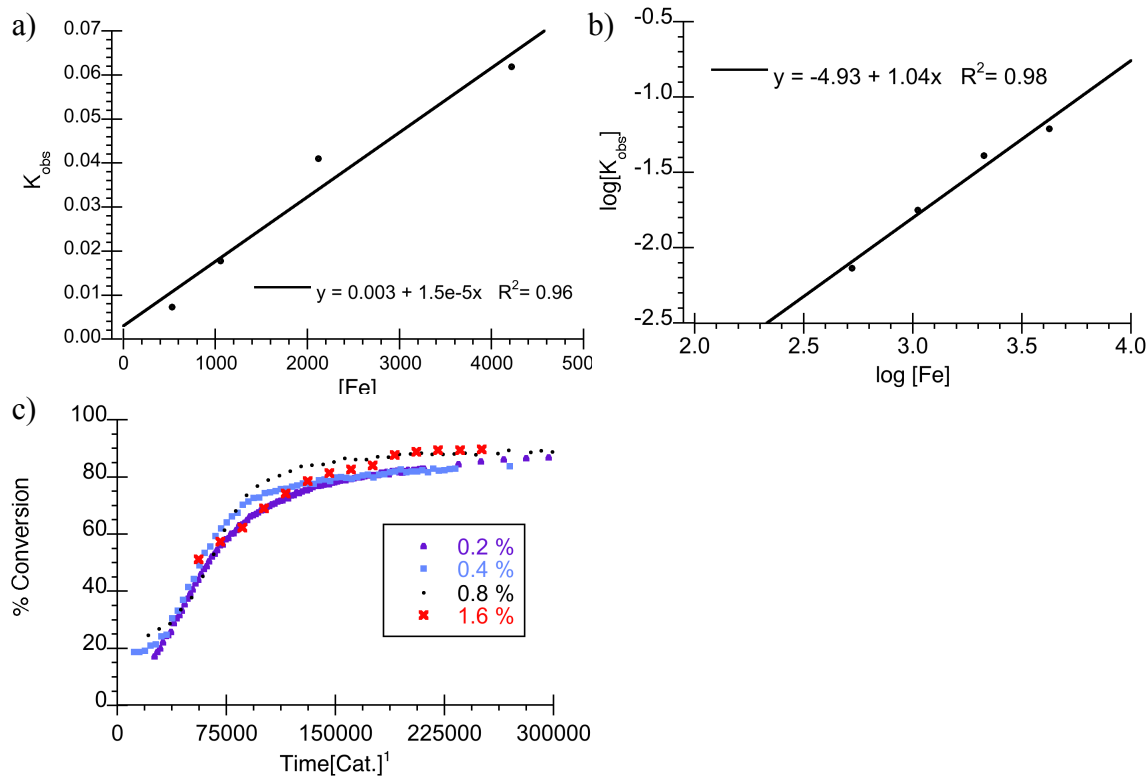


Figure 4.5. Determination of order in iron for cyclohexene oxide polymerization using x mol % of complex 4.2 in deuterated dichloromethane at $-30\text{ }^{\circ}\text{C}$

4.5 Kinetic Modeling

Due to the uncertainty of the second order fit for epoxide concentration, we turned to kinetic modeling with the program COPASI (Complex Pathway Simulator).³⁴ This program allowed us to develop a kinetic model to support a second-order dependence on epoxides for the polymerization. As illustrated in Figure 4.6 we were unable to get a good fit using a model that was first-order in epoxide. Subsequently, we were able to get a good fit using a second-order model. Figure 4.6 shows the best fits obtained for these two models and supports a mechanism that is second-order in epoxide.

While these data demonstrate that the polymerization reaction is first-order in the iron-based catalyst and is suggestive of a reaction that is second-order in epoxide, the kinetic data does not rigorously rule out the possibility for a bimetallic reaction

mechanism in which the catalyst undergoes irreversible aggregation prior to epoxide coordination and insertion.

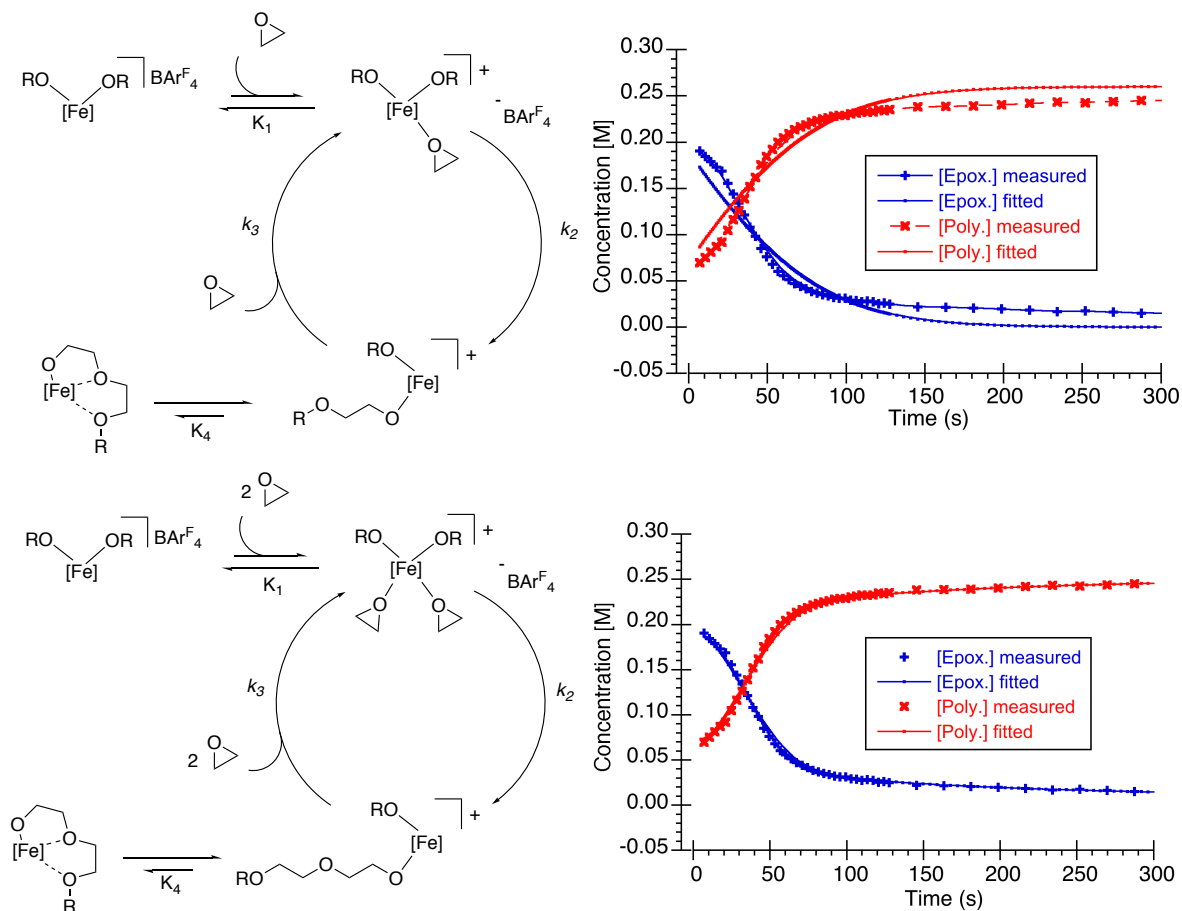


Figure 4.6. Kinetic modeling of 1st order (top: goodness of fit = $1.4e^{-7}$) versus 2nd order (bottom: goodness of fit = $5.4e^{-9}$) in monomer using COPASI. Intermediates shown are used to illustrate the kinetic model used to obtain these fits

It is possible that an iron-based monomer/dimer equilibrium could be a contributing factor to the induction period observed during this reaction. A bimetallic mechanism is important to consider given the long history of epoxide opening reactions that require two metal centers to participate in the ring opening event.^{1,2,12,31} Nevertheless, it is noteworthy that even if a similar mechanism were operative here, the second order dependence on epoxide would make it unique among epoxide opening reactions reported that proceed by a coordination-insertion mechanism.^{1,12} To

accommodate the second-order dependence in epoxide for a reaction mechanism involving two metals that is first-order in **4.2**, it is possible for an equivalent of epoxide to bind to each of the metal centers in a dimeric resting state. After epoxide coordination, simultaneous nucleophilic attack of a metal alkoxide from each of the metal centers onto bound epoxides on the adjacent metal center would result in ring-opening of each of the epoxides with the incorporation of one epoxide into two growing polymer chains and reformation of two new metal alkoxides.

On the other hand, the kinetic data presented above is consistent with a polymerization mechanism that involves a single metal site. One possible way that this configuration would lead to efficient ring opening would be if the cationic metal center pre-organizes the two epoxides about the metal center in a way that allows the iron alkoxide to adopt the proper trajectory for epoxide ring-opening. Whereas coordination of one epoxide would lead to a transition state with poor orbital overlap, incorporation of a second epoxide leads to a six-membered ring transition state that is better suited for alkoxide attack. Subsequent ring opening of both epoxides results in enchainment of two epoxides in one polymer chain and the reformation of a metal alkoxide. As was the case with the bimetallic mechanism, we are unaware of any other epoxide opening reaction proceeding by a similar mechanism.

4.6 Ligand Effects

To further study the epoxide polymerization mechanism, iron-catalysts with different bis(imino)pyridine ligands were explored (Table 4.1). In collaboration with Miao Qi, a small library of bis(imino)pyridine iron complexes was synthesized that containing different imine substituents, and these complexes were evaluated as pre-catalysts for

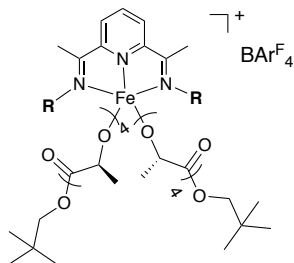
cyclohexene oxide polymerization. As was the case with compound **4.2**, the reaction profiles for these catalysts are most consistent with reactions that are second-order in epoxide. Evaluation of the observed rate constants obtained from the second-order plots revealed that the identity of the bis(imino)pyridine ligand had a notable influence on the rate of the reaction. Rate constants were obtained that spanned four orders of magnitude at room temperature.

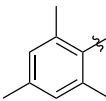
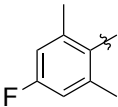
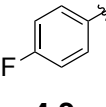
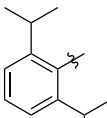
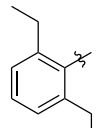
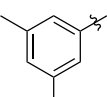
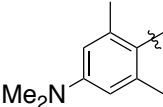
Further comparison of catalysts that demonstrated unusually fast reaction rates were achieved by the collection of kinetic information at -30 °C. Particularly efficient were catalysts that contained 2,6-disubstituted phenyl imines (e.g. **4.2a-d**). These catalysts typically demonstrated rates that were two to three orders of magnitude faster than unsubstituted phenyl imine **4.2i**, 4-fluorophenylimine **4.2g**, aliphatic imine **4.2h**, and two different 2,4,6-trisubstituted aryl imines (**4.2f** and **j**). These complexes reach high conversions in 200 seconds even at -30 °C.

Our current hypothesis is that subtle changes in the steric/electronic environment are affecting the dimer/monomer equilibrium and/or facilitating dissociation of one imine arm. A significant color difference is seen between the catalysts that consume cyclohexene oxide rapidly (complete in less than 200s) and those that are slow. The fast reacting catalysts are pale green, and the slower variants are dark purple (Figure 4.7). We have previously seen this change in color and have attributed it to dissociation of an imine arm from the bis(imino) pyridine ligand.³⁵ In addition to a change in coordination number, which alters the ligand field of the complex, imine arm dissociation disrupts the extended π -conjugation of the bis(imino)pyridine ligand, which affects the ability for the

ligand to serve as a π -accepting ligand. Such factors lead to changes in the UV-Vis spectrum that are manifested as a change in the color of the complex.

Table 4.1. Rate constants (k_{obs}) for different bis(imino)pyridine ligands using 0.2 mol % of the complex in deuterated dichloromethane at -30°C



R	Temp. ($^\circ\text{C}$)	k_{obs}	Catalyst	Temp. ($^\circ\text{C}$)	k_{obs}
 4.2	25	4.50×10^{-1}	 4.2f	25	2.08×10^{-4}
	-30	2.08×10^{-2}			
 4.2b	25	-	 4.2g	25	3.19×10^{-5}
	-30	1.10×10^{-2}			
 4.2c	25	9.78×10^{-2}	 4.2h	25	3.25×10^{-5}
	-30	9.80×10^{-3}			
 4.2d	25	7.72×10^{-2}	 4.2i	25	$<1.00 \times 10^{-5}$
	-30	6.71×10^{-3}			
 4.2e	25	3.44×10^{-2}	 4.2j	25	No Rxn

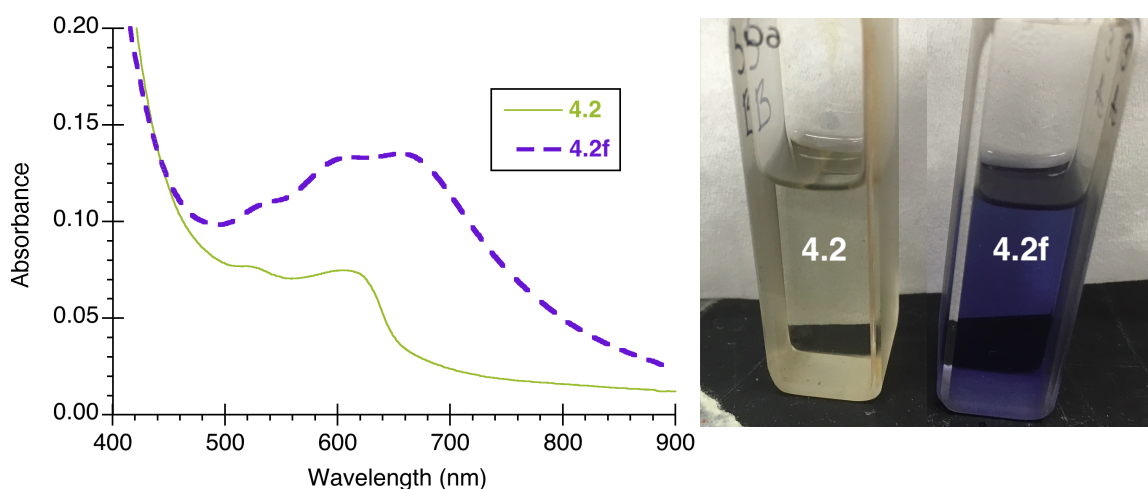


Figure 4.7. UV-vis data for 4.2 and 4.2f at 0.53 M in dichloromethane

The kinetics of complex 4.3 further supports that a complex containing a bidentate ligand gives a more rapid rate^{4.3}. Complex 4.3 contains an imino pyridine ligand, which is incapable of becoming tridentate and was expected to be a superior catalyst for epoxide polymerization. Consistent with this expectation were k_{obs} obtained from the pale green complex 4.3, which was over double the k_{obs} observed with the fastest complex containing the bis(imino)pyridine ligand (Figure 4.8). As was the case with the bis(imino)pyridine complexes, kinetic analysis for cyclohexene oxide polymerization catalyzed by 4.3 was most consistent with a reaction that is second order in epoxide. In contrast to 4.2, however, the order in 4.3 obtained from the Burés method was 0.5, which suggests that a catalyst dimer-to-monomer equilibrium competes with polymer propagation. The capacity for 4.3 to more readily dimerize is consistent with its more sterically open coordination environment in comparison to the bis(imino)pyridine ligands (e.g. 4.2). That the reaction is 0.5 order in 4.3 also suggests that the dimeric structure lies *off* the catalytic cycle and is inconsistent with a bimetallic mechanism for 4.2. Based on this kinetic data, we have adjusted our proposed mechanism so that it has two off-cycle

equilibrium steps (**Scheme 4.3**). We have been able to fit all relevant data with this model and even saw an enhancement of our already good fit in COPASI. Importantly, we were unable to fit the data from complex **4.3** to a model without a dimer/monomer equilibrium.

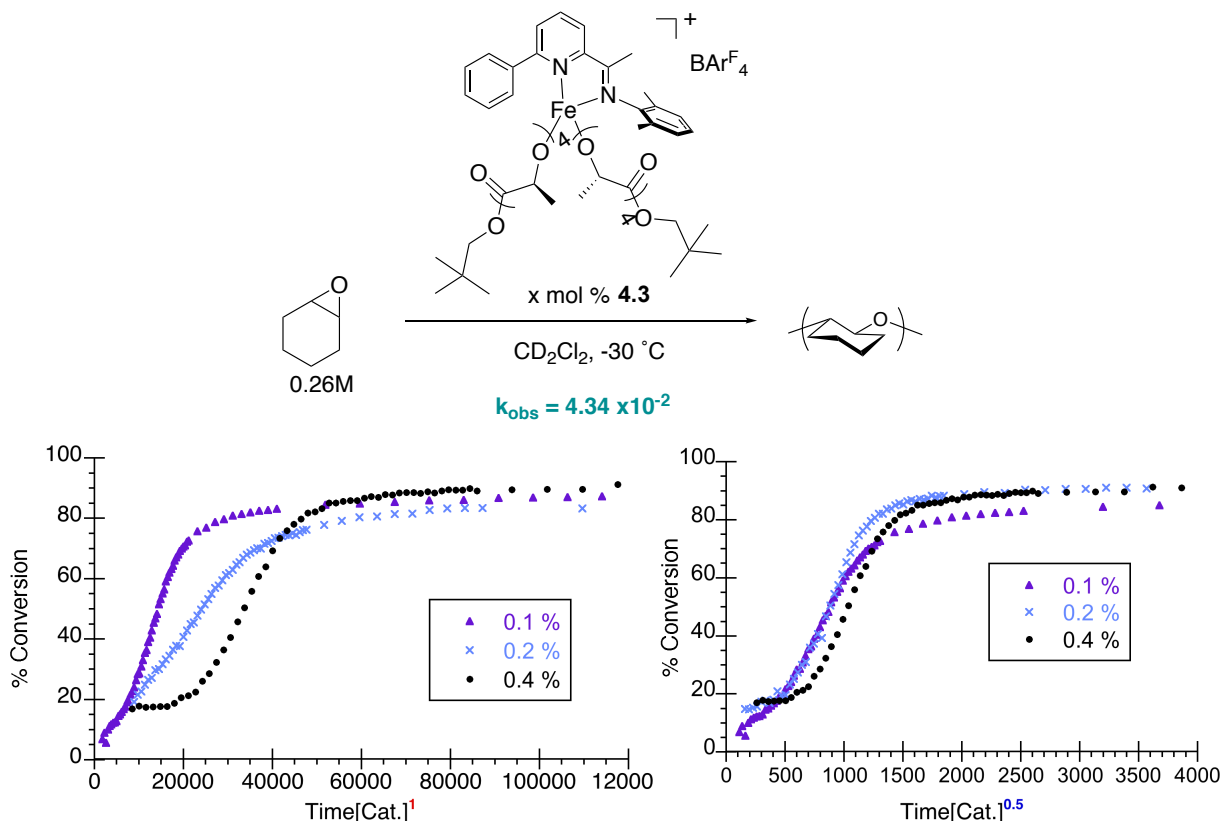
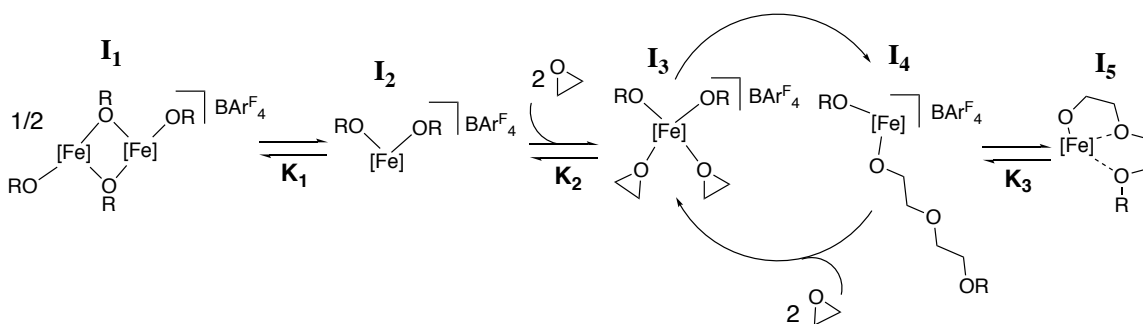


Figure 4.8. Kinetic data and determination of the order in the catalyst for complex **4.3**

Based on this kinetic data, we have proposed a unified mechanism that has three off-cycle equilibrium steps: two that predominate early on in the reaction and involve monomer-dimer dissociation (K_1) as well as imine arm and anion dissociation (K_2) and a third involving product inhibition that predominates at high conversion (K_3). The propagation steps involve simultaneous enchainment of two epoxide molecules (k_3) followed by rapid binding of two additional equivalents of epoxides (k_4) (**Scheme 4.3**). At this point, the data supports a dimer/monomer equilibrium that favors the monomeric iron species under

reaction conditions when epoxide is present. From the monomeric species, the initiation step is complicated and most likely involves a combination of anion dissociation, epoxide coordination, and arm dissociation due to the observations that this step is affected by anion concentration, epoxide concentration, and ligand identity, respectively. Based on the kinetic modeling, it is likely that this equilibrium greatly favors the reverse reaction. Favoring the reverse reaction would mean that the active catalytic species is slowly entering the cycle. This difference between initiation rate and propagation is one factor that could be leading to the somewhat broad molecular weight dispersities we observe. Once in the catalytic cycle, the two propagating steps are irreversible with large rate constants, which leads to the steep conversions observed in the kinetic plots. Lastly, since the reactions do not go to complete conversion, we suspected that there is some inhibition equilibrium that could be attributed to a chelation effect of the growing polymer chain and/or the dissociated anion becoming competitive with the epoxide for binding to the iron-based complex and diminishing reactivity.

Scheme 4.3. Proposed mechanism for iron complex catalyzed epoxide polymerization



Results from the simulations are most consistent with a catalyst dimer to monomer equilibrium that favors the dimer (**Scheme 4.3, I₁**) in most cases. From the monomeric species (**Scheme 4.3, I₂**), the initiation step is further complicated by a combination of anion dissociation, epoxide coordination, and arm dissociation due to the observations that this step is affected by anion concentration, epoxide concentration, and ligand identity, respectively. Based on the kinetic modeling, these equilibrium steps greatly favor the off cycle species **I₂**. Such a scenario is consistent with the fact that the bis(imino)pyridine complex **4.2** demonstrated a first-order dependence on iron whereas the imino pyridine complex **4.3** demonstrated a 0.5 order in the catalyst. Regardless of whether K_1 or K_2 predominates, both catalysts demonstrate induction periods that are most consistent with the active catalytic species being slowly introduced in the cycle. Once in the catalytic cycle, the two propagating steps are irreversible with large rate constants. The irreversible and fast enchainment of the monomers and the second-order dependence on epoxide are consistent with the rapid consumption of monomer observed in the intermediate stage of the reaction. Lastly, since the reactions do not completely convert all of the monomer (95% max.), we suspected that there is some inhibition equilibrium (**Scheme 4.3, K₃**) that could be attributed to product inhibition, which may result from a chelation of the growing polymer chain that becomes competitive with the epoxide for binding to the iron complex.

4.7 Molecular Weight and Dispersity

Overall, for each of the polymerization reactions run there seems to be little effect on the molecular weight of the polymer obtained. All of the reactions produce polymers that are around 100 kg/mol \pm 20. Molecular weight vs. conversion data could not be

obtained due to the fast reaction rates and cold temperatures required for sampling. Additionally, none of the ligand substitutions resulted in a drop in molecular weight distribution (M_w/M_n). The difference between initiation rate and propagation is one factor that is likely leading to the somewhat broad dispersities and the poor molecular weight control that are characteristic features of all of the polymerization reactions (*vide infra*). However, we did notice a narrowing in dispersity from ~ 2.0 to ~ 1.5 when the temperature was raised from $-30\text{ }^\circ\text{C}$ to $40\text{ }^\circ\text{C}$, respectively. We believe elevated temperatures favor the monomer in the dimer/monomer equilibrium and reduce the induction period, getting one step closer to a living system. Kinetic modeling of kinetic data at different temperature will be used to support this hypothesis.

4.8 Conclusions

The study of epoxide polymerization by a family of cationic, bis(imino)pyridine iron(III) alkoxides presented above provides experimental evidence to support the proposed mechanism seen in **Scheme 4.3**. Notably, this is the first in-depth mechanistic investigation of iron-complex catalyzed epoxide polymerizations with a discrete catalyst. Through a combination of a stereochemical probe and the redox-switching capabilities of the reaction, a cationic initiated mechanism for the reaction could be ruled out in favor of an iron-catalyzed coordination-insertion type ring-opening polymerization mechanism. Kinetic analysis revealed an unusual second order dependency for the epoxide monomer and has a first-order dependence on the iron catalyst. Kinetic analysis for the related imino pyridine iron complex **4.3** revealed a half-order dependence on the catalyst, which was explained by a dimer/monomer equilibrium that competes with propagation. These two factors led to the conclusion that the polymerization operates through a monometallic

active species as opposed to a bimetallic species as has been seen in many cobalt catalyzed polymerizations²³ as well as chromium catalyzed hydrolysis reactions.² Modelling of the kinetic data revealed a unified mechanism for the polymerization reaction and provided explanations for the dramatic influence that the identity of the bis(imino)pyridine had on the rate of the reaction. Overall, We have elucidated mechanistic details about iron-catalyzed epoxide polymerization and have proposed, to our best knowledge, a unique mechanism that is second order in monomer and first order in the catalyst. These findings will aid in new catalyst design that will be invaluable for the development of new catalysts used for redox-switchable polymerization reactions.

4.9 Experimental

General Considerations. Unless stated otherwise, all reactions were carried out in oven-dried glassware in nitrogen-filled glove box or using standard Schlenk line techniques. Solvents were used after passage through a solvent purification system under a blanket of argon and then degassed briefly by exposure to vacuum. Sigma-Aldrich, Oakwood Scientific, and Fisher Scientific supplied various anilines. Cyclohexene oxide was purchased from Sigma Aldrich, dried over calcium hydride and distilled. Nuclear magnetic resonance (NMR) spectra were recorded at ambient or cryogenic temperatures on a Varian spectrometer (^1H and $^1\text{H}\{^1\text{H}\}$ 500 MHz, and $^{13}\text{C}\{^1\text{H}\}$ 125 MHz) in CD_2Cl_2 and are referenced versus shifts of solvents containing residual protic impurities. NMR temperature was calibrated using a methanol standard. The line listing for the ^1H NMR spectra are reported as: chemical shift in ppm (peak width at half height). Infrared (IR) spectra were recorded on an OPUS ATR infrared spectrometer. High-resolution mass

spectra were obtained at the Boston College Mass Spectrometry Facility using JEOL AccuTOF DART.

Gel permeation chromatography (GPC) was performed on an Agilent GPC220 in THF at 40 °C with three PL gel columns (10 μ m) in series and recorded with a refractive index detector. Molecular weights and molecular weight distributions were determined from the signal response of the refractive index (RI) detector relative to polystyrene standards.

General procedure of the synthesis of [Bis(imino)pyridine Fe Bis(alkoxide)⁺][Bar^F₄] complexes At room temperature, a solution of neopentyl alcohol (0.030 g, 0.34 mmol) and L-lactide (0.196 mg, 1.36 mmol) in toluene (5 mL) was added slowly to a solution of corresponding bis(imino)pyridine-iron-bis(trimethylsilyl)methyl complex (0.17 mmol, 0.090~0.121 g) in toluene (5 mL) in a 20-mL vial. The reaction mixture was allowed to stir for 2 hours. Ferrocenium BAR^F₄ (0.357 mg, 0.34 mmol) was dissolved in dichloromethane (5 mL) and added to the reaction solution. The solvent was removed and the resulting powder was washed with n-pentane (3 \times 5 mL) and dried in vacuo.

Bis(2,6-dimethylbenzeneamine)-*N,N'*-(2,6-pyridinediyl-diethylidyne) iron-bis(lactic acid) complex **4.2**: yield 0.311g, 90%, ¹H NMR (C₆D₆): δ 38.5 (296), 7.0 (16.4), 6.7(19.4), 4.1 (280), 3.5 (29.1), 3.1 (9.22), 1.2 (37.0), 0.8 (19.4) ppm. IR(neat): 2363, 2340, 1755, 1655, 1455, 1354, 1276, 1122, 886, 839, 713, 682, 567 cm⁻¹.

Bis(2,6-dimethyl-4-fluorobenzene)-*N,N'*-(2,6-pyridinediyl-diethylidynyl)-iron-bis(lactic acid) complex **4.2b**: yield: 0.324g, 92%, ¹H NMR (CD₂Cl₂): δ 29.8 (135), 9.7 (4.6) 8.3(23.4) 7.8 (12.21), 7.6 (9.8) 7.37 (2.7) 7.24(4.33) 7.18 (5.7) 6.92(5.14) 5.14 (19.9),

3.79 (8.7), 2.36 (3.5), 2.1(6.92), 1.52 (37.4) 1.16 (3.8) 0.95 (16.4) ppm. IR(neat): 2363, 2339, 1755, 1664, 1452, 1357, 1276, 1122, 884, 833, 713, 682, 664 cm^{-1} .

Bis(2,6-diisopropylbenzeneamine)-*N,N'*-(2,6-pyridinediyl-diethylidynyl)-iron-bis(lactic acid) complex **4.2c**: yield 0.296 g, 81%, ^1H NMR (C_6D_6): δ 20.54(965), 7.78(11.8), 7.61(9.2), 7.37(2.7), 7.19(16.9), 5.18(9.5), 3.86(5.52), 3.80(10.34), 2.78(2.4), 2.27(13.8), 1.58(6.1), 1.17(21.7), 0.95(4.5)ppm. IR(neat): 3733, 2363, 2339, 1755, 1663, 1455, 1354, 1276, 1122, 886, 839, 769, 715, 682, 671 cm^{-1} .

Bis(2,6-diethylbenzeneamine)-*N,N'*-(2,6-pyridinediyl-diethylidynyl)-iron-bis(lactic acid) complex **4.2d**: yield 0.288 g, 81%, ^1H NMR (C_6D_6): δ 22.53(218), 7.93(20.4), 7.85(12.4), 7.74(13.5), 7.67(9.9), 5.41(3.18), 5.17(10.3), 3.86(7.15), 3.82(8.7), 1.58(30.9), 1.02(3.18), 0.95(10.9) ppm. IR(neat): 2363, 2339, 1755, 1655, 1454, 1354, 1276, 1122, 888, 840, 713, 682, cm^{-1} .

Bis(3,5-dimethylbenzeneamine)-*N,N'*-(2,6-pyridinediyl-diethylidynyl)-iron-bis(lactic acid) complex **4.2e**: yield 0.297 g, 86%, ^1H NMR (C_6D_6): δ 7.75 (11.56), 7.59 (8.3), 7.37(4.3), 5.55(5.7), 5.17(9.5), 2.57(3.7), 2.10(4.4), 1.58(10.4), 1.57(5.32), 0.95(5.08). IR(neat): 2363, 2339, 1755, 1663, 1452, 1357, 1276, 1122, 884, 832, 713, 682, 667 cm^{-1} .

Bis(2,4,6-dimethylbenzeneamine)-*N,N'*-(2,6-pyridinediyl-diethylidynyl)-iron-bis(lactic acid) complex **4.2f**: yield 0.285 g, 81%, ^1H NMR (C_6D_6): δ 28.5 (296), 6.6 (16.4), 6.3(19.4), 4.1 (280), 3.5 (29.1), 3.1 (9.22), 1.2 (37.0), 0.8 (19.4) ppm. IR(neat): 2363, 2339, 1755, 1663, 1453, 1355, 1278, 1122, 884, 832, 713, 682, 662 cm^{-1} .

Bis(4-fluorobenzeneamine)-*N,N'*-(2,6-pyridinediyl-diethylidynyl)-iron-bis(lactic acid) complex **4.2g**: yield 0.261 g, 76%, ^1H NMR (CD_2Cl_2): δ 8.13(20.1), 7.73(13.5), 7.55(10.9), 6.93(12.7), 5.97(15.5), 5.19(20.3), 3.87(10.9), 2.57(10.8), 1.58(10.7),

0.95(7.4) ppm. IR(neat): 2363, 2339, 1755, 1663, 1452, 1354, 1276, 1122, 1088, 884, 832, 713, 682, 667 cm⁻¹.

Bis(cyclohexylamine)-*N,N'*-(2,6-pyridinediyl-diethylidynyl)-iron-bis(lactic acid) complex **4.2h**: yield 0.227 g, 67%, ¹H NMR (CD₂Cl₂): δ 18.51(150), 9.89(131), 8.46(3.3), 7.89(11.3), 7.73(7.05), 7.37(2.7), 7.25(3.7), 7.19(4.45), 6.91(4.18), 5.18(8.75), 4.16(2.6), 3.86(6.4), 2.35(3.4), 2.30(3.6), 2.22(2.8), 2.01(3.4), 1.56(5.6), 0.95(4.4) ppm. IR(neat): 2363, 2339, 1755, 1663, 1452, 1357, 1276, 1122, 884, 832, 713, 682, 667 cm⁻¹.

Bis(benzeneamine)-*N,N'*-(2,6-pyridinediyl-diethylidynyl)-iron-bis(lactic acid) complex **4.2i**: yield 0.289 g, 86%, ¹H NMR (CD₂Cl₂): δ 8.00(13.9), 7.84(5.6), 7.74(10.8), 7.56(6.02), 7.37(2.8), 7.18(14.4), 6.03(18.0), 5.18(5.8), 2.56(25.8), 2.34(5.1), 1.58(9.34), 0.95(3.8).ppm. IR(neat): 2363, 2339, 1755, 1663, 1452, 1354, 1276, 1122, 884, 832, 713, 682, 667 cm⁻¹.

2,6-dimethyl-N-(1-(6-phenylpyridin-2-yl)ethylidene)aniline-iron complex **4.3**: yield 0.288 g, 86%, ¹H NMR (CD₂Cl₂): δ 15.83 (3787), 12.36 (251), 8.28 (4.6), 8.10 (5.8), 7.83 (11.51), 7.66 (7.7), 7.56 (6.0), 7.21 (6.7), 5.17 (7.9), 3.87 (23.6), 2.52 (6.0), 2.15 (4.3), 1.58 (7.24), 0.95 (4.69) ppm. IR(neat): 2363, 2339, 1755, 1663, 1452, 1357, 1276, 1122, 884, 832, 713, 682, 667 cm⁻¹.

General Procedure for the collection of kinetic data of epoxide polymerization reactions.

To a J. Young tube in the glovebox was added cyclohexene oxide (0.30 mL of a 0.527 M stock solution in CD₂Cl₂). This layer was frozen in the cold well that was cooled to -200°C using liquid nitrogen. The desired amount of catalyst (**4.1-4.3**) was added to the tube in the cold well as a solution in CD₂Cl₂ so that the total volume of solvent in the

NMR tube was 0.60 mL. This layer was frozen the J. Young tube was capped. The tube was quickly brought out and immediately submerged into a Dewar containing liquid nitrogen. (NOTE: Importantly, the NMR tube was transferred from the glovebox to the Dewar of liquid N₂ rapidly so that the two layers remained frozen and unmixed.) Immediately prior to collection of the kinetic data, the tube was brought to -78 °C in a Dewar containing dry ice/acetone. Once the tube reached the temperature where CD₂Cl₂ became a liquid, the tube was shaken vigorously to fully mix the two layers. The tube was resubmerged in the dry ice/acetone bath. With the NMR instrument thermostated at the appropriate temperature, the tube was inserted and an pre-acquisition delay array was immediately started. (NOTE: The instrument was shimmed and locked on a sample containing CD₂Cl₂ and **4.2**.) Each acquisition was set to one scan and acquisition time per scan was 2 seconds. After collection of the initial data, acquisitions could be collected every 20 seconds. Subsequent spectra were integrated using VNMRJ software.

4.10 References

- (1) Parker, R. E.; Isaacs, N. S. Mechanisms Of Epoxide Reactions. *Chem. Rev.* **1959**, *59* (4), 737–799.
- (2) Martinez, L. E.; Leighton, J. L.; Carsten, D. H.; Jacobsen, E. N. *Highly Enantioselective Ring Opening of Epoxides Catalyzed by (Salen) Cr (III) Complexes*; 1995; Vol. 117.
- (3) Faiz, S.; Zahoor, A. F. Ring Opening of Epoxides with C-Nucleophiles. *Mol. Divers.* **2016**, *20* (4), 969–987.
- (4) Saddique, F. A.; Zahoor, A. F.; Faiz, S.; Naqvi, S. A. R.; Usman, M.; Ahmad, M. Recent Trends in Ring Opening of Epoxides by Amines as Nucleophiles. *Synth. Commun.* **2016**, *46* (10), 831–868.
- (5) Carlotti, S.; Peruch, F. Cyclic Monomers: Epoxides, Lactide, Lactones, Lactams, Cyclic Silicon-Containing Monomers, Cyclic Carbonates, and Others. In *Anionic Polymerization: Principles, Practice, Strength, Consequences and Applications*; Springer Japan: Tokyo, 2015; pp 191–305.
- (6) Hernandez, Y.; Pang, S.; Feng, X.; Müllen, K. *Polymer Science: A Comprehensive Reference*; Elsevier, 2012.
- (7) Odian, G. *Principles of Polymerization*; John Wiley & Sons, Inc.: Hoboken, NJ, USA, 2004.
- (8) Quirk, R. P.; Lizarraga, G.; Lu, L.-M.; Hasegawa, H.; Zhuo, Q.; Morton, M. *Anionic Polymerization Chemistry of Epoxides. Functionalization, Block Polymerization and Branching*; 1997; Vol. 118.

- (9) Banks, P.; Peters, R. H. Polymerization and Crosslinking of Epoxides: Base-Catalyzed Polymerization of Phenyl Glycidyl Ether. *J. Polym. Sci. Part A-1 Polym. Chem.* **1970**, *8* (9), 2595–2610.
- (10) Crivello, J. V.; Fan, M. Transition Metal Catalyzed Cationic Polymerizations. *Macromol. Symp.* **1995**, *98* (1), 253–268.
- (11) Penczek, S. Cationic Ring-Opening Polymerization (CROP) Major Mechanistic Phenomena. *J. Polym. Sci. Part A Polym. Chem.* **2000**, *38* (11), 1919–1933.
- (12) Herzberger, J.; Niederer, K.; Pohlit, H.; Seiwert, J.; Worm, M.; Wurm, F. R.; Frey, H. Polymerization of Ethylene Oxide, Propylene Oxide, and Other Alkylene Oxides: Synthesis, Novel Polymer Architectures, and Bioconjugation. *Chem. Rev.* **2016**, *116* (4), 2170–2243.
- (13) Pruitt, M. E.; Jackson, L.; Baggett, J. M. Catalysts for the Polymerization of Olefin Oxides. 2706181, 1955.
- (14) Pruitt, M. E.; Baggett, J. M. Solid Composite Propellants Containing Polyalkylene Oxides. US2706189A, October 17, 1957.
- (15) Lal, J. Polymerization of Olefin Oxides and of Olefin Sulfides. US2706182A, June 5, 1966.
- (16) Furukawa, J.; Akutsu, S.; Saegusa, T. Asymmetric-selection Polymerization of d,l-propylene Oxide by (FeCl₃-propylene Oxide) Complex. *Die Makromol. Chemie* **1965**, *81* (1), 100–111.
- (17) Robinson, R. The Polymerisation of Epoxides by Metal Halide Catalysts. *Tetrahedron* **1959**, *5* (1), 96–97.

- (18) Borkovec, A. B. Reaction of Epoxides with Ferric Chloride. *J. Org. Chem.* **1958**, *23* (6), 828–830.
- (19) Osgan, M. Catalytically Active Form of Ferric Acetate Hydroxide for the Insertion Polymerization of Propylene Oxide. *J. Polym. Sci. Part A-1 Polym. Chem.* **1968**, *6* (5), 1249–1257.
- (20) Price, C. C.; Spector, R. Partial Head-to-Head Polymerization of Propylene Oxide by Stereospecific Catalysts. *J. Am. Chem. Soc.* **1965**, *87* (9), 2069–2070.
- (21) Charles Price, B. C.; Osgan, M.; Staudinger, H.; Organische Verbindungen, H.; Pruitt, E.; Baggett, J. M.; Bloomfield, R. J.; Templeton, J. H.; 1956; Vol. 20.
- (22) Corey, E. J. A Theory for the Stereospecific Polymerization of Propylene Oxide by Ferric Chloride. *Tetrahedron Lett.* **1959**, *1* (2), 1–6.
- (23) Hirahata, W.; Thomas, R. M.; Lobkovsky, E. B.; Coates, G. W. Enantioselective Polymerization of Epoxides: A Highly Active and Selective Catalyst for the Preparation of Stereoregular Polyethers and Enantiopure Epoxides. *J. Am. Chem. Soc.* **2008**, *130* (52), 17658–17659.
- (24) Biernesser, A. B.; Delle Chiaie, K. R.; Curley, J. B.; Byers, J. A. Block Copolymerization of Lactide and an Epoxide Facilitated by a Redox Switchable Iron-Based Catalyst. *Angew. Chemie - Int. Ed.* **2016**, *55* (17), 5251–5254.
- (25) Biernesser, A. B.; Li, B.; Byers, J. A. Redox-Controlled Polymerization of Lactide Catalyzed by Bis(imino)pyridine Iron Bis(alkoxide) Complexes. *J. Am. Chem. Soc.* **2013**, *135* (44), 16553–16560.

- (26) Delle Chiaie, K. R.; Yablon, L. M.; Biernesser, A. B.; Michalowski, G. R.; Sudyn, A. W.; Byers, J. A. Redox-Triggered Crosslinking of a Degradable Polymer. *Polym. Chem.* **2016**, *7* (28), 4675–4681.
- (27) Qi, M.; Dong, Q.; Wang, D.; Byers, J. A. Electrochemically Switchable Ring-Opening Polymerization of Lactide and Cyclohexene Oxide. *J. Am. Chem. Soc.* **2018**, *140* (17), 5686–5690.
- (28) Antelmann, B.; Chisholm, M. H.; Iyer, S. S.; Huffman, J. C.; Navarro-Llobet, D.; Pagel, M.; Simonsick, W. J.; Zhong, W. Molecular Design of Single Site Catalyst Precursors for the Ring-Opening Polymerization of Cyclic Ethers and Esters. 2. Can Ring-Opening Polymerization of Propylene Oxide Occur by a Cis-Migratory Mechanism? *Macromolecules* **2001**, *34* (10), 3159–3175.
- (29) Brookhart, M.; Grant, B.; Volpe, A. F. [(3,5-(CF₃)₂C₆H₃)₄B]-[H(OEt₂)₂]⁺: A Convenient Reagent for Generation and Stabilization of Cationic, Highly Electrophilic Organometallic Complexes. *Organometallics* **1992**, *11* (11), 3920–3922.
- (30) Honeychuck, R. V.; Hersh, W. H. Coordination of "noncoordinating" Anions: Synthesis, Characterization, and X-Ray Crystal Structures of Fluorine-Bridged hexafluoroantimonate(1-), tetrafluoroborate(1-), and hexafluorophosphate(1-) Adducts of [R₃P(CO)₃(NO)W]⁺. An Unconventional Order of Anion Donor Strength. *Inorg. Chem.* **1989**, *28* (14), 2869–2886.
- (31) Childers, M. I.; Longo, J. M.; Van Zee, N. J.; Lapointe, A. M.; Coates, G. W. Stereoselective Epoxide Polymerization and Copolymerization. *Chem. Rev.* **2014**, *114* (16), 8129–8152.

- (32) Biernesser, A. B.; Li, B.; Byers, J. A. Redox-Controlled Polymerization of Lactide Catalyzed by Bis(imino)pyridine Iron Bis(alkoxide) Complexes. *J. Am. Chem. Soc.* **2013**, *135* (44), 16553–16560.
- (33) Burés, J. A Simple Graphical Method to Determine the Order in Catalyst. *Angew. Chemie - Int. Ed.* **2016**, *55* (6), 2028–2031.
- (34) Hoops, S.; Sahle, S.; Gauges, R.; Lee, C.; Pahle, J.; Simus, N.; Singhal, M.; Xu, L.; Mendes, P.; Kummer, U. COPASI--a COMplex PATHway SIMulator. *Bioinformatics* **2006**, *22* (24), 3067–3074.
- (35) Manna, C. M.; Kaur, A.; Yablon, L. M.; Haeffner, F.; Li, B.; Byers, J. A. Stereoselective Catalysis Achieved through in Situ Desymmetrization of an Achiral Iron Catalyst Precursor. *J. Am. Chem. Soc.* **2015**, *137* (45), 14232–14235.

Chapter 5 Ring-Opening Polymerization with a Formally Iron(I) Bis(imino)pyridine Mono(alkoxide) Complex

5.1 Introduction

Concern over waste disposal problems and environmental pollution has driven efforts to develop biodegradable alternatives to conventional inert polymeric materials. A promising class of biodegradable materials can be derived from the ring opening polymerization of cyclic esters and carbonates, in particular, from the polymerization of lactide to form poly(lactic acid).¹⁻³ Although numerous catalysts for this transformation have been developed,⁴ we became interested in iron-based systems due to the biocompatibility and low toxicity of iron, as well as the versatility and fine control of catalyst electronic structure available by oxidation state modulation. Whereas a relatively small number of iron complexes have been reported as catalysts for the polymerization of lactide,⁵⁻¹⁶ even fewer have been reported for the polymerization of lactones^{7,8,17-23} and cyclic carbonates.²⁴⁻²⁶ Of the reported catalysts for these last monomers, all are limited by low activity and/or produce a polymer with broad molecular weight distributions.

As seen in Chapter 2, we presented lactide polymerizations that are catalyzed by several bis(imino)pyridine iron(II) bis(alkoxide) complexes (**5.1**, Figure 5.1), and demonstrated that the polymerization reaction was sensitive to the catalyst oxidation state and electron density about the metal center.¹⁶ Lactide polymerization proceeded more rapidly with electron-rich iron(II) complexes as compared to electron-poor analogues,²⁷ which could be achieved by either changing the identity of the alkoxide initiator or using more electron rich bis(imino)-N-heterocyclic carbene ancillary ligands.²⁸ Consistent with

this trend, the activity of the catalyst towards lactide polymerization could be deactivated entirely when oxidized to a cationic, Fe(III) oxidation state (5.2). Interestingly, the complexes demonstrated the ability to undergo redox-switchable polymerization in situ through sequential addition of chemical oxidants and reductants.^{29–31} In sharp contrast to their reactivity towards lactide polymerization, the iron-based complexes displayed orthogonal reactivity towards epoxide polymerization, being active in the cationic Fe(III) oxidation state and inactive in the neutral, Fe(II) oxidation state (Figure 5.1).³² The complementary reactivity of these two monomers was exploited for the redox-controlled synthesis of block copolymers (Chapter 2) and redox-triggered cross-linking of polymers (Chapters 3).^{32,33}

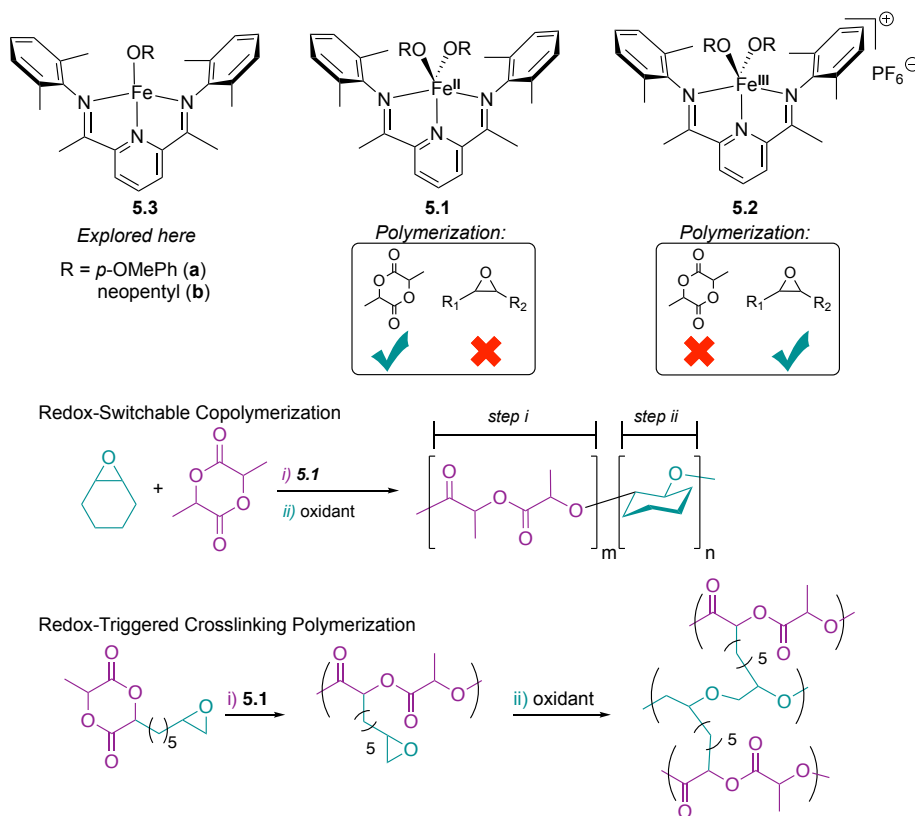


Figure 5.1. Iron bis(imino)pyridine alkoxy complexes used in ring opening polymerization reactions and their application in redox-switchable polymerization reactions

Including our system, all reported examples of iron-based initiators for the ring-opening polymerization of cyclic esters are in the iron(II) and iron(III) oxidation states.^{5–26} However, iron bis(imino)pyridine complexes are highly versatile catalysts for an extensive variety of transformations,^{34–37} due in part to their rich redox chemistry that is facilitated by the redox non-innocent bis(imino)pyridine ligands.^{35–40} Based on our finding that different oxidation states manifest distinct reactivity towards ring-opening polymerization, we turned our attention towards exploring additional redox states of these complexes with the ultimate goal of extending the available monomer scope. In line with the general trends that we have previously observed, we reasoned that a formally iron(I) bis(imino)pyridine alkoxide complex would be a superior catalyst for the ring-opening polymerization of cyclic esters (as compared to the ferrous and ferric complexes) due to the increased electron density at the iron center. In this chapter, the synthesis of such complexes (**5.3**, Scheme 5.1), the elucidation of their electronic structure, and their use as catalysts for the polymerization of a variety of cyclic esters and carbonates are presented (Figure 5.2). These complexes proved to be among the most active iron-based catalysts reported to date for many of the known monomers.

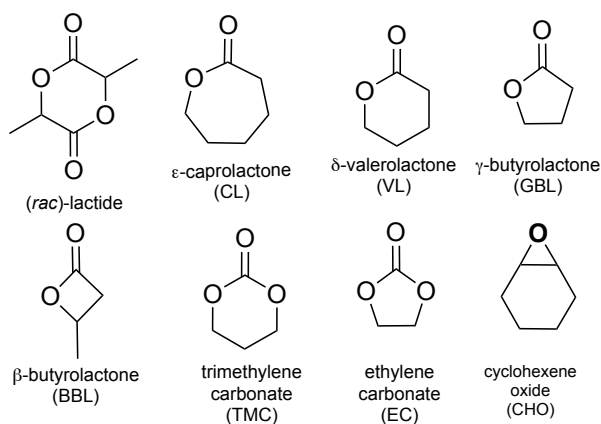
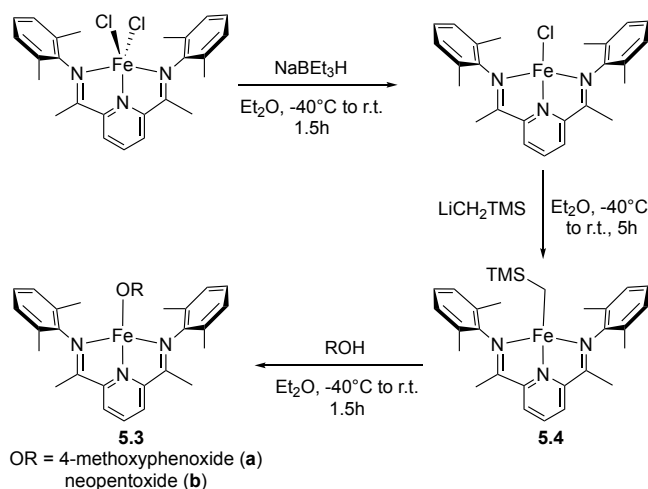


Figure 5.2. Monomers explored for ring-opening polymerization

5.2 Synthesis and Characterization of bis(imino)pyridine iron alkoxides

We have formerly reported the synthesis of bis(imino)pyridine iron(II) bis(alkoxide) complexes by treating a bis(imino)pyridine iron(II) bis(alkyl) complex with a variety of alcohols.¹⁶ We envisioned that similar treatment of a bis(imino)pyridine iron mono(alkyl) might furnish the desired bis(imino)pyridine iron mono(alkoxide) complexes (Scheme 5.1). As reported previously,⁴¹ stepwise reduction of the bis(imino)pyridine iron(II) dichloride complex with NaBEt₃H and alkylation with LiCH₂TMS afforded the bis(imino)pyridine iron(I) mono(alkyl) complex efficiently (Scheme 5.1). In collaboration with Ashley Biernesser, the desired bis(imino)pyridine iron monoalkoxide complexes (**5.3**) were then prepared directly by protonolysis of the corresponding bis(imino)pyridine iron monoalkyl complex (**5.4**) with either *p*-methoxyphenol (**5.3a**) or neopentyl alcohol (**5.3b**, Scheme 5.1). In contrast to the dark purple color of the iron(II) bis(alkoxide) complexes, the iron mono-(alkoxide) complexes are dark red-brown. These are high spin ($S = 3/2$) complexes according to solution state magnetic moment measurements ($M = 3.18 M_B$, *vide infra*).⁴²

Scheme 5.1 Synthesis of iron mono(alkoxide) complexes 5.3



For the bis(imino)pyridine iron(I) neopentoxide complex **5.3b**, X-ray quality crystals were obtained from a concentrated solution in pentane (Figure 5.3). The solid-state molecular structure reveals a slightly distorted square-planar iron center, supported by the bis(imino)pyridine ligand scaffold and containing a single neopentyl alkoxide ligand. Unfortunately, the uncertainty in the ligand bond metrics obscure determination of redox activity of the bis(imino)pyridine ancillary ligand (X-ray data table in Appendix C).^{41,43}

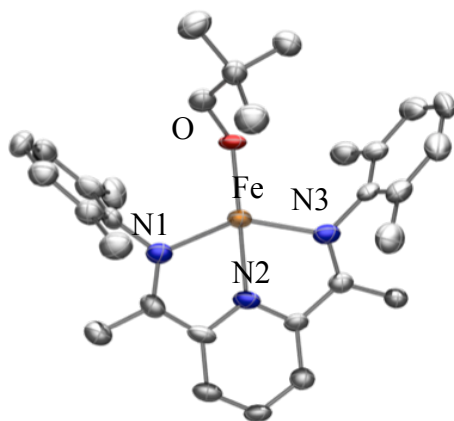


Figure 5.3. X-ray crystal structure of complex 4.3b with thermal ellipsoids represented at the 50% probability level. Hydrogen atoms are omitted for clarity. Fe-N1 = 2.14Å, Fe-N2 = 1.99Å, Fe-N3 = 2.15Å. O-Fe-N1 = 107.9°, O-Fe-N2 = 163.0°, O-Fe-N3 = 105.3°, N1-Fe-N2 = 75.3°, N1-Fe-N3 = 145.6°, N2-Fe-N3 = 75

Because the redox non-innocence of bis(imino)pyridine ligand is well precedented,^{34,41,43} characterization of these complexes by several techniques (EPR, Mössbauer, etc.) is required to understand the electronic structure of the complex and gain information about whether this complex is reduced at the iron center or better described as an iron(II) center with a reduced bis(imino)pyridine ligand. Reports by the Chirik group describe the bis(imino)pyridine iron mono(chloride) as well as

bis(imino)pyridine mono(alkyl) complexes as iron(II) centers with reduced bis(imino)pyridine ligands.^{44,43}

An electron paramagnetic resonance spectrum obtained in frozen toluene of complex **5.3b** displayed an axial signal (Figure 5.4, $g_{\text{eff}} = 2.04$ and 2.37); this signal corresponds to an $S = 1/2$ spin state. Notably, after comparison to a copper standard, it was determined that this $S = 1/2$ signal is due to only 1% of the compound evaluated. Because of this, it is probable that the major iron-containing species in solution is a spin state that we have been unable to observe with X-Band EPR spectroscopy. It would probably be difficult to observe with X-band EPR due to the symmetry of the complex and the spin forbidden-ness of such a transition (Figure 5.4).⁴⁵

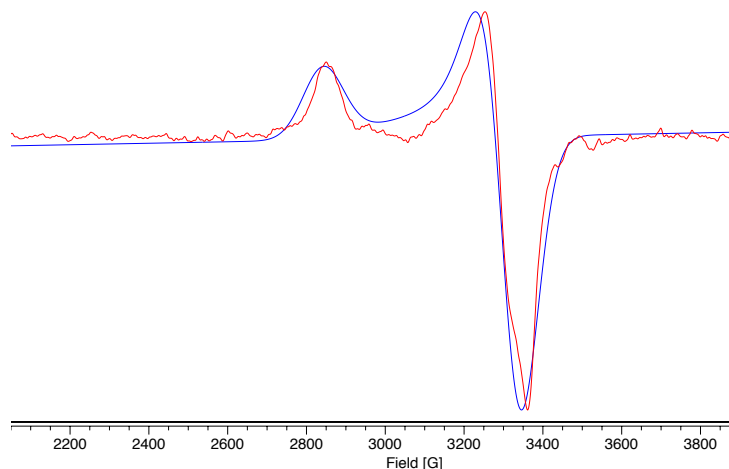


Figure 5.4. Frozen-toluene EPR spectrum of complex 4.3b in red showing simulated spectrum in blue with the parameters given in the text

To further elucidate the electronic environment of the formally iron(I) complexes, **5.3** was characterized by zero-field ⁵⁷Fe Mössbauer spectroscopy with the help of the Betley lab at Harvard (**Table 5.1**). The Mössbauer spectrum of *p*-methoxyphenoxide complex **5.3a** contained two species, the major of which comprises 91% of the mixture.⁴² The two

species had similar Mössbauer parameters with the major species having a slightly higher isomer shift (δ : 1.04 mm/s, $|\Delta E_Q|$: 1.79 mm/s) and smaller quadrupole splitting than that observed for the analogous iron(II) complex **5.1a** (δ : 0.94 mm/s, $|\Delta E_Q|$: 2.19 mm/s) (cf., entry 1 vs. entry 2, **Table 5.1**).⁴² Due to the similarity in Mössbauer parameters of the two components and simplicity of the ¹H NMR spectrum, it is likely that the minor component observed in this compound are solvent adducts of the iron complexes. Consistent with this hypothesis was the much smaller amount of these impurities observed when care was taken to protect the iron complexes from diethyl ether. Similarly, the Mössbauer spectrum of **5.3b** demonstrated evidence for two species with the major species making up 83% of the sample (**Figure 5.5**). This species had isomer shifts and quadrupole splittings smaller than that observed for the analogous Fe(II) complex (entry 4, **Table 5.1**). Regardless, in both cases, the reduction of the complex and effective loss of an alkoxide ligand decreases the quadrupole splitting from the corresponding Fe(II) species, which is consistent with the increase in molecular symmetry that occurs upon reduction of **5.1** to **5.3**.

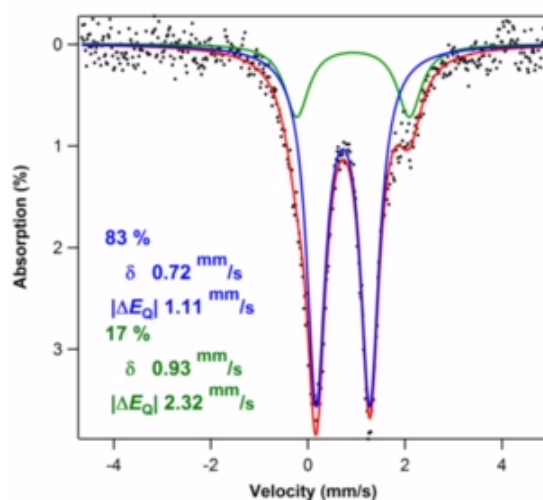


Figure 5.5. Mössbauer spectrum of **5.3b**

The similarity of the isomer shifts between analogous compounds of **5.3** and **5.1** suggests that both compounds exist in the same oxidation state, namely iron(II). However, whereas isomer shift often correlates strongly with oxidation state, these trends are manifested only when structural distortion is minimized upon oxidation or reduction of the complex,⁴⁶ which is not true of the current family of complexes. Whereas it is typical for the oxidation state to outweigh the former, the unambiguous assignment of oxidation states in the present complexes is unfortunately not possible based solely on Mössbauer data. However, we can compare our findings to other reports that have investigated the electronic structure of formally iron(I) bis(imino)pyridine complexes in comparison to closely analogous iron(II) complexes with Mössbauer spectroscopy. For the formally iron(I) bis(imino)pyridine chloride and CH₂SiMe₃ alkyl species, the Mössbauer isomer shifts decrease by around 0.1-0.3 mm/s from the analogous iron(II) species,^{44,43} which is similar to the observed decrease in the isomer shift of complex **5.3b** as compared to complex **5.1b**.

Table 5.1. Zero-field ⁵⁷Fe Mössbauer parameters for iron complexes 5.3 and 5.1^{a,b}

Entry	Complex	δ (mm/s)	$ \Delta E_Q $ (mm/s)
1	5.3a	1.04 (91%)	1.79
		0.99 (9%)	3.10
2	5.1a	0.94 (75%)	2.19
		0.60 (25%)	1.73
3	5.3b	0.72 (83%)	1.11
		0.93 (17%)	2.32
4	5.1b	0.94 (67%)	1.71
		0.36 (33%)	2.06

^aSpectra obtained in frozen benzene at 90K. ^bSamples showed minor impurities in the spectra, the parameters reported are for the major species

The similarity of this trend and the established redox activity of the bis(imino)pyridine ligand in the monochloride and alkyl complexes suggest that the monoalkoxide complexes **5.3a** and **5.3b** are also best described as an iron(II) center with a reduced bis(imino)pyridine ligand.

For a more accurate determination of the spin state and oxidation state of these formally Fe(I) complexes, Superconducting Quantum Interference Device (SQUID) magnetometry measurements were collected on **5.3b** (Figure 5.6). At temperatures above 50 K, magnetic behavior was consistent with the presence of a paramagnetic compound as expected from the paramagnetic NMR spectrum obtained from **5.3b**. The magnetic moment ($\chi \cdot T$) observed above 50 K plateaus at 2.3 ($\text{cm}^3 \text{mol}^{-1} \text{K}$), which is higher than the spin-only value for an $S = 3/2$ system ($\chi \cdot T = 1.88 \text{ cm}^3 \text{mol}^{-1} \text{K}$). The slightly higher magnetic moment observed is consistent with contributions from the spin-orbit coupling, which was expected for spin largely localized on the iron center. Below 50 K, the magnetic moment decreased significantly, which is likely due to contributions from zero-field splitting. These data were in line with the solution state magnetic moment measurements, which indicated that **5.3b** is best described as a high spin $S = 3/2$ system.⁵³

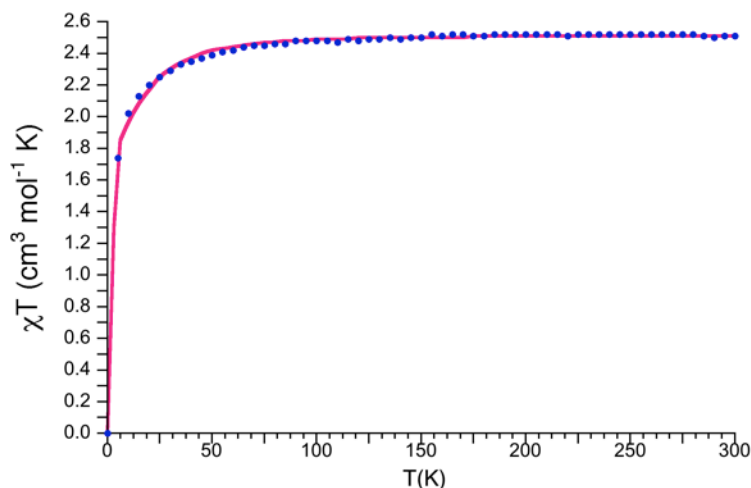


Figure 5.6. Variable temperature magnetic susceptibility (χ^*T) data for complex **3b** obtained in the solid state using a SQUID magnetometer operating at 1.00 Tesla from 5 K to 300 K. The line was a result from a fit to the data to give $g = 2.44$, $D = -21.65$ and $E/D = 0.2$

To complement the suite of experimental data, the electronic structures of complexes **5.3** were investigated computationally with density functional theory (DFT) using the M06-L functional.⁴⁷ **5.3a** and **5.3b** were optimized for both their lowest quartet and doublet spin states. M06-L calculations place the quartet states at 5.7 and 6.5 kcal mol⁻¹ below the doublet states for **5.3a** and **5.3b**, respectively. This result is consistent with the $S = 3/2$ assignment from SQUID measurements (**5.3b**, Figure 5.6). Mulliken spin densities for quartet **5.3a** and doublet **5.3a** are shown in Figure 5.7. These spin states localize roughly two paired and four unpaired (same spin) electrons on the iron center, respectively, and one unpaired electron of opposite spin on the ligand. DFT thus supports the description of these complexes as Fe(II) centers antiferromagnetically coupled to the bis(imino)pyridine ligand, in agreement with previous reports for similar complexes,^{51,49} and, again, demonstrating the ready redox non-innocence of this class of ligands.

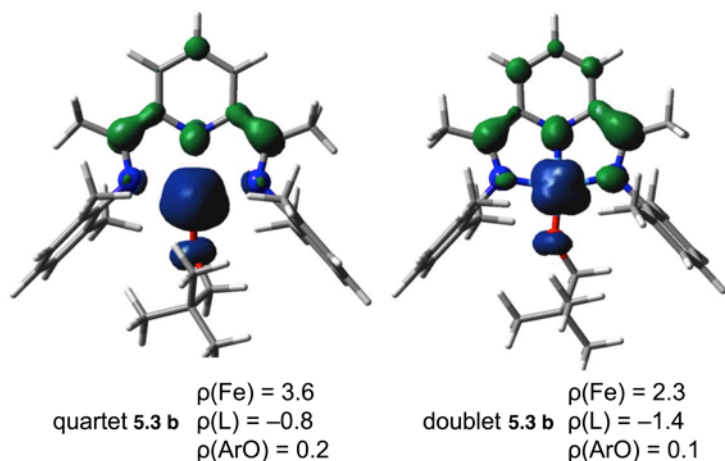


Figure 5.7. Mulliken spin densities (a.u.) for quartet **4.3b** (left) and doublet **4.3b** (right). M06-L electronic energies in kcal mol⁻¹. L = bis(imino)pyridine

Although there is good, qualitative agreement between our M06-L results and experiment for the ground spin state, the considerable sensitivity of predicted Fe spin-state energy separations to density functionals is well documented.⁴⁸ To assess this question, single-point calculations for **5.3b** were performed with two additional functionals: MN15 and TPSSh-D3BJ. MN15 predicts a near degeneracy of the two states, with the doublet 1.4 kcal mol⁻¹ lower in energy than the quartet. TPSSh-D3BJ predicts a doublet ground state by an even still more significant margin, 5.9 kcal mol⁻¹. Compound **5.3b** thus represents another example of an iron coordination compound with spin-state energetics sensitive to density functional selection. While our experience with other systems has generally indicated M06-L to be robust for Fe, we decided to more closely examine predicted structural parameters and Mössbauer spectroscopy to confirm the ground spin-state assignment further.^{49,50}

Optimized M06-L quartet geometries are in good agreement with the X-ray crystal structure of **5.3b** (Figure 5.3). Considering the structural properties of both **5.3a**

and **5.3b**, the doublet geometries display a significant shortening of Fe–N bonds and, as a result, wider N1–Fe–N3 angles (Table 5.2).

Moreover, Mössbauer isomeric shifts were computed at the M06-L level for both complexes. The calculated isomer shifts are 0.86 and 0.63 mm/s for quartet **5.3a** and doublet **5.3a**, respectively, and 0.84 and 0.59 mm/s for quartet **5.3b** and doublet **5.3b**, respectively. The experimental isomer shifts of 1.04 mm/s for **5.3a** and 0.72 mm/s for **5.3b** best fit the calculated values for the quartet state, although it is not clear why a much smaller variation in isomer shift as a function of RO– ligand is predicted with theory compared to the experimental observation (unless it is a condensed-phase effect).

Table 5.2. Selected bond distances and angles for the X-ray crystal structure of 5.3b and structures of 5.3a and 5.3b optimized at the M06-L level

Metric	5.3b	5.3a	5.3b	5.3a	5.3b
	(X-ray)	($S = 3/2$)	($S = 3/2$)	($S = 1/2$)	($S = 1/2$)
(Fe–N2) / Å	1.99	2.024	2.037	1.854	1.888
(Fe–N1) / Å	2.14	2.122	2.129	1.970	1.924
(Fe–N3) / Å	2.15	2.113	2.127	1.969	1.953
(Fe–O) / Å	1.84	1.858	1.847	1.858	1.787
(O–Fe–N2) / °	163.0	164.6	157.7	170.4	172.9
(N1–Fe–N3) / °	145.6	149.0	146.7	160.4	158.9

While the focus of this work is on the formal Fe(I) compounds **5.3a** and **5.3b**, we note that as a computational reference Fe(II) compound **5.1**, M06-L calculations predict a quintet ground state with a high spin Fe(II) center carrying 4 unpaired electrons. While

the localization on the high-spin Fe(II) is unremarkable, there is, nevertheless, substantial charge transfer with associated spin polarization involving the ligands: the bis(imino)pyridine ligand is predicted to be oxidized by about 0.5 electrons with that charge localizing primarily on the oxygen atoms of the two alkoxide groups.

To summarize, experimental and computational investigations describe complexes **5.3** as quartet spin states with a high-spin iron(II) center that is antiferromagnetically coupled to a singly reduced bis(imino)pyridine ligands.

5.3 Polymerizations Catalyzed with Formally Iron(I) Complexes

With the formally iron(I) alkoxide complexes in hand, the activity of aryl alkoxide complex **5.3a** as a catalyst for polymerization was first investigated using (*rac*)-lactide as the monomer (Table 5.3). When (*rac*)-lactide was exposed to 2 mol% **5.3a** in chlorobenzene, poly(lactic acid) was obtained with narrow dispersities ($M_w/M_n = 1.1$) and 86% conversion after 20 minutes (entries 1 and 2, Table 5.3). The activity observed with this catalyst was slightly lower than what was observed with the corresponding iron(II) complex, **5.1a** (entry 4, Table 5.3). Despite the narrow polymer molecular weight distributions obtained with both catalysts, the polymer molecular weights were higher than theoretical values calculated from the monomer to catalyst ratio and the conversion of the reaction by a factor of around 2.5. We hypothesize that slow initiation rates may be contributing to the higher than expected molecular weights of lactide. To test this hypothesis, lactide polymerizations were performed using **5.3a** as the catalyst at higher concentrations of lactide. Previously, we have shown that similar experiments decrease the discrepancy between observed and theoretical molecular weights for catalysts that suffer from slow initiation, which we attribute to the fact that initiation is first-order in

lactide.²⁸ When the concentration of lactide was increased from 0.25 M to 0.86 M, the observed polymer molecular weights were more in line with theoretical values as expected for a slowly initiating reaction (entries 1-3, Table 5.3). However, there were still considerable differences between the observed and theoretical molecular weights even for the highest lactide concentrations tested, which suggested that changes in reaction conditions would not be sufficient to overcome the slow initiation rates from **5.3a**.

In previous studies using the iron(II) bis(alkoxide) complexes, neopentyl alcohol was found to result in the fastest polymerization rates when used as the alkoxide initiator.²⁷ To investigate whether the expected increased nucleophilicity of **5.3b** would lead to efficient polymerization without slow initiation, we next investigated the polymerization of lactide catalyzed by **5.3b**. Satisfyingly, exposure of (*rac*)-lactide to **5.3b** resulted in more efficient polymerization, reaching 90% conversion after 10 minutes with 2 mol% catalyst. Consistent with complete initiation, narrowly disperse polymer was obtained with molecular weights that were close to the theoretical values (entries 5-7, Table 5.3). Highlighting the living characteristics of this polymerization reaction was the linear correlation between M_n and conversion that was observed. Due to the high activity of **5.3b**, the catalyst loading could be lowered to 0.05% to afford high molecular weight polymer in a few hours (entry 7, Table 5.3). Although **5.3b** is highly active toward lactide polymerization, we were surprised to find that the analogous iron(II) complex **5.1b** was even more active for lactide polymerization under the same conditions (entry 8, Table 5.3). For example, with 0.2 mol% catalyst loading, polymerization with **5.1b** was 94% converted after 10 minutes, whereas the same reaction conditions with complex **5.3b** required 90 minutes to reach similar conversions; after 10 minutes only 7% conversion

was seen. Despite the efficiency of reactions catalyzed by **5.1b**, the observed dispersities were broader than what was observed with **5.3b**, which is likely due to transesterification reactions that occur at high conversions.

Table 5.3. Polymerization of (*rac*)-lactide catalyzed by 5.1 and 5.3

Entry	Cat.	Cat. (mol %)	[lactide] (M)	Time (min.)	Conv. (%)	M _n (kg/mol)	M _n theor. (kg/mol)	M _w /M _n
1 ^a	5.3a	2.0	0.25	20	86	16.0	6.2	1.14
2 ^a	5.3a	1.0	0.43	20	86	25.7	12.4	1.16
3 ^a	5.3a	0.5	0.86	20	66	32.2	19.0	1.14
4 ^a	5.1a	2.0	0.25	20	94	16.1	6.8	1.15
5 ^b	5.3b	2.0	0.35	10	91	9.6	6.6	1.12
6 ^b	5.3b	0.2	0.35	90	88	74.1	63.4	1.13
7 ^b	5.3b	0.05	0.35	540	84	214.1	242.1	1.18
8 ^b	5.1b	0.2	0.35	10	94	94.8	67.7	1.37

^aReactions were performed in chlorobenzene at room temperature. ^bReactions were performed in toluene at room temperature.

Next, we next decided to investigate the reactivity of the complexes towards polymerizing other cyclic esters, such as ϵ -caprolactone. Although ϵ -caprolactone has similar ring strain as lactide, iron(II) *p*-methoxyphenoxide complex **5.1a** was completely inactive toward ϵ -caprolactone polymerization at room temperature and only showed moderate reactivity at 70 °C (entries 1 and 2, Table 5.4). In contrast, the formally iron(I) complex **5.3a** was active for ϵ -caprolactone polymerization at room temperature, leading

to 80% conversion after 24 hours (entry 3, Table 5.4). These reactions were characterized by significant induction periods (ca. 4 hours) and broad molecular weight distributions ($M_w/M_n = 2.22$). To accelerate the rate of the reaction, the polymerization of ϵ -caprolactone with **5.3a** was performed at elevated temperatures. At 70 °C in toluene, full conversion was observed after only two hours (entry 4, Table 5.4) with much less significant induction periods compared to reactions carried out at room temperature, although broad and bimodal dispersities were obtained.

As was the case with (*rac*)-lactide, we hypothesized that the slow reaction rates, presence of induction periods, and/or broad dispersities observed with **5.3a** and **5.1a** were due to slow initiation rates. To verify this hypothesis, we explored the reactivity of **5.1b** and **5.3b** for the polymerization of ϵ -caprolactone. Although formally iron(I) neopentoxide complex **5.3b** was found to be less active than the analogous iron(II) complex for (*rac*)-lactide polymerization, we were surprised to find that the neopentyl alkoxide complex **5.3b** demonstrated superior activity for ϵ -caprolactone polymerization at room temperature compared to **5.1b**. When **5.3b** was used as the catalyst, full conversion was obtained in less than 10 minutes, even at low catalyst loadings (0.05 mol%) (entries 5-7, Table 5.4). In contrast, **5.1b** demonstrated significantly lower reaction rates under identical conditions (entry 8, Table 5.4). Although molecular weights were higher than theoretical values, they were closer to theoretical molecular weights compared to when **5.3a** was used in the reaction, and more narrow dispersities were also observed. Moreover, an increase in molecular weight was observed as the catalyst loading was decreased, which further highlighted the living characteristics of the polymerization reaction.

Table 5.4. Polymerization studies with complexes **5.3b** and **5.1b**^a

Entry	Monomer	Cat.	Cat. (mol %)	Time (min.)	Conv. (%)	M _n (kg/mol)	M _n theor. (kg/mol)	M _w /M _n
1	ε-caprolactone	5.1a	2.0	1440	0	-	-	-
2 ^b	ε-caprolactone	5.1a	2.0	1080	99	22.6	5.7	2.14
3	ε-caprolactone	5.3a	2.0	1440	80	30.6	5.7	2.22
4 ^b	ε-caprolactone	5.3a	2.0	120	99	12.0	5.7	6.01
5	ε-caprolactone	5.3b	2.0	10	99	24.2	5.7	1.40
6	ε-caprolactone	5.3b	0.2	10	99	152.2	57.1	1.40
7	ε-caprolactone	5.3b	0.05	10	99	390.3	228.3	1.21
8	ε-caprolactone	5.1b	0.05	10	8	14.7	18.3	1.12
9	cyclohexene oxide	5.3b	0.2	1440	0	N/A	N/A	N/A
10	β-butyrolactone	5.3b	2.0	90	50	1.5	2.2	1.07
11	β-butyrolactone	5.3b	0.2	60	47	0.7	20.4	1.08
12	δ-valerolactone	5.3b	2.0	10	85	5.9	4.2	1.83
13	δ-valerolactone	5.3b	0.2	10	83	47.8	41.6	1.16
14	δ-valerolactone	5.3b	0.05	240	4	10.6	8.0	1.16
15	δ-valerolactone	5.1b	0.2	90	80	36.4	40.1	1.47
16	trimethylene carbonate	5.3b	2.0	10	100	5.0	5.1	6.6

^aReactions were performed in toluene at room temperature. ^bReactions carried out at 70°C.

The difference in reactivity for the iron neopentoxide complex **5.3b** compared to the *p*-methoxyphenoxide complex **5.3a** is remarkable; the former catalyst resulted in rapid conversion at room temperature with controlled molecular weight and molecular weight distributions, while the latter catalyst required prolonged reaction periods or heating and showed bimodal molecular weight distributions. These results illustrate the importance of the identity of the alkoxide ligand as well as the oxidation state of the metal complex, both of which significantly affects the initiation rate of ε-caprolactone polymerizations.

We next investigated the activity for **5.3b** for the ring opening polymerization of other monomers. As expected, complex **5.3b** was found to be completely inactive for epoxide polymerization, which appears to require electron deficient rather than electron rich catalysts to affect polymerization (entry 9, Table 5.4). As was the case with ϵ -caprolactone, complex **5.3b** was found to react quickly with the highly strained monomer β -butyrolactone. Unfortunately, the resulting products were low molecular weight oligomers, and the reactions only proceeded to around 50% completion even after prolonged reaction times (entries 10 and 11, Table 5.4). Polymerizations conducted at lower catalyst loadings did not result in increased molecular weights. We hypothesize that this polymerization must suffer from termination events or depolymerization that cause the molecular weights to be lower than expected based on the monomer to catalyst ratios. Such an outcome is not uncommon for β -butyrolactone polymerization.^{51,52}

When complex **5.3b** was subjected to the less strained 6-membered ring δ -valerolactone,¹⁻³ efficient polymerization was observed using 2.0 or 0.2 mol% catalyst. In either case, 85% conversion was observed within 10 minutes (entries 12 and 13, Table 5.4). Broad molecular weight distributions ($M_w/M_n = 1.83$) were observed when 2 mol% of **5.3b** was used as the catalyst, which is likely due to transesterification because distributions were narrower ($M_w/M_n = 1.16$) when the catalyst loading was lowered to 0.2 mol% or when the reaction was stopped after shorter times. The observed molecular weights were only slightly higher than the theoretical values, but the reaction also did not proceed to full conversion at extended reaction times, which may be due to a competing ring closing depolymerization reaction that is in equilibrium with the ring opening

reaction.⁵² As was the case with ϵ -caprolactone, the analogous iron(II) complex **5.1b** was less active than the formally iron(I) complex (entry 15, Table 5.4).

Because complex **5.3b** was highly active toward the polymerization of many cyclic ester monomers, reactivity toward cyclic carbonates was also investigated. Trimethylene carbonate can be derived from biomass, and its ring-opening polymerization affords an elastomeric biodegradable polymer that is valuable for biomedical and industrial applications.²⁶ Satisfyingly, exposure of trimethylene carbonate to complex **5.3b** resulted in the immediate formation of a gel precipitate in the toluene solution, which indicated its instantaneous polymerization at room temperature. Analysis of the product mixture by ¹H NMR spectroscopy revealed full conversion of the monomer to the polymer. However, GPC analysis of the polymer revealed broad and bimodal molecular weight distributions (entry 16, Table 5.4). We hypothesized that broad dispersities were observed due to the heterogeneity of the reaction mixture that results from the rapid polymerization of this monomer. Unfortunately, lowering catalyst loading or temperature did not slow polymerization reaction rate enough to avoid polymer precipitation.

5.4 Copolymerization Reactions with Low Strain Monomers

Considering the remarkable reactivity that **5.3b** demonstrated as a catalyst for the polymerization of δ -valerolactone and trimethylene carbonate, we explored the reactivity of **5.3b** for the polymerization of γ -butyrolactone and ethylene carbonate.⁵² Both of these monomers are notoriously difficult to engage in ring-opening polymerization due to their low ring strain.^{53,54} Unfortunately, these monomers did not undergo homopolymerization at room temperature when exposed to **5.3b**. Formation of high molecular weight polymer

was also not observed in initial experiments carried out at low reaction temperatures where Chen and coworkers have shown that polymerization of γ -butyrolactone is possible.⁵⁴

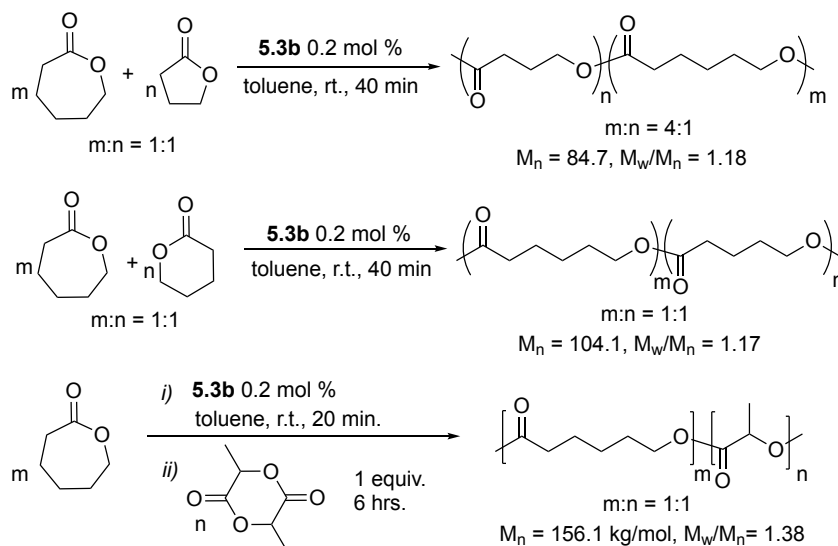
Despite the relative lack of progress in polymerizing γ -butyrolactone homopolymerization reactions, incorporation of γ -butyrolactone into copolymers that also contain more easily polymerized monomers (e.g. ϵ -caprolactone) has previously been reported.^{52,55,56} These copolymers are made thermodynamically possible due to the energy released from ring opening the comonomer. Although homopolymerization of γ -butyrolactone catalyzed by **5.3b** has thus far proven to be elusive, we were excited to find that copolymerization reactions run with an equimolar amount of γ -butyrolactone and ϵ -caprolactone led to the clean conversion of both monomers (Scheme 5.2). Notably, 33% incorporation of γ -butyrolactone in these reactions is near the thermodynamic limit of 43% for incorporating γ -butyrolactone starting with a 1:1 mixture of monomers in the feed,⁵⁵ and is among the highest reported incorporation of γ -butyrolactone in copolymerization reactions with ϵ -caprolactone when starting with an equimolar mixture of monomers in the feed.^{53,54}

The success that **5.3b** had as a catalyst for the copolymerization of ϵ -caprolactone and γ -butyrolactone prompted a brief investigation into the ability for **5.3b** to catalyze other copolymerization reactions (Scheme 5.2). When an equimolar mixture of ϵ -caprolactone and δ -valerolactone was exposed to 0.2 mol% **5.3b** in toluene, evidence for a copolymer containing both monomers was observable by ¹H NMR spectroscopy (Scheme 5.2). Despite **5.3b** being more active toward ϵ -caprolactone than δ -valerolactone in homopolymerization experiments, the two monomers appeared to have similar

conversion rates in the copolymerization experiment. This reactivity is likely due to comparable reactivity ratios for the two monomers in this copolymerization. δ -Valerolactone reached higher ultimate conversion than what was observed in the homopolymerization reactions (93% compared to 83%), which suggests that depolymerization of this monomer is not as accessible under the copolymerization conditions.

In contrast to the other combinations of monomers studied, the combination of (*rac*)-lactide and ϵ -caprolactone did not produce copolymers. When an equimolar mixture of these two monomers was exposed to **5.3b** in toluene at room temperature, full conversion of (*rac*)-lactide was observed without any conversion of ϵ -caprolactone even after prolonged reaction time. This observation was somewhat surprising considering that the homopolymerization of ϵ -caprolactone was significantly faster than the homopolymerization of (*rac*)-lactide.

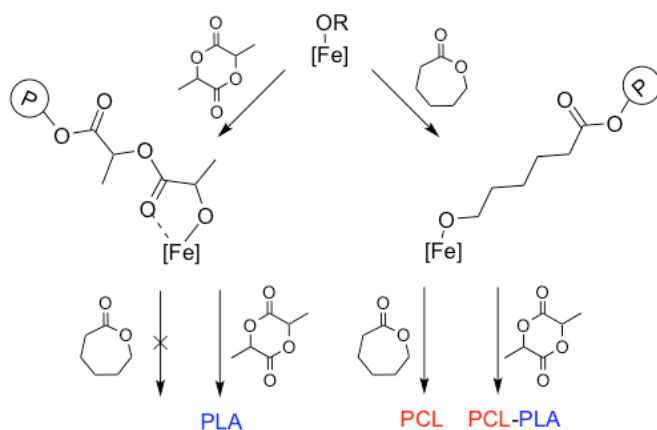
Scheme 5.2. Some copolymerization reactions catalyzed by 5.3b



Although these results precluded the formation of random or statistical copolymers, block copolymers of ϵ -caprolactone and lactide were obtainable by sequential addition of the two monomers in the appropriate order (Scheme 5.2). Whereas reactions involving the initial addition of (*rac*)-lactide polymerization followed by ϵ -caprolactone led to no conversion of the latter monomer, polymerization of both monomers could be obtained if ϵ -caprolactone was added before (*rac*)-lactide. When carried out in this sequence, full conversion of lactide and an increase in molecular weight was observed ($M_w/M_n = 118.3$ to 156.1 kg/mol, respectively), which was evidence for the formation of a block copolymer. Similarly, block copolymers containing δ -valerolactone and (*rac*)-lactide could only be synthesized if δ -valerolactone was used before (*rac*)-lactide and not vice versa. However, block copolymers containing δ -valerolactone and ϵ -caprolactone could be formed using either order of addition of monomers.

The copolymerization results revealed that the active species formed during (*rac*)-lactide polymerization is not active for the insertion of other cyclic esters, such as ϵ -caprolactone (Scheme 5.3). Copolymerization of ϵ -caprolactone and lactide often occur with preferential lactide insertion resulting in gradient or block copolymers, which may be due to the superior coordination ability of lactide.^{56,57} Once lactide inserts into the iron alkoxide bond, an ester functionality adjacent to the growing polymer chain may form a favorable five-membered ring chelate with the iron center (Scheme 5.3, left). To explain the behavior of **5.3b**, we suggest that (*rac*)-lactide polymerization can continue to propagate from this species, but the ϵ -caprolactone monomer is not able to displace this chelate to initiate its polymerization. Conversely, the growing poly(lactone) chain derived

from ϵ -caprolactone polymerization (Scheme 5.3, right) cannot form a similarly stable chelate structure, thereby leaving the iron center accessible for polymerization from either monomer. In this manner, initiation of (*rac*)-lactide polymerization is selective for (*rac*)-lactide propagation, while initiation of ϵ -caprolactone polymerization allows for either monomer to propagate. This explanation also explains the exclusive lactide homopolymerization that occurs when **5.3b** is exposed to a mixture of monomers.



Scheme 5.3. Proposed explanation for the chemoselectivity observed in copolymerization reactions involving (*rac*)-lactide and ϵ -caprolactone

5.5 Conclusions

Formally iron(I) alkoxide complexes supported by bis(imino)pyridine ligands **5.3** were synthesized and found to be excellent catalysts for the ring opening polymerization of several lactones, a cyclic carbonate, and (*rac*)-lactide but completely inactive for the polymerization of epoxides. Our initial hypothesis was that the more electron rich iron center of complex **5.3b** would make it a superior catalyst for ring opening polymerization than the corresponding iron(II) catalyst **5.1b**. This hypothesis proved to be true for most monomers. Remarkably, the formally iron(I) complex **5.3b** was found to be one of the most active iron-based catalysts reported for the polymerization of the lactone monomers

ϵ -caprolactone and δ -valerolactone and afforded accelerated polymerization rates for other monomers compared to the analogous iron(II) complex **5.1b** as expected. Additionally, **5.3b** was able to catalyze statistical copolymerization reactions between caprolactone and the low strain energy monomer γ -butyrolactone, further exemplifying its propensity for ester ring-opening reactions. (*rac*)-Lactide polymerization was an outlier among the cyclic esters tested with the formally iron(II) complex **5.1b** being a more efficient catalyst than the formally iron(I) complex **5.3b**. This discrepancy was attributed to a chelating interaction that is unique to lactide polymerization and tempers the reactivity of **5.3b** more than **5.1b** for reasons that are at present not apparent.

Using a combination of experimental and computational techniques, it was determined that **5.1b** is best described as an iron(II) complex that is antiferromagnetically coupled to a singly reduced ligand. As a result, the differences observed between **5.3** and **5.1** are likely due to the change in the electron donating ability of neutral versus singly reduced bis(imino)pyridine ligands rather than a change in the formal oxidation state of the metal. This result stands in contrast to the significant differences between **5.1** and **5.2** towards ring-opening polymerization reaction of lactide, which we previously have attributed to a change in oxidation state of the metal. However, the differences between **5.1** and **5.2** may also be a consequence of **5.1** being neutral and **5.2** being cationic.

To gain further understanding into the role that charge plays in the reactivity of these complexes, computation studies were performed by the Cramer group on mechanistic exploration of cationic bis(imino)pyridine iron complexes in the ring opening polymerization of ϵ -caprolactone.⁴⁷ The main findings of this computational study were that all the catalysts **5.1-5.3** can best be described as Fe(II) centers with either

a redox-active bis(imino) pyridine or alkoxide ligand. Notably, high-spin species appear to be better Lewis acids and more efficiently bind the monomers for ring-opening polymerization. Aryloxide initiators are likely sluggish catalysts due to the instability of the formed ester intermediates upon their insertion into the monomer. Lastly, it is clear that monomer coordination plays a significant role in determining reactivity trends. Notably, these computations predicted that **5.2b** would be a suitable catalyst for ϵ -caprolactone polymerization. Experimentally, when we tested this prediction, we found that **5.2b** is a competent catalyst for ϵ -caprolactone polymerization and results in full conversion within one hour.

By understanding the characteristic features of the iron-based catalysts that dictate the chemoselectivity in these polymerization reactions, we ultimately aim to develop polymerization reactions that can be controlled at the molecular level so as to produce a variety of degradable materials whose physical and mechanical properties can be tuned appropriately for their application in a wide variety of applications.

5.6 Experimental

General considerations. Unless stated otherwise, all reactions were carried out in oven-dried glassware in a nitrogen-filled glove box or with standard Schlenk line techniques. Solvents were used after passage through a solvent purification system under a blanket of argon and then degassed briefly by exposure to vacuum. Nuclear Magnetic Resonance (NMR) spectra were recorded at ambient temperature on spectrometers operating at 400-600 MHz for ^1H NMR. Resonances for paramagnetic complexes are reported as chemical shift in ppm (peak width at half height, Hz). Infrared (IR) spectra were recorded on an OPUS ATR infrared spectrometer. Magnetic moments were

determined by Evans' method in THF by means of a procedure published by Gibson and coworkers.³⁴ Gel permeation chromatography (GPC) was performed on an Agilent GPC220 in THF at 40°C with three PL gel columns (10µm) in series. Molecular weights and molecular weight distributions were determined from the signal response of the RI detector relative to polystyrene standards. EPR spectra were obtained on a Bruker EleXsys E-500 CW-EPR spectrometer. Spectra were measured as frozen toluene glasses at a microwave power of 0.6325–2 mW at 77 K, 12 K, and 4 K. Effective g-values were obtained from spectral simulations of $S = 1/2$ systems with the program Easyspin. Zero-field ^{57}Fe Mössbauer spectra were measured with a constant acceleration spectrometer (SEE Co, Minneapolis, MN) at 90 K. Isomer shifts are quoted relative to Fe foil at room temperature. Data was analyzed and simulated with Igor Pro 6 software (WaveMetrics, Portland, OR) by means of Lorentzian fitting functions. Samples were prepared by freezing a solution of 20-30 mg compound in benzene. SQUID magnetometry measurements were performed on a Quantum Design MPMS3 Instrument. Samples were prepared by immobilization in eicosane. Data was fit using JulX software to get the zero-field splitting parameters. Statistical molar magnetic susceptibilities were calculated using the usual spin Hamiltonian approach for up to three spins with local multiplicities up to $S = 3/2$ based on:

$$H = H_{\text{ex}} + H_{\text{ZFS}} + H_{\text{Zeeman}} \text{ where,}$$

$$H_{\text{ex}} = -2 \sum_{i=1}^{ns-1} \sum_{j=i+1}^{ns} J_{ij} \bar{S}_i \cdot \bar{S}_j \quad \text{is the exchange Hamiltonian, and}$$

$$H_{\text{ZFS}} = \sum_{i=1}^{ns} D_i \left[S_{z,i}^2 - \frac{1}{3} S_i(S_i + 1) + \frac{E_i}{D_i} (S_{x,i}^2 - S_{y,i}^2) \right] \text{ accounts for zero-field splitting, and}$$

$$H_{\text{Zeeman}} = \sum_{i=1}^{ns} g\beta \bar{S}_i \cdot \bar{B} \quad \text{is the Zeeman interaction.}$$

J_{ij} are the exchange *coupling constants* of spins i and j , n_s is the number of spins (max. four), D_i , E/D_i and g_i are the local axial and rhombic zero field splitting parameters and g -values (isotropic average)

The monomer (*rac*)-lactide was recrystallized from ethyl acetate followed by recrystallization from toluene and dried *in vacuo* prior to polymerization. The monomers ϵ -caprolactone, δ -valerolactone, β -butyrolactone, and γ -valerolactone were dried over CaH_2 and distilled prior to polymerization. Trimethylene carbonate and ethylene carbonate were dried *in vacuo* prior to polymerization. Complexes **5.1** and **5.2** were synthesized as described previously.⁵⁸

Synthesis of Complex 5.3a. In a glove box, a solution of 4-methoxyphenol (0.0249 g, 0.201 mmol) in diethyl ether (10 ml) was cooled to $-40\text{ }^\circ\text{C}$ and added to a solution of **5.4** (0.100 g, 0.196 mmol) in diethyl ether (5ml) that had also been cooled to $-40\text{ }^\circ\text{C}$. The reaction was allowed to stir at room temperature for one hour, and the red mixture was filtered through celite. The solvent was removed from the filtrate to yield a dark red solid (0.103 g, 96%). ^1H NMR (C_6D_6 , broad singlets): 90.3(122.5) *m-py*, 16.5(128.7), -3.9(138.7) *m-aryl*, -12.9(231.4) *p-aryl*, -24.6(146.3), -63.9(1854.6) CCH_3 ppm. IR(neat): 3021, 2914, 2852, 1646, 1592, 1494, 1466, 1437, 1373, 1327, 1250, 1207, 1174, 1109, 1089, 1035, 958, 858, 816, 758, 690, 648, 560, 495 cm^{-1} . EA Found: C, 69.14; H, 6.43; N, 8.38. Calc. for $\text{C}_{32}\text{H}_{34}\text{FeN}_3\text{O}_2$: C, 70.07; H, 6.25; N, 7.66%

Synthesis of Complex 5.3b. In a glove box, a solution of neopentyl alcohol (0.0220 g, 0.250 mmol) in diethyl ether (2 ml) was cooled to $-40\text{ }^\circ\text{C}$ and added to a solution of **5.4** (0.130 g, 0.254 mmol) in diethyl ether (6 ml) that had also been cooled to $-40\text{ }^\circ\text{C}$. The reaction was allowed to stir at room temperature for 30 minutes, and then

solvent was removed *in vacuo*. The resulting residue was lyophilized in frozen benzene. The resulting powder was then dissolved in *n*-pentane and filtered through celite, and the solvent was removed from the filtrate to yield a dark red solid (0.105 g, 82%). Crystallization in *n*-pentane at -40 °C afforded crystals suitable for X-ray analysis. ¹H NMR (C₆D₆, broad singlets): 67.5(109.6) *m*-py, 50.6(235.5), -10.0(51.8) *m*-aryl, -15.9(45.7) *p*-aryl, -50.0(232.4) CCH₃ ppm. IR(neat): 2941, 2856, 1646, 1592, 1467, 1437, 1371, 1327, 1249, 1208, 1170, 1087, 1018, 956, 856, 814, 759, 691, 559, 494 cm⁻¹.

General procedure for the polymerization of (rac)-lactide catalyzed by aryloxy complexes 5.1a and 5.3a. At room temperature in a glove box, iron aryloxy complex **5.1a** or **5.3a** (0.007 mmol) in chlorobenzene (0.9 mL) was added to a seven mL vial containing (*rac*)-lactide (0.050 g, 0.35 mmol) in chlorobenzene (0.5 mL). Aliquots were removed periodically from the reaction mixture and terminated by exposing them to air. Solvent was removed *in vacuo* and conversion was determined by ¹H NMR in CDCl₃ by integrating the methine peak of the remaining lactide versus the methine peak of poly(lactic acid). The aliquots were also analyzed by GPC to determine molecular weight and molecular weight distribution of the polymers.

General procedure for the polymerization of ε-caprolactone catalyzed by aryloxy complexes 5.1a and 5.3a. At room temperature in a glove box, iron aryloxy complex **5.1a** or **5.3a** (0.014 mmol) in toluene (1.8 mL) was added to a seven mL vial containing ε-caprolactone (0.080 g, 0.70 mmol) in toluene (1.0 mL). Aliquots were removed periodically from the reaction mixture and terminated by exposing them to air. Solvent was removed *in vacuo* and conversion was determined by ¹H NMR in CDCl₃ by integrating the α-methylene peak of the remaining ε-caprolactone versus the α-methylene

peak of poly(caprolactone). The aliquots were also analyzed by GPC to determine molecular weight and molecular weight distribution of the polymers.

General procedure for the polymerization of (rac)-lactide catalyzed by neopentoxide complexes 5.1b and 5.3b. At room temperature in a glove box, the desired amount of iron neopentoxide complex **5.1b** or **5.3b** in toluene (1.0 mL) was added to a seven mL vial containing (rac)-lactide (0.10 g, 0.7 mmol) in toluene (1.0 mL). Aliquots were removed periodically from the reaction mixture and terminated by exposing them to air. Solvent was removed *in vacuo* and conversion was determined by ¹H NMR in CDCl₃ by integrating the methine peak of the remaining lactide versus the methine peak of poly(lactic acid). The aliquots were also analyzed by GPC to determine molecular weight and molecular weight distribution of the polymers.

General procedure for the polymerization of ε-caprolactone with neopentoxide complexes 5.1b and 5.3b. Most polymerization reactions were performed at [caprolactone] = 0.34 M: At room temperature in a glove box, the desired amount of iron neopentoxide complex **5.1b** or **5.3b** in toluene (1.0 mL) was added to a seven mL vial containing ε-caprolactone (0.080 g, 0.70 mmol) in toluene (1.0 mL). Aliquots were removed periodically from the reaction mixture and terminated by exposing them to air. Solvent was removed *in vacuo* and conversion was determined by ¹H NMR in CDCl₃ by integrating the α-methylene peak of the remaining ε-caprolactone versus the α-methylene peak of poly(caprolactone). The aliquots were also analyzed by GPC to determine molecular weight and molecular weight distribution of the polymers. Reactions performed at higher concentrations were carried out by increasing the amount of ε-

caprolactone added and reactions performed at lower concentrations were performed by increasing the amount of toluene added.

General procedure for the polymerization of δ -valerolactone with neopentoxide complexes 5.1b and 5.3b. At room temperature in a glove box, the desired amount of iron neopentoxide complex **5.1b** or **5.3b** in toluene (1.0 mL) was added to a seven mL vial containing δ -valerolactone (0.070 g, 0.70 mmol) in toluene (1.0 mL). Aliquots were removed periodically from the reaction mixture and terminated by exposing them to air. Solvent was removed *in vacuo* and conversion was determined by ^1H NMR in CDCl_3 by integrating the α -methylene peak of the remaining δ -valerolactone versus the α -methylene peak of poly(valerolactone). The aliquots were also analyzed by GPC to determine molecular weight and molecular weight distribution of the polymers.

General procedure for the polymerization of β -butyrolactone with neopentoxide complexes 5.1b and 5.3b. At room temperature in a glove box, the desired amount of iron neopentoxide complex **5.1b** or **5.3b** in toluene (1.0 mL) was added to a seven mL vial containing β -butyrolactone (0.070 g, 0.70 mmol) in toluene (1.0 mL). Aliquots were removed periodically from the reaction mixture and terminated by exposing them to air. Solvent was removed *in vacuo* and conversion was determined by ^1H NMR in CDCl_3 by integrating the α -methylene peak of the remaining β -butyrolactone versus the α -methylene peak of poly(butyrolactone). The aliquots were also analyzed by GPC to determine molecular weight and molecular weight distribution of the polymers.

Attempted polymerization of γ -butyrolactone with neopentoxide complexes 5.1b and 5.3b. At room temperature in a glove box, the desired amount of iron

neopentoxide complex **5.1b** or **5.3b** (0.007 mmol) in THF (0.9 mL) was added to a seven mL vial containing γ -butyrolactone (0.070 g, 0.70 mmol) in THF (1.0 mL). The reaction was allowed to stir 24 hours at room temperature. No conversion was observed by ^1H NMR.

Polymerization of trimethylene carbonate with neopentoxide complex 5.3b.

At room temperature in a glove box, the desired amount of iron neopentoxide complex **5.3b** in toluene (0.5 mL) was added to a seven mL vial containing trimethylene carbonate (0.036g, 0.35 mmol) in toluene (0.5 mL). A gel-like precipitate formed immediately. The reaction mixture was allowed to stir for 10 minutes and was quenched by exposing it to air. Solvent was removed *in vacuo* and conversion was determined by ^1H NMR in CDCl_3 by integrating the α -methylene peak of the remaining β -butyrolactone versus the α -methylene peak of poly(butyrolactone). The aliquots were also analyzed by GPC to determine molecular weight and molecular weight distribution of the polymers.

Attempted polymerization of ethylene carbonate with neopentoxide complexes 5.1b and 5.3b. At room temperature in a glove box, the desired amount of iron neopentoxide complex **5.1b** or **5.3b** in THF (0.9 mL) was added to a seven mL vial containing ethylene carbonate (0.032 g, 0.36 mmol) in toluene (0.5 mL). The reaction mixture was allowed to stir at room temperature for 24 hours. No conversion was observed by ^1H NMR.

Attempted copolymerization of lactide and ϵ -caprolactone in one reaction pot. At room temperature in a glove box, the desired amount of complex **5.3b** in toluene (1.0 mL) was added to a seven mL vial containing (*rac*)-lactide (0.10 g, 0.70mmol) and ϵ -caprolactone (0.080g, 0.70mmol) in toluene (1.0 mL). Aliquots were removed

periodically from the reaction mixture and terminated by exposing them to air. Solvent was removed *in vacuo* and conversion of lactide was determined by ^1H NMR in CDCl_3 by integrating the methine peak of the remaining lactide versus the methine peak of poly(lactic acid). No conversion of ϵ -caprolactone was observed by ^1H NMR. The aliquots were also analyzed by GPC to determine molecular weight and molecular weight distribution of the polymers.

Attempted copolymerization of lactide and ϵ -caprolactone by sequential lactide-caprolactone addition. At room temperature in a glove box, iron alkoxide complex **5.3b** (350 μL of a 0.0040 M solution in toluene, 0.0014 mmol) was added to a seven mL vial containing (*rac*)-lactide (0.10 g, 0.70 mmol) in toluene (2.0 mL). The reaction was allowed to stir at room temperature for six hours, and then ϵ -caprolactone (0.080 g, 0.70 mmol) was added. Aliquots were removed periodically from the reaction mixture and terminated by exposing them to air. Solvent was removed *in vacuo* and conversion of lactide was determined by ^1H NMR in CDCl_3 by integrating the methine peak of the remaining lactide versus the methine peak of poly(lactic acid). No conversion of ϵ -caprolactone was observed by ^1H NMR. The aliquots were also analyzed by GPC to determine molecular weight and molecular weight distribution of the polymers.

Block copolymerization of lactide and ϵ -caprolactone by sequential caprolactone-lactide addition. At room temperature in a glove box, complex **5.3b** (350 μL of a 0.0040 M solution in toluene, 0.0014 mmol) was added to a seven mL vial containing ϵ -caprolactone (0.080 g, 0.7 mmol) in toluene (2.0 mL). The reaction was allowed to stir at room temperature for 20 minutes, and then (*rac*)-lactide (0.10 g, 0.70 mmol) was added. Aliquots were removed periodically from the reaction mixture and

terminated by exposing them to air. Solvent was removed *in vacuo* and conversion of lactide was determined by ^1H NMR in CDCl_3 by integrating the methine peak of the remaining lactide versus the methine peak of poly(lactic acid). Conversion of ϵ -caprolactone was determined by ^1H NMR in CDCl_3 by integrating the α -methylene peak of the remaining ϵ -caprolactone versus the α -methylene peak of poly(caprolactone). The aliquots were also analyzed by GPC to determine molecular weight and molecular weight distribution of the polymers.

Attempted copolymerization of lactide and δ -valerolactone in one reaction pot. At room temperature in a glove box, the desired amount of iron alkoxide complex **5.3** (350 μL of a 0.0040 M solution in toluene, 0.0014 mmol) was added to a seven mL vial containing (*rac*)-lactide (0.10 g, 0.70 mmol) and δ -valerolactone (0.080 g, 0.70 mmol) in toluene (2.0 mL). Aliquots were removed periodically from the reaction mixture and terminated by exposing them to air. Solvent was removed *in vacuo* and conversion of lactide was determined by ^1H NMR in CDCl_3 by integrating the methine peak of the remaining lactide versus the methine peak of poly(lactic acid). No conversion of δ -valerolactone was observed by ^1H NMR. The aliquots were also analyzed by GPC to determine molecular weight and molecular weight distribution of the polymers.

Copolymerization of ϵ -caprolactone and δ -valerolactone in one reaction pot. At room temperature in a glove box, the desired amount of iron alkoxide complex **5.3b** (350 μL of a 0.0040 M solution in toluene, 0.0014 mmol) was added to a seven mL vial containing ϵ -caprolactone (0.080 g, 0.70 mmol) and δ -valerolactone (0.080 g, 0.70 mmol) in toluene (2.0 mL). Aliquots were removed periodically from the reaction mixture and terminated by exposing them to air. Solvent was removed *in vacuo* and conversions of

both monomers were determined by ^1H NMR in CDCl_3 by integrating the α -methylene peak of the remaining lactone monomer versus the α -methylene peak of poly(lactone). The aliquots were also analyzed by GPC to determine molecular weight and molecular weight distribution of the polymers.

General procedure for the polymerization of ϵ -caprolactone with 5.2b. In a 7 mL vial with stir bar was added 2,6-dimethylphenyl bis(imino)pyridine iron bis(neopentoxide) (1.05 mg, 1.75 μmol) in toluene (2.00 mL). ϵ -caprolactone (1mg, 8.76 μmol) was then added to the vial and allowed to stir for 10 minutes to allow the complex to initiate. Ferrocenium hexafluorophosphate (0.6 mg, 1.81 μmol) was then added to the vial. Reaction was allowed to stir for 10 minutes at room temperature, solution turned blue. Additional ϵ -caprolactone (99.0 mg, 867 μmol) was then added to the vial and allowed to stir at room temperature. Complete conversion was seen after 60 minutes to yield a polymer with $M_n = 48.9 \text{ kg mol}^{-1}$ and $M_w/M_n = 1.2$.

Computational Details

Electronic structure. All calculations were performed at the density functional theory (DFT)⁵⁹ level with Gaussian 09.⁶⁰ Geometry optimizations were carried using the M06-L local density functional.^{61,62} Numerical integrations were performed with an ultrafine grid. An automatic density-fitting set generated by the Gaussian program was employed to reduce the computational cost. Def2-TZVP basis sets were used for all atoms.⁶³ Selected species were re-optimized at TPSSh-D3BJ⁶⁴⁻⁶⁶ level. Single point calculations on M06-L geometries were computed using a variety of density functionals (DFs): τ -HCTH,⁶⁷ B3LYP-D3BJ,^{65,66,68} MN15,⁶⁹ B97D3,^{65,66,70} OPBE-D3BJ,^{65,66,71,72} and

TPSSh-D3BJ.⁶⁴⁻⁶⁶ Some of these DFs have been recommended for complexes bearing redox non-innocent ligands⁷³ and iron spin-state splitting energies.⁷⁴

All quartet and doublet energies were corrected from spin contamination through sextet single point calculations following the Yamaguchi broken-spin-symmetry procedure,⁷⁵

$${}^{\text{LS}}E = \frac{{}^{\text{BS}}E(\langle S^2 \rangle^{\text{HS}}) - {}^{\text{HS}}E(\langle S^2 \rangle^{\text{BS}})}{\langle S^2 \rangle^{\text{HS}} - \langle S^2 \rangle^{\text{BS}}}$$

where $\langle S^2 \rangle^{\text{HS}}$ and $\langle S^2 \rangle^{\text{BS}}$ refer to the computed expectation values of the total spin operator for sextet (HS) and quartet or doublet (BS), and $\langle S^2 \rangle^{\text{LS}}$ corresponds to the ideal expectation value of the total spin operator for quartet (3.75) or doublet (0.75).

Sensitivity of geometries. All species were optimized at M06-L level, which predicts a quartet ground state. To address the influence of the density functional on the geometry, we re-optimized species **5.3a** using TPSSh-D3BJ, a density functional that favors a doublet ground state. Despite the somehow smaller O–Fe–N2 angle shown by TPSSh-D3BJ, the computed bond distances are quite similar and follow the same trend; shorter values are predicted for the doublet state.

⁵⁷Fe Mössbauer calculations. ⁵⁷Fe Mössbauer parameters (isomer shift δ and quadrupole splitting ΔE_Q) were computed following the procedure reported by Neese et al.^{76,77} For the prediction of isomer shifts we first need to correlate theoretical electron densities ρ_0 with experimental isomer shifts δ_{exp} . We employed most of the species of the calibration set reported by Neese et al.⁷⁷ plus two additional iron complexes **S** and **T**. **S** ($\delta = 1.13$ mm/s)⁴⁵ was considered as an example of bis(imino)pyridine complex, whereas **T**

($\delta = -0.32$ mm/s)⁷⁸ was included to expand the under-represented section of negative isomer shift values within the calibration set.

All calculations were carried out at the density functional theory using the M06-L local density functional as implemented in ORCA.⁷⁹ Geometry optimizations were performed with Def2-TZVP basis sets for all atoms; subsequent single point calculations were performed with Def2-TZVPP for Fe and Def2-TZVPPD for the rest of atoms.^{63,80} Def2-TZVP/J auxiliary basis sets were employed. We used an integration accuracy of 11 for Fe and 7 for the rest of atoms. All calculations regarding the calibration set were carried out in an aqueous environment using the COSMO model.⁸¹ Complexes **5.3a** and **5.3b** were reoptimized in SMD=water³¹ as implemented in Gaussian 09 and the resulting geometries were used to compute ρ_0 and ΔE_Q using the above-mentioned procedure in ORCA.

5.7 References

- (1) Dove, A. P. Controlled Ring-Opening Polymerisation of Cyclic Esters: Polymer Blocks in Self-Assembled Nanostructures. *Chem. Commun.* **2008**, No. 48, 6446–6470.
- (2) Dechy-Cabaret, O.; Martin-Vaca, B.; Bourissou, D. Controlled Ring-Opening Polymerization of Lactide and Glycolide. *Chem. Rev.* **2004**, *104* (12), 6147–6176.
- (3) Mehta, R.; Kumar, V.; Bhunia, H.; Upadhyay, S. N. Synthesis of Poly(lactic Acid): A Review. *J. Macromol. Sci. - Polym. Rev.* **2005**, *45* (4), 325–349.
- (4) Byers, J. A.; Biernesser, A. B.; Delle Chiaie, K. R.; Kaur, A.; Kehl, J. A. Catalytic Systems for the Production of Poly(lactic Acid); 2017; pp 67–118.
- (5) Stolt, M.; Södergård, A. Use of Monocarboxylic Iron Derivatives in the Ring-Opening Polymerization of L-Lactide. *Macromolecules* **1999**, *32* (20), 6412–6417.
- (6) O’Keefe, B. J.; Monnier, S. M.; Hillmyer, M. A.; Tolman, W. B. Rapid and Controlled Polymerization of Lactide by Structurally Characterized Ferric Alkoxides. *J. Am. Chem. Soc.* **2001**, *123* (2), 339–340.
- (7) O’Keefe, B. J.; Breyfogle, L. E.; Hillmyer, M. A.; Tolman, W. B. Mechanistic Comparison of Cyclic Ester Polymerizations by Novel iron(III)-Alkoxide Complexes: Single vs Multiple Site Catalysis. *J. Am. Chem. Soc.* **2002**, *124* (16), 4384–4393.
- (8) Gibson, V. C.; Marshall, E. L.; Navarro-Llobet, D.; White, A. J. P.; Williams, D. J. A Well-Defined iron(II) Alkoxide Initiator for the Controlled Polymerisation of Lactide. *J. Chem. Soc. Dalton Trans.* **2002**, *0* (23), 4321–4322.

- (9) McGuinness, D. S.; Marshall, E. L.; Gibson, V. C.; Steed, J. W. Anionic iron(II) Alkoxides as Initiators for the Controlled Ring-Opening Polymerization of Lactide. *J. Polym. Sci. Part A Polym. Chem.* **2003**, *41* (23), 3798–3803.
- (10) Wang, X.; Liao, K.; Quan, D.; Wu, Q. Bulk Ring-Opening Polymerization of Lactides Initiated by Ferric Alkoxides. *Macromolecules* **2005**, *38* (11), 4611–4617.
- (11) Idage, B. B.; Idage, S. B.; Kasegaonkar, A. S.; Jadhav, R. V. Ring Opening Polymerization of Dilactide Using Salen Complex as Catalyst. *Mater. Sci. Eng. B Solid-State Mater. Adv. Technol.* **2010**, *168* (1), 193–198.
- (12) Södergård, A.; Stolt, M. Ring-Opening Polymerization of L-Lactide by Means of Different Iron Compounds. *Macromol. Symp.* **1998**, *130* (1), 393–402.
- (13) Nakayama, A.; Kawasaki, N.; Arvanitoyannis, I.; Yamamoto, N. Synthesis and Degradability of a Novel Aliphatic Polyester: *Polymer (Guildf)*. **1995**, *36* (4), 1295–1301.
- (14) Kricheldorf, H. R.; Boettcher, C. Polylactones .21. Polymerization of L,L-Lactide and Rac-D,L-Lactide With Hematin and Related Porphyrin Complexes. *Makromol. Chemie-Macromolecular Chem. Phys.* **1993**, *194* (2), 463–473.
- (15) Kricheldorf, H. R.; Damrau, D. O. Polylactones, 38: Polymerization of L-Lactide with Fe(II) Lactate and Other Resorbable Fe(II) Salts. *Macromol. Chem. Phys.* **1997**, *198* (6), 1767–1774.
- (16) Biernesser, A. B.; Li, B.; Byers, J. A. Redox-Controlled Polymerization of Lactide Catalyzed by Bis(imino)pyridine Iron Bis(alkoxide) Complexes. *J. Am. Chem. Soc.* **2013**, *135* (44), 16553–16560.

- (17) Arbaoui, A.; Redshaw, C.; Elsegood, M. R. J.; Wright, V. E.; Yoshizawa, A.; Yamato, T. Iron(III) and Zinc(II) Calixarene Complexes: Synthesis, Structural Studies, and Use as Procatalysts for ϵ -Caprolactone Polymerization. *Chem. - An Asian J.* **2010**, *5* (3), 621–633.
- (18) Gowda, R. R.; Chakraborty, D. Environmentally Benign Process for Bulk Ring Opening Polymerization of Lactones Using Iron and Ruthenium Chloride Catalysts. *J. Mol. Catal. A Chem.* **2009**, *301* (1–2), 84–92.
- (19) Chen, M. Z.; Sun, H. M.; Li, W. F.; Wang, Z. G.; Shen, Q.; Zhang, Y. Synthesis, Structure of Functionalized N-Heterocyclic Carbene Complexes of Fe(II) and Their Catalytic Activity for Ring-Opening Polymerization of ϵ -Caprolactone. *J. Organomet. Chem.* **2006**, *691* (11), 2489–2494.
- (20) Geng, C.; Peng, Y.; Wang, L.; Roesky, H. W.; Liu, K. A Multimetallic iron(II)-Lithium Complex as a Catalyst for ϵ -Caprolactone Polymerization. *Dalt. Trans.* **2016**, *45* (40), 15779–15782.
- (21) Hege, C. S.; Schiller, S. M. Non-Toxic Catalysts for Ring-Opening Polymerizations of Biodegradable Polymers at Room Temperature for Biohybrid Materials. *Green Chem.* **2014**, *16* (3), 1410–1416.
- (22) Estrina, G. A.; Grishchuk, A. A.; Karateyev, A. M.; Rozenberg, B. A. Polymerization of ϵ -Caprolactone with Photoreduction of an Iron Chloride Complex Catalyst. *Polym. Sci. U.S.S.R.* **1988**, *30* (3), 615–620.
- (23) Fang, Y. Y.; Gong, W. J.; Shang, X. J.; Li, H. X.; Gao, J.; Lang, J. P. Synthesis and Structure of a Ferric Complex of 2,6-di(1H-Pyrazol-3-yl) Pyridine and Its

- Excellent Performance in the Redox-Controlled Living Ring-Opening Polymerization of ϵ -Caprolactone. *Dalt. Trans.* **2014**, *43* (22), 8282–8289.
- (24) Dobrzynski, P.; Pastusiak, M.; Bero, M. Less Toxic Acetylacetonates as Initiators of Trimethylene Carbonate and 2,2-Dimethyltrimethylene Carbonate Ring Opening Polymerization. *J. Polym. Sci. Part A Polym. Chem.* **2005**, *43* (9), 1913–1922.
- (25) Kricheldorf, H. R.; Lee, S. R.; Weegen-Schulz, B. Polymers of Carbonic Acid: Spontaneous and Hematin-Initiated Polymerizations of Trimethylene Carbonate and Neopentylene Carbonate. *Macromol. Chem. Phys.* **1996**, *197* (3), 1043–1054.
- (26) Helou, M.; Miserque, O.; Brusson, J.-M.; Carpentier, J.-F.; Guillaume, S. M. Poly(trimethylene Carbonate) from Biometals-Based Initiators/Catalysts: Highly Efficient Immortal Ring-Opening Polymerization Processes. *Adv. Synth. Catal.* **2009**, *351* (9), 1312–1324.
- (27) Biernesser, A. B.; Li, B.; Byers, J. A. Redox-Controlled Polymerization of Lactide Catalyzed by Bis(imino)pyridine Iron Bis(alkoxide) Complexes. *J. Am. Chem. Soc.* **2013**, *135* (44), 16553–16560.
- (28) Manna, C. M.; Kaplan, H. Z.; Li, B.; Byers, J. A. High Molecular Weight Poly(lactic Acid) Produced by an Efficient Iron Catalyst Bearing a Bis(amidinato)-N-Heterocyclic Carbene Ligand. *Polyhedron* **2014**, *84*, 160–167.
- (29) Teator, A. J.; Lastovickova, D. N.; Bielawski, C. W. Switchable Polymerization Catalysts. *Chem. Rev.* **2016**, *116* (4), 1969–1992.
- (30) Guillaume, S. M.; Kirillov, E.; Sarazin, Y.; Carpentier, J. F. Beyond Stereoselectivity, Switchable Catalysis: Some of the Last Frontier Challenges in

- Ring-Opening Polymerization of Cyclic Esters. *Chem. - A Eur. J.* **2015**, *21* (22), 7988–8003.
- (31) Blanco, V.; Leigh, D. A.; Marcos, V. Artificial Switchable Catalysts. *Chem. Soc. Rev.* **2015**, *44* (15), 5341–5370.
- (32) Biernesser, A. B.; Chiaie, K. R. D.; Curley, J. B.; Byers, J. A. Block Copolymerization of Lactide and an Epoxide Facilitated by a Redox Switchable Iron-Based Catalyst. *Angew. Chemie - Int. Ed.* **2016**, *55* (17), 5251–5254.
- (33) Delle Chiaie, K. R.; Yablon, L. M.; Biernesser, A. B.; Michalowski, G. R.; Sudyn, A. W.; Byers, J. A. Redox-Triggered Crosslinking of a Degradable Polymer. *Polym. Chem.* **2016**, *7* (28), 4675–4681.
- (34) Britovsek, G. J. P.; Gibson, V. C.; Spitzmesser, S. K.; Tellmann, K. P.; White, A. J. P.; Williams, D. J. Cationic 2,6-Bis(imino)pyridine Iron and Cobalt Complexes: Synthesis, Structures, Ethylene Polymerisation and Ethylene/polar Monomer Co-Polymerisation Studies. *J. Chem. Soc. Dalton Trans.* **2002**, No. 6, 1159.
- (35) Britovsek, G. J. P.; Bruce, M.; Gibson, V. C.; Kimberley, B. S.; Maddox, P. J.; Mastroianni, S.; McTavish, S. J.; Redshaw, C.; Solan, G. A.; Strömberg, S.; et al. Iron and Cobalt Ethylene Polymerization Catalysts Bearing 2,6-Bis(imino)pyridyl Ligands: Synthesis, Structures, and Polymerization Studies. *J. Am. Chem. Soc.* **1999**, *121* (38), 8728–8740.
- (36) Trovitch, R. J.; Lobkovsky, E.; Bill, E.; Chirik, P. J. Functional Group Tolerance and Substrate Scope in Bis(imino)pyridine Iron Catalyzed Alkene Hydrogenation. *Organometallics* **2008**, *27* (7), 1470–1478.

- (37) Tondreau, A. M.; Atienza, C. C. H.; Weller, K. J.; Nye, S. A.; Lewis, K. M.; Delis, J. G. P.; Chirik, P. J. Iron Catalysts for Selective Anti-Markovnikov Alkene Hydrosilylation Using Tertiary Silanes. *Science* (80-.). **2012**, *335* (6068), 567–570.
- (38) Small, B. L.; Brookhart, M.; Bennett, A. M. A. Highly Active Iron and Cobalt Catalysts for the Polymerization of Ethylene. *J. Am. Chem. Soc.* **1998**, *120* (16), 4049–4050.
- (39) Monfette, S.; Turner, Z. R.; Semproni, S. P.; Chirik, P. J. Enantiopure C 1-Symmetric Bis(imino)pyridine Cobalt Complexes for Asymmetric Alkene Hydrogenation. *J. Am. Chem. Soc.* **2012**, *134* (10), 4561–4564.
- (40) Russell, S. K.; Lobkovsky, E.; Chirik, P. J. Iron-Catalyzed Intermolecular $[2\pi + 2\pi]$ Cycloaddition. *J. Am. Chem. Soc.* **2011**, *133* (23), 8858–8861.
- (41) Bouwkamp, M. W.; Bart, S. C.; Hawrelak, E. J.; Trovitch, R. J.; Lobkovsky, E.; Chirik, P. J. Square Planar Bis(imino)pyridine Iron Halide and Alkyl Complexes. *Chem. Commun.* **2005**, *104* (27), 3406–3408.
- (42) Biernesser, A. B. Synthesis of Divers Degradable Polymers by Redox-Switchable Iron-Based Catalysis, Boston College, 2016.
- (43) Tondreau, A. M.; Milsman, C.; Patricks, A. D.; Hoyt, H. M.; Lobkovsky, E.; Wiegardt, K.; Chirik, P. J. Synthesis and Electronic Structure of Cationic, Neutral, and Anionic Bis(imino)pyridine Iron Alkyl Complexes: Evaluation of Redox Activity in Single-Component Ethylene Polymerization Catalysts. *J. Am. Chem. Soc.* **2010**, *132* (42), 15046–15049.

- (44) Bart, S. C.; Chłopek, K.; Bill, E.; Bouwkamp, M. W.; Lobkovsky, E.; Neese, F.; Wiegardt, K.; Chirik, P. J. Electronic Structure of Bis(imino)pyridine Iron Dichloride, Monochloride, and Neutral Ligand Complexes: A Combined Structural, Spectroscopic, and Computational Study. *J. Am. Chem. Soc.* **2006**, *128* (42), 13901–13912.
- (45) Tondreau, A. M.; Stieber, S. C. E.; Milsmann, C.; Lobkovsky, E.; Weyhermüller, T.; Semproni, S. P.; Chirik, P. J. Oxidation and Reduction of Bis(imino)pyridine Iron Dinitrogen Complexes: Evidence for Formation of a Chelate Trianion. *Inorg. Chem.* **2013**, *52* (2), 635–646.
- (46) Gütllich, P.; Bill, E.; Trautwein, A. X. *Mössbauer Spectroscopy and Transition Metal Chemistry*; Springer, 2011.
- (47) Ortuño, M. A.; Dereli, B.; Chiaie, K. R. D.; Biernesser, A. B.; Qi, M.; Byers, J. A.; Cramer, C. J. The Role of Alkoxide Initiator, Spin State, and Oxidation State in Ring-Opening Polymerization of ϵ -Caprolactone Catalyzed by Iron Bis(imino)pyridine Complexes. *Inorg. Chem.* **2018**, *57* (4), 2064–2071.
- (48) Swart, M.; Gruden, M. Spinning around in Transition-Metal Chemistry. *Acc. Chem. Res.* **2016**, *49* (12), 2690–2697.
- (49) Isley, W. C.; Zarra, S.; Carlson, R. K.; Bilbeisi, R. A.; Ronson, T. K.; Nitschke, J. R.; Gagliardi, L.; Cramer, C. J. Predicting paramagnetic ^1H NMR Chemical Shifts and State-Energy Separations in Spin-Crossover Host-Guest Systems. *Phys. Chem. Chem. Phys.* **2014**, *16* (22), 10620–10628.
- (50) Verma, P.; Varga, Z.; Klein, J. E. M. N.; Cramer, C. J.; Que, L.; Truhlar, D. G. Assessment of Electronic Structure Methods for the Determination of the Ground

- Spin States of Fe(II), Fe(III) and Fe(IV) Complexes. *Phys. Chem. Chem. Phys.* **2017**, *19* (20), 13049–13069.
- (51) Saiyasombat, W.; Molloy, R.; Nicholson, T. M.; Johnson, A. F.; Ward, I. M.; Poshyachinda, S. Ring Strain and Polymerizability of Cyclic Esters. *Polymer (Guildf)*. **1998**, *39* (23), 5581–5585.
- (52) Duda, A.; Kowalski, A. Thermodynamics and Kinetics of Ring-Opening Polymerization. In *Handbook of Ring-Opening Polymerization*; Duda, A.; Kowalski, A., Ed.; Wiley-VCH Verlag GmbH & Co., 2009; pp 1–51.
- (53) Myers, D.; Cyriac, A.; Williams, C. K. Polymer Synthesis: To React the Impossible Ring. *Nat. Chem.* **2016**, *8* (1), 3–4.
- (54) Hong, M.; Chen, E. Y. X. Completely Recyclable Biopolymers with Linear and Cyclic Topologies via Ring-Opening Polymerization of γ -Butyrolactone. *Nat. Chem.* **2016**, *8* (1), 42–49.
- (55) Duda, A.; Libiszowski, J.; Mosnáček, J.; Penczek, S. Copolymerization of Cyclic Esters at the Living Polymer-Monomer Equilibrium. *Macromol. Symp.* **2005**, *226* (1), 109–119.
- (56) Nomura, N.; Akita, A.; Ishii, R.; Mizuno, M. Random Copolymerization of ϵ -Caprolactone with Lactide Using a Homosalen-Al Complex. *J. Am. Chem. Soc.* **2010**, *132* (6), 1750–1751.
- (57) Vion, J. M.; Jérôme, R.; Teyssié, P.; Aubin, M.; Prud'homme, R. E. Synthesis, Characterization, and Miscibility of Caprolactone Random Copolymers. *Macromolecules* **1986**, *19* (7), 1828–1838.

- (58) Delle Chiaie, K. R.; Biernesser, A. B.; Ortuño, M. A.; Dereli, B.; Iovan, D. A.; Wilding, M. J. T.; Li, B.; Cramer, C. J.; Byers, J. A. The Role of Ligand Redox Non-Innocence in Ring-Opening Polymerization Reactions Catalysed by Bis(imino)pyridine Iron Alkoxide Complexes. *Dalton Trans.* **2017**, *46* (38), 12971–12980.
- (59) Cramer, C. J.; Truhlar, D. G. Density Functional Theory for Transition Metals and Transition Metal Chemistry. *Phys. Chem. Chem. Phys.* **2009**, *11* (46), 10757–10816.
- (60) 8. M. J. Frisch et al. Gaussian 09, Revision E.01; Gaussian, Inc.: Wallingford, CT, 2016. <http://gaussian.com/g09citation/> (accessed Aug 6, 2018).
- (61) Zhao, Y.; Truhlar, D. G. A New Local Density Functional for Main-Group Thermochemistry, Transition Metal Bonding, Thermochemical Kinetics, and Noncovalent Interactions. *J. Chem. Phys.* **2006**, *125* (19), 194101.
- (62) Zhao, Y.; Truhlar, D. G. Density Functionals with Broad Applicability in Chemistry. *Acc. Chem. Res.* **2008**, *41* (2), 157–167.
- (63) Weigend, F.; Ahlrichs, R. Balanced Basis Sets of Split Valence, Triple Zeta Valence and Quadruple Zeta Valence Quality for H to Rn: Design and Assessment of Accuracy. *Phys. Chem. Chem. Phys.* **2005**, *7* (18), 3297–3305.
- (64) Staroverov, V. N.; Scuseria, G. E.; Tao, J.; Perdew, J. P. Comparative Assessment of a New Nonempirical Density Functional: Molecules and Hydrogen-Bonded Complexes. *J. Chem. Phys.* **2003**, *119* (23), 12129–12137.

- (65) Grimme, S.; Antony, J.; Ehrlich, S.; Krieg, H. A Consistent and Accurate Ab Initio Parametrization of Density Functional Dispersion Correction (DFT-D) for the 94 Elements H-Pu. *J. Chem. Phys.* **2010**, *132* (15), 154104.
- (66) Grimme, S.; Ehrlich, S.; Goerigk, L. Effect of the Damping Function in Dispersion Corrected Density Functional Theory. *J. Comput. Chem.* **2011**, *32* (7), 1456–1465.
- (67) Boese, A. D.; Handy, N. C. New Exchange-Correlation Density Functionals: The Role of the Kinetic-Energy Density. *J. Chem. Phys.* **2002**, *116* (22), 9559–9569.
- (68) Becke, A. D. Density-Functional Thermochemistry. III. The Role of Exact Exchange. *J. Chem. Phys.* **1993**, *98* (7), 5648–5652.
- (69) Yu, H. S.; He, X.; Li, S. L.; Truhlar, D. G. MN15: A Kohn-Sham Global-Hybrid Exchange-Correlation Density Functional with Broad Accuracy for Multi-Reference and Single-Reference Systems and Noncovalent Interactions. *Chem. Sci.* **2016**, *7* (8), 5032–5051.
- (70) Becke, A. D. Density-Functional Thermochemistry. V. Systematic Optimization of Exchange-Correlation Functionals. *J. Chem. Phys.* **1997**, *107* (20), 8554–8560.
- (71) Perdew, J. P.; Burke, K.; Ernzerhof, M. Generalized Gradient Approximation Made Simple. *Phys. Rev. Lett.* **1996**, *77* (18), 3865–3868.
- (72) Handy, N. C.; Cohen, A. J. Left-Right Correlation Energy. *Mol. Phys.* **2001**, *99* (5), 403–412.
- (73) Milko, P.; Iron, M. A. On the Innocence of Bipyridine Ligands: How Well Do DFT Functionals Fare for These Challenging Spin Systems? *J. Chem. Theory Comput.* **2014**, *10* (1), 220–235.

- (74) Swart, M. Accurate Spin-State Energies for Iron Complexes. *J. Chem. Theory Comput.* **2008**, *4* (12), 2057–2066.
- (75) Yamaguchi, K.; Jensen, F.; Dorigo, A.; Houk, K. N. A Spin Correction Procedure for Unrestricted Hartree-Fock and Møller-Plesset Wavefunctions for Singlet Diradicals and Polyradicals. *Chem. Phys. Lett.* **1988**, *149* (5–6), 537–542.
- (76) Neese, F. Prediction and Interpretation of the ^{57}Fe Isomer Shift in Mössbauer Spectra by Density Functional Theory. *Inorganica Chim. Acta* **2002**, *337*, 181–192.
- (77) Römelt, M.; Ye, S.; Neese, F. Calibration of Modern Density Functional Theory Methods for the Prediction of ^{57}Fe Mössbauer Isomer Shifts: Meta-GGA and Double-Hybrid Functionals. *Inorg. Chem.* **2009**, *48* (3), 784–785.
- (78) Zhang, H.; Ouyang, Z.; Liu, Y.; Zhang, Q.; Wang, L.; Deng, L. (Aminocarbene)(divinyltetramethyldisiloxane)iron(0) Compounds: A Class of Low-Coordinate iron(0) Reagents. *Angew. Chemie - Int. Ed.* **2014**, *53* (32), 8432–8436.
- (79) Neese, F. The ORCA Program System. *Wiley Interdiscip. Rev. Comput. Mol. Sci.* **2012**, *2* (1), 73–78.
- (80) Rappoport, D.; Furche, F. Property-Optimized Gaussian Basis Sets for Molecular Response Calculations. *J. Chem. Phys.* **2010**, *133* (13), 134105.
- (81) Klamt, A.; Schuurmann, G. COSMO: A New Approach to Dielectric Screening in Solvents with Explicit Expressions for the Screening Energy and Its Gradient. *J. Chem. Soc. Perkin Trans. 2* **1993**, *0* (5), 799–805.

Appendix A Differential Scanning Calorimetry and Thermogravimetric Analysis Thermograms

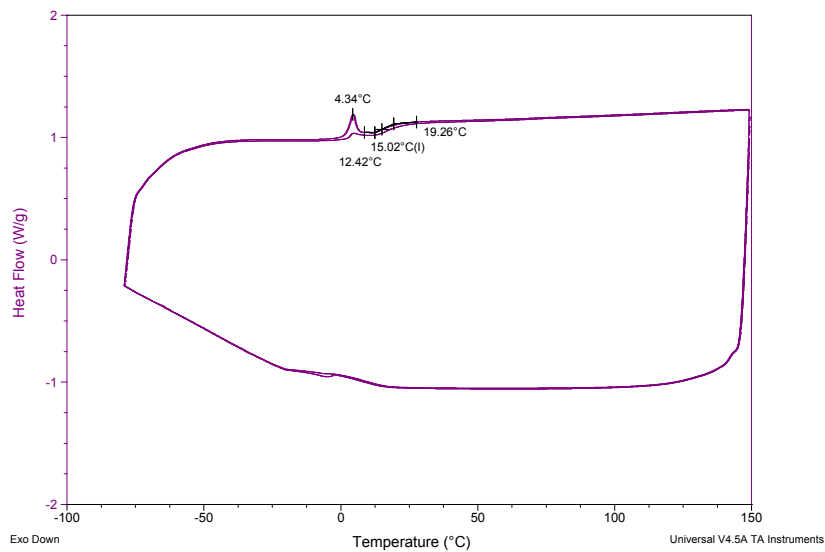


Figure A. 1 DSC trace of a 3.9 homopolymerization catalyzed by 3.1.

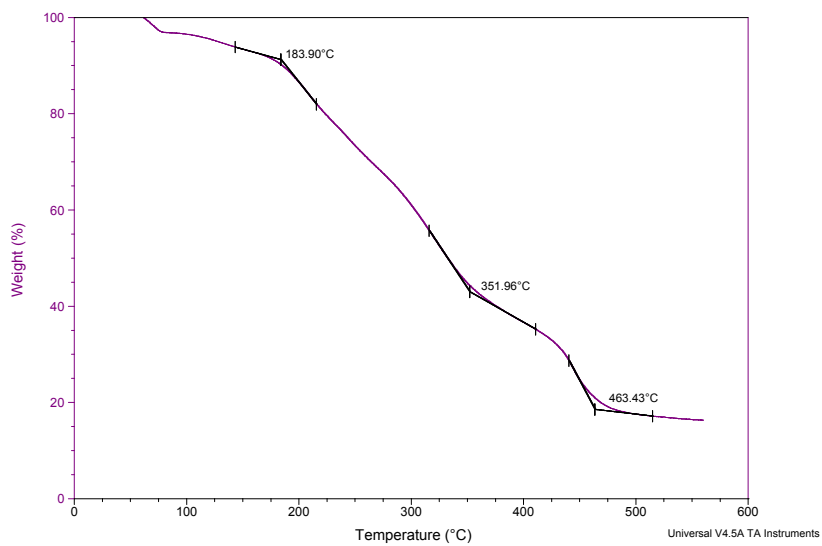


Figure A. 2 TGA trace of a 3.9 homopolymerization catalyzed by 3.1.

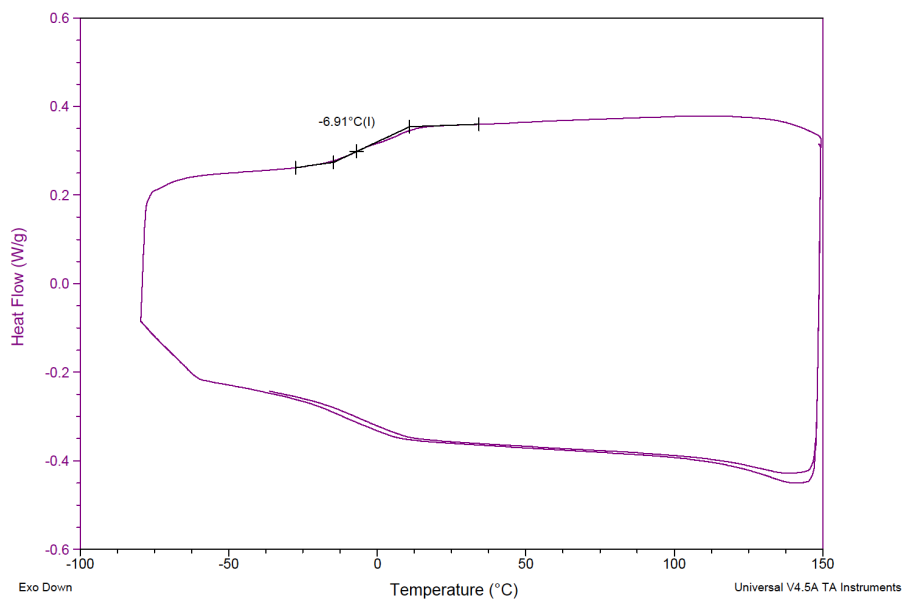


Figure A. 3 DSC trace of a 3.9 homopolymerization catalyzed by 3.2.

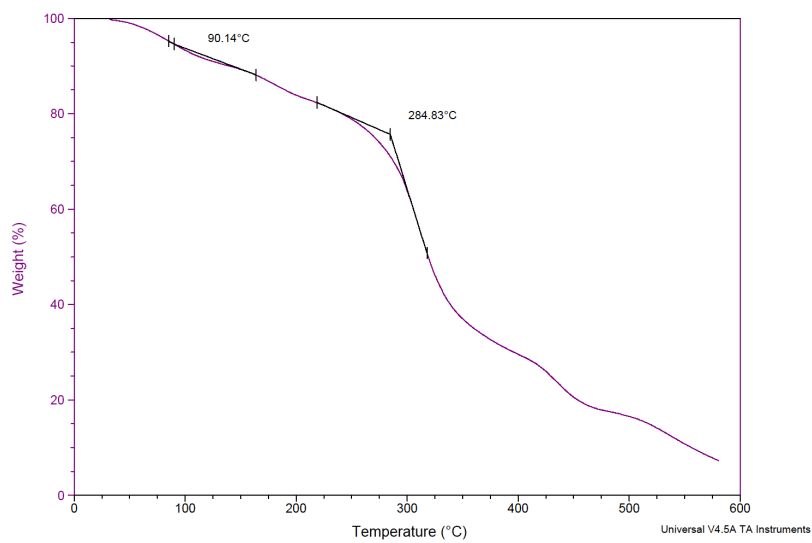


Figure A. 4 TGA trace of 3.9 homopolymerization catalyzed by 3.2.

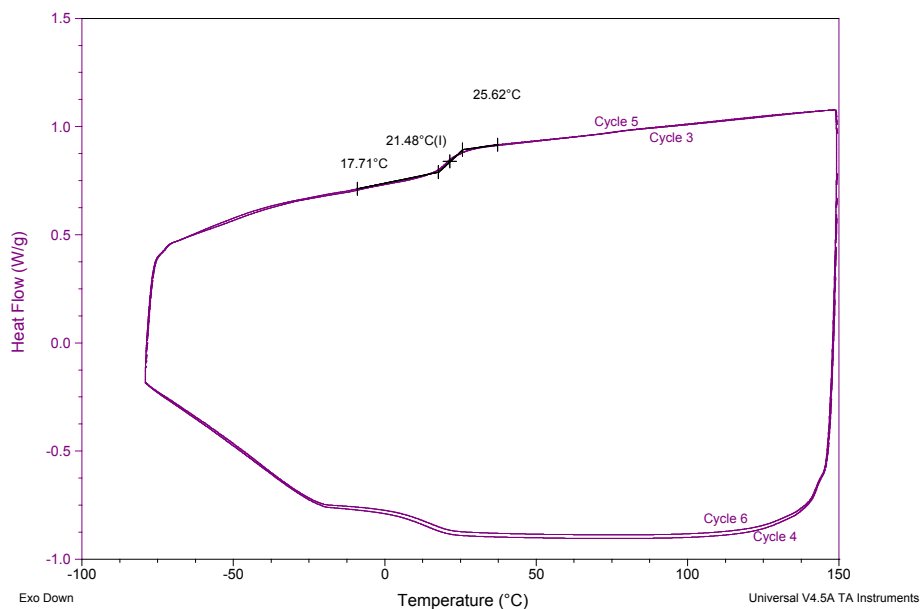


Figure A. 5 DSC trace of a 3.9:lactide (9:1) copolymerization before oxidation.

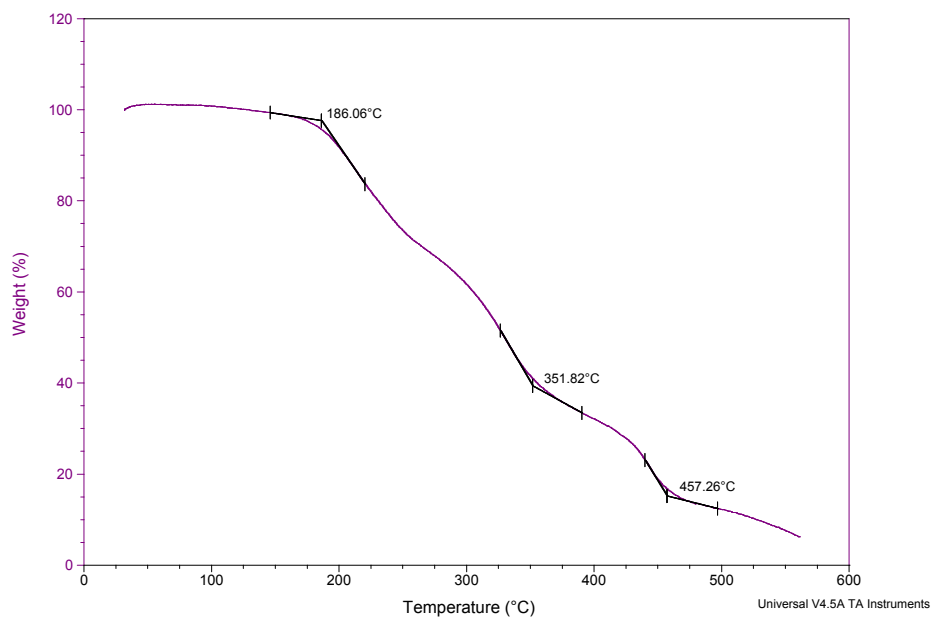


Figure A. 6 TGA trace of a 3.9:lactide (9:1) copolymerization before oxidation.

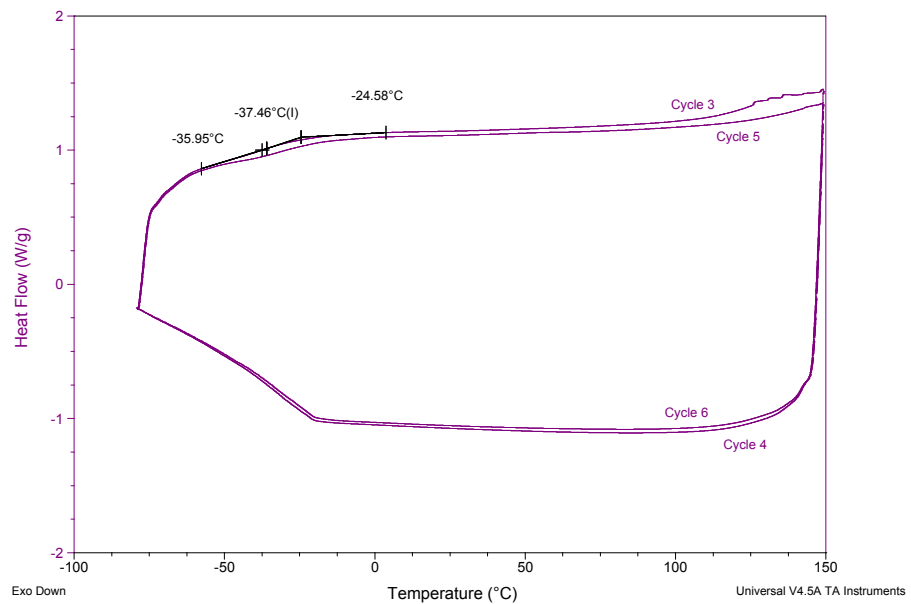


Figure A. 7 DSC trace of a 3.9:lactide (3:1) copolymerization before oxidation.

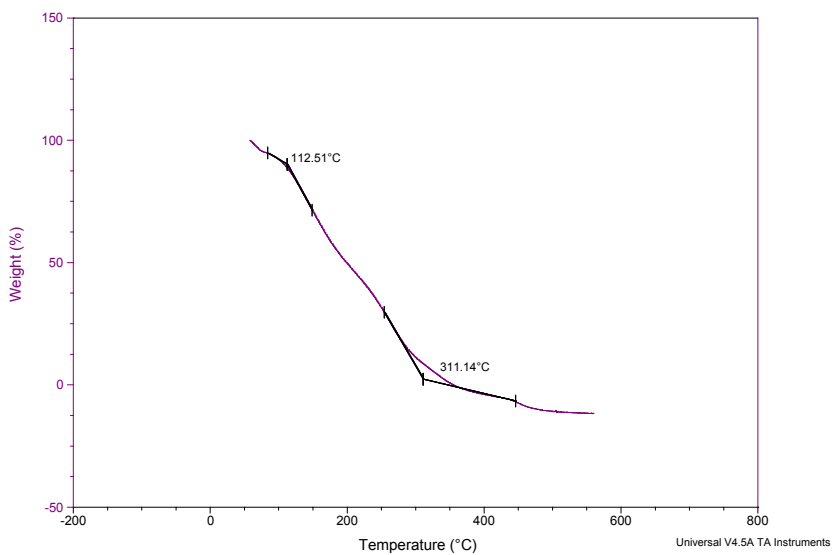


Figure A. 8 TGA trace of a 3.9:lactide (3:1) copolymerization before oxidation.

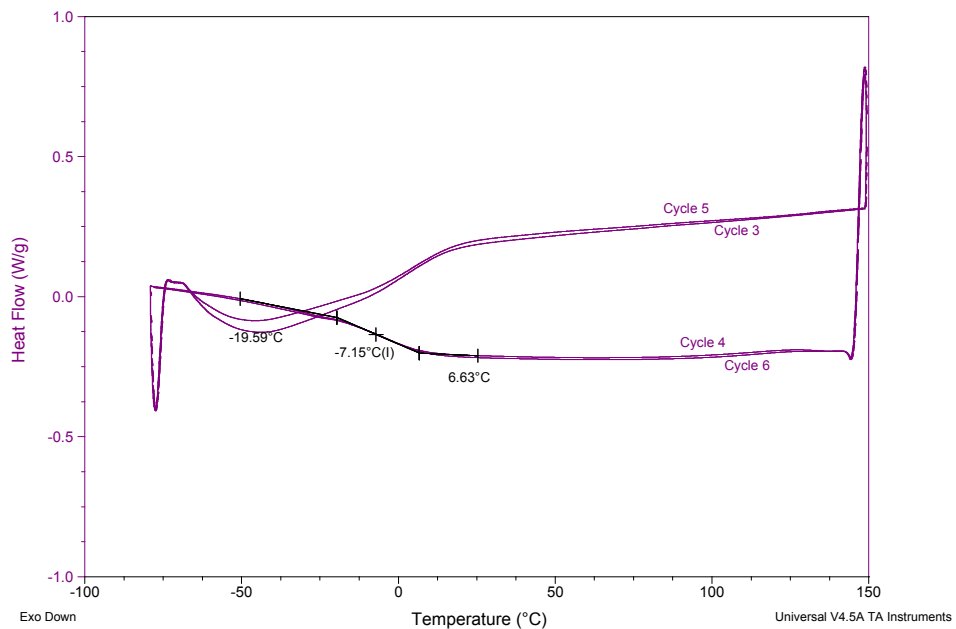


Figure A. 9. DSC trace of a 3.9:lactide (1:1) copolymerization before oxidation.

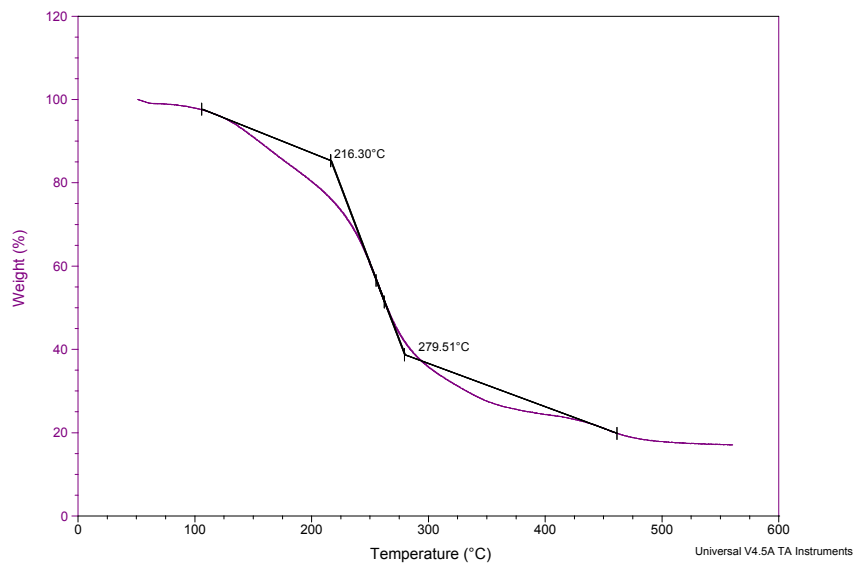


Figure A. 10 TGA trace of a 3.9:lactide (1:1) copolymerization before oxidation.

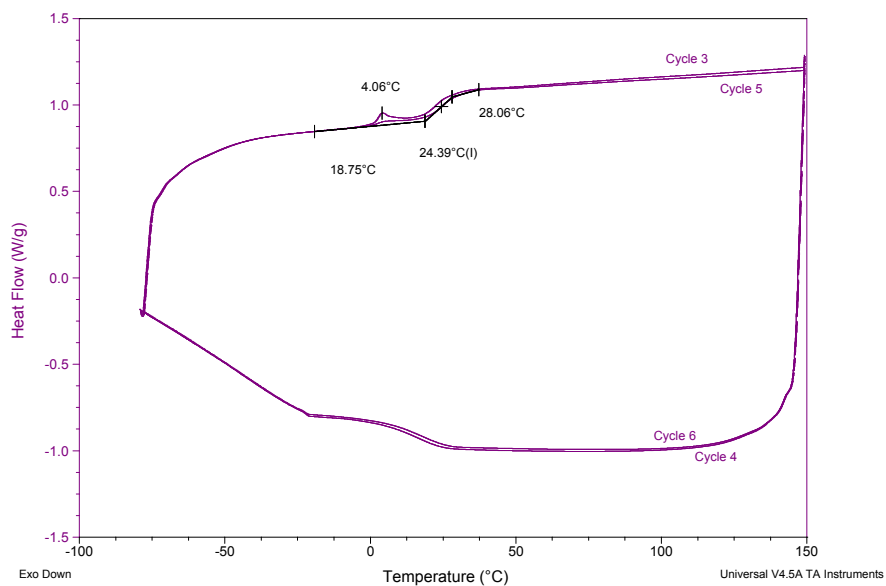


Figure A. 11 DSC trace of a 3.9:lactide (1:3) copolymerization before oxidation.

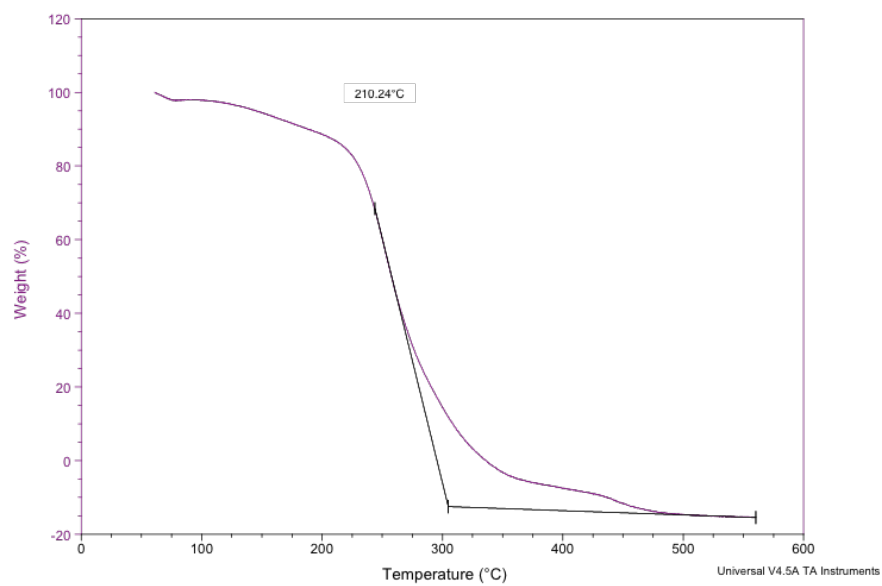


Figure A. 12 TGA trace of a 3.9:lactide (1:3) copolymerization before oxidation.

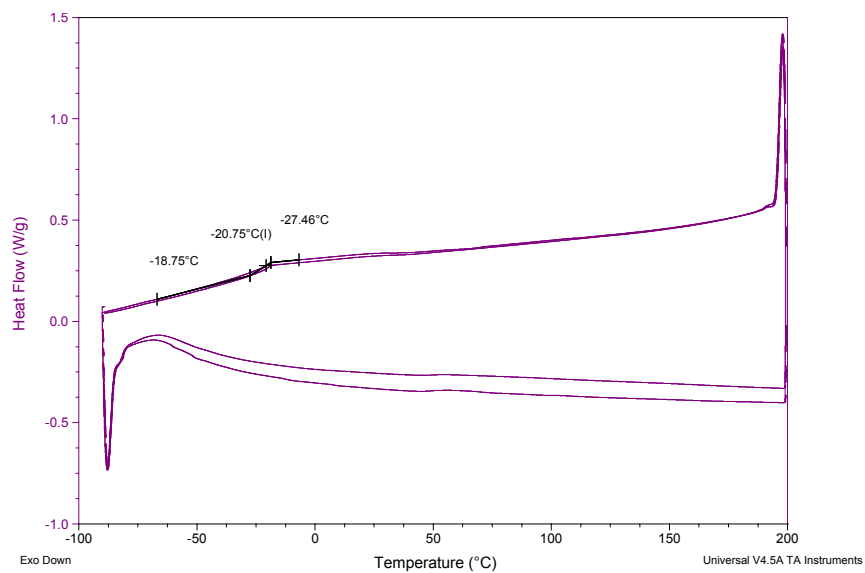


Figure A. 13 DSC trace of a 3.9:lactide (1:9) copolymerization before oxidation.

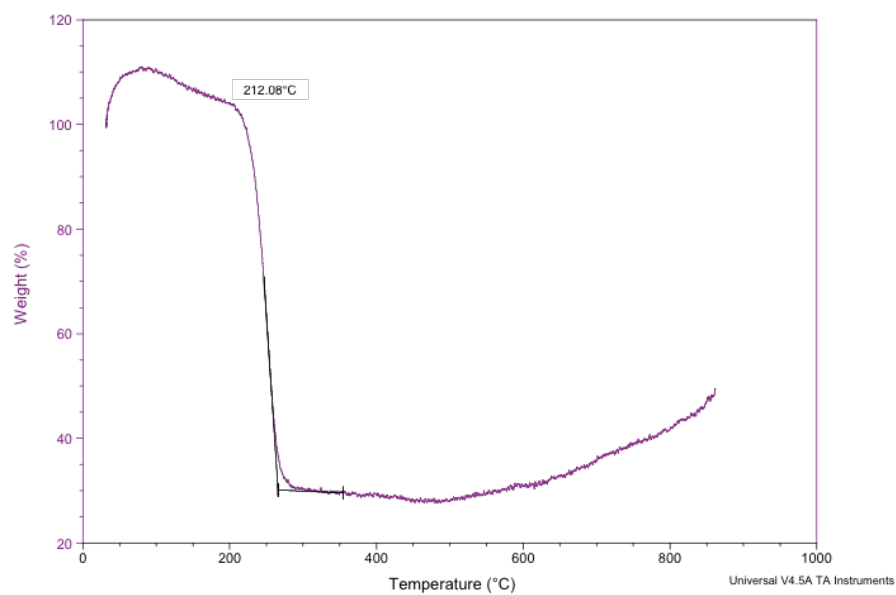


Figure A. 14 TGA trace of a 3.9:lactide (1:9) copolymerization before oxidation.

Sample: KDC_BC1_194_xlink
Size: 3.2960 mg
Method: Cyclic

DSC

File: C:\TAData\DSC\KDC (BC)\194_xlink.001
Operator: Kayla (BC)
Run Date: 26-Jun-2015 12:34
Instrument: DSC Q10 V9.9 Build 303

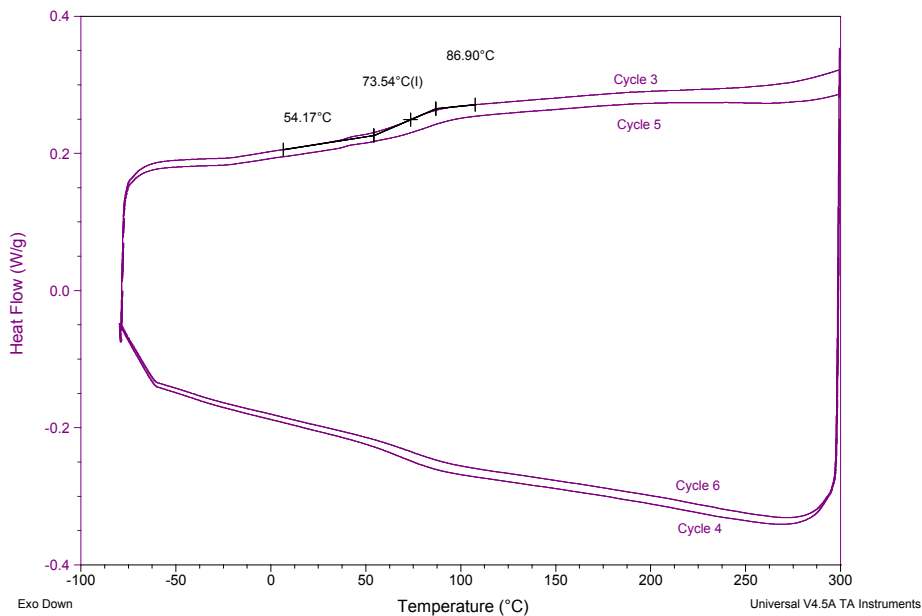


Figure A. 15 DSC trace of a 3.9 homopolymerization after the iron(II) to iron(III) switch.

Sample: KDC_BC1_crosslink_196
Size: 1.2790 mg
Method: Ramp

TGA

File: C:\...KDC (BC)\KDC_BC1_crosslink_196.001
Operator: Kayla (BC)
Run Date: 24-Jun-2015 12:23
Instrument: TGA Q50 V6.7 Build 203

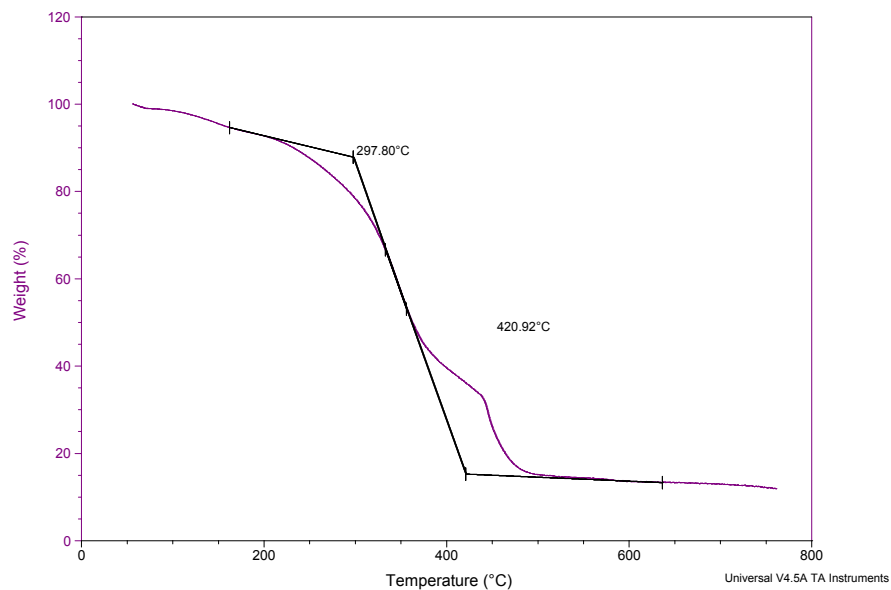


Figure A. 16 TGA trace of a 6 homopolymerization after the iron(II) to iron(III) switch.

Sample: KDC_BC2_154
Size: 1.8490 mg
Method: Cyclic

DSC

File: C:\TA\Data\DSC\KDC (BC)\BC2_154.001
Operator: Kayla (BC)
Run Date: 24-May-2016 10:16
Instrument: DSC Q10 V9.9 Build 303

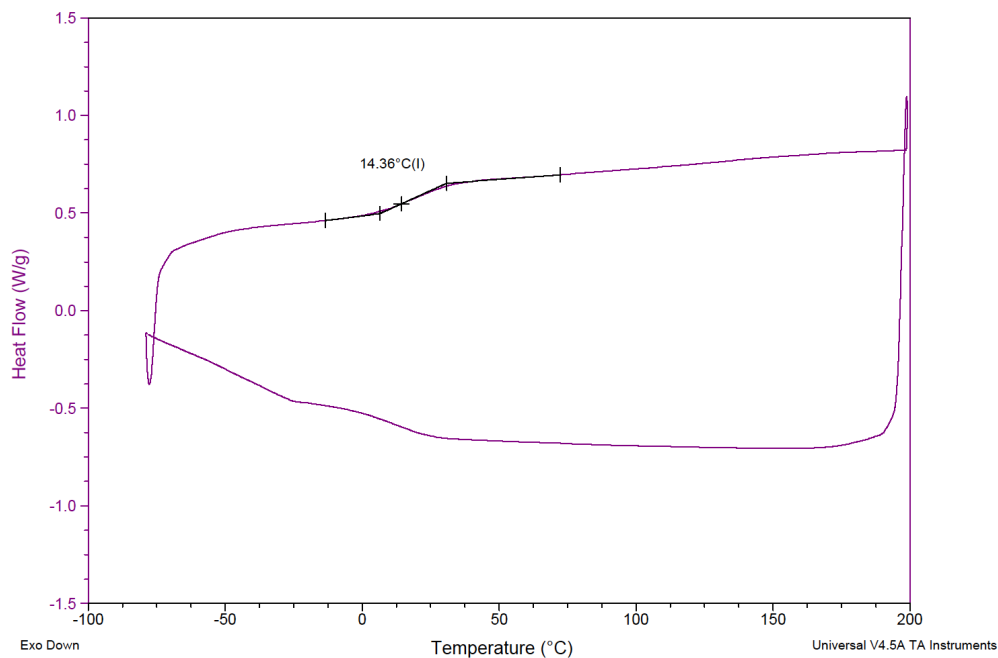


Figure A. 17 DSC trace of a 63.9 homopolymerization obtained after the iron(III) to iron(II) switch.

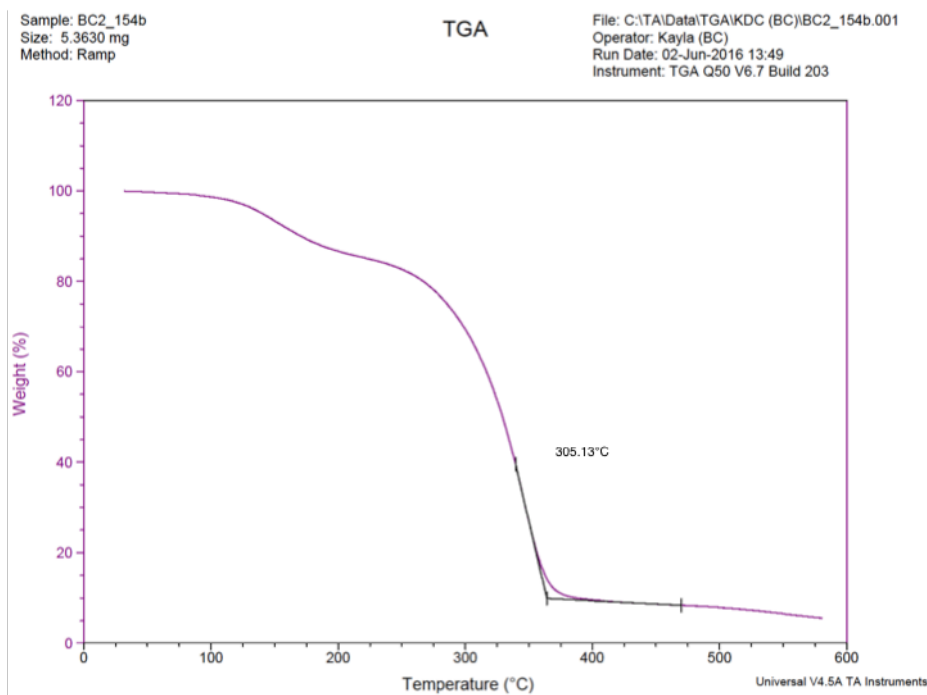


Figure A. 18 TGA trace of a 3.9 homopolymerization obtained after the iron(III) to iron(II) switch.

Sample: KDC_BC1_260F
Size: 1.2110 mg
Method: Cyclic

DSC

File: C:\TA\Data\DSC\KDC (BC)\260F.003
Operator: KDC (BC)
Run Date: 21-Sep-2015 08:54
Instrument: DSC Q10 V9.9 Build 303

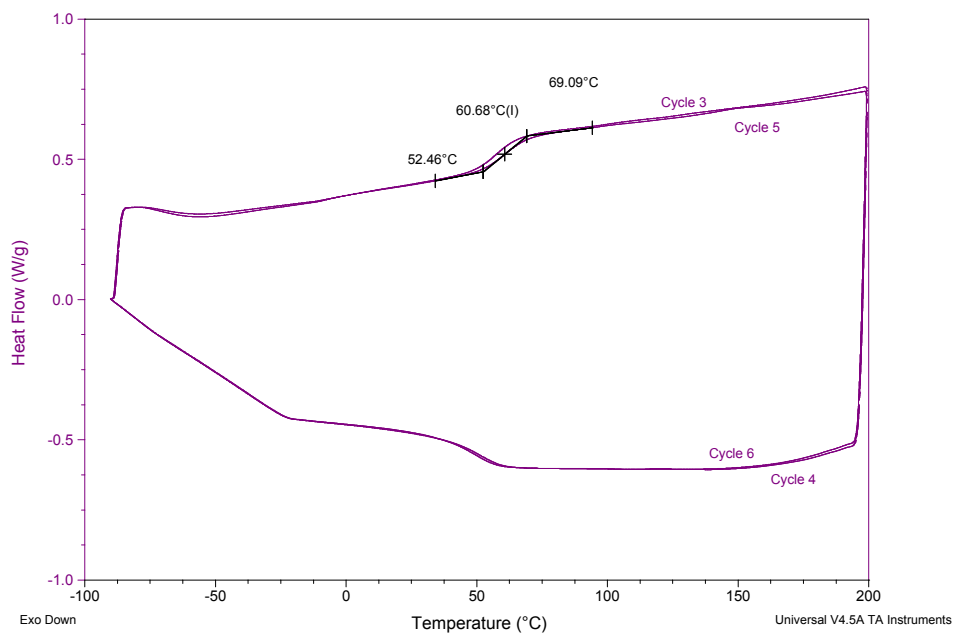


Figure A. 19 DSC trace of a 3.9:lactide (9:1) copolymerization after oxidation.

Sample: KDC_BC1_260F
Size: 0.7760 mg
Method: Ramp

TGA

File: C:\TA\Data\TGA\KDC (BC)\260F.001
Operator: KDC (BC)
Run Date: 21-Sep-2015 12:36
Instrument: TGA Q50 V6.7 Build 203

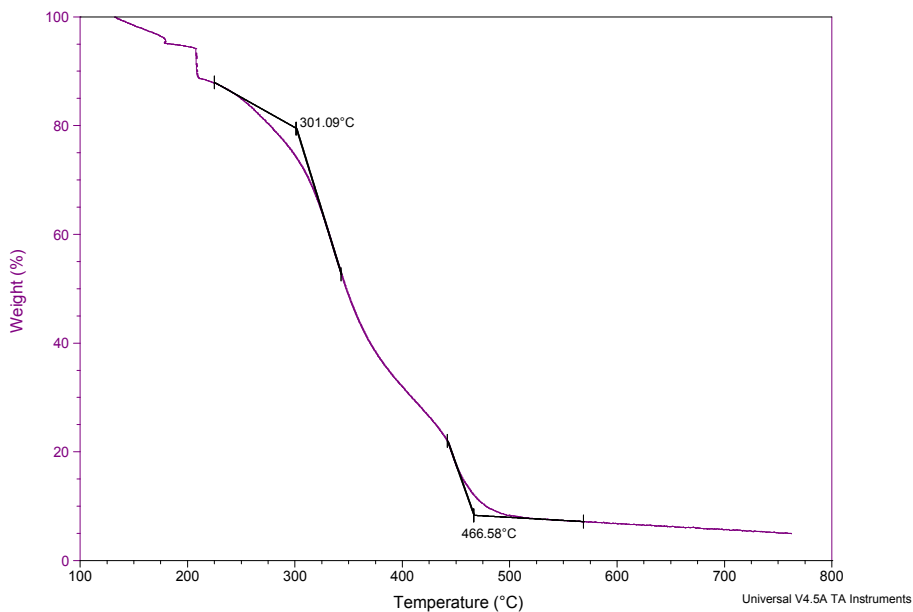


Figure A. 20 TGA trace of a 3.9 lactide (9:1) copolymerization after oxidation.

Sample: KDC_BC1_252A
Size: 2.3720 mg
Method: Cyclic

DSC

File: C:\TA\Data\DSC\KDC (BC)\252A.002
Operator: Kayla (BC)
Run Date: 24-Jun-2015 10:38
Instrument: DSC Q10 V9.9 Build 303

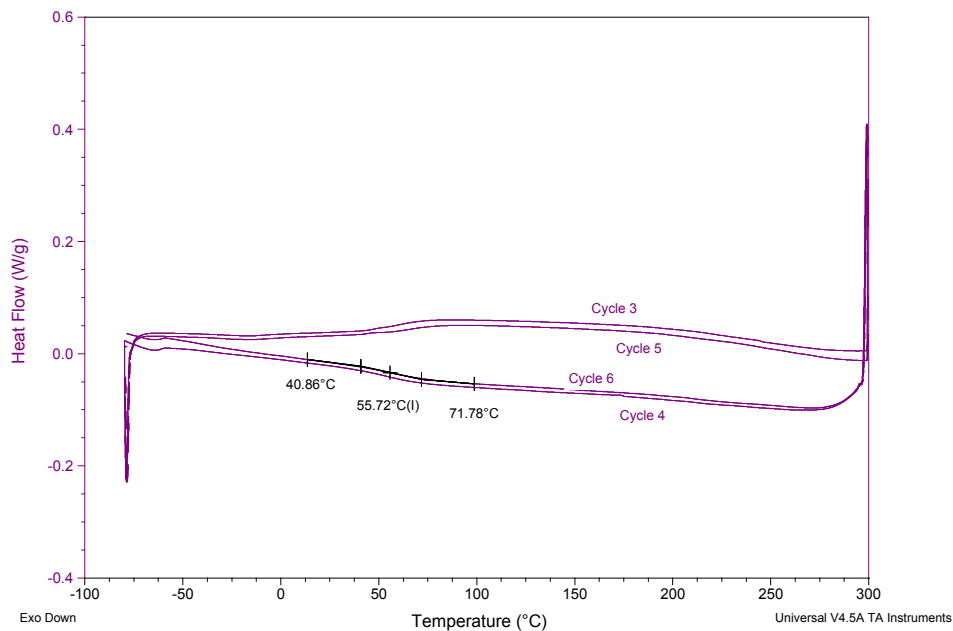


Figure A. 21 DSC trace of a 3.9:lactide (3:1) copolymerization after oxidation.

Sample: KDC_BC1_252_A
Size: 1.1080 mg
Method: Ramp

TGA

File: C:\...TGA\KDC (BC)\KDC_BC1_252_A.001
Operator: Kayla (BC)
Run Date: 12-Jun-2015 16:16
Instrument: TGA Q50 V6.7 Build 203

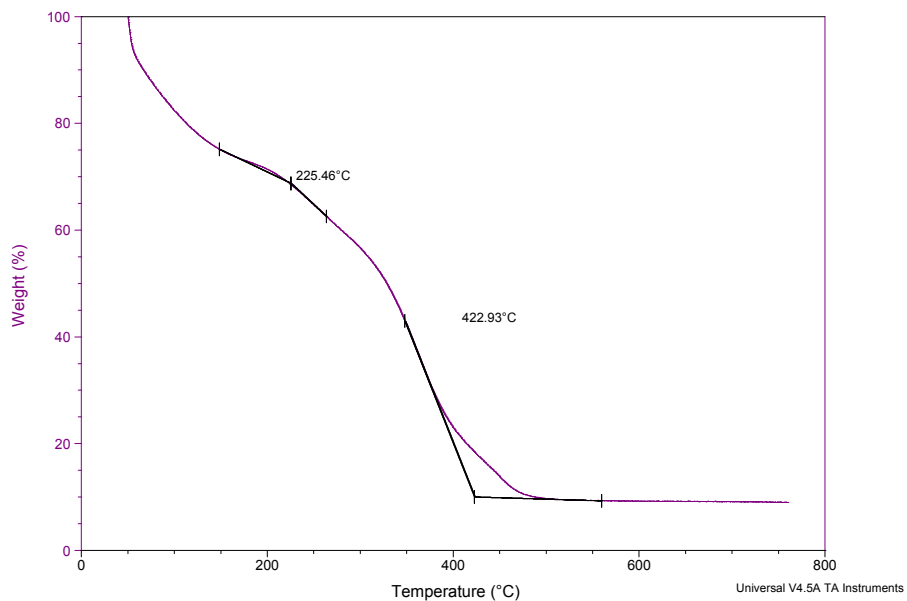


Figure A. 22 TGA trace of a 3.9:lactide (3:1) copolymerization after oxidation.

Sample: KDC_BC1_252B
Size: 4.1690 mg
Method: Cyclic

DSC

File: C:\TA\Data\DSC\KDC (BC)\252B.001
Operator: Kayla (BC)
Run Date: 25-Jun-2015 08:57
Instrument: DSC Q10 V9.9 Build 303

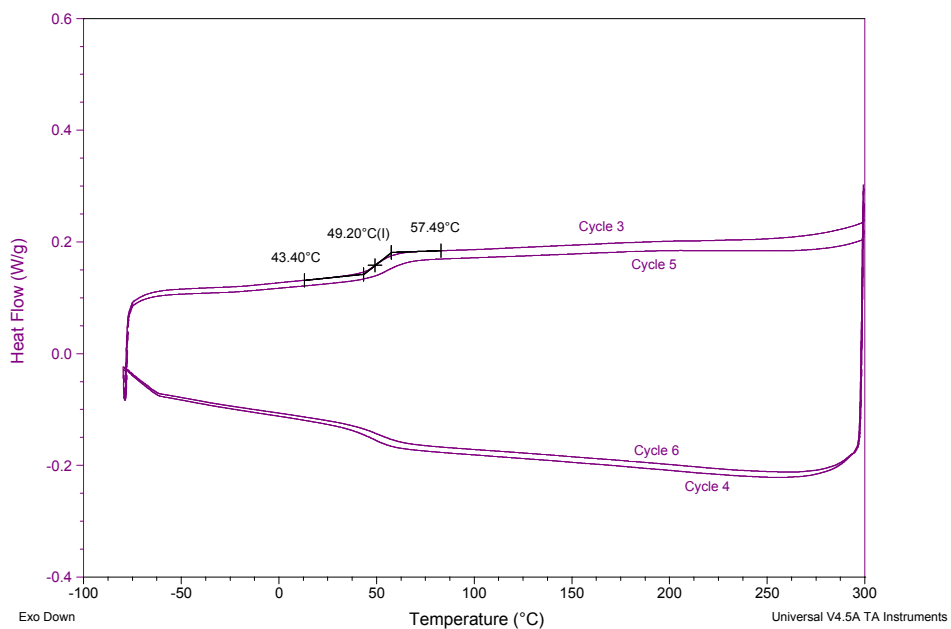


Figure A. 23 DSC trace of a 3.9:lactide (1:1) copolymerization after oxidation.

Sample: KDC_BC1_252_B
Size: 0.8790 mg
Method: Ramp

TGA

File: C:\...TGA\KDC (BC)\KDC_BC1_252_B.001
Operator: Kayla (BC)
Run Date: 24-Jun-2015 08:41
Instrument: TGA Q50 V6.7 Build 203

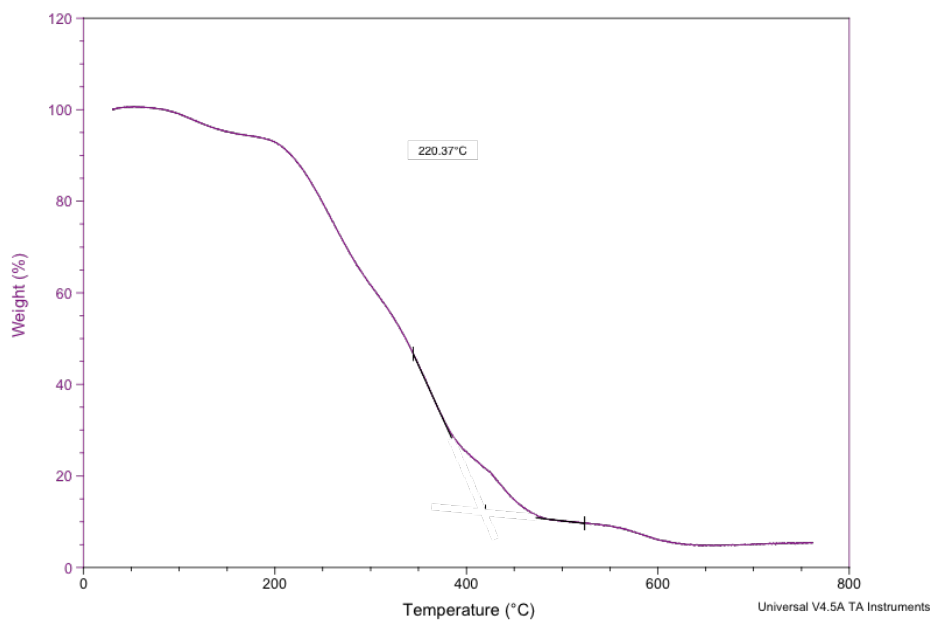


Figure A. 24 TGA trace of a 6:lactide (1:1) copolymerization after oxidation.

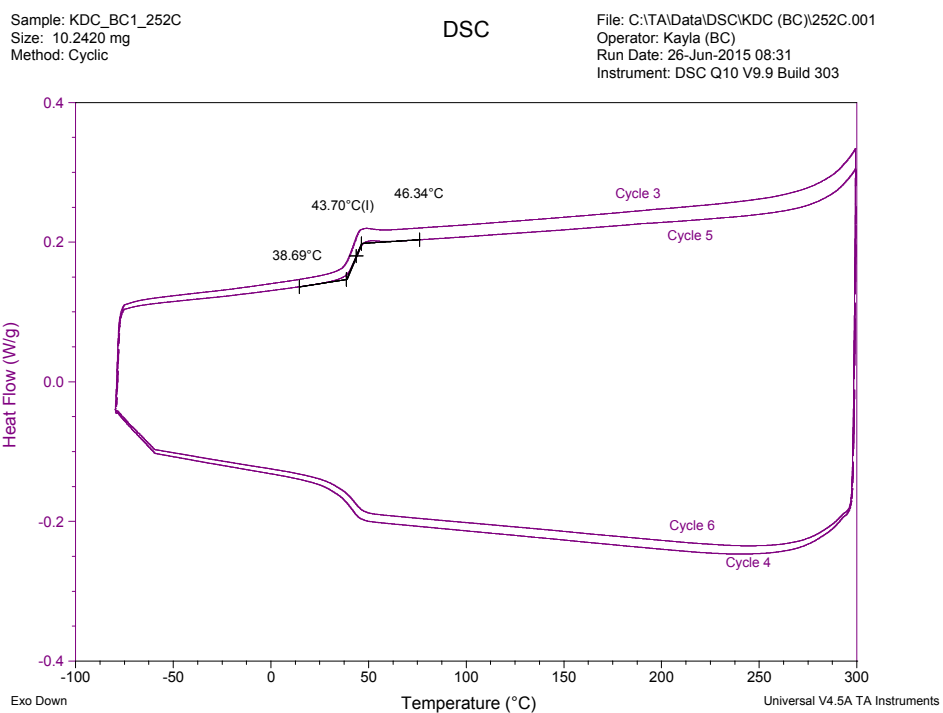


Figure A. 25 DSC trace of a 3.9:lactide (1:3) copolymerization after oxidation.

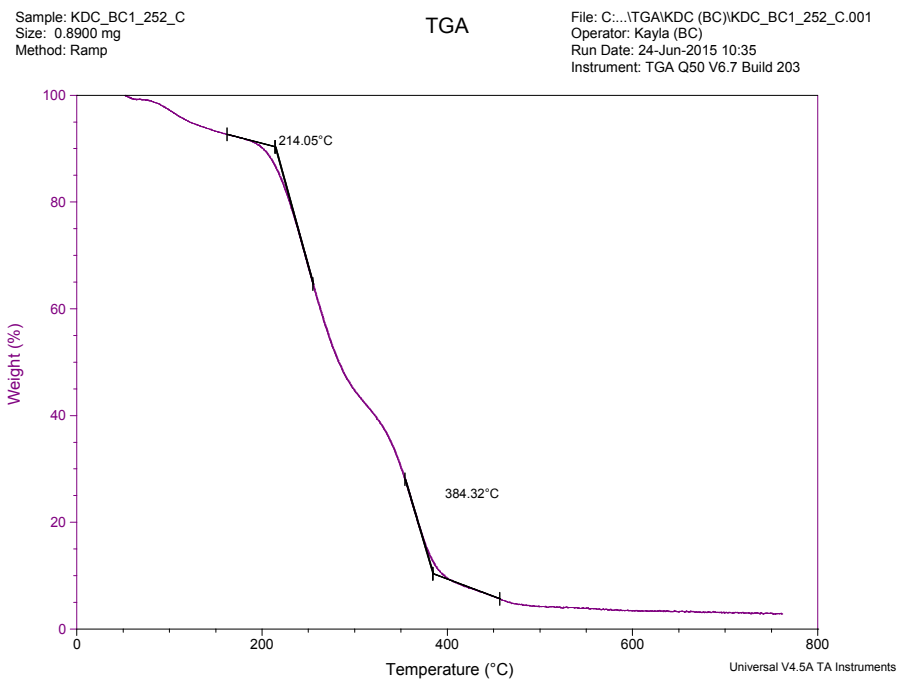


Figure A. 26 TGA trace of a 6:lactide (1:3) copolymerization after oxidation.

Sample: KDC_BC1_260F
Size: 1.2110 mg
Method: Cyclic

DSC

File: C:\TA\Data\DSC\KDC (BC)\260B
Operator: KDC (BC)
Run Date: 22-Sep-2015 08:14
Instrument: DSC Q10 V9.9 Build 303

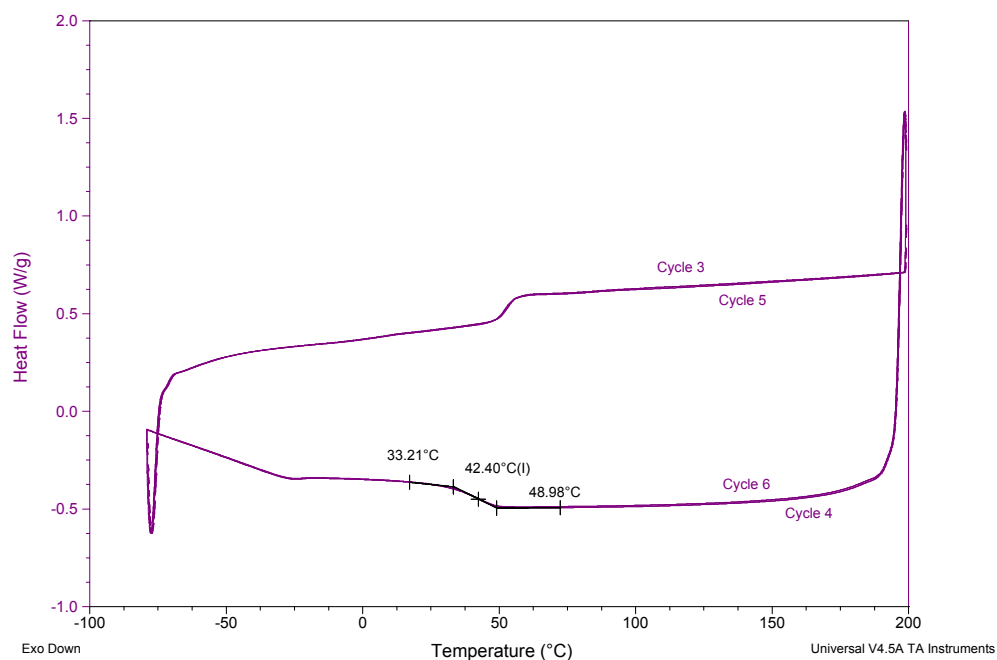


Figure A. 27 DSC trace of a 3.9:lactide (1:9) copolymerization after oxidation.

Sample: KDC_BC1_260B
Size: 0.9740 mg
Method: Ramp

TGA

File: C:\TA\Data\TGA\KDC (BC)\260B.001
Operator: KDC (BC)
Run Date: 22-Sep-2015 08:23
Instrument: TGA Q50 V6.7 Build 203

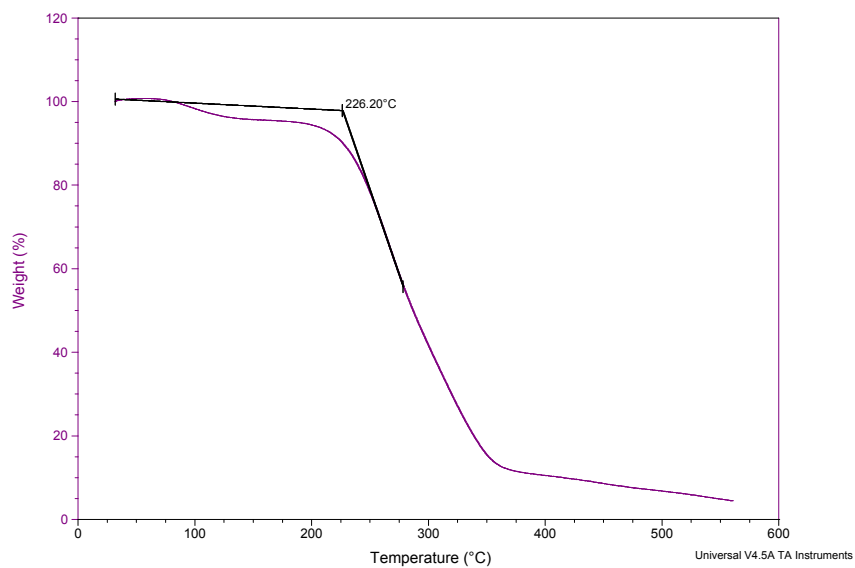


Figure A. 28 TGA trace of a 3.9:lactide (1:9) copolymerization after oxidation.

Appendix B Nuclear Magnetic Resonance (NMR) Spectra

B.1 NMR Spectra from Chapter 3

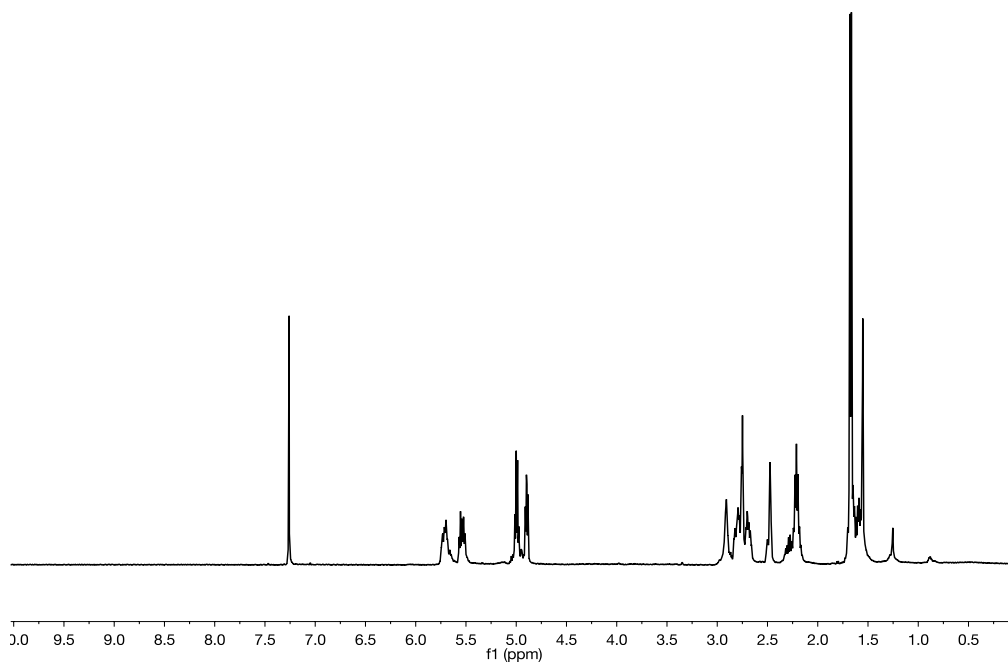


Figure B. 1 ^1H NMR (600 MHz) of 3.8 CDCl_3

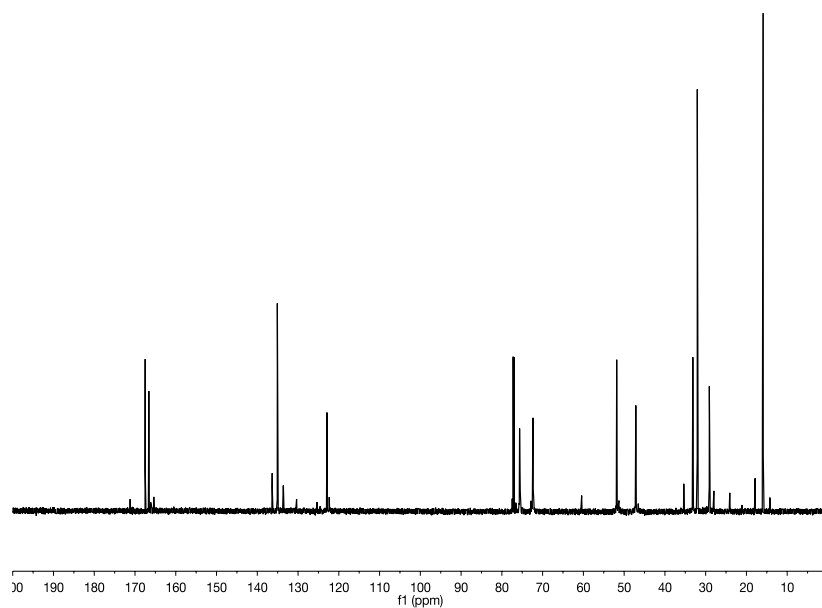


Figure B. 2 ^{13}C NMR(600 MHz) of 3.8 CDCl_3

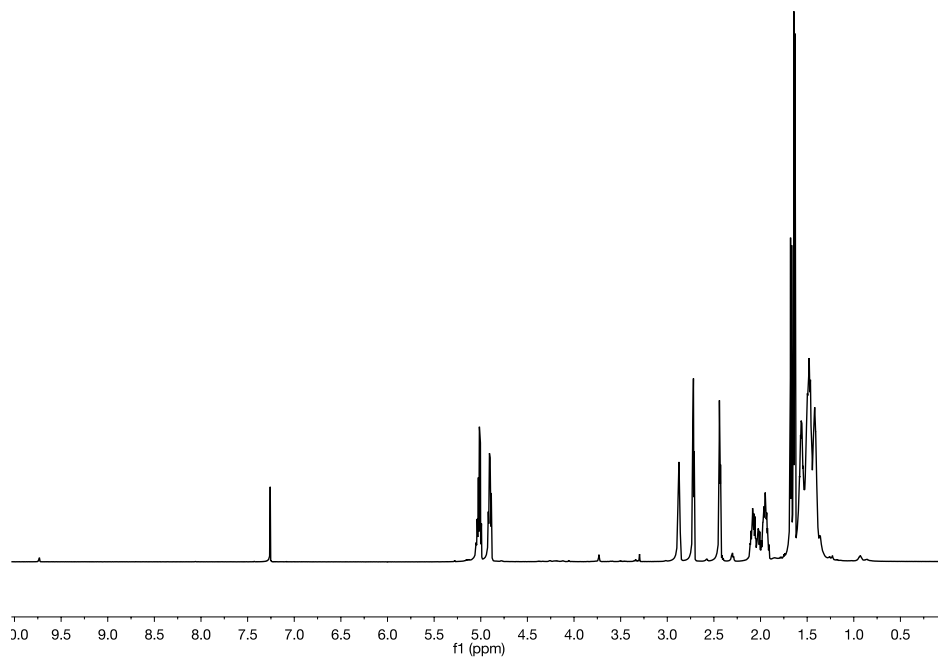


Figure B. 3 ^1H NMR (600 MHz) of 3.9 CDCl_3

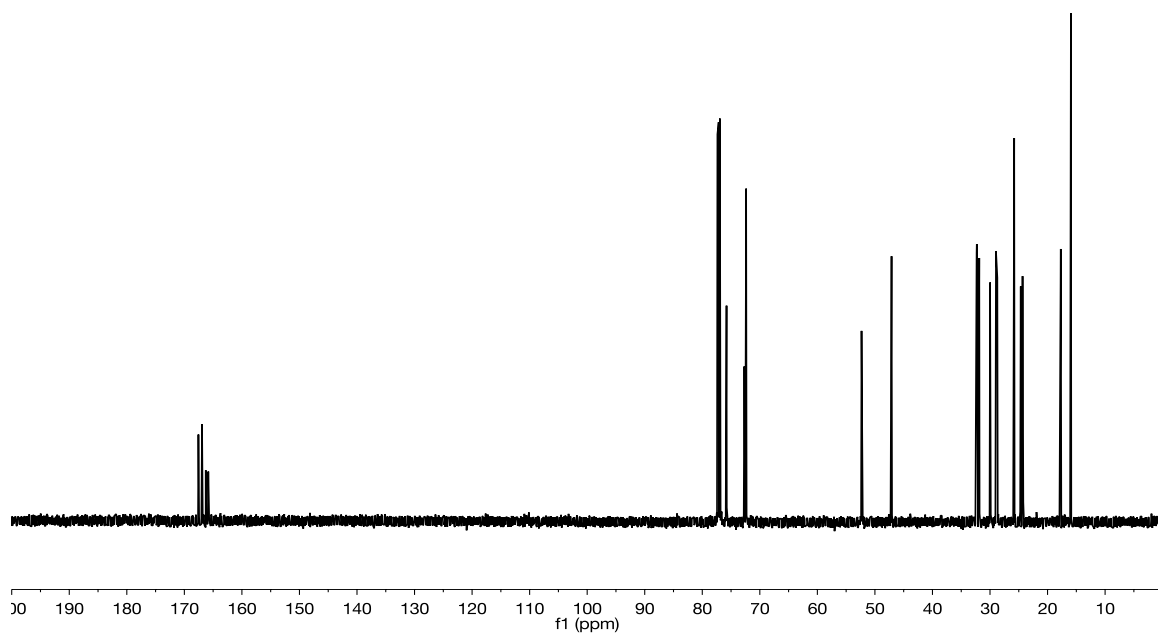


Figure B. 4 ^{13}C NMR(600 MHz) of 3.9 CDCl_3

B.2 NMR Spectra from Chapter 4

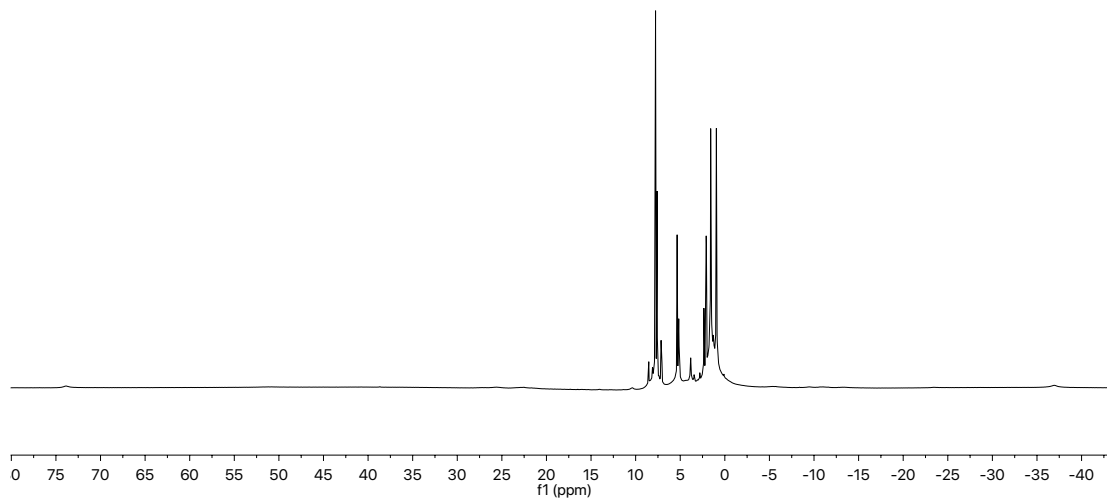


Figure B. 5 ^1H -NMR (500MHz) of 4.2 in CD_2Cl_2

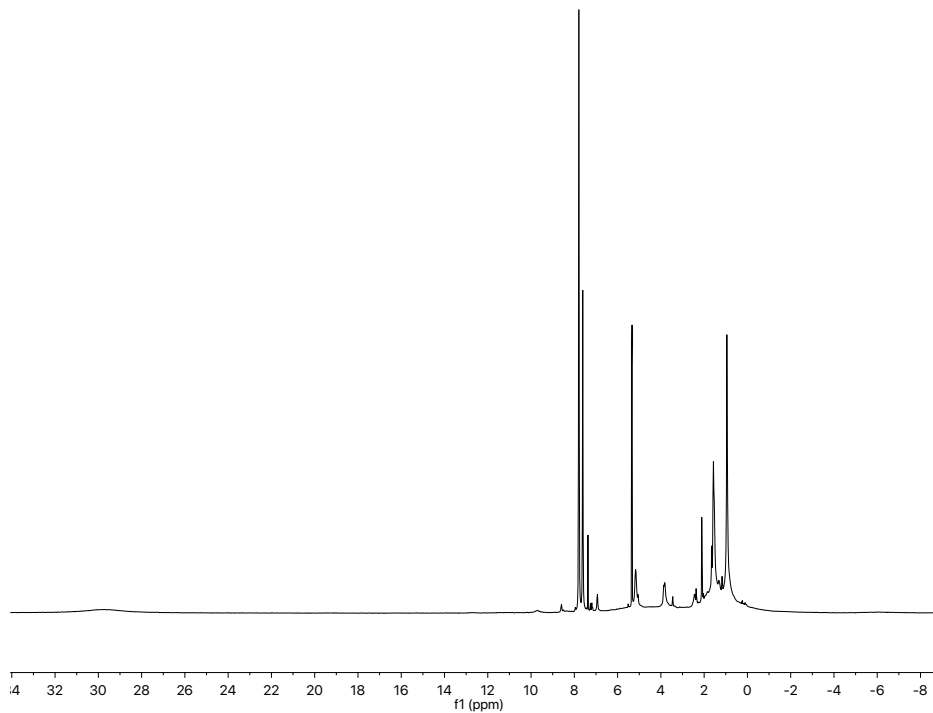


Figure B. 6 ^1H -NMR (500MHz) of 4.2b in CD_2Cl_2

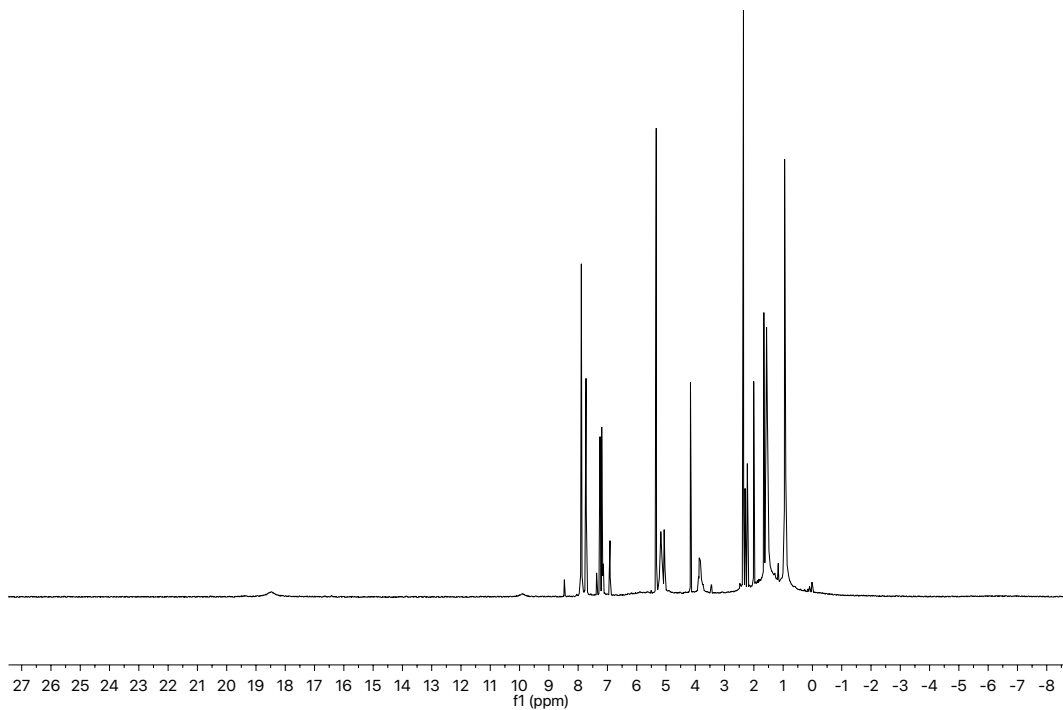


Figure B. 7 ¹H-NMR (500MHz) of 4.2c in CD₂Cl₂

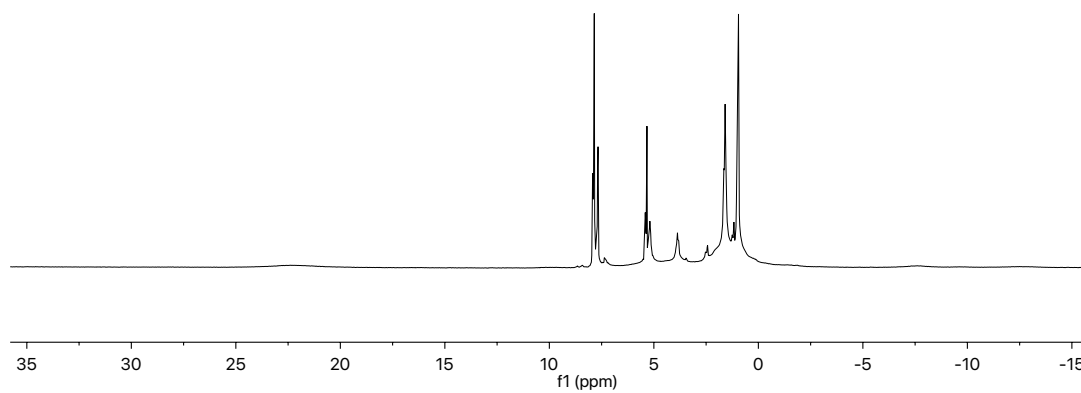


Figure B. 8 ¹H-NMR (500MHz) of 4.2d in CD₂Cl₂

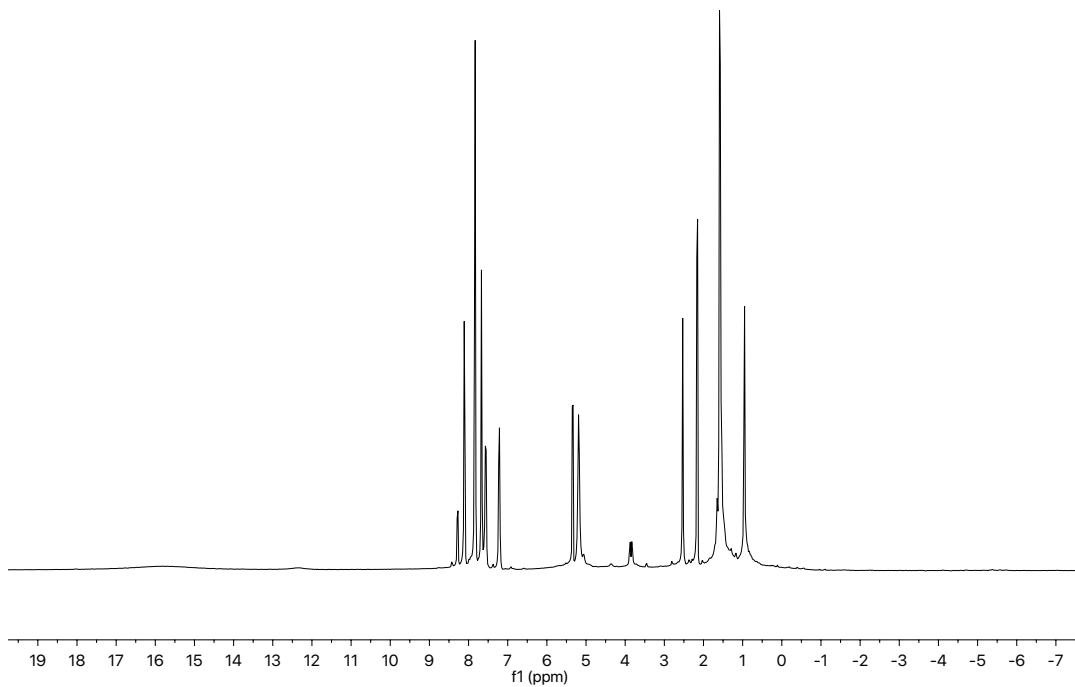


Figure B. 9 $^1\text{H-NMR}$ (500MHz) of 4.2e in CD_2Cl_2

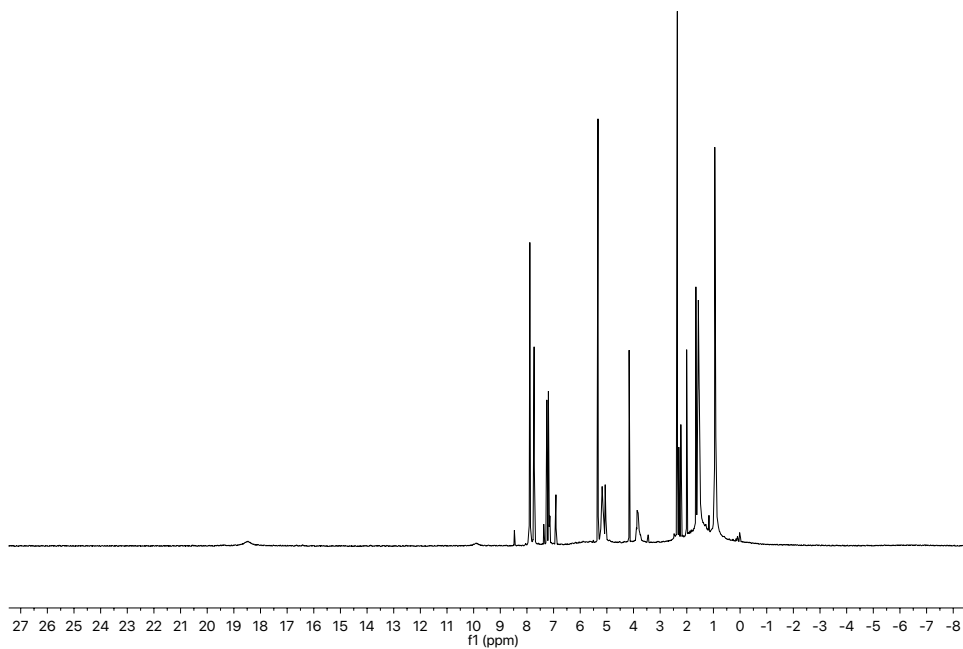


Figure B. 10 $^1\text{H-NMR}$ (500MHz) of 4.2f in CD_2Cl_2

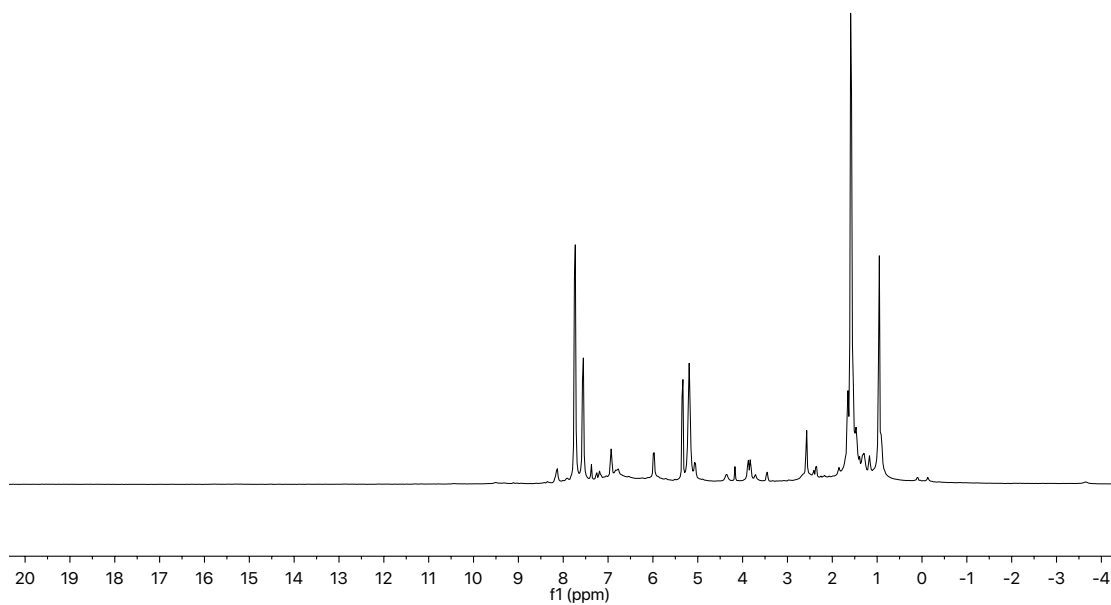


Figure B. 11 ¹H-NMR (500MHz) of 4.2g in CD₂Cl₂

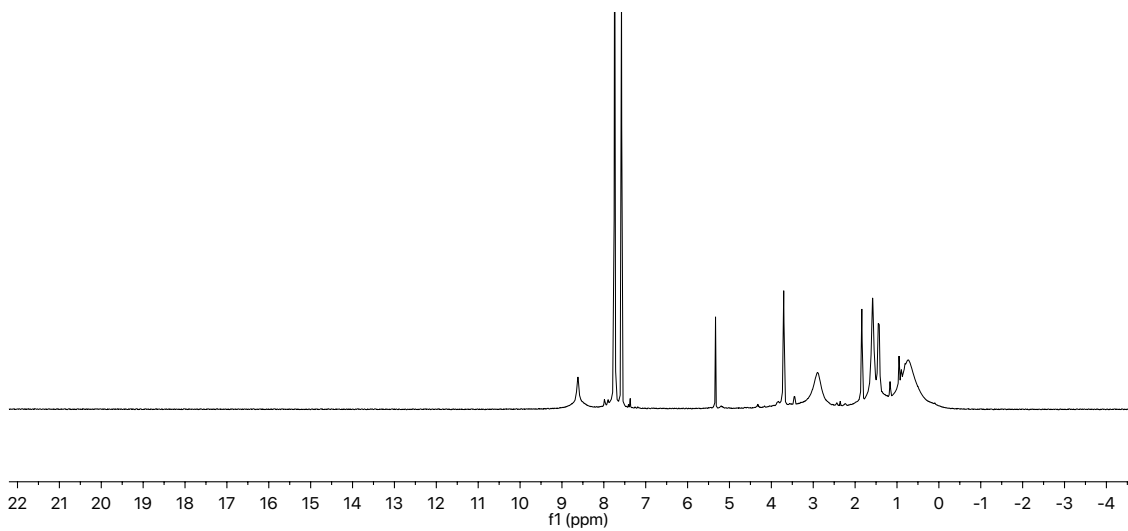


Figure B. 12 ¹H-NMR (500MHz) of 4.2h in CD₂Cl₂

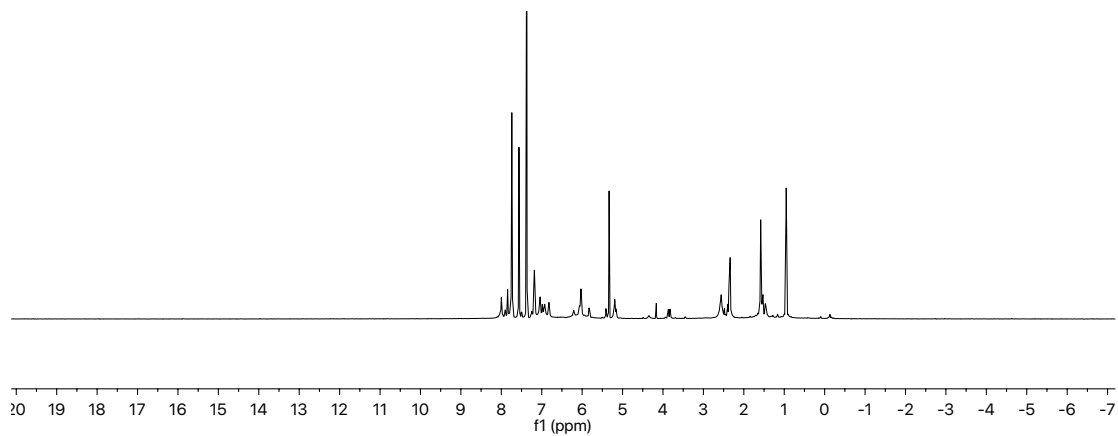


Figure B. 13 ¹H-NMR (500MHz) of 4.2i in CD₂Cl₂

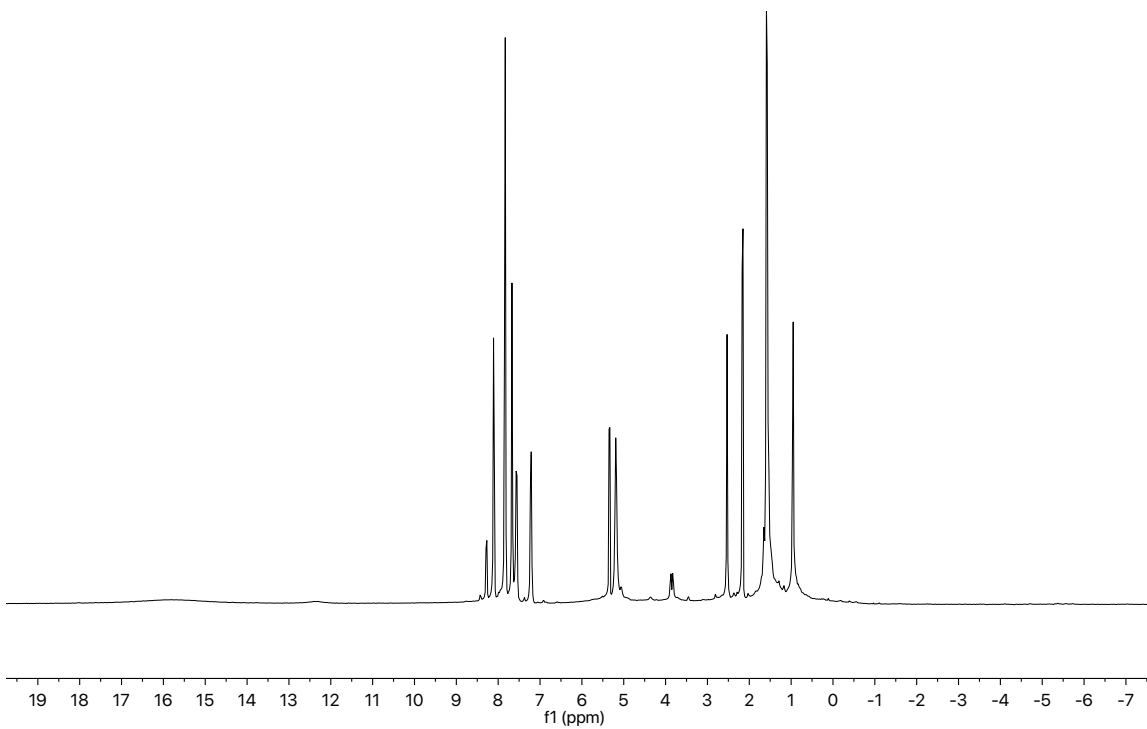


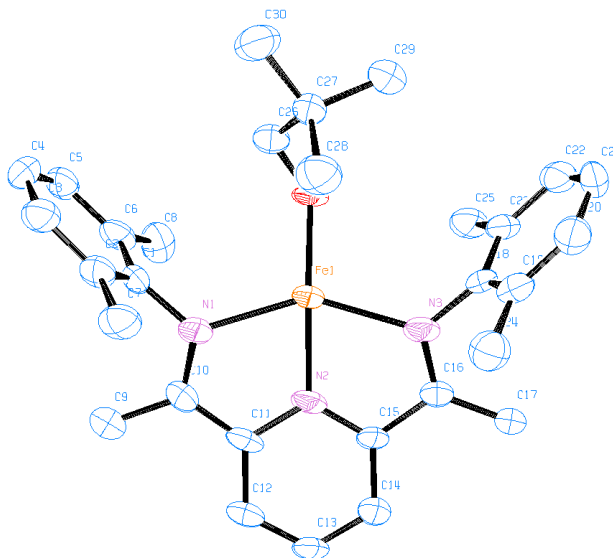
Figure B. 14 ¹H-NMR (500MHz) of 4.3 in CD₂Cl₂

Appendix C X-ray crystal structure data from Chapter 5

Table C. 1 Crystal data and structure refinement for Fe(PDI)(neopentoxide) (5.3b)

Identification code	$C_{30}H_{38}FeN_3O$
Empirical formula	$C_{30} H_{38} Fe N_3 O$
Formula weight	512.48
Temperature	100(2) K
Wavelength	1.54178 Å
Crystal system	Triclinic
Space group	P-1
Unit cell dimensions	$a = 9.6160(6) \text{ \AA}$ $\alpha = 80.409(4)^\circ$. $b = 15.1762(8) \text{ \AA}$ $\beta = 89.607(4)^\circ$. $c = 18.9657(11) \text{ \AA}$ $\gamma = 89.916(4)^\circ$.
Volume	$2729.0(3) \text{ \AA}^3$
Z	4
Density (calculated)	1.247 Mg/m^3
Absorption coefficient	4.624 mm^{-1}
F(000)	1092
Crystal size	$0.200 \times 0.080 \times 0.070 \text{ mm}^3$
Theta range for data collection	$2.363 \text{ to } 67.771^\circ$.
Index ranges	$-11 \leq h \leq 11, -18 \leq k \leq 18, -21 \leq l \leq 22$
Reflections collected	31006
Independent reflections	9543 [R(int) = 0.0732]
Completeness to theta = 67.679°	98.4 %
Absorption correction	Semi-empirical from equivalents
Max. and min. transmission	0.7528 and 0.4940
Refinement method	Full-matrix least-squares on F^2
Data / restraints / parameters	9543 / 0 / 650
Goodness-of-fit on F^2	1.230
Final R indices [$I > 2\sigma(I)$]	R1 = 0.1087, wR2 = 0.2768
R indices (all data)	R1 = 0.1365, wR2 = 0.3238
Largest diff. peak and hole	2.156 and $-1.485 \text{ e.\AA}^{-3}$

Table C. 2 Bond lengths [Å] and angles [°] for Fe(PDI)(neopentoxide) (5.3b)



Fe(1)-O(1)	1.842(5)	C(13)-C(14)	1.377(13)
Fe(1)-N(2)	1.991(7)	C(13)-H(13)	0.9500
Fe(1)-N(1)	2.143(7)	C(14)-C(15)	1.405(12)
Fe(1)-N(3)	2.147(8)	C(14)-H(14)	0.9500
O(1)-C(26)	1.411(11)	C(15)-C(16)	1.459(12)
N(1)-C(10)	1.309(12)	C(16)-C(17)	1.473(12)
N(1)-C(1)	1.428(10)	C(17)-H(17A)	0.9800
N(2)-C(15)	1.356(11)	C(17)-H(17B)	0.9800
N(2)-C(11)	1.378(12)	C(17)-H(17C)	0.9800
N(3)-C(16)	1.326(11)	C(18)-C(19)	1.394(15)
N(3)-C(18)	1.439(12)	C(18)-C(23)	1.401(13)
C(1)-C(6)	1.395(13)	C(19)-C(20)	1.371(15)
C(1)-C(2)	1.398(13)	C(19)-C(24)	1.487(15)
C(2)-C(3)	1.387(13)	C(20)-C(21)	1.415(16)
C(2)-C(7)	1.512(13)	C(20)-H(20)	0.9500
C(3)-C(4)	1.397(14)	C(21)-C(22)	1.350(18)
C(3)-H(3)	0.9500	C(21)-H(21)	0.9500
C(4)-C(5)	1.366(14)	C(22)-C(23)	1.398(15)
C(4)-H(4)	0.9500	C(22)-H(22)	0.9500
C(5)-C(6)	1.394(13)	C(23)-C(25)	1.493(16)

C(5)-H(5)	0.9500	C(24)-H(24A)	0.9800
C(6)-C(8)	1.529(13)	C(24)-H(24B)	0.9800
C(7)-H(7A)	0.9800	C(24)-H(24C)	0.9800
C(7)-H(7B)	0.9800	C(25)-H(25A)	0.9800
C(7)-H(7C)	0.9800	C(25)-H(25B)	0.9800
C(8)-H(8A)	0.9800	C(25)-H(25C)	0.9800
C(8)-H(8B)	0.9800	C(26)-C(27)	1.526(16)
C(8)-H(8C)	0.9800	C(26)-H(26A)	0.9900
C(9)-C(10)	1.475(14)	C(26)-H(26B)	0.9900
C(9)-H(9A)	0.9800	C(27)-C(29)	1.505(13)
C(9)-H(9B)	0.9800	C(27)-C(28)	1.523(13)
C(9)-H(9C)	0.9800	C(27)-C(30)	1.547(13)
C(10)-C(11)	1.420(13)	C(28)-H(28A)	0.9800
C(11)-C(12)	1.415(12)	C(28)-H(28B)	0.9800
C(12)-H(12)	0.9500	C(28)-H(28C)	0.9800
C(29)-H(29A)	0.9800	C(39)-H(39A)	0.9800
C(29)-H(29B)	0.9800	C(39)-H(39B)	0.9800
C(29)-H(29C)	0.9800	C(39)-H(39C)	0.9800
C(30)-H(30A)	0.9800	C(40)-C(41)	1.453(13)
C(30)-H(30B)	0.9800	C(41)-C(42)	1.365(12)
C(30)-H(30C)	0.9800	C(42)-C(43)	1.378(15)
Fe(2)-O(2)	1.811(7)	C(42)-H(42)	0.9500
Fe(2)-N(5)	1.985(7)	C(43)-C(44)	1.379(15)
Fe(2)-N(6)	2.144(7)	C(43)-H(43)	0.9500
Fe(2)-N(4)	2.147(7)	C(44)-C(45)	1.393(12)
O(2)-C(56)	1.393(12)	C(44)-H(44)	0.9500
N(4)-C(40)	1.304(11)	C(45)-C(46)	1.437(13)
N(4)-C(31)	1.455(11)	C(46)-C(47)	1.516(13)
N(5)-C(45)	1.369(13)	C(47)-H(47A)	0.9800
N(5)-C(41)	1.385(12)	C(47)-H(47B)	0.9800
N(6)-C(46)	1.323(11)	C(47)-H(47C)	0.9800
N(6)-C(48)	1.428(12)	C(48)-C(53)	1.403(13)
C(31)-C(36)	1.369(15)	C(48)-C(49)	1.409(13)
C(31)-C(32)	1.413(13)	C(49)-C(50)	1.396(13)
C(32)-C(33)	1.393(15)	C(49)-C(54)	1.501(13)

C(32)-C(37)	1.508(17)	C(50)-C(51)	1.394(15)
C(33)-C(34)	1.390(18)	C(50)-H(50)	0.9500
C(33)-H(33)	0.9500	C(51)-C(52)	1.349(15)
C(34)-C(35)	1.359(15)	C(51)-H(51)	0.9500
C(34)-H(34)	0.9500	C(52)-C(53)	1.399(14)
C(35)-C(36)	1.398(16)	C(52)-H(52)	0.9500
C(35)-H(35)	0.9500	C(53)-C(55)	1.491(14)
C(36)-C(38)	1.528(14)	C(54)-H(54A)	0.9800
C(37)-H(37A)	0.9800	C(54)-H(54B)	0.9800
C(37)-H(37B)	0.9800	C(54)-H(54C)	0.9800
C(37)-H(37C)	0.9800	C(55)-H(55A)	0.9800
C(38)-H(38A)	0.9800	C(55)-H(55B)	0.9800
C(38)-H(38B)	0.9800	C(55)-H(55C)	0.9800
C(38)-H(38C)	0.9800	C(56)-C(57)	1.540(12)
C(39)-C(40)	1.511(13)	C(56)-H(56A)	0.9900
C(56)-H(56B)	0.9900	C(1)-C(2)-C(7)	120.8(8)
C(57)-C(60)	1.491(17)	C(2)-C(3)-C(4)	119.0(9)
C(57)-C(59)	1.504(18)	C(2)-C(3)-H(3)	120.5
C(57)-C(58)	1.544(16)	C(4)-C(3)-H(3)	120.5
C(58)-H(58A)	0.9800	C(5)-C(4)-C(3)	121.1(8)
C(58)-H(58B)	0.9800	C(5)-C(4)-H(4)	119.4
C(58)-H(58C)	0.9800	C(3)-C(4)-H(4)	119.4
C(59)-H(59A)	0.9800	C(4)-C(5)-C(6)	120.7(9)
C(59)-H(59B)	0.9800	C(4)-C(5)-H(5)	119.6
C(59)-H(59C)	0.9800	C(6)-C(5)-H(5)	119.6
C(60)-H(60A)	0.9800	C(5)-C(6)-C(1)	118.6(9)
C(60)-H(60B)	0.9800	C(5)-C(6)-C(8)	120.7(9)
C(60)-H(60C)	0.9800	C(1)-C(6)-C(8)	120.7(9)
		C(2)-C(7)-H(7A)	109.5
O(1)-Fe(1)-N(2)	163.7(3)	C(2)-C(7)-H(7B)	109.5
O(1)-Fe(1)-N(1)	107.8(3)	H(7A)-C(7)-H(7B)	109.5
N(2)-Fe(1)-N(1)	75.3(3)	C(2)-C(7)-H(7C)	109.5
O(1)-Fe(1)-N(3)	105.3(3)	H(7A)-C(7)-H(7C)	109.5
N(2)-Fe(1)-N(3)	75.6(3)	H(7B)-C(7)-H(7C)	109.5
N(1)-Fe(1)-N(3)	145.6(3)	C(6)-C(8)-H(8A)	109.5

C(26)-O(1)-Fe(1)	131.9(5)	C(6)-C(8)-H(8B)	109.5
C(10)-N(1)-C(1)	120.4(8)	H(8A)-C(8)-H(8B)	109.5
C(10)-N(1)-Fe(1)	115.7(6)	C(6)-C(8)-H(8C)	109.5
C(1)-N(1)-Fe(1)	122.2(5)	H(8A)-C(8)-H(8C)	109.5
C(15)-N(2)-C(11)	119.2(7)	H(8B)-C(8)-H(8C)	109.5
C(15)-N(2)-Fe(1)	120.2(6)	C(10)-C(9)-H(9A)	109.5
C(11)-N(2)-Fe(1)	119.8(6)	C(10)-C(9)-H(9B)	109.5
C(16)-N(3)-C(18)	120.0(7)	H(9A)-C(9)-H(9B)	109.5
C(16)-N(3)-Fe(1)	115.1(6)	C(10)-C(9)-H(9C)	109.5
C(18)-N(3)-Fe(1)	124.1(5)	H(9A)-C(9)-H(9C)	109.5
C(6)-C(1)-C(2)	120.7(8)	H(9B)-C(9)-H(9C)	109.5
C(6)-C(1)-N(1)	119.5(8)	N(1)-C(10)-C(11)	115.1(8)
C(2)-C(1)-N(1)	119.8(8)	N(1)-C(10)-C(9)	122.6(8)
C(3)-C(2)-C(1)	119.9(8)	C(11)-C(10)-C(9)	122.3(8)
C(3)-C(2)-C(7)	119.2(9)	N(2)-C(11)-C(12)	120.1(9)
N(2)-C(11)-C(10)	113.1(7)	C(21)-C(22)-C(23)	121.2(10)
C(12)-C(11)-C(10)	126.8(9)	C(21)-C(22)-H(22)	119.4
C(13)-C(12)-C(11)	119.4(9)	C(23)-C(22)-H(22)	119.4
C(13)-C(12)-H(12)	120.3	C(22)-C(23)-C(18)	117.2(11)
C(11)-C(12)-H(12)	120.3	C(22)-C(23)-C(25)	120.9(9)
C(14)-C(13)-C(12)	120.3(8)	C(18)-C(23)-C(25)	121.9(9)
C(14)-C(13)-H(13)	119.9	C(19)-C(24)-H(24A)	109.5
C(12)-C(13)-H(13)	119.9	C(19)-C(24)-H(24B)	109.5
C(13)-C(14)-C(15)	119.1(8)	H(24A)-C(24)-H(24B)	109.5
C(13)-C(14)-H(14)	120.5	C(19)-C(24)-H(24C)	109.5
C(15)-C(14)-H(14)	120.5	H(24A)-C(24)-H(24C)	109.5
N(2)-C(15)-C(14)	121.5(8)	H(24B)-C(24)-H(24C)	109.5
N(2)-C(15)-C(16)	113.5(7)	C(23)-C(25)-H(25A)	109.5
C(14)-C(15)-C(16)	124.9(8)	C(23)-C(25)-H(25B)	109.5
N(3)-C(16)-C(15)	113.4(7)	H(25A)-C(25)-H(25B)	109.5
N(3)-C(16)-C(17)	125.1(8)	C(23)-C(25)-H(25C)	109.5
C(15)-C(16)-C(17)	121.3(7)	H(25A)-C(25)-H(25C)	109.5
C(16)-C(17)-H(17A)	109.5	H(25B)-C(25)-H(25C)	109.5
C(16)-C(17)-H(17B)	109.5	O(1)-C(26)-C(27)	114.3(8)
H(17A)-C(17)-H(17B)	109.5	O(1)-C(26)-H(26A)	108.7

C(16)-C(17)-H(17C)	109.5	C(27)-C(26)-H(26A)	108.7
H(17A)-C(17)-H(17C)	109.5	O(1)-C(26)-H(26B)	108.7
H(17B)-C(17)-H(17C)	109.5	C(27)-C(26)-H(26B)	108.7
C(19)-C(18)-C(23)	122.4(9)	H(26A)-C(26)-H(26B)	107.6
C(19)-C(18)-N(3)	119.3(8)	C(29)-C(27)-C(28)	109.5(8)
C(23)-C(18)-N(3)	118.2(9)	C(29)-C(27)-C(26)	110.0(8)
C(20)-C(19)-C(18)	118.5(10)	C(28)-C(27)-C(26)	111.0(8)
C(20)-C(19)-C(24)	120.8(10)	C(29)-C(27)-C(30)	109.2(8)
C(18)-C(19)-C(24)	120.7(9)	C(28)-C(27)-C(30)	109.0(9)
C(19)-C(20)-C(21)	119.8(11)	C(26)-C(27)-C(30)	108.2(8)
C(19)-C(20)-H(20)	120.1	C(27)-C(28)-H(28A)	109.5
C(21)-C(20)-H(20)	120.1	C(27)-C(28)-H(28B)	109.5
C(22)-C(21)-C(20)	120.8(10)	H(28A)-C(28)-H(28B)	109.5
C(22)-C(21)-H(21)	119.6	C(27)-C(28)-H(28C)	109.5
C(20)-C(21)-H(21)	119.6	H(28A)-C(28)-H(28C)	109.5
H(28B)-C(28)-H(28C)	109.5	C(34)-C(33)-C(32)	121.6(10)
C(27)-C(29)-H(29A)	109.5	C(34)-C(33)-H(33)	119.2
C(27)-C(29)-H(29B)	109.5	C(32)-C(33)-H(33)	119.2
H(29A)-C(29)-H(29B)	109.5	C(35)-C(34)-C(33)	119.1(11)
C(27)-C(29)-H(29C)	109.5	C(35)-C(34)-H(34)	120.4
H(29A)-C(29)-H(29C)	109.5	C(33)-C(34)-H(34)	120.4
H(29B)-C(29)-H(29C)	109.5	C(34)-C(35)-C(36)	121.7(12)
C(27)-C(30)-H(30A)	109.5	C(34)-C(35)-H(35)	119.2
C(27)-C(30)-H(30B)	109.5	C(36)-C(35)-H(35)	119.2
H(30A)-C(30)-H(30B)	109.5	C(31)-C(36)-C(35)	118.8(10)
C(27)-C(30)-H(30C)	109.5	C(31)-C(36)-C(38)	121.3(10)
H(30A)-C(30)-H(30C)	109.5	C(35)-C(36)-C(38)	119.9(10)
H(30B)-C(30)-H(30C)	109.5	C(32)-C(37)-H(37A)	109.5
O(2)-Fe(2)-N(5)	148.8(3)	C(32)-C(37)-H(37B)	109.5
O(2)-Fe(2)-N(6)	106.7(3)	H(37A)-C(37)-H(37B)	109.5
N(5)-Fe(2)-N(6)	75.8(3)	C(32)-C(37)-H(37C)	109.5
O(2)-Fe(2)-N(4)	109.6(3)	H(37A)-C(37)-H(37C)	109.5
N(5)-Fe(2)-N(4)	75.6(3)	H(37B)-C(37)-H(37C)	109.5
N(6)-Fe(2)-N(4)	143.5(3)	C(36)-C(38)-H(38A)	109.5
C(56)-O(2)-Fe(2)	137.1(7)	C(36)-C(38)-H(38B)	109.5

C(40)-N(4)-C(31)	119.3(7)	H(38A)-C(38)-H(38B)	109.5
C(40)-N(4)-Fe(2)	116.2(6)	C(36)-C(38)-H(38C)	109.5
C(31)-N(4)-Fe(2)	123.2(5)	H(38A)-C(38)-H(38C)	109.5
C(45)-N(5)-C(41)	120.2(8)	H(38B)-C(38)-H(38C)	109.5
C(45)-N(5)-Fe(2)	119.7(6)	C(40)-C(39)-H(39A)	109.5
C(41)-N(5)-Fe(2)	119.8(6)	C(40)-C(39)-H(39B)	109.5
C(46)-N(6)-C(48)	119.1(7)	H(39A)-C(39)-H(39B)	109.5
C(46)-N(6)-Fe(2)	114.6(6)	C(40)-C(39)-H(39C)	109.5
C(48)-N(6)-Fe(2)	125.5(6)	H(39A)-C(39)-H(39C)	109.5
C(36)-C(31)-C(32)	121.5(9)	H(39B)-C(39)-H(39C)	109.5
C(36)-C(31)-N(4)	120.1(8)	N(4)-C(40)-C(41)	114.5(8)
C(32)-C(31)-N(4)	118.3(9)	N(4)-C(40)-C(39)	123.7(8)
C(33)-C(32)-C(31)	117.3(10)	C(41)-C(40)-C(39)	121.9(8)
C(33)-C(32)-C(37)	122.3(9)	C(42)-C(41)-N(5)	119.7(9)
C(31)-C(32)-C(37)	120.4(9)	C(42)-C(41)-C(40)	127.3(8)
N(5)-C(41)-C(40)	112.9(7)	C(51)-C(52)-H(52)	118.9
C(41)-C(42)-C(43)	120.2(9)	C(53)-C(52)-H(52)	118.9
C(41)-C(42)-H(42)	119.9	C(52)-C(53)-C(48)	118.7(9)
C(43)-C(42)-H(42)	119.9	C(52)-C(53)-C(55)	121.4(9)
C(42)-C(43)-C(44)	120.2(9)	C(48)-C(53)-C(55)	119.9(8)
C(42)-C(43)-H(43)	119.9	C(49)-C(54)-H(54A)	109.5
C(44)-C(43)-H(43)	119.9	C(49)-C(54)-H(54B)	109.5
C(43)-C(44)-C(45)	119.3(10)	H(54A)-C(54)-H(54B)	109.5
C(43)-C(44)-H(44)	120.3	C(49)-C(54)-H(54C)	109.5
C(45)-C(44)-H(44)	120.3	H(54A)-C(54)-H(54C)	109.5
N(5)-C(45)-C(44)	119.6(9)	H(54B)-C(54)-H(54C)	109.5
N(5)-C(45)-C(46)	113.1(7)	C(53)-C(55)-H(55A)	109.5
C(44)-C(45)-C(46)	127.2(9)	C(53)-C(55)-H(55B)	109.5
N(6)-C(46)-C(45)	115.1(8)	H(55A)-C(55)-H(55B)	109.5
N(6)-C(46)-C(47)	122.4(8)	C(53)-C(55)-H(55C)	109.5
C(45)-C(46)-C(47)	122.5(8)	H(55A)-C(55)-H(55C)	109.5
C(46)-C(47)-H(47A)	109.5	H(55B)-C(55)-H(55C)	109.5
C(46)-C(47)-H(47B)	109.5	O(2)-C(56)-C(57)	114.1(9)
H(47A)-C(47)-H(47B)	109.5	O(2)-C(56)-H(56A)	108.7
C(46)-C(47)-H(47C)	109.5	C(57)-C(56)-H(56A)	108.7

H(47A)-C(47)-H(47C)	109.5	O(2)-C(56)-H(56B)	108.7
H(47B)-C(47)-H(47C)	109.5	C(57)-C(56)-H(56B)	108.7
C(53)-C(48)-C(49)	120.3(8)	H(56A)-C(56)-H(56B)	107.6
C(53)-C(48)-N(6)	119.8(8)	C(60)-C(57)-C(59)	112.4(12)
C(49)-C(48)-N(6)	119.3(8)	C(60)-C(57)-C(56)	112.6(9)
C(50)-C(49)-C(48)	117.9(9)	C(59)-C(57)-C(56)	108.5(10)
C(50)-C(49)-C(54)	121.9(9)	C(60)-C(57)-C(58)	107.8(11)
C(48)-C(49)-C(54)	120.3(8)	C(59)-C(57)-C(58)	108.7(11)
C(51)-C(50)-C(49)	121.9(10)	C(56)-C(57)-C(58)	106.6(9)
C(51)-C(50)-H(50)	119.1	C(57)-C(58)-H(58A)	109.5
C(49)-C(50)-H(50)	119.1	C(57)-C(58)-H(58B)	109.5
C(52)-C(51)-C(50)	119.0(9)	H(58A)-C(58)-H(58B)	109.5
C(52)-C(51)-H(51)	120.5	C(57)-C(58)-H(58C)	109.5
C(50)-C(51)-H(51)	120.5	H(58A)-C(58)-H(58C)	109.5
C(51)-C(52)-C(53)	122.2(10)	H(58B)-C(58)-H(58C)	109.5
C(57)-C(59)-H(59A)	109.5		
C(57)-C(59)-H(59B)	109.5		
H(59A)-C(59)-H(59B)	109.5		
C(57)-C(59)-H(59C)	109.5		
H(59A)-C(59)-H(59C)	109.5		
H(59B)-C(59)-H(59C)	109.5		
C(57)-C(60)-H(60A)	109.5		
C(57)-C(60)-H(60B)	109.5		
H(60A)-C(60)-H(60B)	109.5		
C(57)-C(60)-H(60C)	109.5		
H(60A)-C(60)-H(60C)	109.5		
H(60B)-C(60)-H(60C)	109.5		
